A COMPARISON STUDY OF ONE- AND TWO-DIMENSIONAL HYDRAULIC MODELS FOR RIVER ENVIRONMENTS

By

Evan C. Deal

Submitted to the graduate degree program in Civil, Environmental and Architectural Engineering and the Graduate Faculty of the University of Kansas in partial fulfillment of the requirements for the degree of Master of Science.

_____
Chairperson Alfred D. Parr

_____
Co-chair C. Bryan Young

_____
Bruce McEnroe

Date Defended: June 10, 2015

The Thesis Committee for Evan C. Deal

certifies that this is the approved version of the following thesis:

A Comparison Study of One- and Two-Dimensional

Hydraulic Models for River Environments

_____

Chairperson Alfred D. Parr

Date approved: June 10, 2016

Abstract

Computer models are used every day to analyze river systems for a wide variety of reasons vital to the public interest. For decades most hydraulic engineers have been limited to models that simplify the fluid mechanics to the unidirectional case. With the advent of easy access to higher quality data and greater computational power, two-dimensional hydrodynamic models have become practical for widespread use. Two such models are considered in this report – HEC-RAS v.5.0.1 and SRH-2D v.3.0. These two-dimensional models were compared to the most common one-dimensional model HEC-RAS. While the latest version of HEC-RAS is capable of both one- and two-dimensional analyses, previous versions were restricted to one-dimensional flow. Findings in this report include: differences in the flow divisions for multiple opening bridges for all three models, less subjectivity in the construction of the 2D models than for the 1D, differences in the sensitivity of each 2D model to the Manning's roughness coefficient, great similarity in the expansion and contraction rates at bridges for the 2D models when using the full momentum equations with HEC-RAS 2D, differences in the response of the two-dimensional models at steady state conditions to vortex shedding through bridge openings with cylindrical piers, shorter computation times for HEC-RAS 2D than SRH-2D using highly comparable model setups, and in general, higher depths predicted by SRH-2D than HEC-RAS 1D but the highest depths overall predicted by the HEC-RAS 2D full momentum model.

Acknowledgements

I would like to thank my committee members Dr. Parr, Dr. Young, and Dr. McEnroe for allowing me the opportunity to achieve things that bring me great joy, and for providing me with the guidance and knowledge to do so. Additional thanks goes to Dr. Parr, who has given me tremendous feedback on this report and who also built the HEC-RAS 1D model featured in Chapter 7. I am grateful for the direction given by the project monitor for this study, Michael Orth, P.E., of the Kansas Department of Transportation, and also for his interest in our work. My gratitude goes out to my parents, Michael and Deborah Deal, whose unconditional love and support has always been there for me, to my brother, Logan, my sister, Carla, and of course, to the love of my life, Fadia.

Table of Contents

List of Tables

List of Figures

Chapter 1

Introduction

The reasons for performing hydraulic modeling are vast and varied across many fields – through mathematics, the sciences, and virtually every engineering discipline. For the civil engineer alone, the reasons for performing hydraulic modeling vary greatly still – as do the locations that require the services of the civil engineer, from water treatment plants to municipal water distribution systems, from groundwater sites to the atmosphere, from natural lakes to man-made reservoirs, and from natural streams and rivers to constructed channels. Even narrowing our focus to this last group, the channelized flow, natural or otherwise, the motivations for building a computerized model still span across a multitude. Issues of concern are: potential backwater profiles caused by the construction or modification of a bridge that could result in flooding upstream from the structure, scour at bridge piers and abutments that could compromise the structural integrity of the entire bridge, determination of floodplain extents as part of the National Flood Insurance Program, the regulation of floodway encroachments, dam-break studies to help assess risk and create a priority list for maintenance schedules, the proper sizing of culverts and selection of end treatments, appraisal of suitable sites for fish habitat restoration along a reach, sediment transport studies to estimate long-term aggradation or degradation within rivers, and studies of sedimentation of dams to predict when, where, and how much dredging in a reservoir should occur. The agencies that address such topics include state and federal Departments of Transportation, federal water management agencies such as the Bureau of Reclamation, Army Corps of Engineers, and Geological Survey, researchers and educators at universities around the world, and private contracting firms of all shapes and sizes.

Most early models dealt with unidirectional flow, not because the mathematics to do more did not exist, but because the computational power and the availability of detailed terrain data did not. Thus, two-dimensional models were simply not practical for general use. These one-dimensional models, such as HEC-2 and all versions of HEC-RAS up to and including the previous release of the software, HEC-RAS 4.1, have proven exceptionally useful over their decades of use. In large part due to the great amount of time and resources invested by countless researchers and practicing engineers in making sure the empirical equations that are used to compensate for shortcomings of the one-dimensional assumption, such as in the case of rapidly varied flow through a channel constriction under bridges, can accurately predict upstream and downstream flow parameters like depth and bed shear stress.

However, not only are computers now faster and more powerful than ever before, but the quality of and access to the data that serves as the inputs to hydraulic models is much better. The advent of the internet and such resources as the National Map Viewer, a repository for digital elevation data managed by the United States Geological Survey, and the Web Soil Survey, a national map for soil types managed by the United States Department of Agriculture, have aided in the widespread practice of complex hydraulic modeling. Thus, the latest trend in the world of hydraulic river modeling is towards the two-dimensional model, of which there are many.

- HEC-RAS (Hydrologic Engineering Center's River Analysis System): a product of the United States Army Corps of Engineers.
- SRH-2D (Sedimentation and River Hydraulics – Two-Dimensional River Flow Model): of the United States Bureau of Reclamation (this program along with HEC-RAS are the main focus of this report).

- FESWMS (Finite-Element Surface-Water Modeling System): of the United States Geological Survey.
- FST2DH (Flow and Sediment Transport Two-Dimensional Hydraulics): a module of FESWMS sponsored by the Federal Highway Administration.
- AdH (Adaptive Hydraulics): yet another product of the USACE.
- TELEMAC-MASCARET: a model managed by a consortium of European agencies based in France, Germany, and United Kingdom.
- FLO-2D: produced by FLO-2D Software, Inc., a privately owned company.
- RiverFlow-2D: from another privately owned company, Hydronia, LLC.
- Many more.

Much has changed since the early days of computerized river modeling when in 1966 the Hydrologic Engineering Center at the United States Army Corps of Engineers developed the first FORTRAN version of HEC-2, the predescessor of today's HEC-RAS software package, to calculate backwater profiles. HEC-2 "was capable of computing water surface profiles in channels with irregularly shaped cross sections", something other models could not do, and it "represented a significant step in the development of modern computational techniques for hydraulic analysis" (HEC-2 User Manual Section 1.1). The computing power of today's machines greatly exceeds that which was available 50 years ago, and so while the questions engineers and scientists would like to answer by running hydraulic simulations may be the same as they were five decades ago, our ability to answer those questions has improved dramatically.

The industry is on the verge of great change, and care must be taken to ensure that these new two-dimensional models are adopted responsibly. A great many structures have been designed based on the results of one-dimensional analyses, and engineers have grown to understand and

trust those designs. As with any decision that can have great consequences for the public and its safety, the adoption of 2D models should be made only with all reasonable confidence in their efficacy. That is why this report seeks to compare these programs – HEC-RAS 4.1, HEC-RAS 5.0, and SRH-2D v.3.0 – and to provide guidance for good hydraulic modeling practices, such as those for terrain conditioning, mesh development, and model parameterization. Comparisons will be made on the basis of flood plain extent and velocity calculations across the spatial domain.

Chapter 2

Theory

2.1. Overview of the Model Theory and Hydraulics

A one-dimensional model is based on the assumption that all discharge through any cross-section is normal to the cross-section. That is, all flow is assumed to travel in the longitudinal direction, none in the lateral or vertical directions. Obviously, this is not true for an actual river, but in many cases it is an assumption that provides quite reasonable results. The strength of this assumption lies in the placement and orientation of each cross-section within the area of interest such that the one-dimensional simplification is as close to reality as possible. This often requires that cross sections have breaks with individual lines segments perpendicular to the terrain contours. The hydraulic engineer responsible must be able to visualize the flow patterns which are likely to occur and to draw the cross-sections accordingly. This can be a challenging task and one which greatly depends upon the complexity of the terrain. In the end, the engineers must rely on their best judgement to properly model a reach.

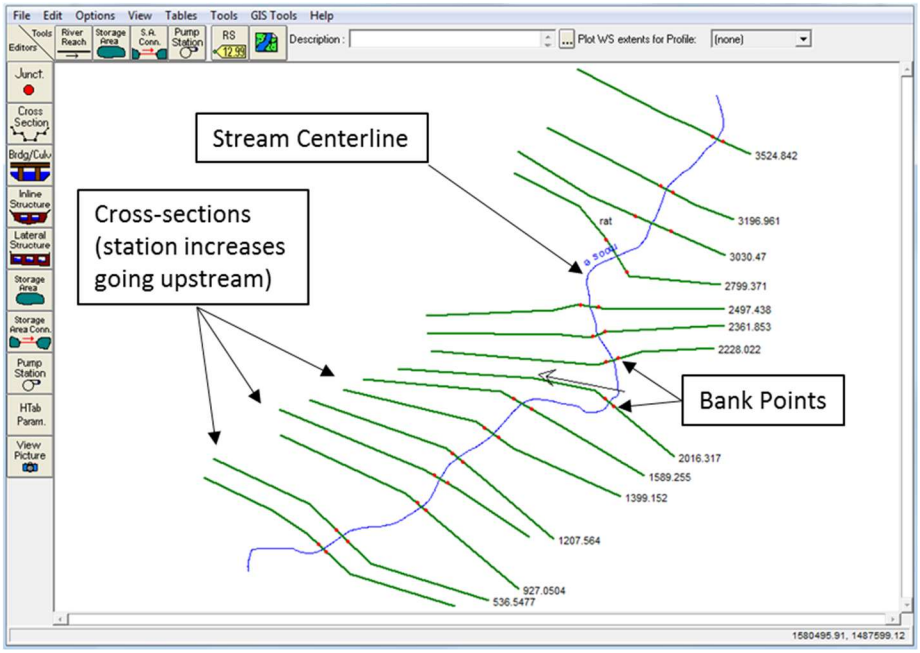

Figure 2-1. Plan View of Typical HEC-RAS Model

Figure 2-1 shows the Geometric Data Editor window from a simple HEC-RAS project. As the cross-sections were placed, it was necessary to consider the stream lines of the water through the study region. Also, by scrutinizing the elevation contours (or the hill shade) within a GIS application (in this case ArcMap), the overbank flow paths can be visualized. This is best accomplished by drawing the cross-sections perpendicular to the elevation contours, though the maximum angle recommended between breaks in a cross section is 20 degrees. Furthermore, by taking into account the fact that if the flow were to overtop the road (located between cross section stations 2361.853 and 2497.438) then the road would function as a weir, meaning that the flow would move perpendicular to the road centerline.

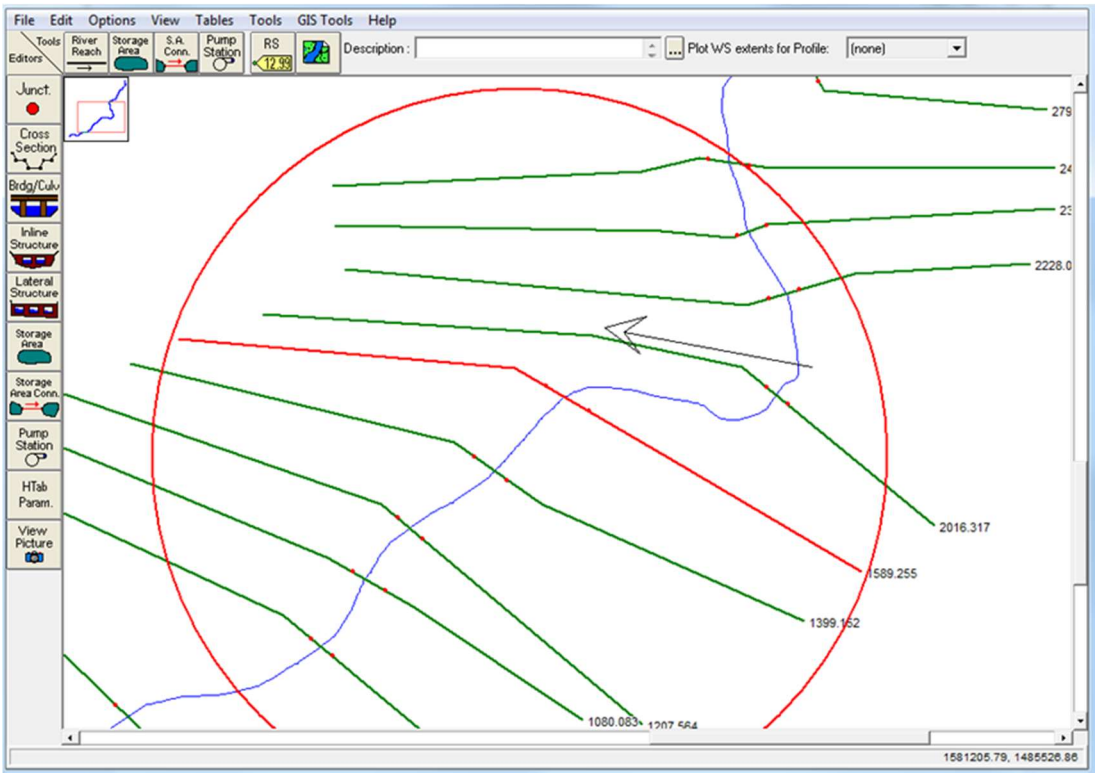

Figure 2-2.Selection of Example Cross Section 1589.255

If just one cross-section is considered, it can easily be shown how the one-dimensional assumption operates in practice. Figure 2-3shows the flux across a sample cross-section from a

HEC-RAS project, and while it may seem that there are indeed two components to the velocity, that is in truth merely an artifact of how the section is represented in the GUI (graphical user interface) of HEC-RAS.

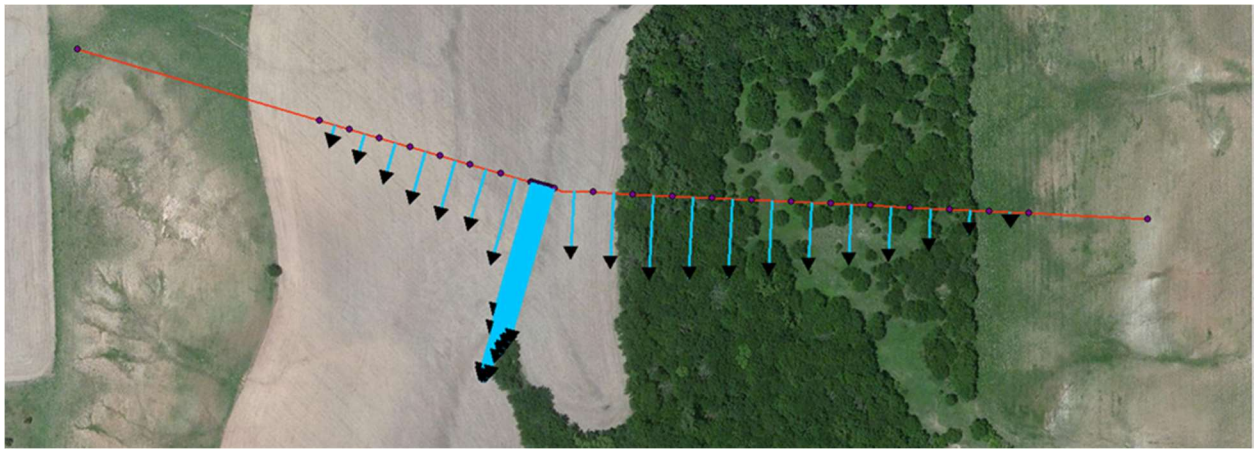

Figure 2-3. Representation of Assumed Flow Directions for a Single Cross Section

It should be noted that the velocity is allowed to vary across the cross section in a HEC-RAS model. In Figure 2-3 the magnitudes of these velocities correspond to the length of the vector drawn from the cross section (this was accomplished manually within ArcMap). HEC-RAS can compute these velocities as it determines the conveyance through each subdivision of the cross section (see Section 2.2.1 for more details). In order to see these values, displayed graphically in Figure 2-4, one must set the option in HEC-RAS by going to Run > Steady Flow Data > Options > Flow Distribution Locations before running the model. Also, from Figure 2-4 the result of how HEC-RAS extracts data from the underlying DEM (digital elevation model) and uses it for a cross section is shown.

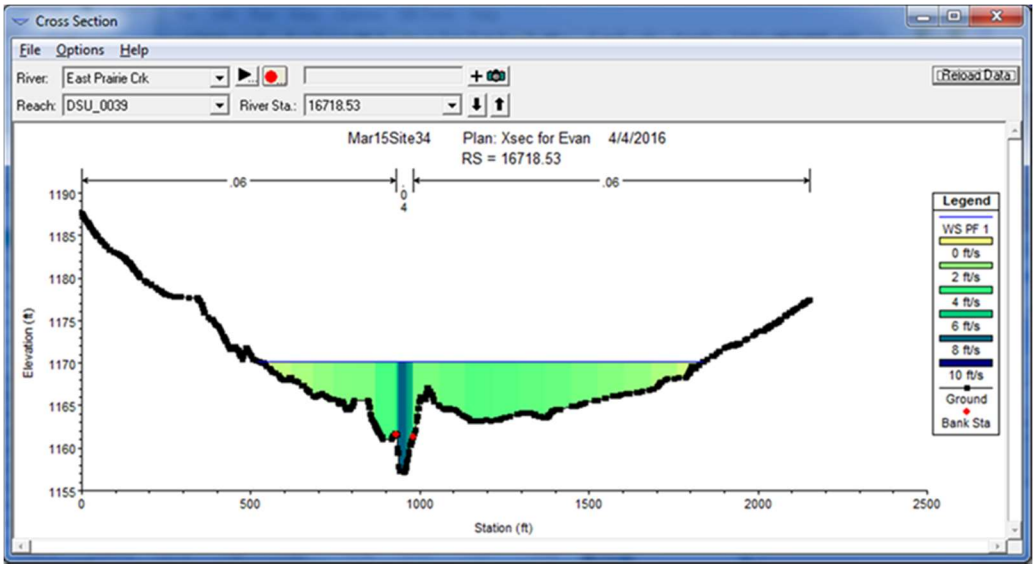

Figure 2-4. HEC-RAS Interpretation of Given Cross Section

Thus, as shown in Figures 2-1 through 2-3, each cross-section is made up of a single line or a line with multiple segments. This display, however, is merely for the benefit of the engineer in constructing the model and interpreting the model results. A more accurate representation of how HEC-RAS truly models the reach is shown in Figure 2-5. Mathematically, the program treats the river as if it were straight and all the flow were moving in one direction, albeit at different depths and velocities from one cross-section to the next. One caveat here is that is the model generally uses different reach lengths for the main channel and each overbank.

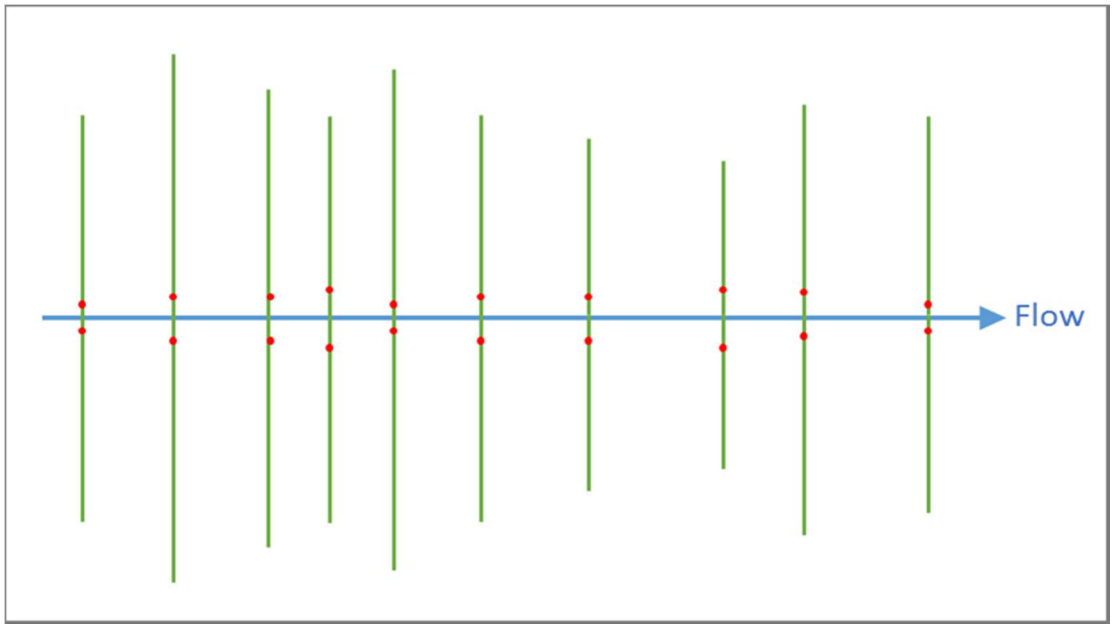

Figure 2-5. Schematic of a Typical HEC-RAS Reach Model.

However, a two-dimensional model allows for velocity vector components along a horizontal plane in two directions while neglecting any vertical component. Clearly, this mathematical treatment of the flow lends itself to a much more realistic solution of the hydraulics occurring in a given reach. The theoretical construct referred to as a "cross section" is necessary to proceed with a one-dimensional analysis, but requires various properties of the flow, such as velocity and water surface elevation, to be averaged over large distances. This averaging of properties is not nearly so drastic when using a two-dimensional model. HEC-RAS 2D still uses something like scaled-down cross sections for each side of a 2D element. SRH-2D uses a finite element approach to define the model space rather than cross-sections. The result of each method is that water is allowed to flow from a computational mesh element to adjacent elements.

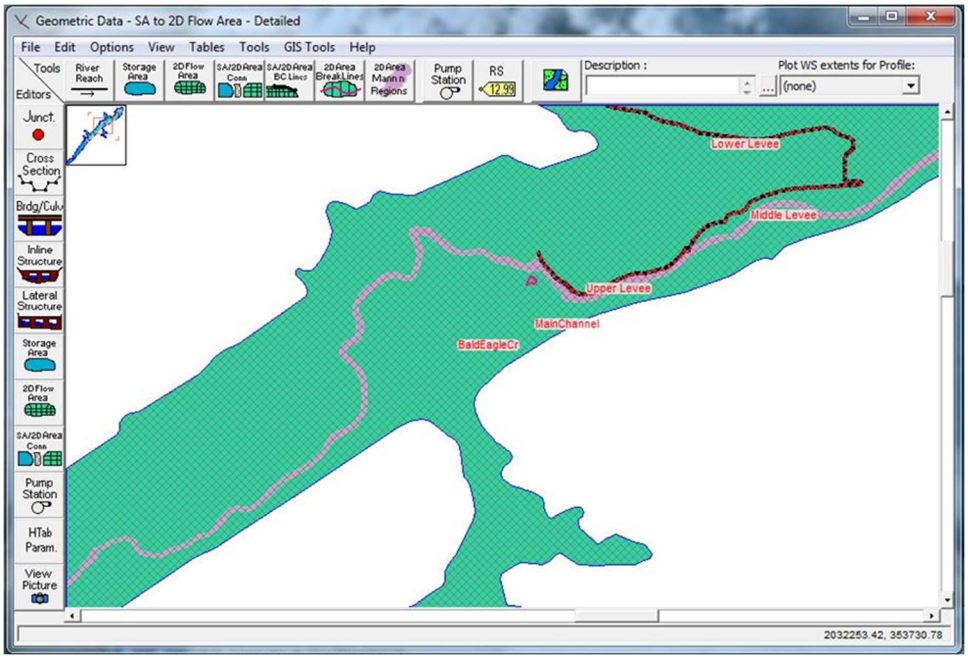

Figure 2-6. Geometric Data Editor Window for HEC-RAS 5.0 Bald Eagle Creek Dam Break Example Project

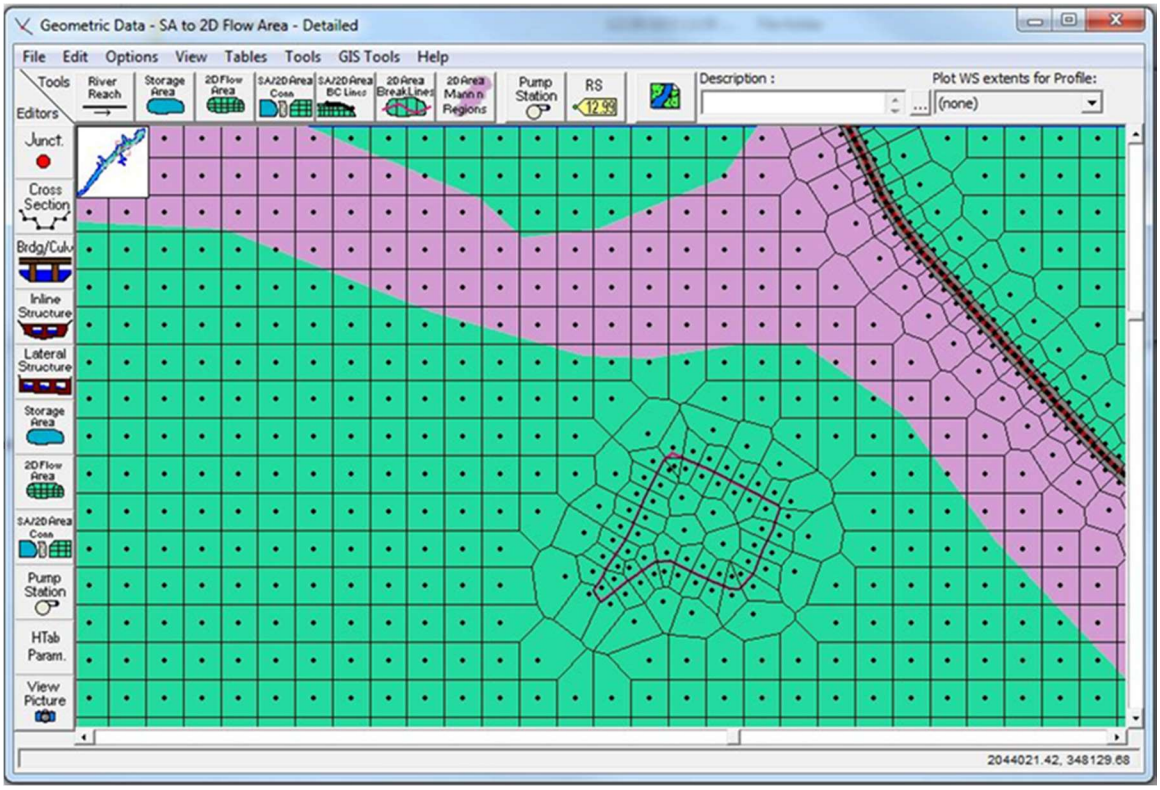

Figure 2-7. Zoomed-in View for HEC-RAS 5.0 Bald Eagle Creek Example Project Showing Mesh Details

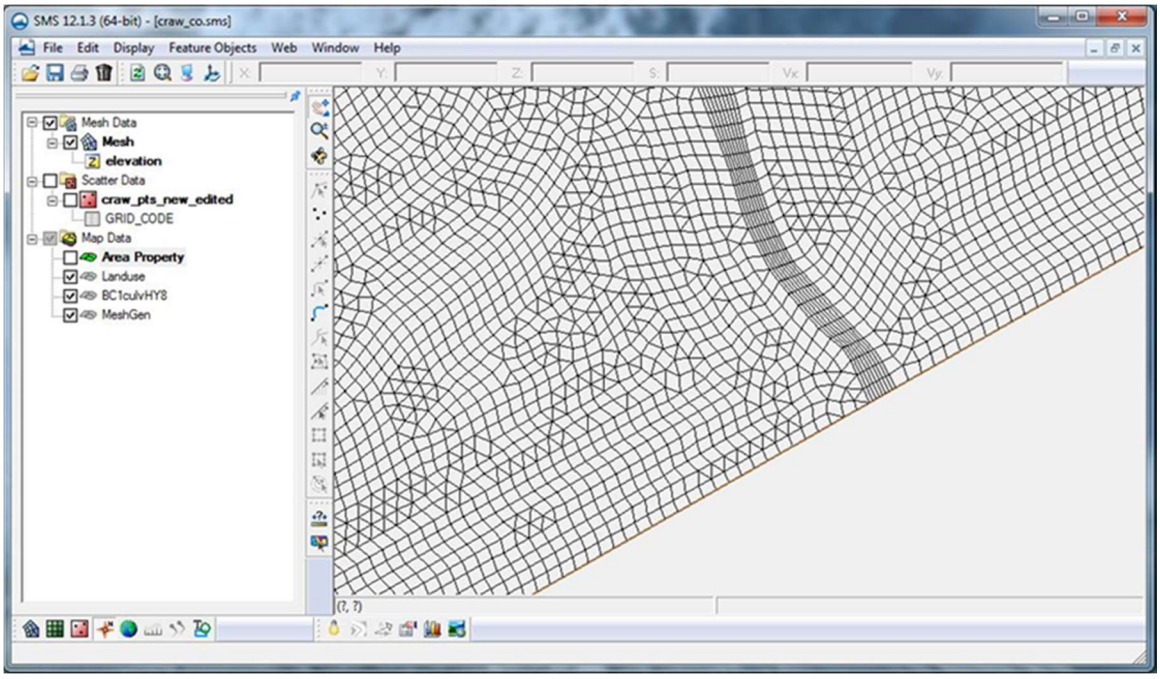

Figure 2-8. SRH-2D Mesh Viewed in SMS 12.1 for a Site in Crawford County, KS

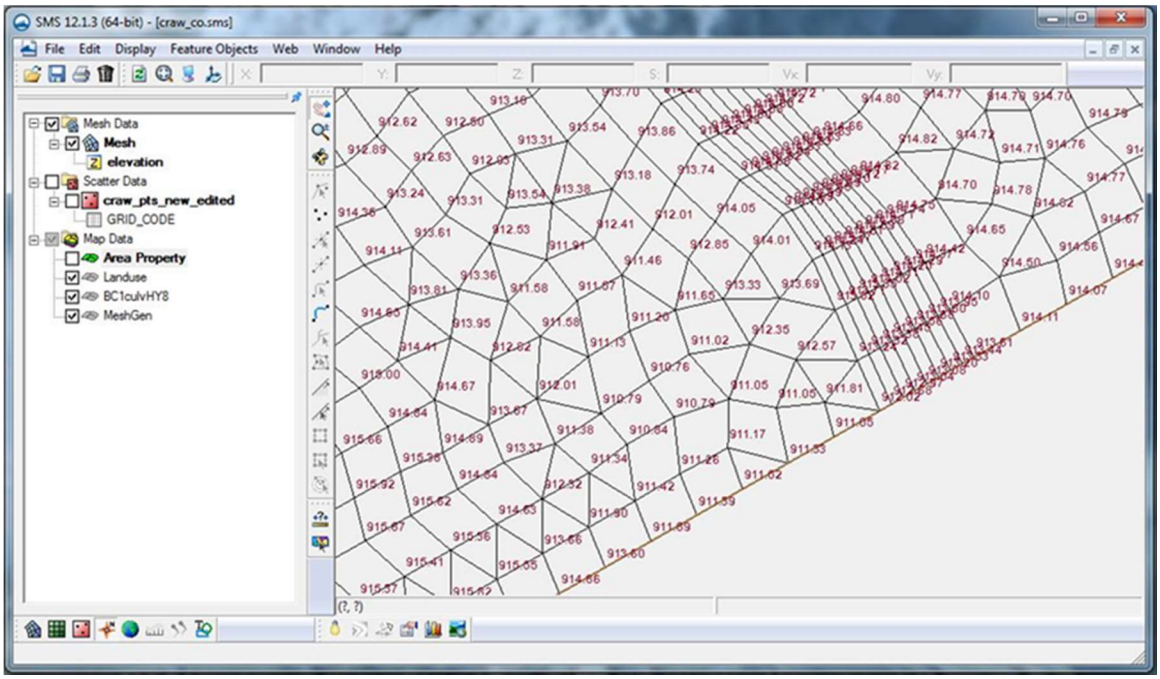

Figure 2-9. Zoomed-in View of SRH-2D Mesh from Fig. 2.7 Showing Elevation Values at Corner Nodes

2.2. Model Equations

2.2.1. One-Dimensional HEC-RAS Equations

During a steady-state simulation for HEC-RAS 1D the flow profile is determined from one cross section to the next by solving the Energy equation and by also employing the standard step method.

$$Z_2 + Y_2 + \frac{\alpha_2 V_2^2}{2g} = Z_1 + Y_1 + \frac{\alpha_1 V_1^2}{2g} + h_e \qquad (EQN: 2.1)$$

For the above equation, the terms accompanied by a subscript of "1" denote the downstream section, while those with a "2" represent the cross-section immediately upstream. "Z" represents the channel invert elevations, "Y" the water depth, "α" is a velocity weighting coefficient, "V" is the average velocity for the entire cross-section, "g" is the gravitational acceleration, and "h_e" is the energy loss term from section 2 to 1.

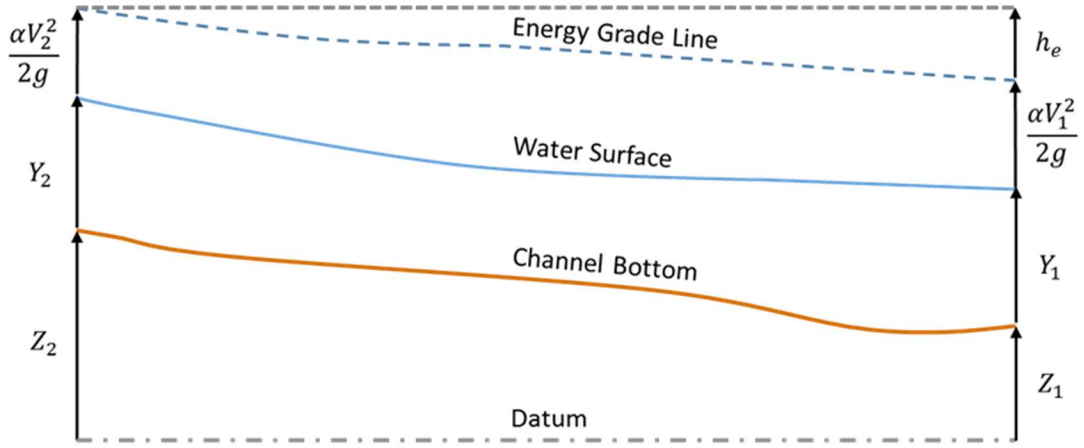

Figure 2-10. Diagram Showing Terms Used in HEC-RAS Energy Equation

$$h_e = L\bar{S_f} + C\left|\frac{\alpha_2 V_2^2 - \alpha_1 V_1^2}{2g}\right| \qquad (EQN: 2.2)$$

The above equation used to calculate head loss between sections and is required to apply the energy equation. "L" is the discharge-weighted reach length, $\bar{S_f}$ is the representative friction slope, and "C" is either an expansion or contraction loss coefficient.

$$L = \frac{L_{lob}\bar{Q}_{lob} + L_{ch}\bar{Q}_{ch} + L_{rob}\bar{Q}_{rob}}{\bar{Q}_{lob} + \bar{Q}_{ch} + \bar{Q}_{rob}} \qquad (EQN: 2.3)$$

For the above equation the subscript "lob" stands for left overbank, "ch" for channel, and "rob" for right overbank. "L" is the cross section reach length between sections while "$\bar{Q}$" is the arithmetic mean of discharge.

$$S_f = \left(\frac{Q}{K}\right)^2 \rightarrow \bar{S}_f = \left(\frac{Q_1 + Q_2}{K_1 + K_2}\right)^2 \qquad (EQN: 2.4)$$

By default, HEC-RAS uses the arithmetic mean of the friction slope at each section to calculate the representative friction slope (although, the geometric and harmonic means are also options within the program). In the above, "Q" represents discharge and "K" the conveyance for each subdivision within an individual cross-section.

$$Q = KS_f^{1/2} \qquad (EQN: 2.5)$$

$$K = \frac{1.486}{n}AR^{2/3} \qquad (EQN: 2.6)$$

Discharge is computed for each conveyance subdivision using Manning's equation with English units as shown above. The basis for each subdivision is n-value break points within the cross section, and at breaks between the overbanks and the main channel (where transitions in n-values typically occur). "A" is the cross-sectional area of each section, "n" is the Manning's roughness coefficient, and "R" is the hydraulic radius which is defined as the cross-sectional area divided by the wetted perimeter ($R = A/P$).

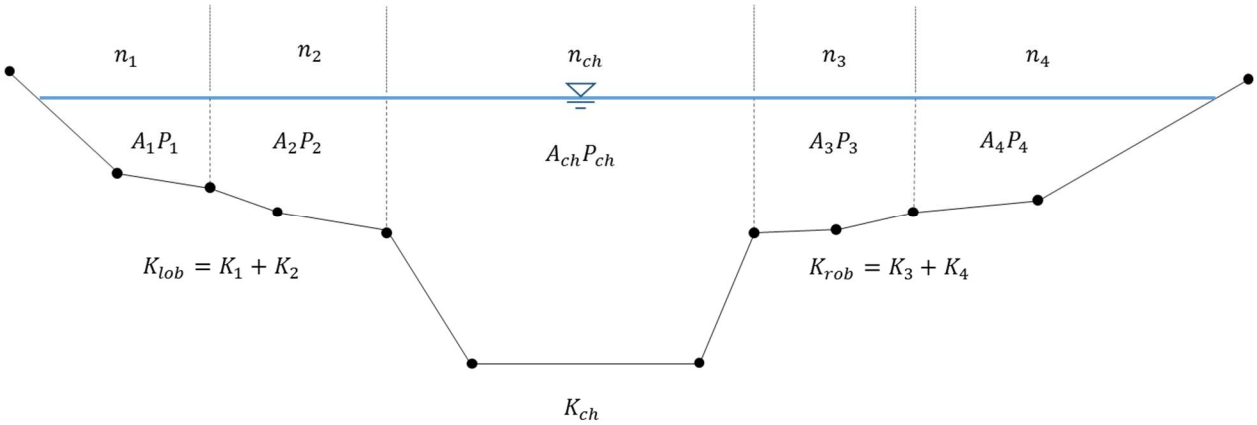

Figure 2-11. Channel Subdivisions Used in HEC-RAS Cross Section Model

HEC-RAS then determines the total conveyance for the cross section by summing up all of the incremental K-values. It's also possible that the Manning's n-values vary within the main channel itself. If such is the case then the following equation is used to determine a composite roughness coefficient.

$$n_c = \left[\frac{\sum_{i=1}^{N}(P_i n_i^{1.5})}{P}\right]^{2/3} \qquad (EQN: 2.7)$$

The velocity weighting coefficient, α, used in Equation 2.1, is determined using the following equation. Where "A_t" is the total area for the cross-section and "K_t" is the total conveyance.

$$\alpha = \frac{(A_t)^2\left[\frac{K_{lob}^3}{A_{lob}^2} + \frac{K_{ch}^3}{A_{ch}^2} + \frac{K_{rob}^3}{A_{rob}^2}\right]}{K_t^3} \qquad (EQN: 2.8)$$

In order to determine the head losses due to either the expansion or contraction of flow, which are the the second group of terms on the right-hand side of Equation 2.2, the following equation is used.

$$h_{ce} = C\left|\frac{\alpha_1 V_1^2}{2g} - \frac{\alpha_2 V_2^2}{2g}\right| \qquad (EQN: 2.9)$$

Whether the "C" value used in the equation corresponds with the expansion or contraction coefficient for the cross-section depends on V_1 and V_2. When the velocity upstream, V_2, is less than the velocity downstream then the contraction coefficient is applied, but when the reverse is true then the expansion coefficient is used. For more information on expansion and contraction coefficients, see Chapter 3 of the HEC-RAS 4.1 User's Manual, "Basic Data Requirements".

Two key assumptions in a steady state HEC-RAS simulation, in addition to the one-dimensional requirement, are that the discharge is constant and that the water surface profile is gradually varied except at locations where the flow is rapidly varied. Such locations include channel constrictions (culverts, weirs, and bridges) and sites where a hydraulic jump may exist. Empirical equations or momentum analyses are used at these locations. The momentum equation is shown below.

$$\frac{Q_2^2\beta_2}{gA_2} + A_2\bar{Y}_2 + \left(\frac{A_1 + A_2}{2}\right)LS_0 - \left(\frac{A_1 + A_2}{2}\right)L\bar{S}_f = \frac{Q_1^2\beta_1}{gA_1} + A_1\bar{Y}_1 \qquad (EQN: 2.10)$$

The above form of the momentum equation includes terms for the momentum flux in and out of the control volume between cross-sections. It includes hydrostatic pressure terms, a term for the water weight component acting parallel to the channel bed, and a term for the frictional forces between the water and the ground opposing the motion of the water. The "β" terms are momentum coefficients that account for the velocity distribution in irregular channels, and "$\bar{Y}$" represents the depth measured from the water surface to the centroid of the cross-sectional area.

A discussion of the unsteady flow routing portion of one-dimensional HEC-RAS is especially relevant because these equations also serve as the basis for the two-dimensional HEC-RAS model. These equations are based on the St. Venant equations, which are in turn based on the Navier-Stokes equation for an incompressible fluid.

$$\rho \frac{D\boldsymbol{u}}{Dt} = -\nabla p + \rho \boldsymbol{g} + \mu \nabla^2 \boldsymbol{u} \qquad (EQN: 2.11)$$

In the equation above "ρ" is the density of the fluid. "$\frac{D\boldsymbol{u}}{Dt}$" is the total time differential of the velocity vector, "$\boldsymbol{u}$", "$\boldsymbol{g}$" is the gravitional acceleration expressed as a vector, "μ" is the dynamic viscosity of the fluid, and "∇^2" is the Laplace operator $\left(\frac{\partial^2}{\partial x^2} + \frac{\partial^2}{\partial y^2} + \frac{\partial^2}{\partial z^2}\right)$. The Navier-Stokes equation is derived from Newton's second law concerning conservation of momentum.

$$\sum F_x = \frac{d\vec{M}}{dt} \qquad (EQN: 2.12)$$

From this the one-dimensional St. Venant equation for shallow water free surface flow may be derived (see HEC-RAS User's Manual for more information).

$$\frac{\partial Q}{\partial t} + \frac{\partial QV}{\partial x} + gA\left(\frac{\partial z}{\partial x} + S_f\right) = 0 \qquad (EQN: 2.13)$$

If all terms in the above equation are included, then it is what is referred to as the "full momentum equation" within HEC-RAS (but is also known as the "dynamic wave equation"). If the first term, $\frac{\partial Q}{\partial t}$, which represents the local acceleration of the fluid, is excluded, then what remains is known as the "diffusion wave equation". "$\frac{\partial QV}{\partial x}$" represents the convective acceleration of the fluid. "$\frac{\partial z}{\partial x}$" is the change in the z-direction with respect to the x-direction, and is then clearly equal to the negative of the ground slope, S_O. The friction slope, "S_f", is calculated by the following equation (based on Manning's equation) when performing an unsteady flow analysis.

$$S_f = \frac{Q|Q|n^2}{2.208R^{4/3}A^2} \qquad (EQN: 2.14)$$

The continuity equation for unsteady HEC-RAS is defined as the following.

$$\frac{\partial A_T}{\partial t} + \frac{\partial Q}{\partial x} - q_l = 0 \qquad (EQN: 2.15)$$

where "A_T" represents the total flow area and "q_l" the lateral inflow per unit length.

2.2.2. Two-Dimensional HEC-RAS Equations

The HEC-RAS 2D system differs from the 1D model in that "cross section-like" properties are defined for each cell face. Thus the rate that water flows through each cell face is dependent on the face properties. This is important in that it allows the hydraulic engineer to more accurately represent the terrain of the entire reach within the model. The outcome is that less averaging of the flow and terrain properties occurs for a 2D model since it embodies the properties of the entire area of interest.

The computational mesh employed within HEC-RAS 2D differs from most two-dimensional models in that the ground elevation within an element is not assumed to be a plane. The model uses what is called a "high resolution subgrid model" that within the interface is referred to as the 2D Computational Mesh which is linked to a Hydraulic Property Table. Cells can have anywhere from 3 to 8 sides and these edges of an element are not required to be straight lines (in that their elevation does not vary linearly). Within the hydraulic property table is stored various details about the cell faces such as elevation versus wetted perimeter, area, roughness, etc. Discharge moving across a cell face uses this information. The next several figures seek to clarify the nature of these cells with "cross section-like" edges.

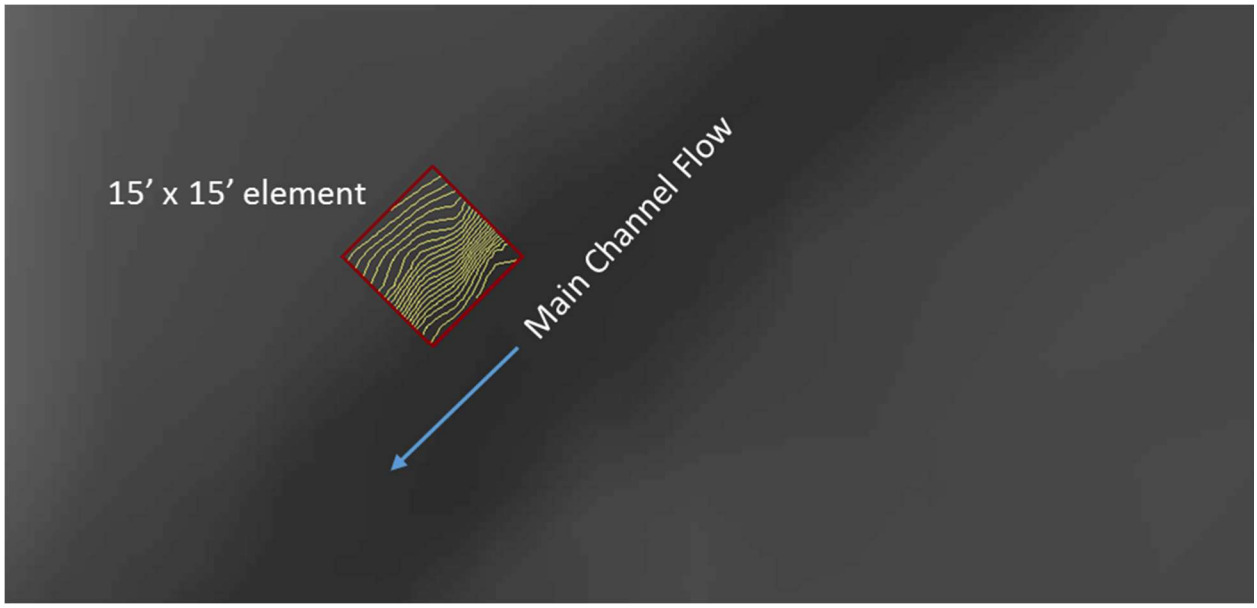

Figure 2-12. Square Mesh Element atop Grid with Elevation Contours Spaced at 0.2’ Intervals

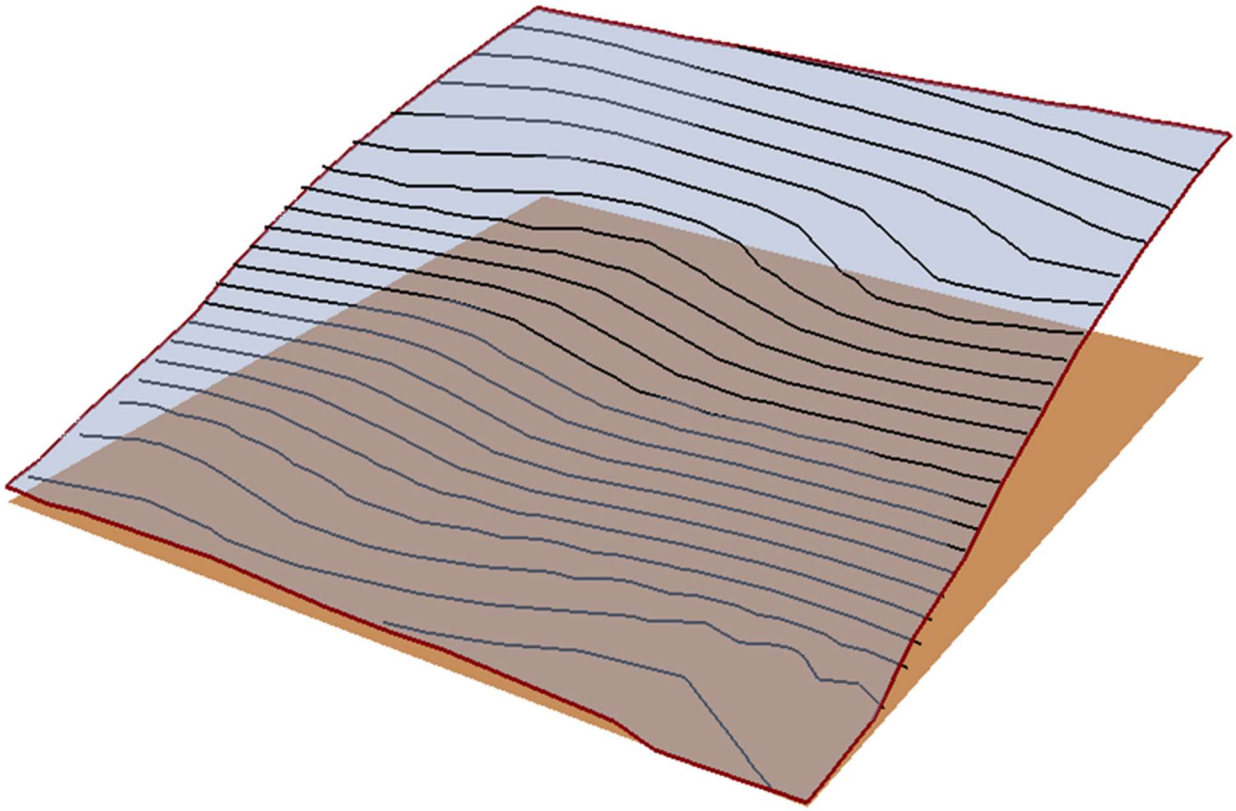
Figure 2-13. Three-Dimensional Representation of the Mesh Element from Figure 2.12

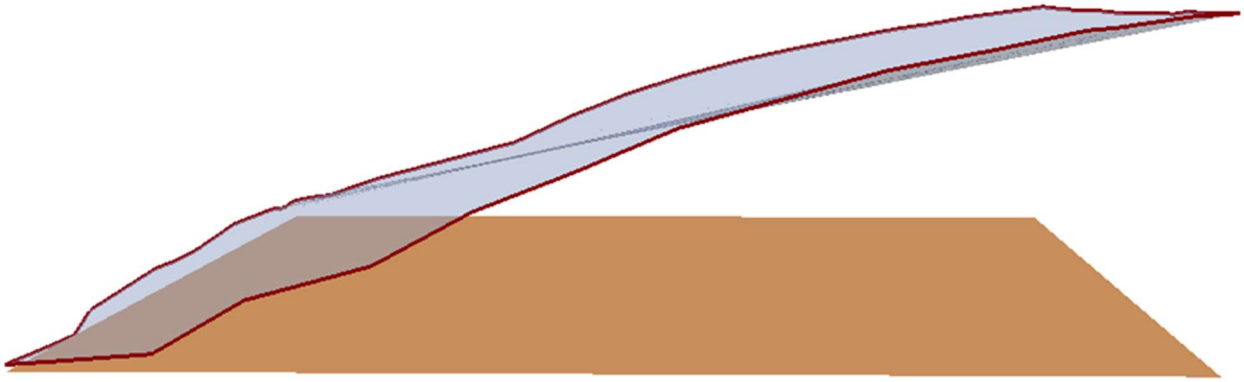

Figure 2-14: View from Upstream Looking Downstream

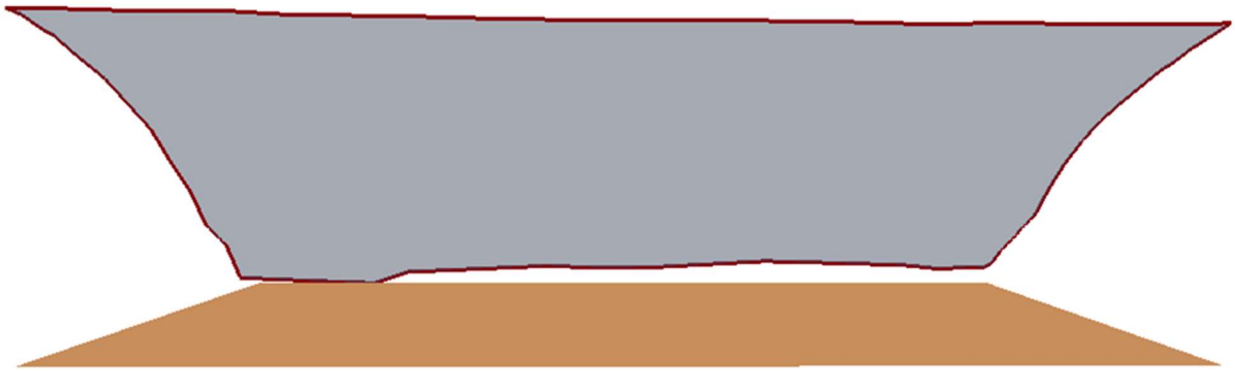

Figure 2-15. View Perpendicular to that in Figure 2.14 Looking Towards the Main Channel Flowline

Each of the four faces of the element described in the figures above is analogous to a one-dimensional HEC-RAS cross section, except that flow across any face possesses two components for velocity. Treating the mesh this way allows for a cell to be partially wet and yet still contain the correct volume of water. It also allows for larger mesh sizes that still accurately account for storage versus stage within an individual cell. Even if all elements within the model are 40 feet by 40 feet, but the river being modeled is only 10 feet wide, at low flows when the water should stay in the channel it will indeed do that. This system makes it possible to use fewer cells as well as a larger computational timestep than do most other models, meaning fewer calculations are required, yet accurate results are still achievable.

The equations used for a HEC-RAS 2D simulation are based upon those outlined in the previous section for a HEC-RAS 1D unsteady state simulation. The full momentum or the diffusive

wave versions of the St. Venant equations can be selected before starting a simulation. The full momentum equation should provide more accurate solutions, but it takes more time to compute than the diffusive wave equation. Often, the results from the two equations are similar enough that either solution is acceptable, but situations in which the diffusive wave equation is grossly inadequate include places where large eddy losses occur such as in places of recirculating flow like those found upstream and downstream of bridge openings. Usually, sections such as bridge constrictions should be handled by the one-dimensional HEC-RAS bridge routines. This is accomplished by creating a combined one- and two-dimensional HEC-RAS model, where a one-dimensional section is placed between two-dimensional sections.

2.2.3. SRH-2D Equations

SRH-2D uses a finite-element approach to generating the mesh used for its hydraulic calculations. Elements can be either triangles or quadrilaterals, and a model may contain all of one or the other type, or some combination of the two. Each element is a plane defined by a single elevation, although within the mesh generation application, the Surface Water Modeling System (SMS, a product of Aquaveo) interpolates elevation values to the mesh nodes on the corners of each element.

The flow equations used by SRH-2D are derived from the three-dimensional Navier-Stokes equation presented in Section 2.2.1 by integrating across the vertical dimension, thus leading to the depth-averaged, two-dimensional St. Venant equations.

The form of the continuity equation used is the following.

$$\frac{\partial h}{\partial t} + \frac{\partial hU}{\partial x} + \frac{\partial hV}{\partial y} = e \qquad (EQN: 2.16)$$

where "h" is the water depth, "t" is time, "U" and "V" are depth-averaged velocity components in the x and y directions, respectively, and "e" is the excess rainfall rate.

$$\frac{\partial hU}{\partial t}+\frac{\partial hUU}{\partial x}+\frac{\partial hVU}{\partial y}=\frac{\partial hT_{xx}}{\partial x}+\frac{\partial hT_{xy}}{\partial y}-gh\frac{\partial z}{\partial x}-\frac{\tau_{bx}}{\rho}+D_{xx}+D_{xy} \qquad (EQN: 2.17a)$$

$$\frac{\partial hV}{\partial t}+\frac{\partial hUV}{\partial x}+\frac{\partial hVV}{\partial y}=\frac{\partial hT_{xy}}{\partial x}+\frac{\partial hT_{yy}}{\partial y}-gh\frac{\partial z}{\partial y}-\frac{\tau_{by}}{\rho}+D_{yx}+D_{yy} \qquad (EQN: 2.17b)$$

The two equations above are the full momentum equations used by SRH-2D." T_{xx}","T_{xy}", and "T_{yy}" are depth-averaged turbulent stresses. "D_{xx}","D_{xy}", "D_{yx}", and "D_{yy}" are dispersion terms that arise due to depth averaging. "z" is the water surface elevation and is equal to "z_b" the bed elevation, plus "h". "ρ" is the water density. "τ_{bx}" and "τ_{by}" are both frictional stresses between the water and the ground and they are calculated using the following equations based upon Manning's roughness equation.

$$\begin{pmatrix}\tau_{bx}\\ \tau_{by}\end{pmatrix}=\rho C_f\begin{pmatrix}U\\ V\end{pmatrix}\sqrt{U^2+V^2} \qquad (EQN: 2.18)$$

$$C_f=\frac{gn^2}{h^{1/3}} \qquad (EQN: 2.19)$$

The following equations are used to calculate the turbulent stresses and are based on the Boussinesq equations:

$$T_{xx}=2(\nu+\nu_t)\frac{\partial U}{\partial x}-\frac{2}{3}k \qquad (EQN: 2.20a)$$

$$T_{xy}=(\nu+\nu_t)\left(\frac{\partial U}{\partial y}+\frac{\partial V}{\partial x}\right) \qquad (EQN: 2.20b)$$

$$T_{yy}=2(\nu+\nu_t)\frac{\partial V}{\partial y}-\frac{2}{3}k \qquad (EQN: 2.20c)$$

where "ν" is the kinematic viscosity of water, "ν_t" is the turbulent eddy viscosity, and "k" is the turbulent kinetic energy. There are two ways of modeling turbulence within SRH-2D. One method is called the k-ϵ model and is not the standard setting within SRH-2D and will not be

discussed (for more information see SRH-2D manual, Chapter 6). The second method, the parabolic turbulence model, is the standard in SRH-2D. In this second approach to modeling turbulence, the terms with k are dropped, and ν_t is calculated using the following equation:

$$\nu_t = C_t U_* h \qquad (EQN: 2.21)$$

where "U_*" is the bed frictional velocity and "C_t" is the parabolic turbulence constant. While C_t can range from 0.3 to 1.0, the default is 0.7. For most applications the default value should be acceptable. Section 4.2 presents a simple test to evaluate model sensitivity to this value.

The distribution of flow in the SRH-2D model is determined according to a conveyance method described by the following equation:

$$K = Q \Big/ \sum_i \frac{h_i^{5/3}}{n_i} \Delta s_i \qquad (EQN: 2.22)$$

where "i" is the i-th boundary face of the inlet, "h_i" is the water depth, "n_i" is the Manning's coefficient, and "Δs_i" is the i-th boundary face distance. The velocity at each face is assumed to be normal to the inlet boundary and is calculated using the following equation.

$$v_i = K\, h_i^{2/3} / n_i \qquad (EQN: 2.23)$$

Chapter 3

Computation Test and Basic Flow around a Bend

3.1. Overview of the Computation Test and Basic Flow around a Bend

A factor of great interest to a hydraulic modeler is the amount of time it takes to execute a simulation – a consideration of great practical importance due to the very iterative nature of hydraulic modeling. Consider, for example, a project that involves the design of a new bridge with scour limitations. If the team designing the bridge is seeking the optimal configuration in terms of cost, structural integrity, and hydraulic performance, models with run times of several days may be impractical for many design offices. This sort of consideration is why only recently two-dimensional hydraulic models have started to enter the mainstream for projects such as floodplain mapping and bridge hydraulics.

A few simulations were performed in this study using RAS-2D and SRH-2D with model parameters as similar as possible between the two to gauge their differences in computation time (RAS-1D was not considered since even for very complicated sites its simulation time is extremely short – several seconds at most). For RAS-2D both the diffusive wave and full momentum equation sets were considered. A Dell Precision T1770 workstation with 4 cores that have 2 threads each was used to perform the tests.

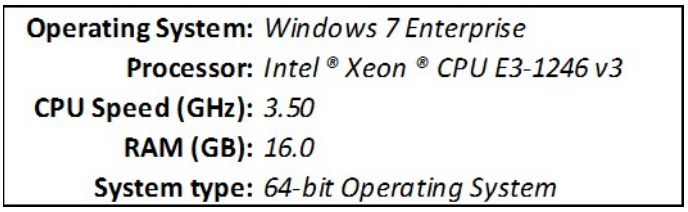

Figure 3-1. Significant Properties of the Machine Used to Perform the Computational Tests

As can be seen in Figures 3-2 and 3-3, the channel used for these tests was sinusoidal in the x-y plane, and due to this feature the basic characteristics of flow around a bend

as described in Section 7.3 of Henderson's "Open Channel Flow" were examined in brief. This channel was developed in ArcMap with the recommendations put forth for developing meander patterns from the K-TRAN report "Guidelines for Stream Realignment Design" (McEnroe, Young, and Shelley, 2009). A series of parallel polylines were used to define the channel through its length and across its width. These lines were created from the generated centerline using the "Copy Parallel" tool during an editing session. Each line was assigned upstream and downstream elevation values, and these 2D polylines were converted to 3D ones using the 3D Analyst tool "Feature To 3D By Attribute" where the upstream elevation field was used as the required "Height Field" input and the downstream elevation field was used as the optional "To Height Field". The resulting 3D shapefile was used to create a TIN, and from this TIN a Raster was created on a 1' by 1' grid (which needed to be made slightly larger than the test section to avoid errors later when the models were developed).

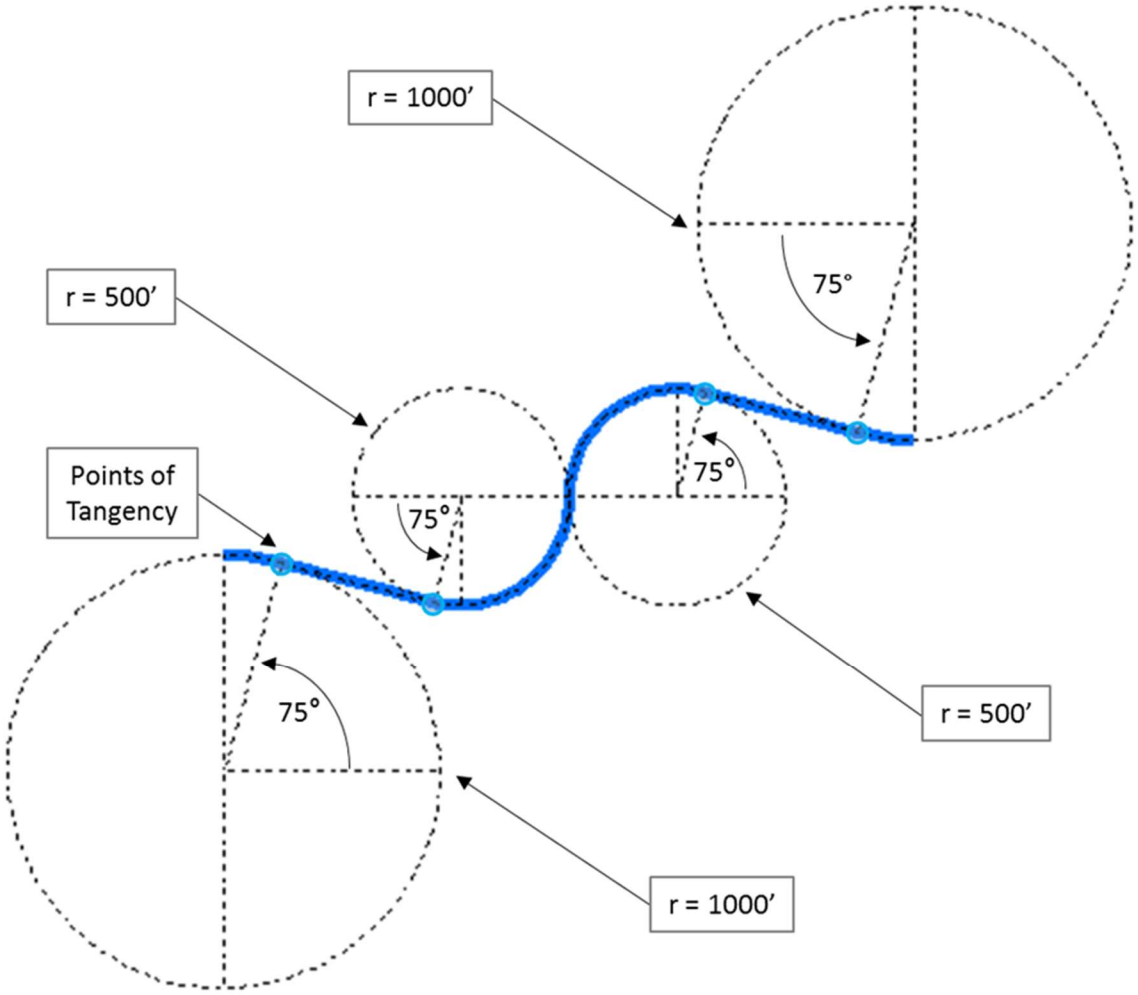

Figure 3-2. Plan View Showing Geometric Basis for Computational Test Reach

The stream centerline (represented by the blue line) was constructed from four arc segments and two straight lines. The arcs were derived from four different circles with the two types of geometry featured above – those with a radius of 500 feet and those with a radius of 1000 feet. The straight segments were connected to points of tangency on the circles corresponding to the angles in the figure. The distance in the x-direction spanned by both straight segments was based on a geometric mean of the two different radii of curvature used for this reach – that is, $\sqrt{r_{big} \cdot r_{small}} = \sqrt{1000ft \cdot 500ft} = 707ft$. The distance in the y-direction for each segment was thus dictated by this length and angles involved (see figure below).

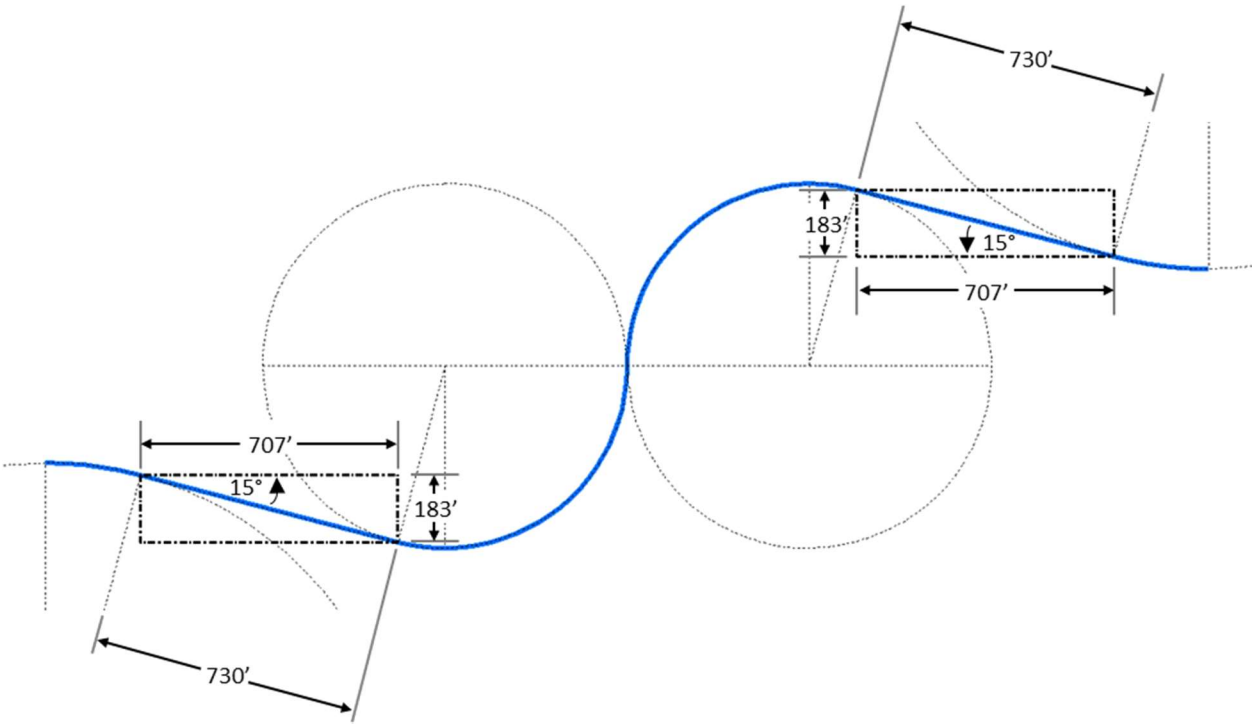

Figure 3-3. Close-up of View Describing Straight Segments of Computational Test Reach

A representative cross section was created for the downstream end of the test reach in an Excel spreadsheet. The channel possessed a circular bottom except out of the main-channel area where two different straight side slopes were used. The flow was not expected to be outside the main channel, but the side slopes were included just in case this happened. The low point of the cross-section was along its centerline, and at the downstream end this was specified to have an elevation of zero feet. The following three equations were used to determine the elevations of points spaced every one foot horizontally across the cross-section in the manner described by Figure 3-4. In the end, the main channel was defined for a radius of curvature equal to 40 feet and spanned a horizontal distance of 68 feet.

$$\beta_i = sin^{-1}\left(\frac{STA.}{r}\right) + \beta_o \qquad (EQN: 3.1)$$

$$y_i = r \cdot sin\beta_i \qquad (EQN: 3.2)$$

$$z_i = z_o + r + y_i \qquad (EQN: 3.3)$$

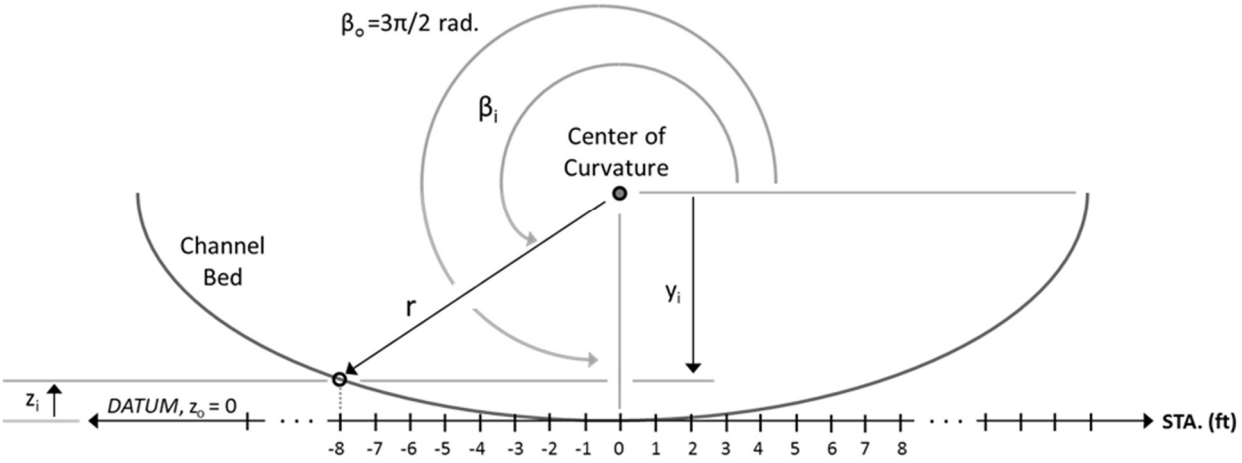

Figure 3-4. Elevation View of Geometric Basis for Cross-Sections of the Computational Test Reach

Also, within this spreadsheet, Manning's equation was applied as if the channel were straight to estimate a roughness coefficient and discharge that would return an acceptable normal depth for the tests. Using a roughness coefficient of 0.045 and a discharge of 3001 cfs the normal depth calculated was 16.27 feet. This value for normal depth was used as the downstream boundary condition for each simulation. The bed possessed a constant slope in the longitudinal direction of 0.2% as well as a length of 3816.34 feet (determined from ArcMap) and so elevations for points along the upstream cross-section were calculated. The side slopes outside of the circular portion of the channel were extended at first using a 1:2 (H:V) side slope for a horizontal distance of 6 feet, and then extended at 1:1 for 8 feet. Using the average velocity for uniform flow of 6.25 fps, an approximate travel time for flow through the channel was calculated equal to 10.2 minutes. Considering this, the hydrograph used for the simulations was one that ramped up linearly from 150 cfs to 3000 cfs over a 15-minute period and maintained that flowrate for another 15 minutes, slightly longer than the estimated travel time of 10.2 minutes to account for discrepancies resulting

from the bends. A visual check was made on all models to ensure steady state conditions had been reached.

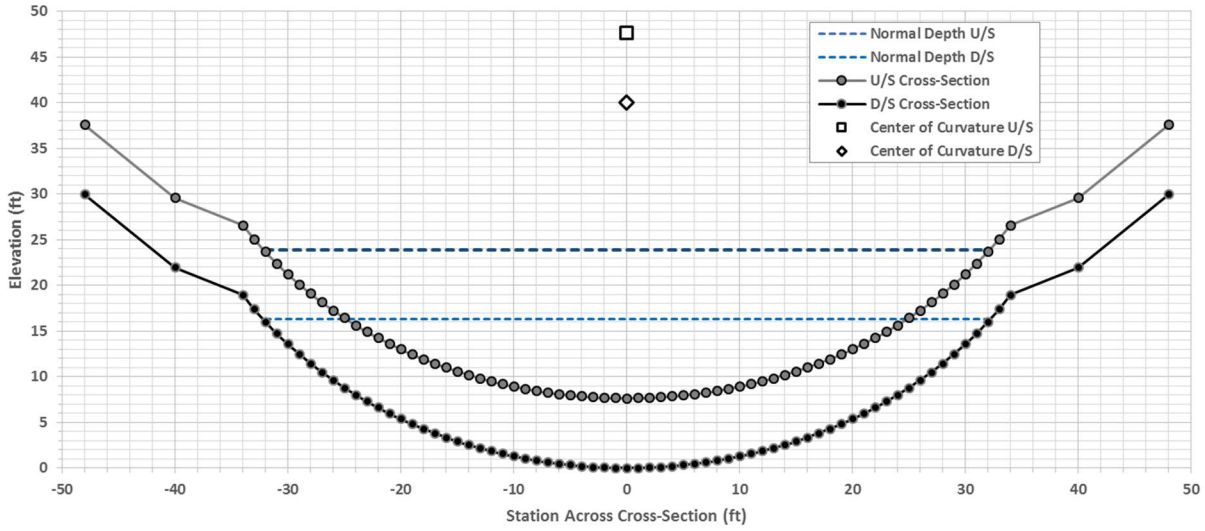

Figure 3-5. Representative Cross Sections for the Computational Test Terrain

3.2. Computational Test Results

Table 3-1. Major Inputs and Results of the Computational Tests

Model	Timestep, Δt	Spacing	Total Simulation Time, T	No. of Elements	CPU Runtime	Result output time	Initial Condition	Max. Cell	Min. Cell	Avg. Cell	Approx. Courant Number
-	(s)	(ft)	(hr)	-	(s)	(min)	-	(sq.ft)	(sq.ft)	(sq.ft)	-
SRH-2D	1.0	10	0.50	3826	34.44	1.00	Dry	113.14	50.97	95.76	0.63
	0.5	8	0.50	5724	134.64	1.00	Dry	76.61	49.24	64.01	0.39
HR-2D	1.0	10	0.50	3476	10.00	1.00	Dry	184.37	80.35	105.40	0.63
Diff.	0.5	8	0.50	5495	23.00	1.00	Dry	135.30	47.61	66.67	0.39
HR-2D	1.0	10	0.50	3476	26.00	1.00	Dry	184.37	80.35	105.40	0.63
Mom.	0.5	8	0.50	5495	54.00	1.00	Dry	135.30	47.61	66.67	0.39

Table 3-1 contains much of the relevant information concerning the computational tests performed. From these results it can be seen that for comparable model set-ups, HEC-RAS 2D is faster than SRH-2D even when using the full momentum equation set. SRH-2D took from about 32% to about 149% longer than RAS-2D (using full momentum) for the models with 10 foot and 8 foot spacing, respectively.

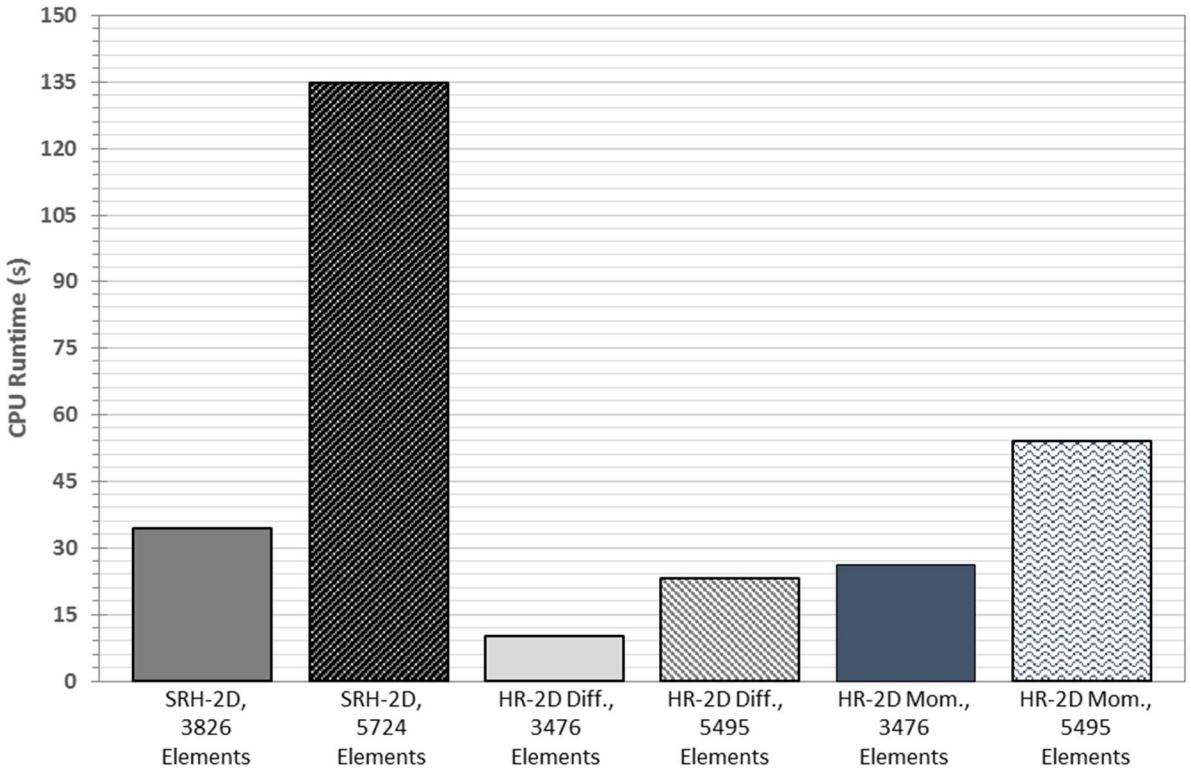

Figure 3-6. Comparison of the Six Trials Performed for the Computational Test

From Figure 3-6 it is obvious that HEC-RAS 2D with the diffusion wave equation set is by far the fastest, with the longest CPU runtime for those trials shorter than either HEC-RAS simulation using the full momentum equation set or either SRH-2D trial. However, some physics are sacrificed for that added computational benefit, the effects of which are investigated later in this chapter. It should be noted that there were no applications being run in the foreground of the operating system, and by watching the real time system details visible on the Performance tab of the Windows Task Manager that at no point during the simulations neither the CPU usage nor was the physical memory in use was ever significantly above 50%.

An attempt was made to quantify the speed of each model by devising a rate for results produced by the model. By considering that each model needed to determine results for every element for every timestep for the entire duration of the simulation, a total number of element-

results per simulation could be defined. By dividing this value by the CPU runtime recorded for each trial an element-results per unit time could be determined. The equations used to do this are as follows and the results are included in the subsequent figure.

$$\frac{Total\ Simul.Time * No.of\ Elements\ in\ Model}{Timestep} = Element\ Results\ per\ Simulation \qquad (EQN: 3.4)$$

$$\frac{Element\ Results\ per\ Simulation}{CPU\ Runtime} = Element\ Results\ per\ Second \qquad (EQN: 3.5)$$

Table 3-2. Estimation of Calculation Speed for each Model

Model	Timestep, Δt (s)	Total Simulation Time (hr)	No. of Elements -	CPU Runtime (s)	Element Results per Simulation	Element Results per Second
SRH-2D	1.0	0.50	3826	34.44	6886800	199937
	0.5	0.50	5724	134.64	20606400	153048
HR-2D Diff.	1.0	0.50	3476	10.00	6256800	625680
	0.5	0.50	5495	23.00	19782000	860087
HR-2D Mom.	1.0	0.50	3476	26.00	6256800	240646
	0.5	0.50	5495	54.00	19782000	366333

The calculation made to obtain the results above ignore the fact that each model produces different results for each mesh element (in the case of SRH-2D) or computational cell (in the case of HEC-RAS 2D), however there were enough similarities that this comparison should be useful. Interestingly, the comparisons in speed, in terms of element results per second, between SRH-2D and HEC-RAS 2D with the full momentum equations are very similar to those made above by simply comparing the CPU runtime between models – although, this should be a better comparison since it takes directly into account the discrepancies in the number of elements in each model. Strangely, for SRH-2D the denser mesh with the shorter timestep had fewer element results per second while for both HEC-RAS equation sets the reverse was true. Likely, in the case of SRH-2D this has to do with the Courant number (discussed below), which was larger for the less dense mesh with the longer timestep meaning that the code needed to perform more iterations for each

timestep to solve for the desired variables. It is not understood why the opposite would be true for the HEC-RAS simulations.

$$Courant\ Number, C = \frac{V\Delta t}{\Delta x} \qquad (EQN: 3.6)$$

The Courant Number (shown above) is a ratio between the distance water in the simulation could travel in a given timestep to the length of the element it is travelling through. Thus it is a dimensionless quantity, where values lower than 1 mean that the water entering an element will have at least 1 computational timestep coincide with its residence in that cell, while Courant numbers greater than 1 indicate that the water would bypass an element entirely before another computational timestep occurs. Generally speaking, to increase model stability, the Courant number should be decreased. In chapter 4 of the HEC-RAS 5.0 User's Manual (2016) there are recommendations for the Courant number provided – it states that when using the full momentum equations the value should be less than or equal to 1.0 (yet with a maximum of 3.0), but when using the diffusion wave equations a larger timestep is permissible, with the recommended value being less than or equal to 2.0 (with a maximum of 5.0). In order to approximate a representative Courant number for these models the average velocity for uniform flow of 6.252 fps was used in EQN 3.6 in place of V, Δt was equal to the computational timestep for each model, and the value used for Δx was the spacing criteria used when generating each mesh. These values are reflected in Table 3-1, and upon closer examination of the results of each model using SMS 12.1 and the RAS-Mapper, the approximate Courant number calculated was quite accurate.

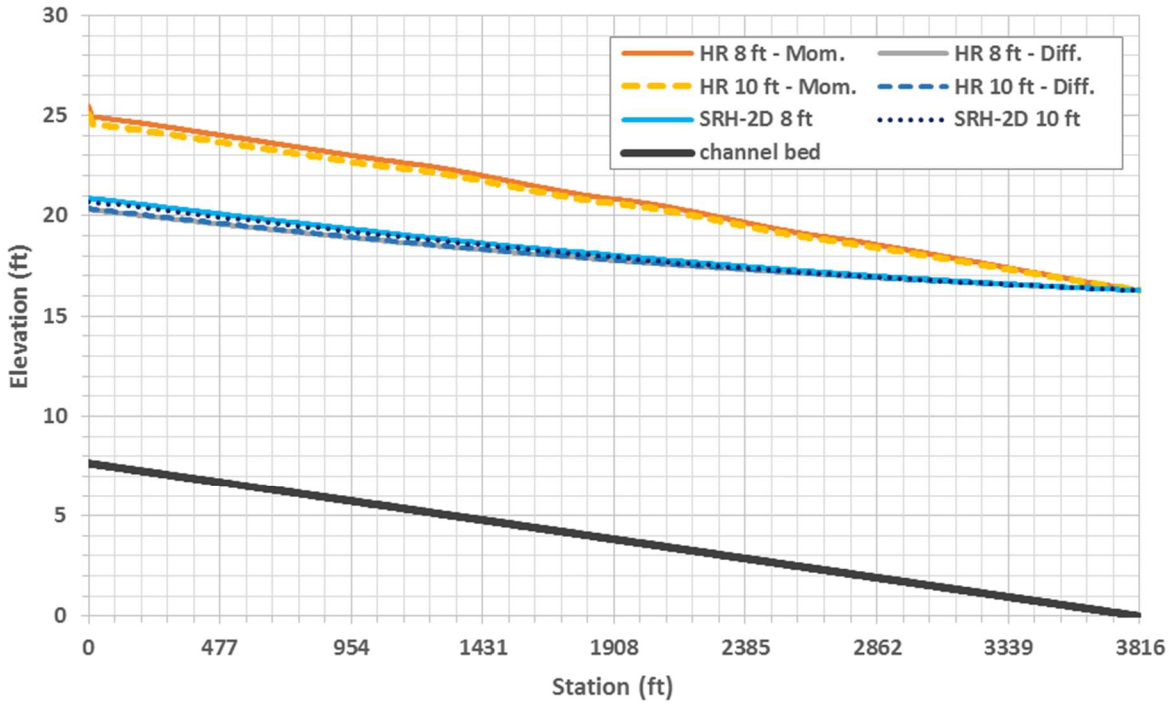

Figure 3-7. Steady State Profiles from along the Channel Centerline for the Computational Tests

Figure 3-7 shows models results for SRH-2D and HEC-RAS 2D using both the diffusion and full momentum equations for two different mesh densities, and while the differences between the models are small amongst themselves, there are obvious differences between the separate models. Surprisingly, the HEC-RAS models using the diffusion wave equations are more similar to the SRH-2D results than those from HEC-RAS with the full momentum equations. Both the SRH-2D and the diffusion wave profiles resemble a standard M1 gradually varied flow profile in which depth increases in the downstream direction -- behavior which seems entirely reasonable for this reach. However, the HEC-RAS 2D models with the full momentum equation enter the model space above the uniform depth of 16.27 feet, at 17.82 feet and 17.42 feet for the 8 foot and 10 foot spacing models, respectively. This is despite using an EGL equal to the ground slope of 0.002 in order to determine conveyance at the upstream boundary condition. Also curiously, for both HEC-RAS full momentum simulations the flow enters at the depths mentioned, decreases

rapidly over some relatively short distance, 18.7 feet and 14.7 feet for the 8 foot and 10 foot spacing models, respectively, and then hardly changes for the entire length of the channel, staying near 17 feet for the bulk of the distance yet decreasing very gradually until the depth reaches the downstream boundary condition of 16.27 feet.

3.3. Basic Flow around a Bend

In natural streams, it is extremely common to see bends where the bank on the outside of the turn is steeper than that on the inside. This is because of the stresses incurred on the outside bank by the flow as it is forced to change direction which in turn causes erosion of that bank. The water surface elevation of the flow on the outside of the bend tends to be higher, and due to larger hydrostatic forces near the channel bed caused by this deeper flow, a secondary, circular pattern of flow is induced through the cross-section which deposits the eroded soil on the inside bank. This phenomenon is discussed in Henderson's Open Channel Flow section on "Changes of Direction", and while these secondary flow patterns through bends result in highly three-dimensional situations, the fact that flow is expected to be deeper on the outside of a channel bend can investigated using the software discussed in this report. Only the HEC-RAS 2D full momentum and the SRH-2D models with 8-foot spacing were used in this analysis. All data shown is from the steady-state portion of each simulation.

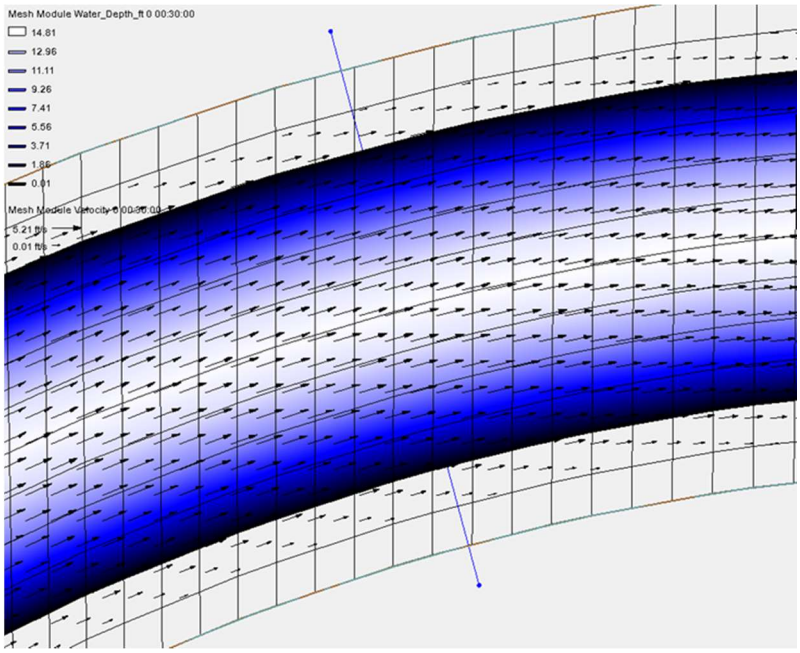

Figure 3-8. View from SMS 12.1 of Cross- Section used for Basic Flow around a Bend Analysis

At a cross-section 1253.81 feet upstream from the downstream boundary (32.9% of the entire channel length) data were taken from the SRH-2D and RAS-2D models. SMS could only provide values for each element, and thus has data at approximately 8 foot spacing, while RAS Mapper writes output to the terrain used, in this case the elevation raster, and since it had a grid spacing of 1 foot by 1 foot, the RAS-2D data are much denser. In Figures 3-9 and 3-10 stationing increases from inside the bend to out.

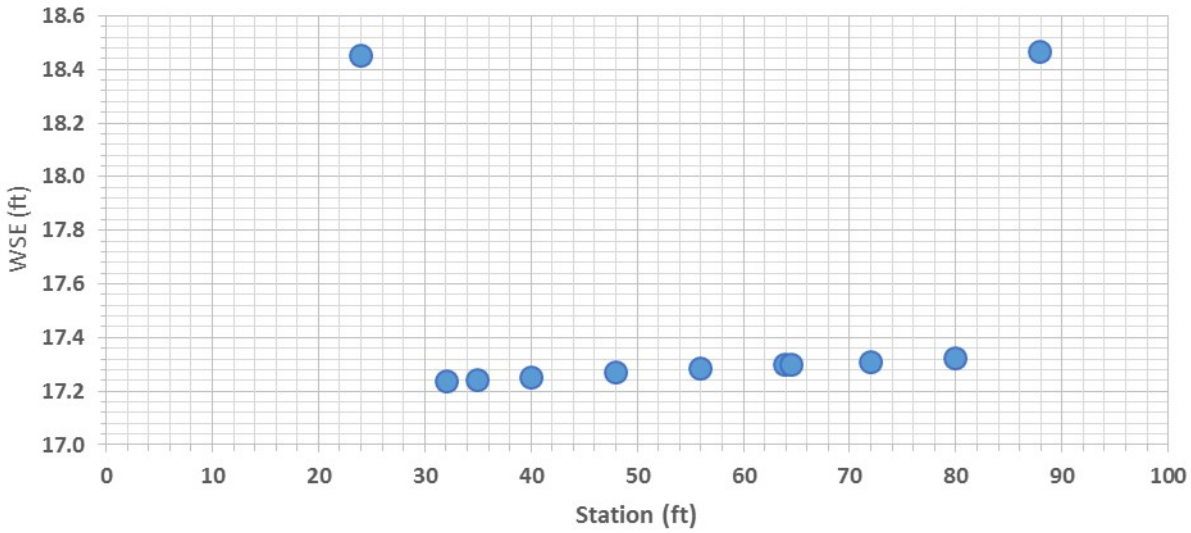

Figure 3-9. SRH-2D Data for Cross-Section Located 1253.81 feet upstream

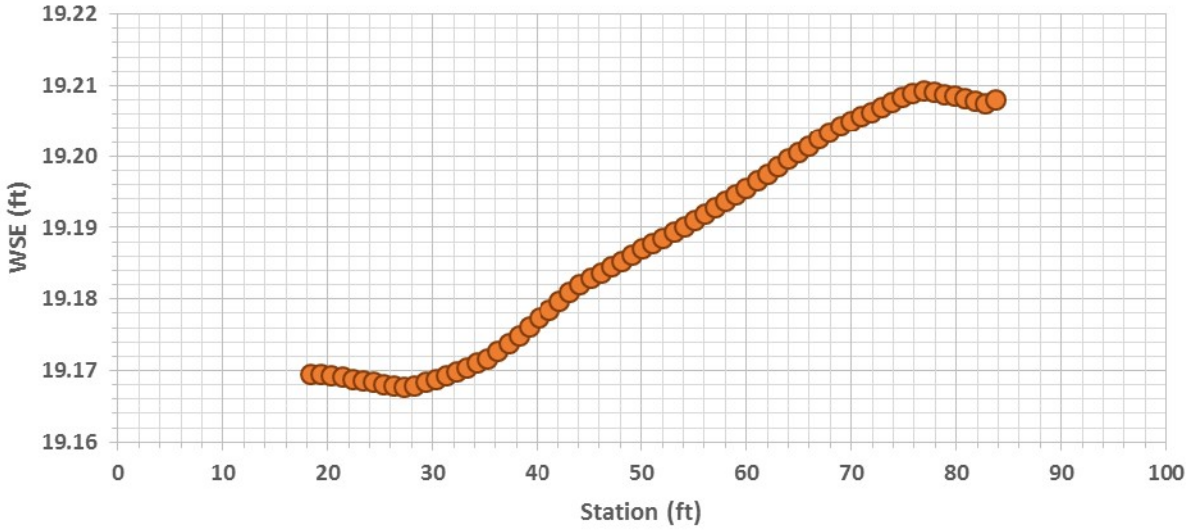

Figure 3-10. HEC-RAS 2D Data for Cross-Section Located 1253.81 feet upstream

From the two figures above it can be clearly seen that the water surface does indeed tend to be higher on the outside of the bend. Interestingly, this was not true from every cross-section along the channel – in fact, frequently the opposite was true and the water surface was higher on the inside of the bend. This is believed to be caused by series of reflections caused by the two major bends in this channel that are being elsewhere throughout the channel. It would appear that the cross-section at a station 1253.81 feet upstream is far enough away from these disturbances.

One more test was conducted using the data from this station, and that was to check the validity of what in Henderson's text is equation 7-17 and is as follows.

$$\frac{dv}{dn} + \frac{v}{r} = 0 \qquad (EQN: 3.7)$$

In the above v is the depth averaged velocity at a point, n is the distance measured outwards across the width of the cross-section, and r is the radius of curvature drawn in the horizontal plane of the streamlines at any vertical section. From the velocity vectors in Figure 3-8 it is apparent that all flow travels normal to the cross-section, and thus the radius of curvature for the streamlines should be determined based on their position relative to the stream centerline, where a radius of curvature of 500 feet exists. For the purposes of this analysis, the derivatives in Equation 3.7 were approximated using finite differences, and thus became the following.

$$\frac{\Delta v}{\Delta n} + \frac{v}{r} = 0 \qquad (EQ \quad : 3.8)$$

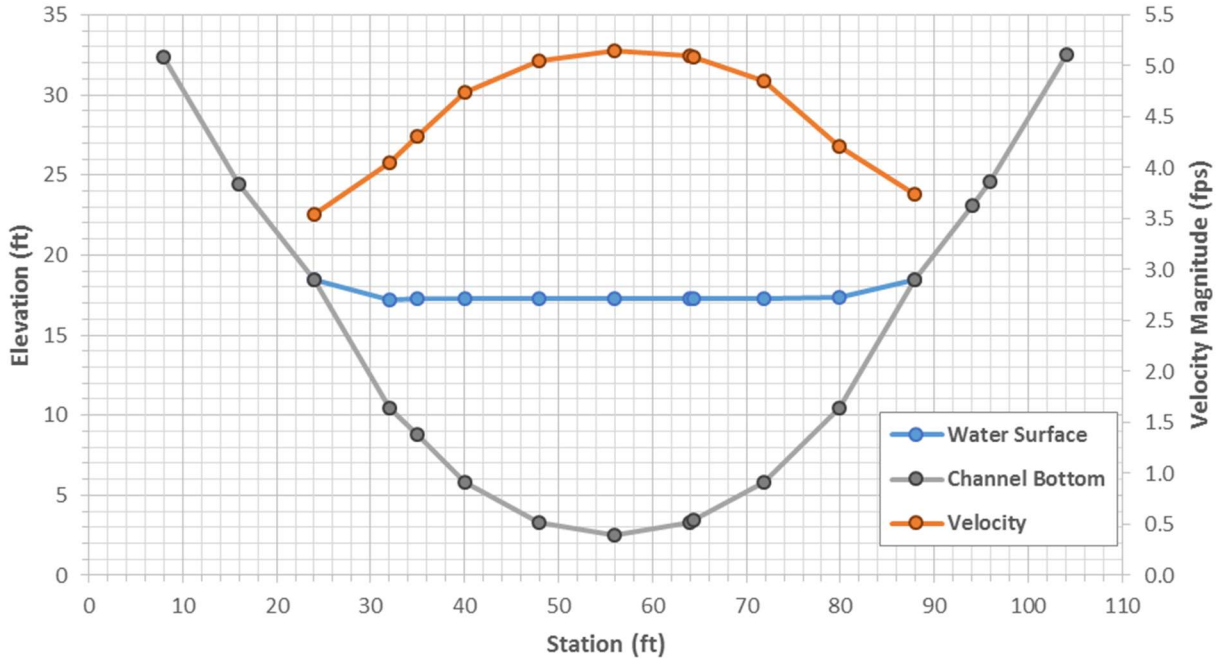

Figure 3-11. Detailed SRH-2D Data for Cross-Section Located 1253.81 feet upstream

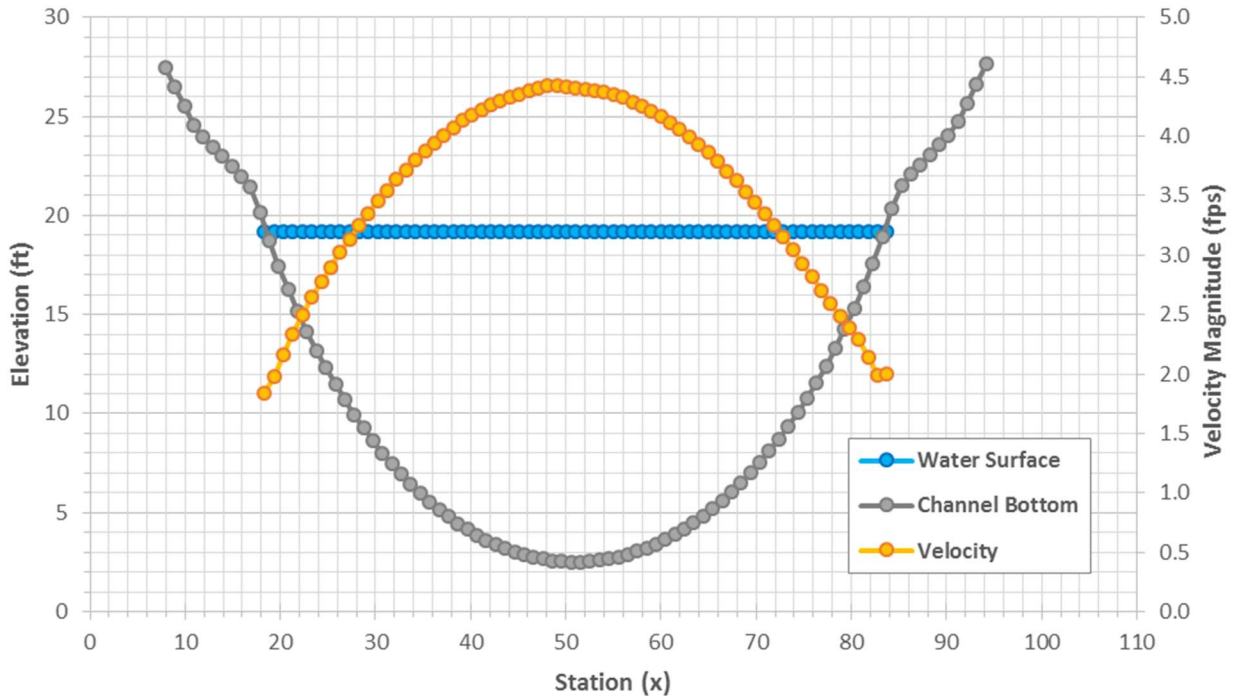

Figure 3-12. Detailed HEC-RAS 2D Data for Cross-Section Located 1253.81 feet upstream

Table 3-3. Solution of Equation 3-8 (Henderson's 7-17) with Data from SRH-2D Model

Sta. (ft)	Elev. (ft)	Vel.Mag. (fps)	WSE (ft)	H (ft)	Δv (fps)	Δn (ft)	(7-17)* -
8.000	32.360	-	-	-	-	-	-
15.993	24.428	-	-	-	-	-	-
23.992	18.450	3.545	18.453	18.648	-	-	-
31.998	10.471	4.053	17.239	17.494	0.508	8.005	0.072
34.912	8.778	4.308	17.244	17.533	0.256	2.914	0.096
39.976	5.834	4.745	17.255	17.605	0.437	5.064	0.096
47.945	3.315	5.046	17.270	17.666	0.301	7.969	0.048
55.924	2.512	5.151	17.285	17.697	0.105	7.979	0.023
63.913	3.319	5.100	17.299	17.703	-0.052	7.989	0.004
64.410	3.476	5.084	17.300	17.701	-0.015	0.498	-0.020
71.881	5.831	4.855	17.311	17.677	-0.230	7.471	-0.021
79.873	10.466	4.210	17.324	17.599	-0.645	7.992	-0.072
87.891	18.465	3.738	18.468	18.685	-0.472	8.018	-0.052
94.005	23.098	-	-	-	-	-	-
95.934	24.565	-	-	-	-	-	-
104.004	32.514	-	-	-	-	-	-

**Derivatives approximated by finite differences*

Table 3-4. Solution of Equation 3-8 (Henderson's 7-17) with Data from HEC-RAS 2D Model

Station* (ft)	WSE (ft)	Vel. Mag. (fps)	H (ft)	Δv (fps)	Δn (ft)	(7-17)** -
18.337	19.170	1.841	19.222	-	-	-
19.329	19.170	1.979	19.230	0.1376	0.991	0.143
20.320	19.169	2.159	19.242	0.1807	0.991	0.187
36.179	19.173	3.944	19.414	0.0684	0.991	0.077
44.108	19.182	4.327	19.473	0.0307	0.991	0.040
45.099	19.183	4.356	19.478	0.0286	0.991	0.038
46.091	19.184	4.383	19.482	0.0273	0.991	0.036
47.082	19.185	4.409	19.486	0.0259	0.991	0.035
49.064	19.186	4.422	19.490	-0.0015	0.991	0.007
50.055	19.187	4.414	19.490	-0.0074	0.991	0.001
51.046	19.188	4.407	19.489	-0.0072	0.991	0.002
52.038	19.189	4.399	19.489	-0.0085	0.991	0.000
53.029	19.189	4.386	19.488	-0.0128	0.991	-0.004
54.020	19.190	4.370	19.487	-0.0159	0.991	-0.007
82.764	19.208	1.989	19.269	-0.1511	0.991	-0.149
83.756	19.208	2.000	19.270	0.0112	0.991	0.015

**Many interior rows hidden*

***Derivatives approximated by finite differences*

Tables 3-3 and 3-4 show that the Henderson equation, while not perfectly represented here (possibly due to the introduction of finite differences), is not entirely inaccurate for this cross section. The range of values is greatest for those determined from the data derived from the HEC-RAS 2D model, ranging from 0.143 to 0.000, and yet both sets of data yielded solutions to Equation 3-8 that were qualitatively near zero. Also, it can be seen that the assumption in Henderson's Equation 7-14, that all stream filaments across the width will have the same total energy, is very nearly satisfied here – except at the far lateral extents of the flow in the SRH-2D data.

Chapter 4

Turbulence and Roughness Sensitivity Tests

4.1. Overview of the Turbulence and Roughness Sensitivity Tests

A river model must often be calibrated against historical data such as high water marks for historical floods before it can be used to predict behavior of the reach, say after construction of a new bridge over the river. There are many inputs required by a proper model, and the collection of this data is often a large part of the modelling task, but not all of these inputs are appropriate candidates for calibration. Two important considerations for any hydraulic model is how energy losses due to friction and turbulence are included, both of which can have a large effect on the flow behavior, and both of which are good candidates for model calibration.

Friction losses are accounted for through the use of Manning's equation for one-dimensional river models, and one important parameter in this equation is the familiar roughness coefficient, "n", known as "Manning's roughness coefficient". This parameter (with units of $\text{seconds} \cdot \text{meters}^{-1/3}$) depends upon the type of land cover the water is flowing over – whether it be concrete, dense brush, tall grass, short grass, rocky channels, bare earth, etc. Much research has been performed to empirically determine Manning's n values for many possible scenarios (Chow, 1959), and hydraulic engineers have used them for many years and are familiar with how changes in this parameter will affect their models. Due to their familiarity – and all of the time invested in laboratory work, calibration studies, and compiling tables of these coefficients – classic Manning's n values have been adapted for use in two-dimensional models such as HEC-RAS 2D and SRH-2D. Losses due to turbulence must be accounted for when using the full momentum equations employed by HEC-RAS 2D and SRH-2D. HEC-RAS 2D accomplishes this by use of an eddy viscosity model (Kundu and Cohen – Fluid Mechanics, 4th Ed.) that can be adjusted by changing

the value of the eddy viscosity coefficient. SRH-2D uses a parabolic-turbulence model (or a κ-ε model – which was not investigated in this report) to account for these losses with a constant coefficient that can be adjusted in the model control menu of SMS 12.1 (see SRH-2D User's Manual v.2, 2008). The one-dimensional HEC-RAS model attempts to account for these sorts of losses in part by use of the expansion and contraction coefficients discussed in Chapter 1 of this report.

Hydraulic engineers are far less familiar with how variations in these new parameters will affect their two-dimensional models, and for this reason, a simple sensitivity test was conducted for a reach using both HEC-RAS 2D and SRH-2D. As of version 5.0.1, in HEC-RAS 2D the eddy viscosity term apparently cannot be adjusted for use with the full momentum equation and as such was not included in this study. However, the parabolic turbulence model of SRH-2D can have its coefficient adjusted, and both models accept changes to the Manning's roughness coefficients.

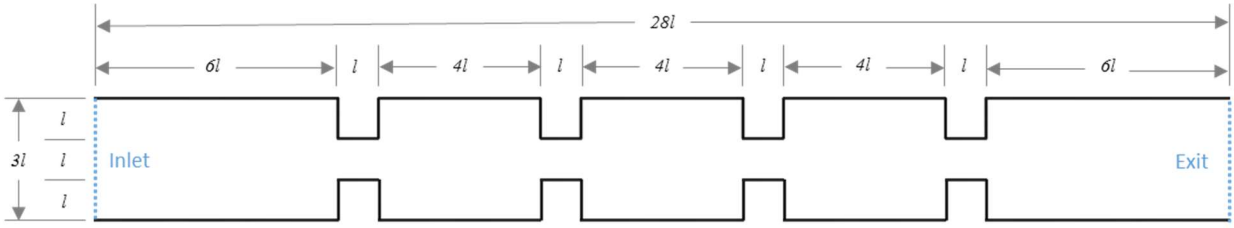

Figure 4-1. Plan View of the Geometric Basis for Tests where l = 6 feet

Figure 4-1 describes the layout used for these sensitivity tests. The channel has a horizontal bed, a flat bottom, and infinitely high walls oriented perpendicular to the flat bottom. Each constriction reduces the channel width by two-thirds, to 6 feet from 18 feet, before opening again to the full width. These four constrictions are intended to cause a large amount of local losses due to turbulent dissipation of energy. For comparison, the same channel was used for both the turbulence constant test and the roughness coefficient test. Some model preparation was performed in ArcMap for use in both SMS 12.1 and HEC-RAS 5.0. For SMS 12.1, and consequently SRH-

2D, only the shapefile defining the outside limits where the flow could traverse needed to be defined – thus, what would become the inlet and exit, and the walls of the channel. For use in HEC-RAS 2D, a raster defining the elevations for the model had to be created, and to simulate the sheer walls of the channel, a rapidly sloping wall was used – from the channel bottom at an elevation of zero feet, to a height of 70 feet over a horizontal distance of 0.5 feet. One-foot square mesh elements were used for both models, a computational timestep of 0.1 seconds for all tests, and the simulation time for every run was 12 minutes. The discharge every test ramped linearly up to 2000 cfs from 20 cfs over of 6 minutes, and stayed at 2000 cfs for the 6 remaining minutes of each test. The downstream boundary condition used was a constant depth of 12 feet. All profiles shown are representative of the channel's centerline and the final timestep at 12 minutes. The method used for distributing the flow at the inlet for SRH-2D was by selecting the "conveyance" option for the inlet boundary. Similarly for HEC-RAS 2D the flow was distributed according to conveyance at the inlet, however a slope for the energy grade line had to be specified, and this value was chosen, somewhat arbitrarily, to be equal to 0.0006 for all trials. For every SRH-2D turbulence test the Manning's roughness coefficient was set to 0.01 to minimize the influence of friction on the results.

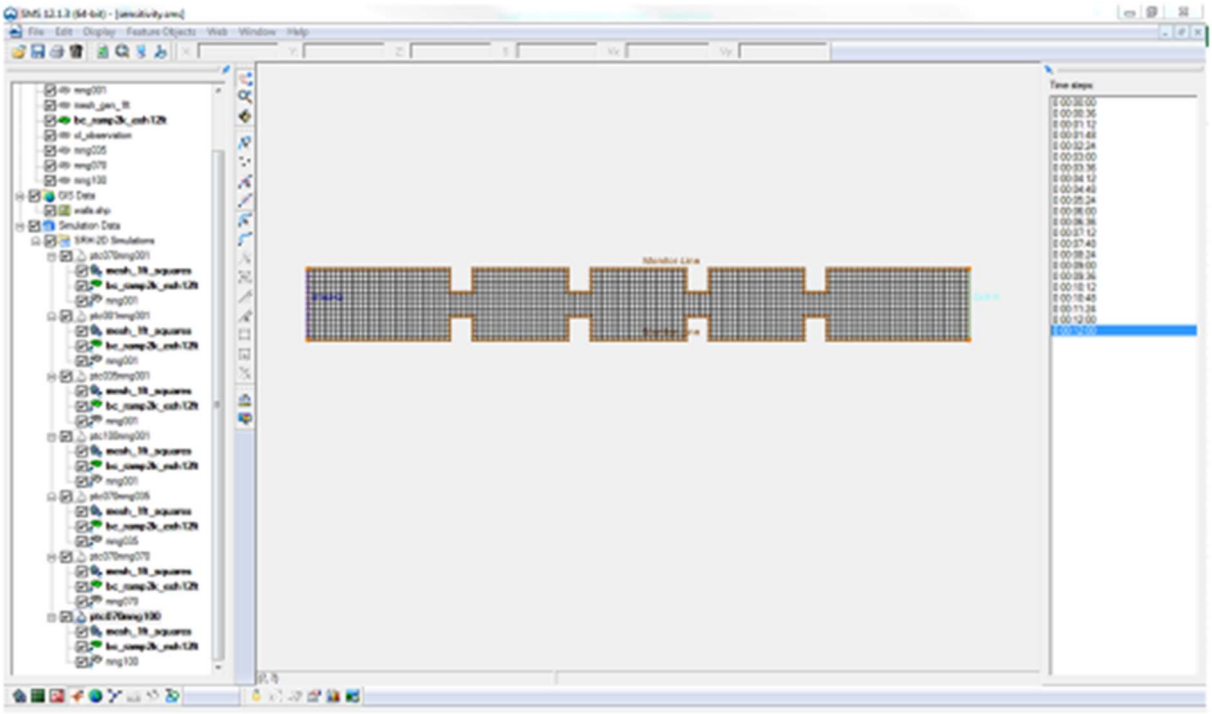

Figure 4-2. SMS 12.1 Project Overview and Grid Display for SRH-2D Sensitivity Tests

Figure 4-3. Representative Plan View from HEC-RAS 2D Showing Typical Flow Patterns from the Simulations.

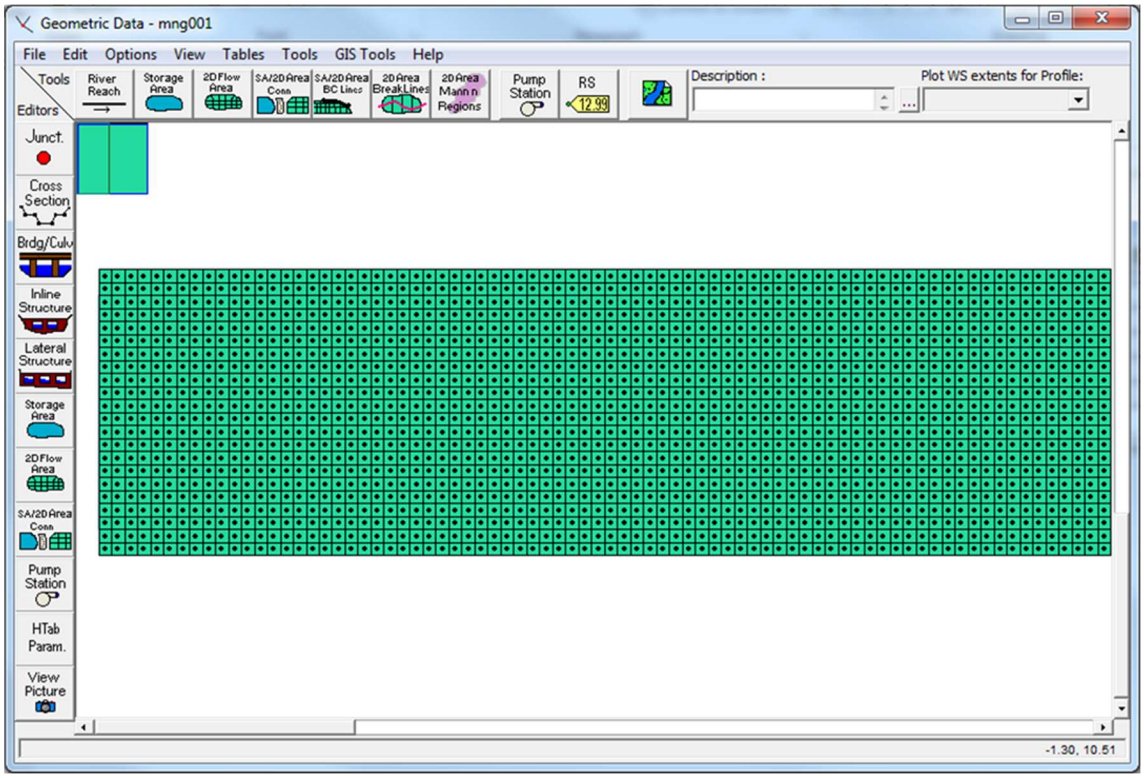

Figure 4-4. HEC-RAS 2D Flow Area Elements for Sensitivity Tests

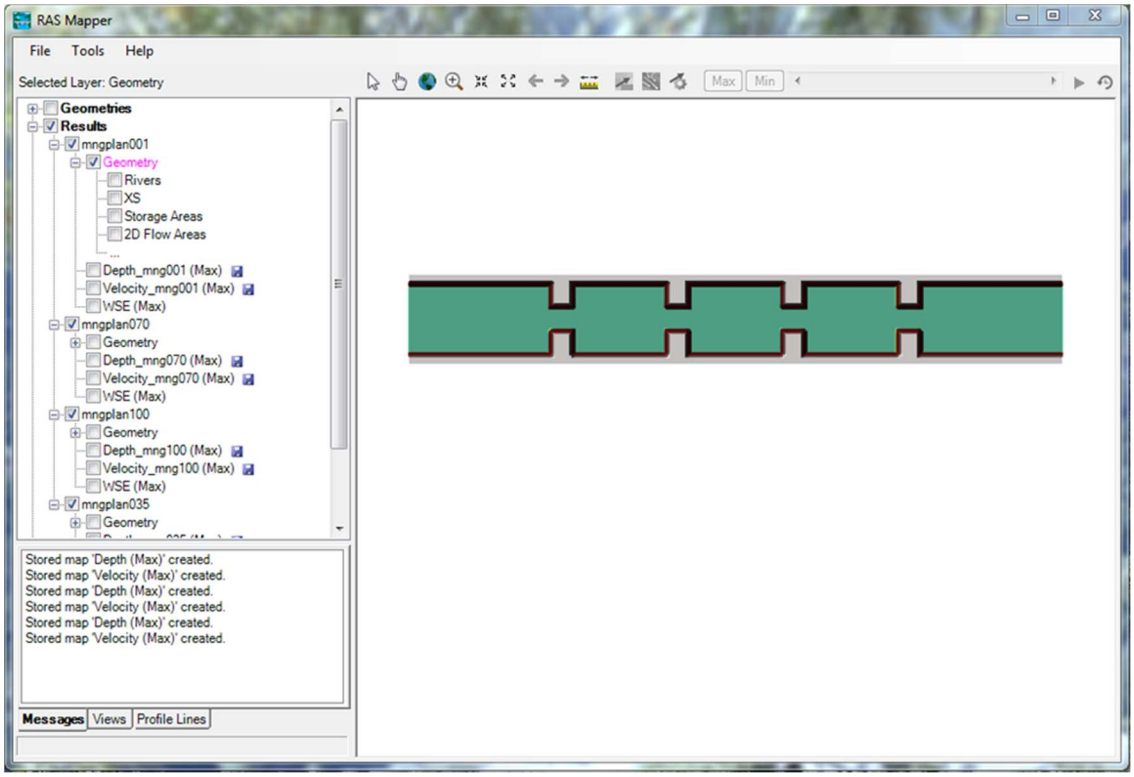

Figure 4-5. Triangulated Irregular Network for Model Elevations for HEC-RAS 2D Sensitivity Tests as Seen in RAS Mapper

4.2. Results of Sensitivity Tests.

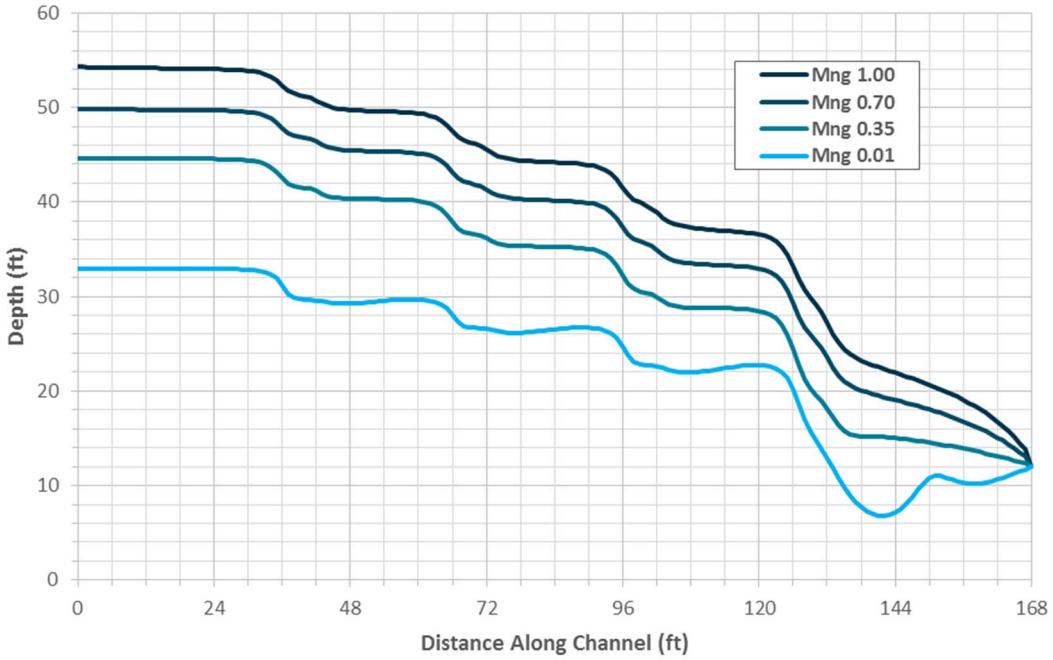

Figure 4-6. SRH-2D Roughness Coefficient Tests with Parabolic Turbulence Equal to 0.7 for all Trials

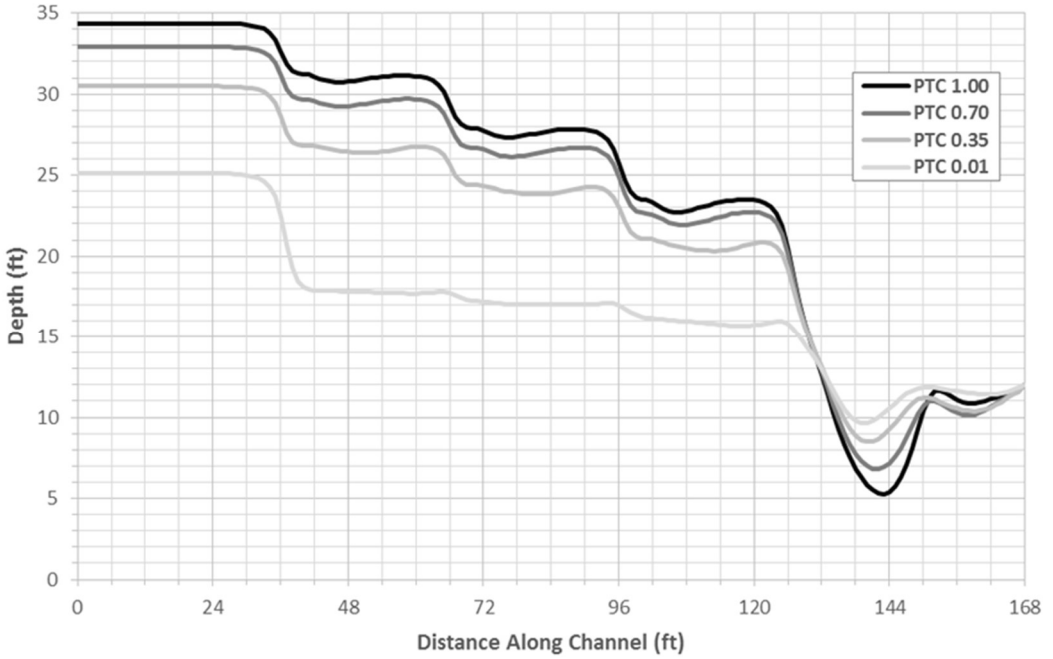

Figure 4-7. SRH-2D Parabolic Turbulence Constant Tests with Manning's Roughness Coefficient Equal to 0.01 for all Tests

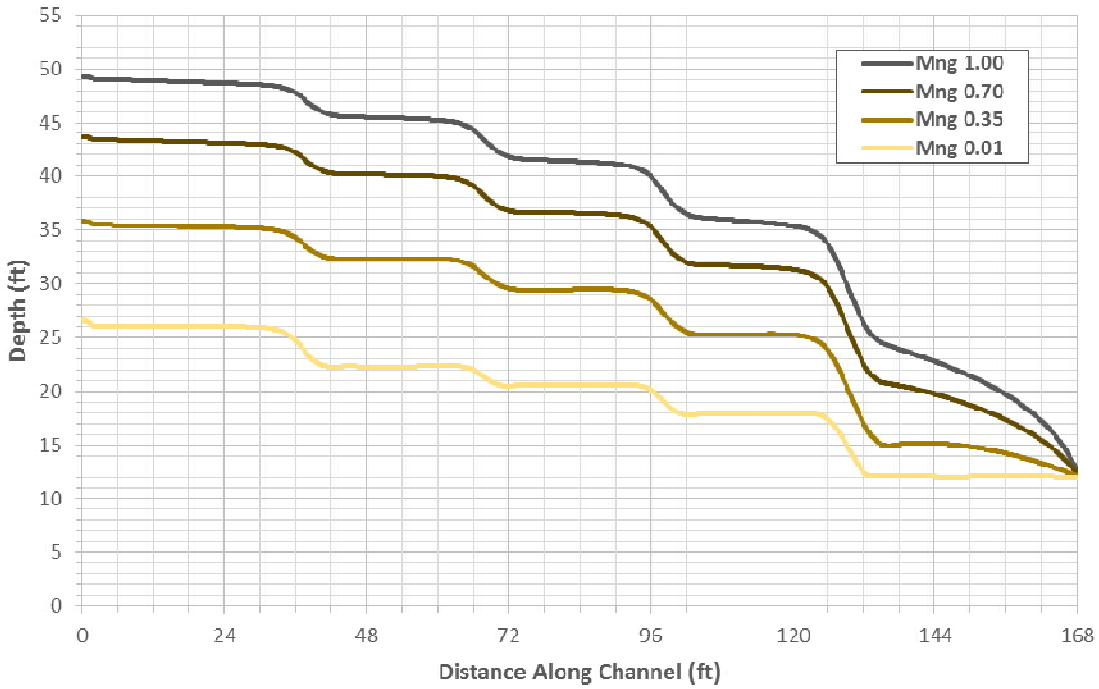

Figure 4-8. HEC-RAS 2D Roughness Coefficient Tests.

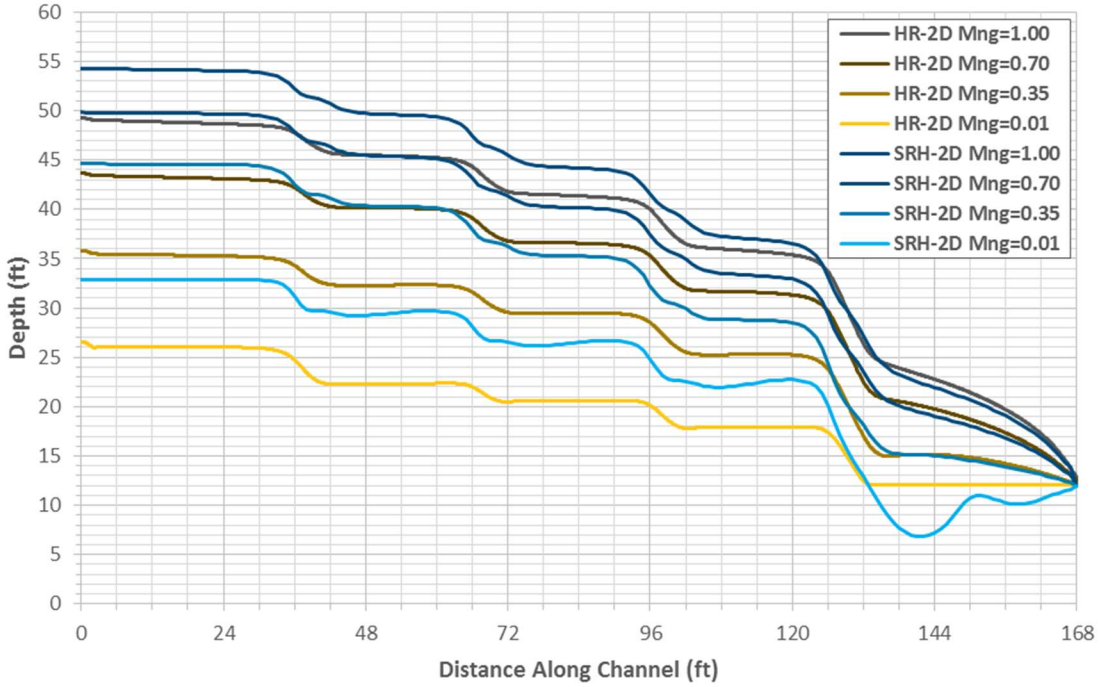

Figure 4-9. Comparison between Roughness Coefficient Test Results for SRH-2D and HEC-RAS 2D

Table 4-1. Change in Depth from Upstream to Downstream Normalized by the Channel Length

Test Parameter Value	0.01	0.35	0.70	1.00
			-Δy/L	
SRH-2D PTC*	0.08	0.11	0.12	0.13
SRH-2D Manning's n*	0.12	0.19	0.23	0.25
HEC-RAS 2D Manning's n	0.09	0.14	0.19	0.22

**Manning's Roughness Coefficient, n=0.01 for all SRH-2D PTC Tests.*

***PTC=0.70 (default) for all SRH-2D Manning's n Tests.*

For the SRH-2D Turbulence Test with PTC = 0.01,

$$\frac{-(change\ in\ depth\ from\ x = 0\ ft\ to\ x = 168ft)}{length\ of\ channel} = \frac{-\Delta y}{L} = \frac{-(12.00ft - 25.13ft)}{168ft} = \boxed{0.08}$$

From the data it can be seen that between the SRH-2D parabolic turbulence tests the increase in upstream depth from minimum to maximum trials was 36.7%, while there was an increase of 64.9% from the SRH-2D roughness trials. The increase in upstream depth between the minimum and maximum trials for the HEC-RAS 2D roughness trials was 85.3%. Although, for the HEC-RAS tests the upstream depths were all lower than for the SRH-2D trials with the same roughness coefficients. This could be explained by the constant friction slope used for the HEC-RAS models to determine conveyance at the inlet; however, the pattern that as roughness increases, there are more losses, and so the water must gain hydraulic head by gaining depth upstream to pass the same discharge, and so the results exhibit physically realistic behavior. It is likely that the friction slope used as an input to the HEC-RAS models could itself be a source of calibration. It would seem that the effect of the parabolic turbulence constant is not especially large, and unless the modeler has a special reason to do so, this parameter should not be considered when trying to calibrate a model (it should be noted that the actual value of the parabolic turbulence constant for the PTC = 1.00 test is PTC = 0.999999, the maximum value allowed by SRH-2D). Small changes in the roughness coefficient have a large impact on the depth of flow, and these coefficients can vary over an even wider range than the turbulence constant values, and as such should be a primary

concern when calibrating a model. Also, the roughness coefficients are often, initially, just educated guesses based upon aerial photographs of the site in question, and it can be difficult to say whether the crop field seen in the image should have a roughness coefficient of 0.025 or 0.030 after consulting the descriptions within a Manning's roughness coefficient table. It is not surprising that the coefficients used within a model may require some fine-tuning.

Chapter 5

Mixed Flow Regime Test

5.1. Overview of the Mixed Flow Regime Test

This chapter evaluates the mixed flow regime capability of SRH-2D by addressing a two-lake problem where water flows between two lakes through a channel with two slope breaks. The objective was to conduct a simple test to assess how well the two-dimensional models simulate well-established one-dimensional principles. This was done by analyzing the problem within an Excel spreadsheet by applying the standard Depth Step Method then by using both one and two-dimensional HEC-RAS 5.0, and SRH-2D. The water surface profiles extracted from the channel centerline served as a major basis of comparison between these methods.

The channel connecting these two water bodies is a straight reach that possesses a prismatic, trapezoidal cross section. The base width is 20 feet and the side slopes are 1:1 (H:V). Within the channel there are two breaks-in-grade. The first break was a transition from a grade of 0.2% to 2%, and the next returned to 0.2%. The first and third sections are hydraulically mild and the middle section is steep. The Manning's roughness coefficient, n, is a uniform 0.025 everywhere. The discharge is 1000 cfs. This channel is represented in the following figures (channel elevations provided are representative of the channel's centerline). A hydraulic jump was expected to occur somewhere in the channel.

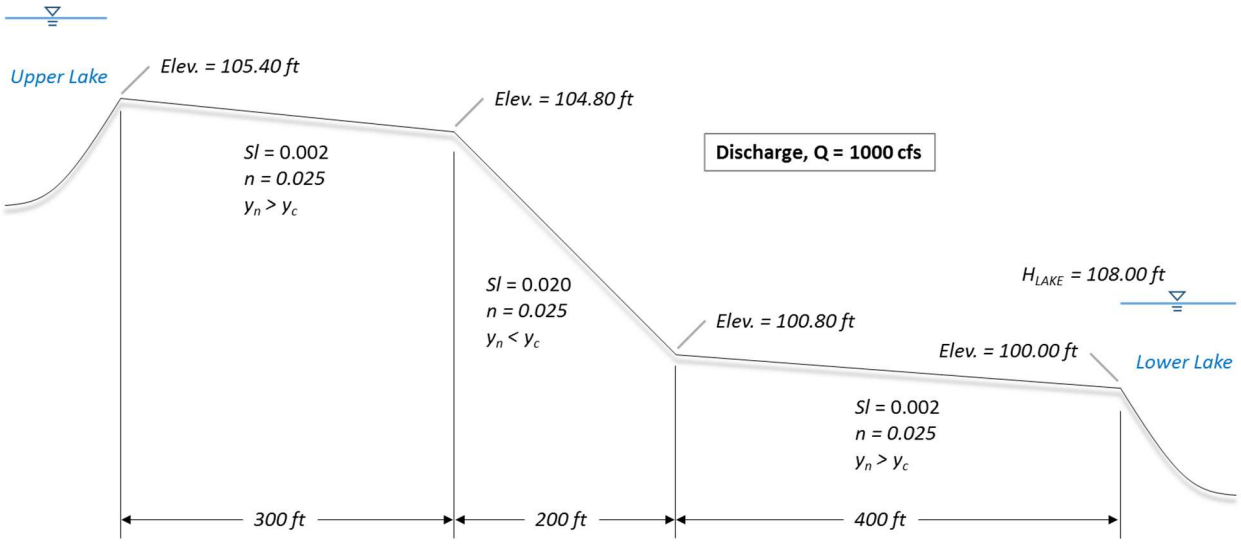

Figure 5-1. Elevation View of Reach with Exaggerated Z-Scale

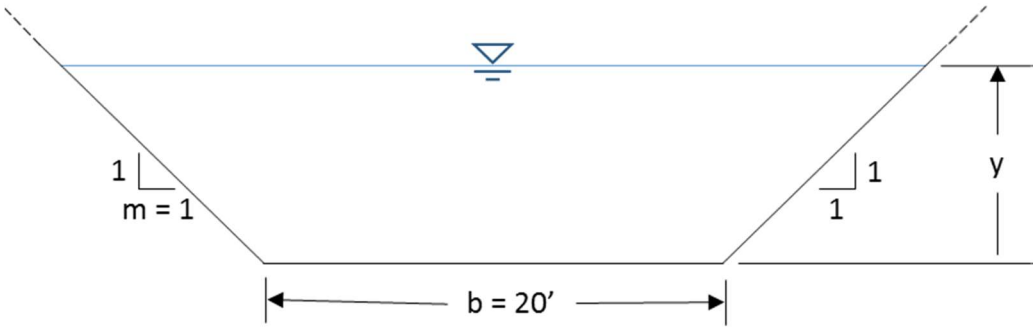

Figure 5-2. Representative Cross Section for Channel

5.2. Direct Step Method and Solution Procedure for Test Reach

The Depth Step Method is an explicit scheme for computing gradually varied flow profiles. A starting depth must be known at a location in the reach. Generally, this is a control section such as a free overfall with the resultant critical depth, a lake with a known water surface elevation, uniform depth upstream or downstream, or some other such control section. A change in depth is then specified and a new horizontal position within the reach is directly calculated and the process is repeated. This change in depth can be either positive or negative depending upon the situation. Supercritical profiles are calculated from upstream to downstream while the opposite is true for

subcritical profiles. Friction losses between horizontal stations are calculated using Manning's equation (all equations used in this spreadsheet are presented in Section 5.4).

The Excel add-in Solver was used extensively to quickly arrive at solutions satisfying user-specified criteria. When using Solver the user must specify an objective cell. This cell must contain a formula. The user must also specify what cell or cells contain the variable that should be changed in order to satisfy the requirements placed on the objective cell. Variable cells must contain an initial value – they cannot be empty cells. A good initial guess on the user's part at these variables will aid Solver in converging on a solution. Solver is not guaranteed to find an answer – even if one exists. This can be a problem if the initial guess is a poor one. Often further constraints are required in order for Solver to find a solution. This was the case when applying to Depth Step Method to this problem. Tables 5-1 and 5-2 as well as Figures 5-3 through 5-6 detail the use of this tool.

Table 5-1. Depth Step Method Spreadsheet with Incorrect Solution

Bottom Width, b (ft)	20
Side Slope, m (H:V)	1
Bottom Slope, S_o (ft/ft)	0.002
Manning's n	0.025
Discharge, Q (cfs)	1000
Initial Station for Profile (ft)	500
Final Station for Profile (ft)	900
Initial Bottom Elevation for Profile (ft)	100.80
Final Bottom Elevation for Profile (ft)	100.00
Initial Depth for Profile (ft)	8.00
Depth Step, Δy (ft)	0.100000

Changing
Constraint
Objective

Step n	y (ft)	A (sq.ft)	V (fps)	E (ft)	P_w (ft)	R (ft)	Fr	Avg. V (fps)	Avg. R (ft)	Avg. Sf (ft/ft)	Avg. Fr	Δx (ft)	x (ft)	z (ft)	y+z (ft)	M (cu.ft)
0	8.00	224.00	4.464	8.309	42.627	5.255	0.315	-	-	-	-	-	900.000	100.00	108.00	949.309
1	8.10	227.61	4.393	8.400	42.910	5.304	0.309	4.429	5.280	0.000601	0.312	64.502	964.502	99.87	107.97	969.690
2	8.20	231.24	4.325	8.490	43.193	5.354	0.302	4.359	5.329	0.000575	0.306	63.608	1028.111	99.74	107.94	990.491
3	8.30	234.89	4.257	8.581	43.476	5.403	0.296	4.291	5.378	0.000550	0.299	62.793	1090.903	99.62	107.92	1011.710
4	8.40	238.56	4.192	8.673	43.759	5.452	0.290	4.225	5.427	0.000527	0.293	62.046	1152.949	99.49	107.89	1033.349
5	8.50	242.25	4.128	8.765	44.042	5.500	0.284	4.160	5.476	0.000505	0.287	61.360	1214.309	99.37	107.87	1055.406
6	8.60	245.96	4.066	8.857	44.324	5.549	0.279	4.097	5.525	0.000484	0.281	60.728	1275.037	99.25	107.85	1077.883
7	8.70	249.69	4.005	8.949	44.607	5.598	0.273	4.035	5.573	0.000464	0.276	60.146	1335.183	99.13	107.83	1100.779
8	8.80	253.44	3.946	9.042	44.890	5.646	0.268	3.975	5.622	0.000445	0.270	59.607	1394.790	99.01	107.81	1124.095
9	8.90	257.21	3.888	9.135	45.173	5.694	0.263	3.917	5.670	0.000427	0.265	59.107	1453.897	98.89	107.79	1147.831
10	9.00	261.00	3.831	9.228	45.456	5.742	0.258	3.860	5.718	0.000410	0.260	58.643	1512.539	98.77	107.77	1171.988
49	12.90	424.41	2.356	12.986	56.487	7.513	0.136	2.369	7.492	0.000108	0.137	51.851	3620.873	94.56	107.46	2452.837
50	13.00	429.00	2.331	13.084	56.770	7.557	0.135	2.344	7.535	0.000105	0.135	51.793	3672.666	94.45	107.45	2494.725

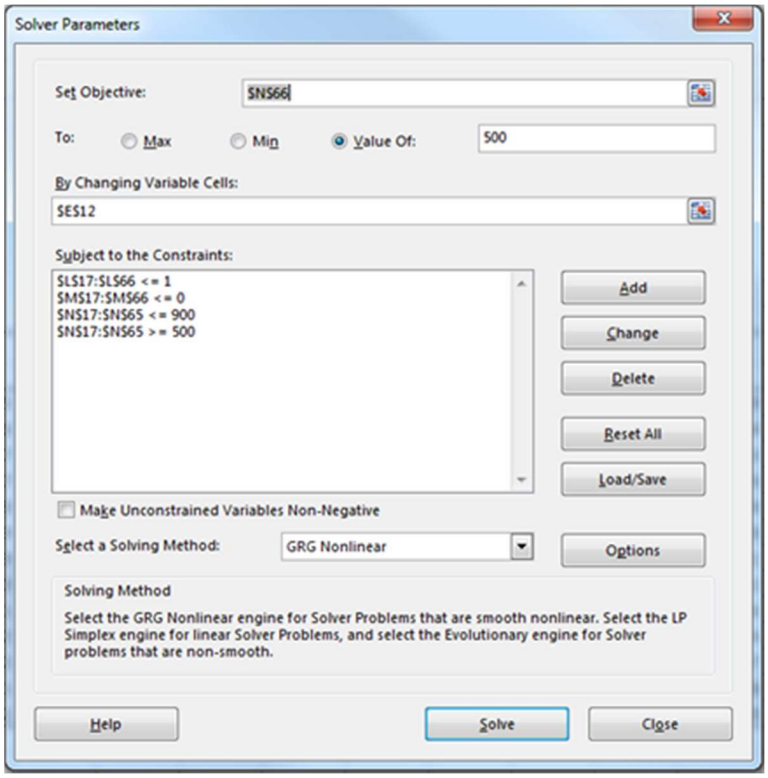

Figure 5-3. Main Solver Interface Window with Criteria for Solution

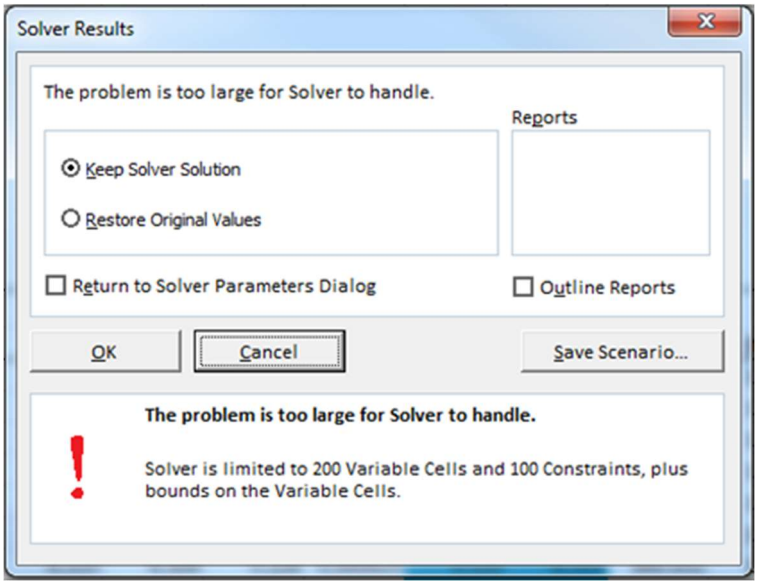

Figure 5-4. Error Message Due to Excess Number of Cells Included

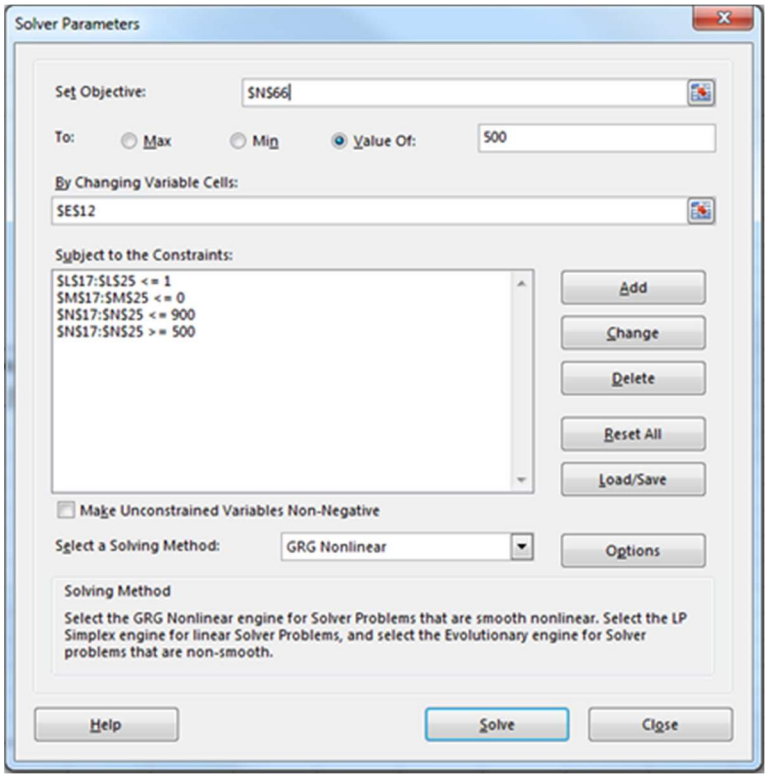

Figure 5-5. Revised Solver Constraints

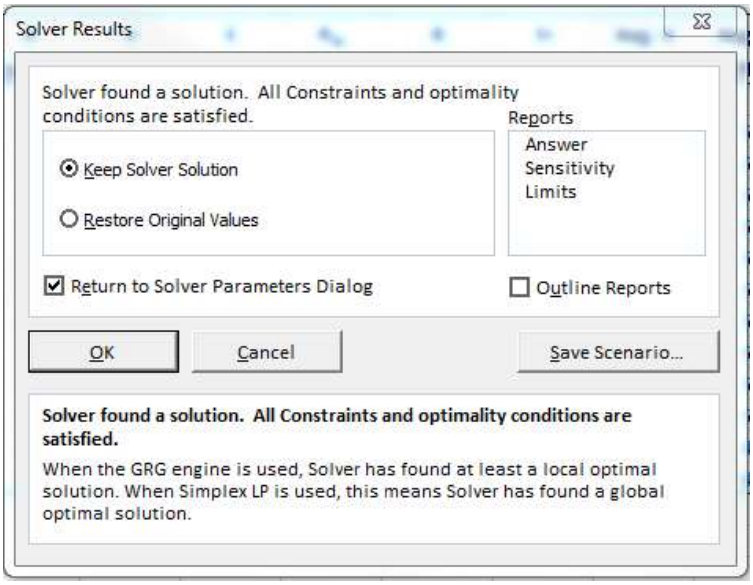

Figure 5-6. Successfully Applied Solver Tool

Table 5-2. Depth Step Method Spreadsheet with Correct Solution

Bottom Width, b (ft)	20
Side Slope, m (H:V)	1
Bottom Slope, S_o (ft/ft)	0.002
Manning's n	0.025
Discharge, Q (cfs)	1000
Initial Station for Profile (ft)	500
Final Station for Profile (ft)	900
Initial Bottom Elevation for Profile (ft)	100.80
Final Bottom Elevation for Profile (ft)	100.00
Initial Depth for Profile (ft)	8.00
Depth Step, Δy (ft)	-0.011676

Changing
Constraint
Objective

Step	y	A	V	E	P_w	R	Fr	Avg. V	Avg. R	Avg. Sf	Avg. Fr	Δx	x	z	y+z	M
n	(ft)	(sq.ft)	(fps)	(ft)	(ft)	(ft)		(fps)	(ft)	(ft/ft)		(ft)	(ft)	(ft)	(ft)	(cu.ft)
0	8.00	224.00	4.464	8.309	42.627	5.255	0.315	-	-	-	-	-	900.000	100.00	108.00	949.309
1	7.99	223.58	4.473	8.299	42.594	5.249	0.316	4.468	5.252	0.000616	0.316	-7.594	892.406	100.02	108.00	946.957
2	7.98	223.16	4.481	8.288	42.561	5.243	0.317	4.477	5.246	0.000619	0.317	-7.607	884.799	100.03	108.01	944.610
3	7.96	222.74	4.490	8.278	42.528	5.237	0.318	4.485	5.240	0.000622	0.317	-7.621	877.178	100.05	108.01	942.269
4	7.95	222.32	4.498	8.267	42.495	5.232	0.319	4.494	5.235	0.000625	0.318	-7.635	869.543	100.06	108.01	939.934
5	7.94	221.90	4.507	8.257	42.462	5.226	0.319	4.502	5.229	0.000629	0.319	-7.649	861.894	100.08	108.02	937.604
6	7.93	221.48	4.515	8.246	42.429	5.220	0.320	4.511	5.223	0.000632	0.320	-7.663	854.231	100.09	108.02	935.280
7	7.92	221.06	4.524	8.236	42.396	5.214	0.321	4.519	5.217	0.000635	0.321	-7.677	846.553	100.11	108.03	932.962
8	7.91	220.65	4.532	8.226	42.363	5.208	0.322	4.528	5.211	0.000639	0.321	-7.692	838.861	100.12	108.03	930.650
9	7.89	220.23	4.541	8.215	42.330	5.203	0.323	4.536	5.206	0.000642	0.322	-7.707	831.154	100.14	108.03	928.343
10	7.88	219.81	4.549	8.205	42.297	5.197	0.323	4.545	5.200	0.000646	0.323	-7.721	823.433	100.15	108.04	926.042
49	7.43	203.73	4.908	7.802	41.009	4.968	0.358	4.904	4.971	0.000798	0.357	-8.473	508.498	100.78	108.21	840.774
50	7.42	203.32	4.918	7.792	40.976	4.962	0.359	4.913	4.965	0.000802	0.358	-8.498	500.000	100.80	108.22	838.703

The solution procedure for this reach was to first determine the GVF (gradually-varied flow) profile backwards from the lower lake to the horizontal station where the channel transitions from steep to mild (Table 5.3). The next step was to simultaneously solve two GVF profiles in the steep section (Table 5.4). boundary condition was located at the upstream end of the third section and was the depth determined from the previous GVF profile. The main constraints for the solution here was that the horizontal stations and the specific forces between the super- and subcritical profiles were equal. Lastly, the GVF profile for the uppermost section of the reach was back calculated to the upper lake using critical depth as the downstream boundary condition (Table 5.5).

5.3. Direct Step Method Results

Table 5-3. Depth Step Method Results for M1 Profile from Station 500 to 900

Depth Step, Δy (ft)	-0.0117															
Step	y	A	V	E	P_W	R	Fr	Avg. V	Avg. R	Avg. Sf	Avg. Fr	Δx	x	z	y+z	M
n	(ft)	(sq.ft)	(fps)	(ft)	(ft)	(ft)		(fps)	(ft)	(ft/ft)		(ft)	(ft)	(ft)	(ft)	(cu.ft)
0	8.000	224.000	4.464	8.309	42.627	5.255	0.315	-	-	-	-	-	900.000	100.000	108.000	949.309
1	7.988	223.580	4.473	8.299	42.594	5.249	0.316	4.468	5.252	0.00062	0.316	-7.594	892.406	100.015	108.004	946.957
2	7.977	223.160	4.481	8.288	42.561	5.243	0.317	4.477	5.246	0.00062	0.317	-7.607	884.799	100.030	108.007	944.610
3	7.965	222.740	4.490	8.278	42.528	5.237	0.318	4.485	5.240	0.00062	0.317	-7.621	877.178	100.046	108.011	942.269
4	7.953	222.321	4.498	8.267	42.495	5.232	0.319	4.494	5.235	0.00063	0.318	-7.635	869.543	100.061	108.014	939.934
...	...	...	...	...	...	...	...	...	...	...	...	...	...	...	...	...
47	7.451	204.545	4.889	7.822	41.075	4.980	0.356	4.884	4.983	0.00079	0.355	-8.424	525.420	100.749	108.200	844.934
48	7.440	204.138	4.899	7.812	41.042	4.974	0.357	4.894	4.977	0.00079	0.356	-8.449	516.971	100.766	108.206	842.851
49	7.428	203.730	4.908	7.802	41.009	4.968	0.358	4.904	4.971	0.00080	0.357	-8.473	508.498	100.783	108.211	840.774
50	7.416	203.324	4.918	7.792	40.976	4.962	0.359	4.913	4.965	0.00080	0.358	-8.498	500.000	100.800	108.216	838.703

Table 5-4: Combined Depth Step Method Results for S2 and S1 Profiles from Station 300 to 500

Depth Step, Δy (ft)	-0.0193															
Step	y	A	V	E	P_W	R	Fr	Avg. V	Avg. R	Avg. Sf	Avg. Fr	Δx	x	z	y+z	M
n	(ft)	(sq.ft)	(fps)	(ft)	(ft)	(ft)		(fps)	(ft)	(ft/ft)		(ft)	(ft)	(ft)	(ft)	(cu.ft)
0	3.979	95.399	10.482	5.685	31.253	3.052	1.000	-	-	-	-	-	300.000	104.800	108.779	504.815
1	3.959	94.861	10.542	5.685	31.198	3.041	1.008	10.512	3.047	0.00704	1.004	0.012	300.012	104.800	108.759	504.829
2	3.940	94.323	10.602	5.685	31.144	3.029	1.016	10.572	3.035	0.00716	1.012	0.036	300.047	104.799	108.739	504.872
3	3.921	93.787	10.663	5.686	31.089	3.017	1.024	10.632	3.023	0.00728	1.020	0.060	300.108	104.798	108.719	504.944
4	3.901	93.251	10.724	5.687	31.035	3.005	1.032	10.693	3.011	0.00740	1.028	0.086	300.194	104.796	108.698	505.046
...	...	...	...	...	...	...	...	...	...	...	...	...	...	...	...	...
47	3.073	70.902	14.104	6.162	28.692	2.471	1.509	14.054	2.478	0.01659	1.502	7.086	376.369	103.273	106.346	542.113
48	3.054	70.399	14.205	6.187	28.637	2.458	1.524	14.154	2.465	0.01694	1.517	8.192	384.561	103.109	106.162	543.884
49	3.034	69.896	14.307	6.213	28.583	2.445	1.540	14.256	2.452	0.01730	1.532	9.631	394.191	102.916	105.951	545.704
50	3.015	69.395	14.410	6.240	28.528	2.432	1.555	14.359	2.439	0.01768	1.548	11.580	405.772	102.685	105.700	547.576

Depth Step, Δy (ft)	-0.0461															
Step	y	A	V	E	P_W	R	Fr	Avg. V	Avg. R	Avg. Sf	Avg. Fr	Δx	x	z	y+z	M
n	(ft)	(sq.ft)	(fps)	(ft)	(ft)	(ft)		(fps)	(ft)	(ft/ft)		(ft)	(ft)	(ft)	(ft)	(cu.ft)
0	7.416	203.324	4.918	7.792	40.976	4.962	0.359	-	-	-	-	-	500.000	100.800	108.216	838.703
1	7.370	201.719	4.957	7.752	40.846	4.939	0.363	4.938	4.950	0.00081	0.361	-2.092	497.908	100.842	108.212	830.574
2	7.324	200.118	4.997	7.712	40.715	4.915	0.366	4.977	4.927	0.00083	0.364	-2.087	495.821	100.884	108.207	822.535
3	7.278	198.521	5.037	7.672	40.585	4.892	0.370	5.017	4.903	0.00085	0.368	-2.082	493.738	100.925	108.203	814.587
4	7.232	196.929	5.078	7.632	40.454	4.868	0.374	5.058	4.880	0.00087	0.372	-2.077	491.661	100.967	108.198	806.729
...	...	...	...	...	...	...	...	...	...	...	...	...	...	...	...	...
47	5.248	132.490	7.548	6.132	34.843	3.803	0.638	7.508	3.816	0.00266	0.634	-1.593	410.403	102.592	107.840	557.946
48	5.201	131.085	7.629	6.105	34.712	3.776	0.647	7.588	3.789	0.00274	0.643	-1.569	408.834	102.623	107.825	554.378
49	5.155	129.685	7.711	6.079	34.582	3.750	0.657	7.670	3.763	0.00283	0.652	-1.544	407.290	102.654	107.810	550.921
50	5.109	128.288	7.795	6.053	34.451	3.724	0.667	7.753	3.737	0.00292	0.662	-1.518	405.772	102.685	107.794	547.576

Table 5-5. Depth Step Method Results for M2 Profile from Station 0 to 300

Depth Step, Δy (ft)	0.0252															
Step	y	A	V	E	P_W	R	Fr	Avg. V	Avg. R	Avg. Sf	Avg. Fr	Δx	x	z	y+z	M
n	(ft)	(sq.ft)	(fps)	(ft)	(ft)	(ft)		(fps)	(ft)	(ft/ft)		(ft)	(ft)	(ft)	(ft)	(cu.ft)
0	3.979	95.399	10.482	5.685	31.253	3.052	1.000	-	-	-	-	-	300.000	104.800	108.779	504.815
1	4.004	96.104	10.405	5.685	31.324	3.068	0.990	10.444	3.060	0.00691	0.995	-0.052	299.948	104.800	108.804	504.839
2	4.029	96.811	10.329	5.686	31.396	3.084	0.980	10.367	3.076	0.00676	0.985	-0.158	299.790	104.800	108.829	504.912
3	4.054	97.518	10.254	5.687	31.467	3.099	0.970	10.292	3.091	0.00662	0.975	-0.268	299.522	104.801	108.855	505.032
4	4.079	98.227	10.180	5.689	31.538	3.115	0.961	10.217	3.107	0.00648	0.965	-0.382	299.139	104.802	108.881	505.200
...	...	...	...	...	...	...	...	...	...	...	...	...	...	...	...	...
47	5.163	129.913	7.697	6.083	34.603	3.754	0.655	7.720	3.747	0.00288	0.658	-16.184	55.866	105.288	110.451	551.478
48	5.188	130.678	7.652	6.097	34.674	3.769	0.650	7.675	3.762	0.00283	0.653	-17.326	38.540	105.323	110.511	553.362
49	5.213	131.444	7.608	6.112	34.745	3.783	0.645	7.630	3.776	0.00279	0.648	-18.579	19.961	105.360	110.573	555.280
50	5.238	132.211	7.564	6.127	34.817	3.797	0.640	7.586	3.790	0.00274	0.643	-19.961	0.000	105.400	110.638	557.230

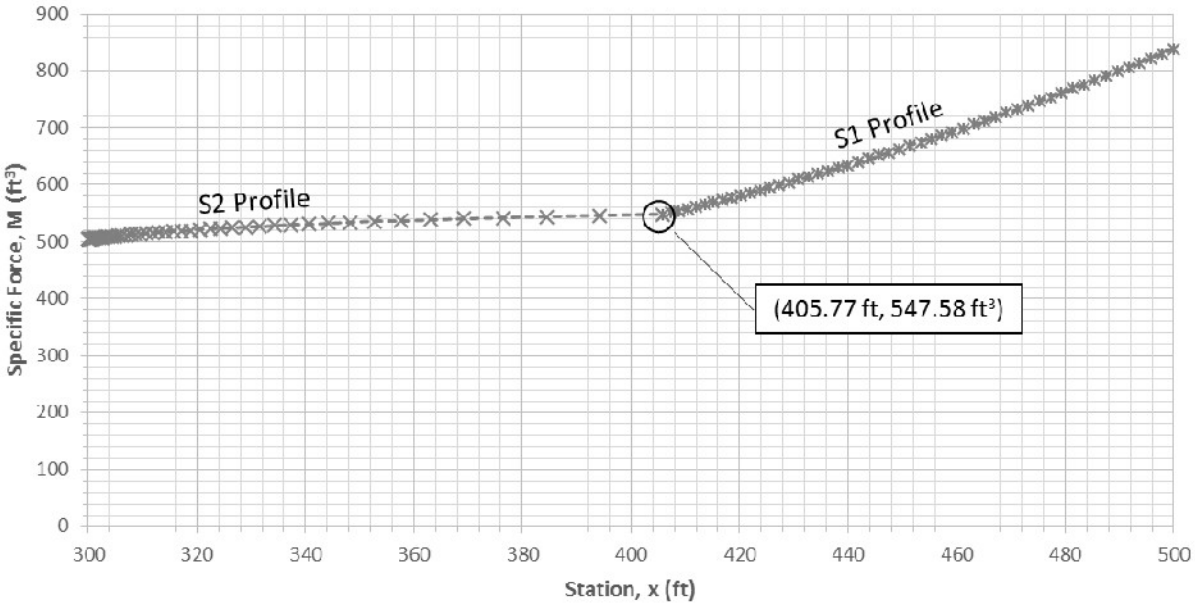

Figure 5-7. Locating Hydraulic Jump on the Hydraulically Steep Section

The profile characteristics found through the channel from upstream to downstream were M2, S2, the occurrence of a hydraulic jump at a horizontal station of 405.77 feet, S1, and then M1. Since each step involves averaging properties between horizontal locations the large number of depth steps used in calculating each profile was to ensure the greatest and most reasonable accuracy for this method. An even greater number of steps could have been used, but this would not have had any significant impact on the results.

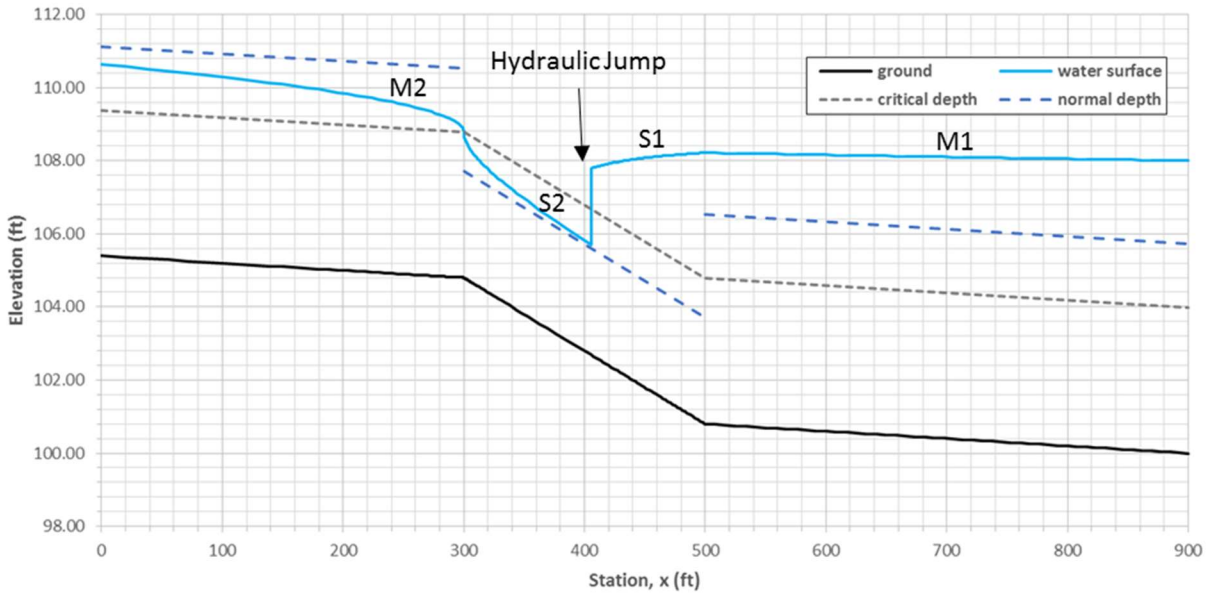

Figure 5-8. Composite Water Surface Profile from the Depth Step Method

5.4. Equations Used for Depth Step Method

$$A = y(b + my) \qquad (EQ\ \ :5.1)$$

$$V = Q/A \qquad (EQN: 5.2)$$

$$E = y + \frac{Q^2}{2gA^2} \qquad (EQN: 5.3)$$

$$P = b + 2y\sqrt{1 + m^2} \qquad (EQ\ \ :5.4)$$

$$R = A/P \qquad (EQN: 5.5)$$

$$Fr \quad \frac{V}{\sqrt{gD}} = \frac{V}{\sqrt{g\frac{A}{T}}} = \frac{V}{\sqrt{g\frac{A}{b + 2my}}} \qquad (EQ\ \ :5.6)$$

$$\bar{V} = \frac{V_n + V_{n+1}}{2} \qquad (EQN: 5.7)$$

$$\bar{R} = \frac{R_n + R_{n+1}}{2} \qquad (EQN: 5.8)$$

$$\bar{S_f} = \left(\frac{\bar{V} \cdot n}{c \cdot \bar{R}^{2/3}}\right) \qquad (EQN: 5.9)$$

$$\overline{Fr} = \frac{Fr_n + Fr_{n+1}}{2} \qquad (EQN: 5.10)$$

$$\Delta x = \frac{\Delta E}{S_o - \bar{S}_f} \qquad (EQN: 5.11)$$

$$x_{n+1} = x_n + \Delta x \qquad (EQN: 5.12)$$

$$z_{n+1} = z_n + \Delta x \cdot S_o \qquad (EQN: 5.13)$$

$$M = \frac{Q^2}{gA} + A\bar{y} \rightarrow M_{TRAP.} = \frac{Q^2}{gy(b+my)} + \frac{by^2}{2} + \frac{my^3}{3} \qquad (EQN: 5.14)$$

5.5. SRH-2D Hydraulic Jump Test Terrain Setup and Determining Results for Comparison

One major capability of SRH-2D is that "all flow regimes, i.e., subcritical, transcritical, and supercritical flows, may be simulated simultaneously without the need for special treatments" (Manual-SRH2D-v2.0-Nov2008 Chapter 1.2 – Modeling Concept and Capabilities). So, locating the hydraulic jump should be as straightforward as inputing the channel geometry, roughness, appropriate boundary conditions, and running the simulation for an appropriate length of time in order to reach steady state conditions. The files used to define the site in SMS 12.1 were prepared in ArcMap 10.2. The elevations for the channel were defined by scatter points arranged in a 1' x 1' grid pattern. These scatter points were first calculated in Excel, imported into ArcMap, and then converted into a shapefile. This shapefile was used to generate a DEM raster (not used with the SRH-2D but with HEC-RAS 2D) as well as a text file with xyz data for easy importation into SMS. The scatter points were used to define an area slightly larger than the Manning's n coverage that would become the extents of the model space. This was done to ensure SMS would not extrapolate elevations at the outermost limits of the mesh. The dimensions of the coverage were selected as 900' x 48' in order to include the entire length of the channel and to accommodate the maximum top width of the water surface of 36 feet located at the downstream lake but to also give some additional space in case of unforeseen differences in the two-dimensional model and yet not be unecessarily large.

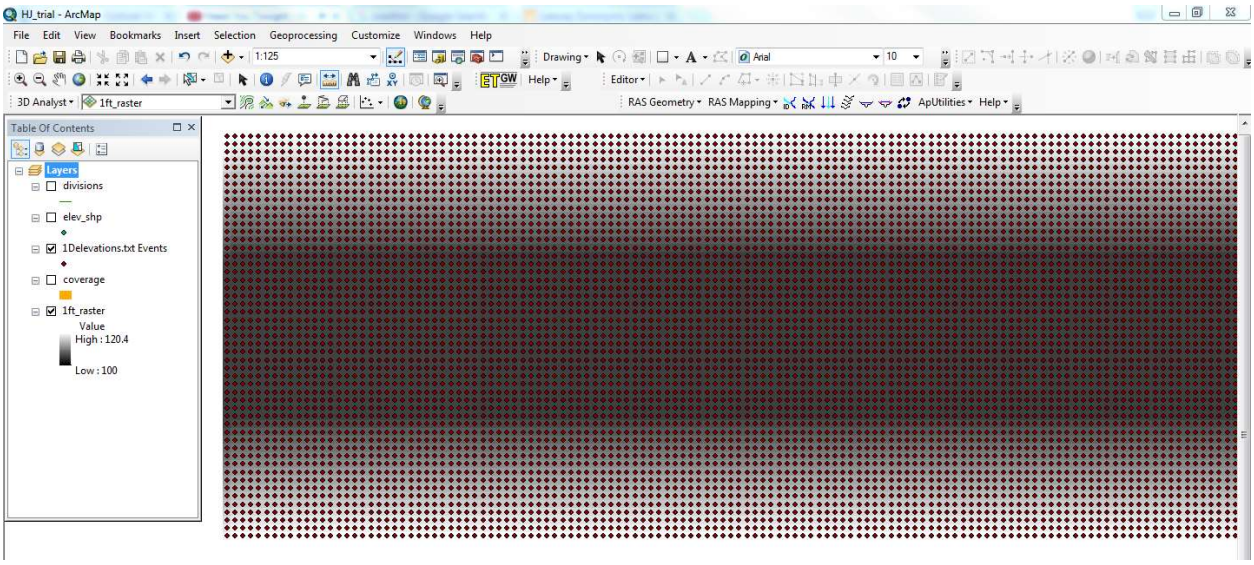

Figure 5-9. ArcMap 10.2 Data View Showing Scatter Points and Raster Generated from Them

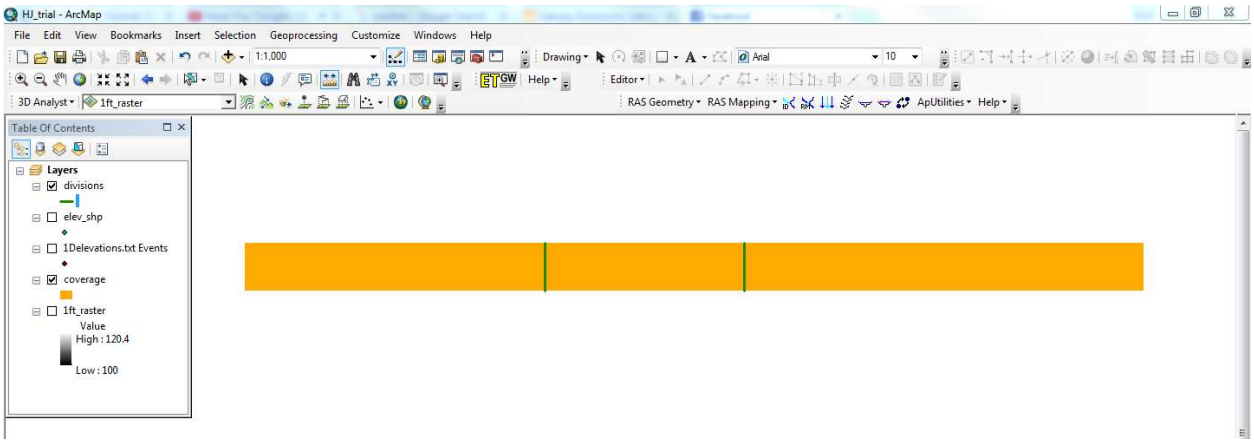

Figure 5-10. ArcMap Data View Showing Manning's Roughness Coverage and Lines Denoting Channel Slope Changes

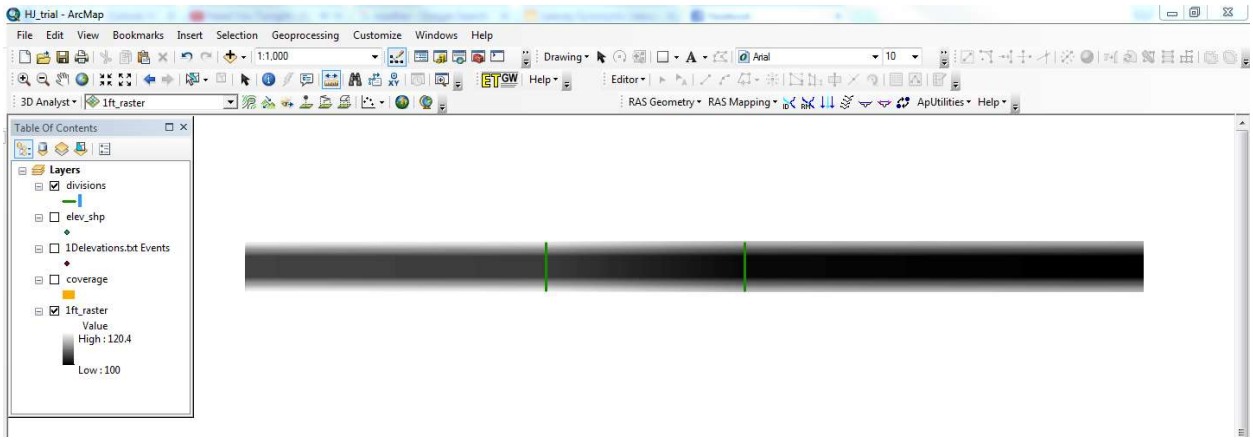

Figure 5-11. ArcMap Data View Showing Raster and Lines Denoting Channel Slope Changes

In order to locate hydraulic jump using SRH-2D, three different meshes were created, each composed of perfectly square elements. Each mesh possessed smaller elements than the preceding one. First, 4-foot elements were used, then 2 foot, and then 1 foot. Images of these meshes, along with the hydraulic jumps from each simulation, are shown in the following figures.

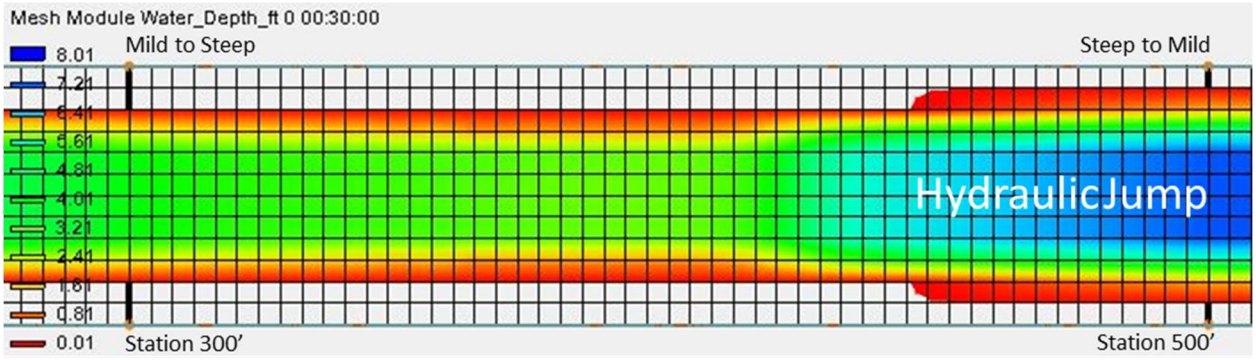

Figure 5-12. Plan View in SMS 12.1 with Color Fill Contours of SRH-2D Hydraulic Jump Trial Results Using Square 4-foot Elements

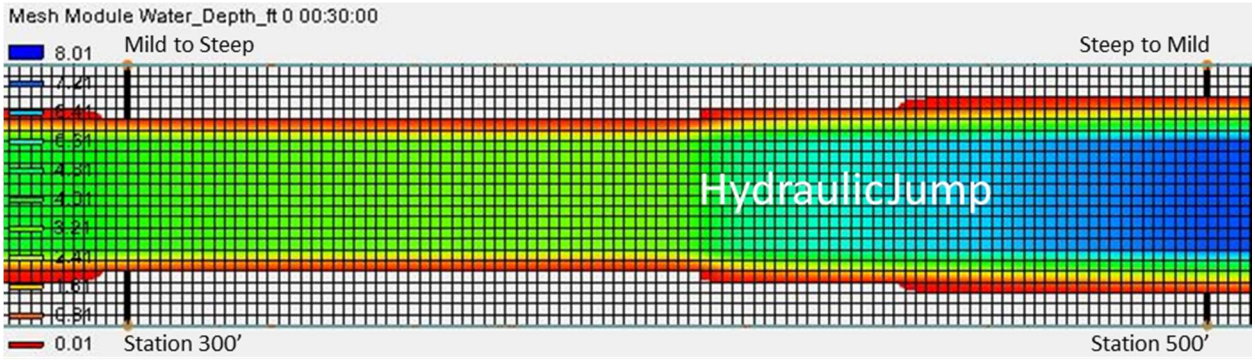

Figure 5-13. Plan View in SMS 12.1 with Color Fill Contours of SRH-2D Hydraulic Jump Trial Results Using Square 2-foot Elements

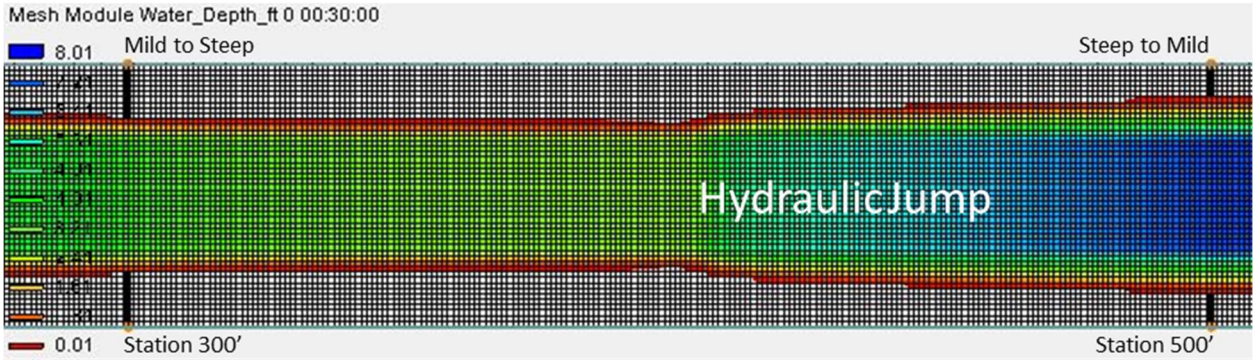

Figure 5-14. Plan View in SMS 12.1 with Color Fill Contours of SRH-2D Hydraulic Jump Trial Results Using Square 1-foot Elements

Comparing Figures 5-13 and 5-14 and noting how similarly each simulation placed the hydraulic jump in the channel, it was deemed unnecessary to use a tighter mesh size with the necessarily smaller computational time step. The model that employed the mesh with 4-foot square elements encompassed one full hour of simulated time, and from this it was determined that a much less time than that would be required to reach steady state conditions. For both the models that used the 2-foot and the 1-foot mesh elements the simulated times spanned half an hour (although, upon further inspection of the results, ten minutes would have been adequate). Results from the simulation using the 1-foot mesh elements were used for comparisons between methods.

5.6. SRH-2D Results for Hydraulic Jump Test from Simulation with Square 1-foot Elements

Figure 5-15 shows the final, steady state output from this simulation. This information was extracted from SMS using the Plot Wizard display tool to graph the results for an Observation Profile drawn along the channel's centerline. The data was then taken from the plot by right clicking it, selecting "view values", and then copying and pasting these values into an Excel spreadsheet.

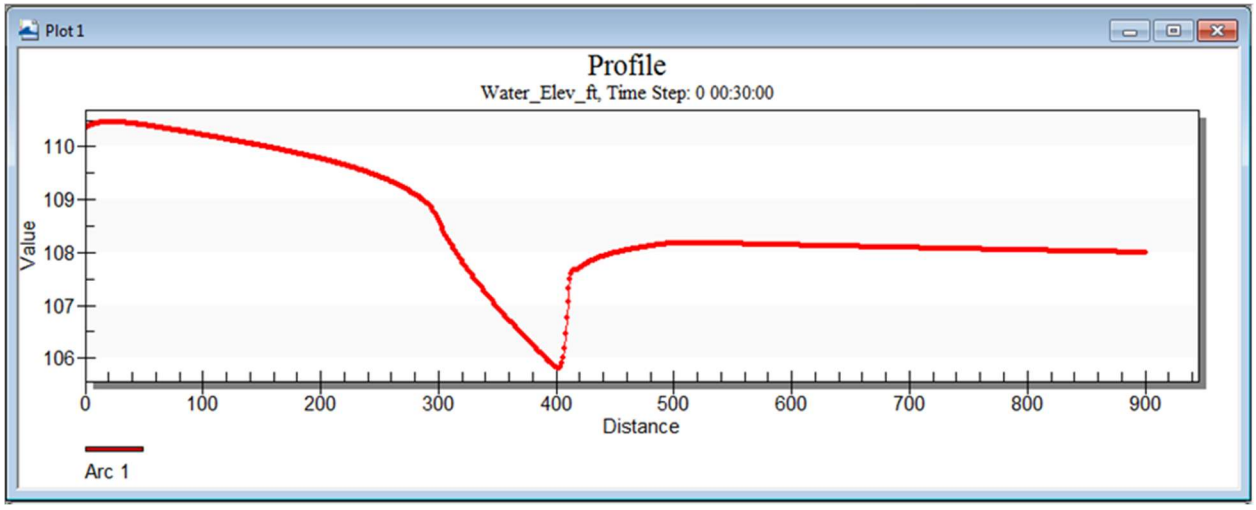

Figure 5-15. SMS 12.1 Output for Centerline Water Surface Elevation Data from Hydraulic Jump Test with 1-foot Square Mesh Elements

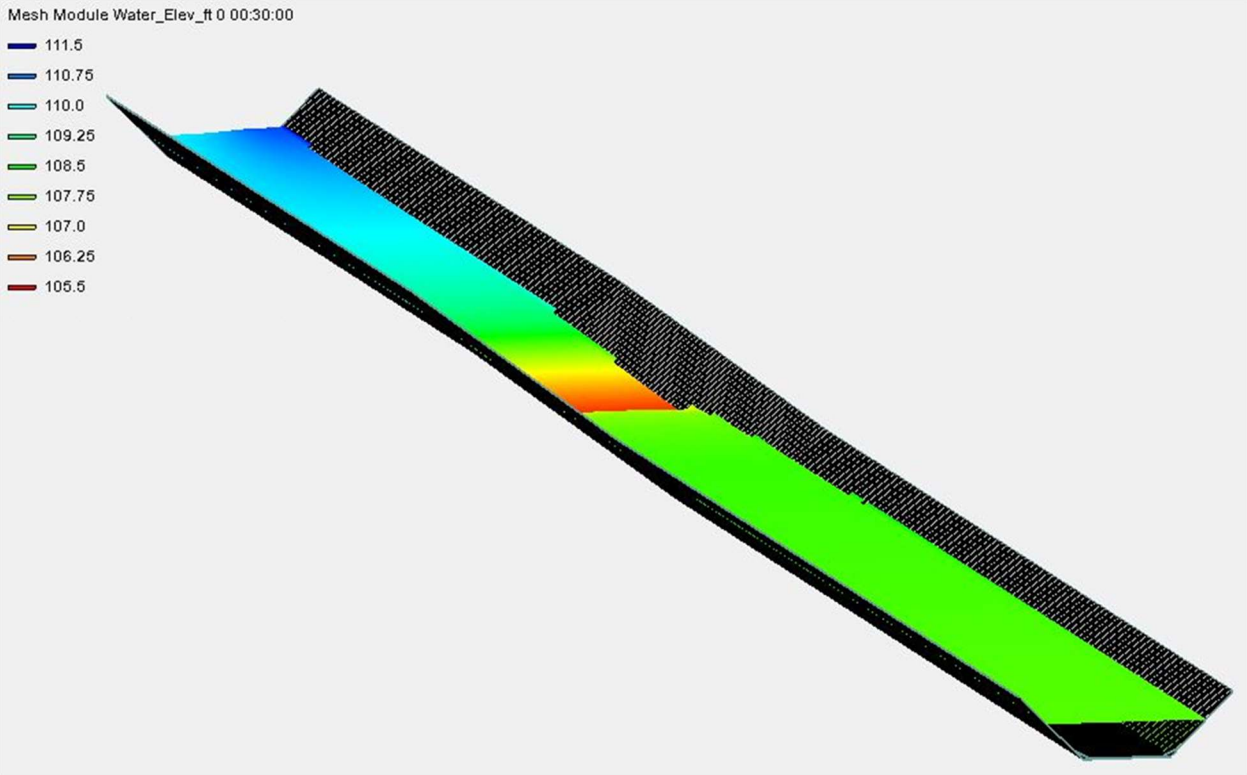

Figure 5-16. Oblique View of Simulation Output without Exaggerated Z-Scale

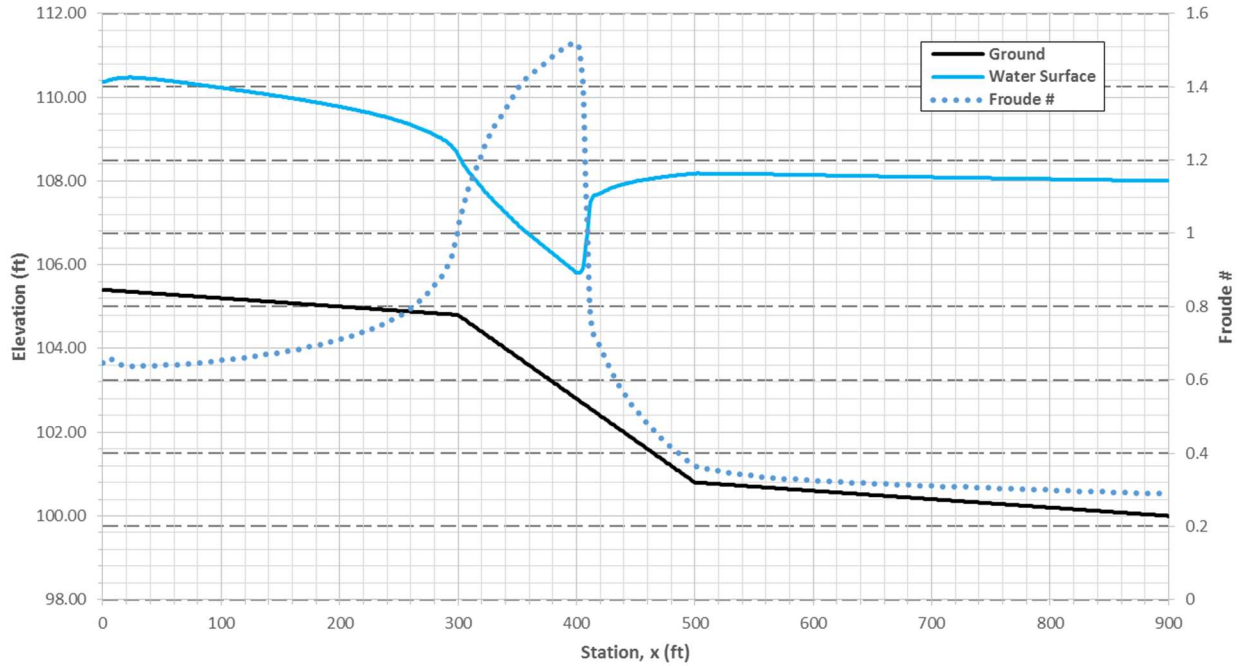

Figure 5-17. Complete Water Surface Profile along Channel Centerline for SRH-2D Hydraulic Jump Test

From Figure 5-17 it is immediately apparent that the hydraulic jump occurs in roughly the same vicinity as calculated from using the step method at a station of 405.77 feet. The next thing that becomes obvious is that unlike in the output from applying the step method where the water surface profile is assumed to instantly transition straight from the depth upstream of the jump to that downstream, with both depths applying at the same station, the hydraulic jump occurs over some horizontal distance. While this is a much more physically realistic result it makes the determination of a specific station where the hydraulic jump occurs, and the comparison between methods, rather difficult. However, if the definition that a hydraulic jump is an abrupt transition

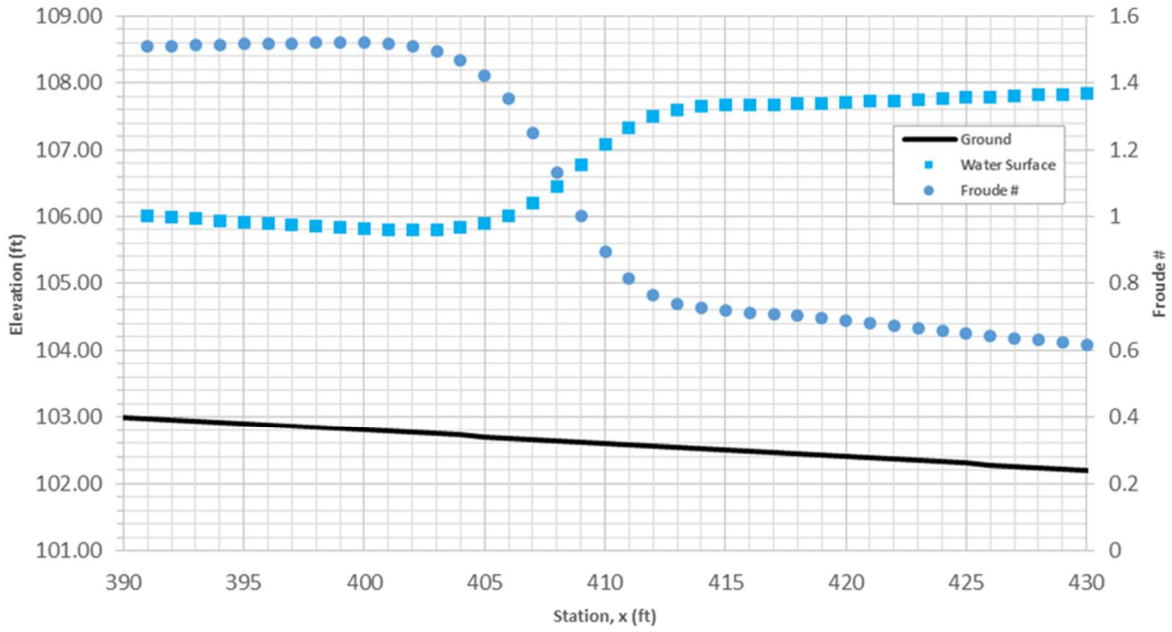

Figure 5-18. Data from Figure 5-17 near the Location of the Hydraulic Jump

from supercritical to subcritical flow is strictly applied, then the position where this change occurs is between stations 409.00’ and 410.00’ with Froude numbers of 1.004 and 0.895, respectively. But this does not seem satisfactory, as the maximum Froude number found along the channel centerline occurs at a station of 399.00’ has a value of 1.520, and the Froude number at a station

of 417.00', where the rollers on the surface of the hydraulic jump have dissipated and something resembling the typical S1 type curve begins, has a value of 0.708, thus the jump could be said to occur over a horizontal distance of 18 feet, which, relative to the 200 foot length of the steep section, may be deemed "abrupt". Worth noting is that the two stations, 399.00' and 417.00', do properly bracket the hydraulic jump's location.

An approximate length for the hydraulic jump then is 18 feet. In order to assess this value, the eminent resource, "Open Channel Hydraulics", Chow – 1959 was consulted. In that book, in Chapter 15 titled "Hydraulic Jump and Its Use as an Energy Dissipater" there is a chart relating upstream Froude number to the ratio of the length of the hydraulic jump to the downstream depth, and while this chart "was developed primarily for jumps occurring in rectangular channels" the author also states "In the absence of adequate data, this curve may also be applied approximately to jumps formed in trapezoidal channels." Since the horizontal to vertical side slope of this test reach is not extreme (1:1), this was considered appropriate. After rounding the maximum Froude number found upstream to 1.5 for simplicity's sake, and entering the chart mentioned, from the curve a ratio of the hydraulic jump's length to the downstream depth obtained was approximately 3.75. Using the depth at station 417.00', equal to 5.214 feet, a length of 19.55 feet was calculated. Subtracting this length from station 417.00' places the beginning of the hydraulic jump at station 397.45'. This estimate is near station 399.00', previously suggested as the initial station of the hydraulic jump. It seems reasonable that for a trapezoidal channel the hydraulic jump could occur over a shorter distance than for a rectangular one, since in the case of the trapezoidal channel, the flow can move up the side slopes to match the downstream depth. Another source of discrepancy may be precision errors involved in rounding or reading the chart, or from the fact that the chart from Chow was also intended for horizontal channels, while this channel was sloped. However,

over a horizontal distance of 18 feet (the first estimate for the hydraulic jump's length) the drop in bed elevation for this steep section is 0.36 feet and thus probably not an enormous source of error, but is not negligible considering the depths involved (3.016 feet at station 399.00' and 5.214 feet at station 417.00').

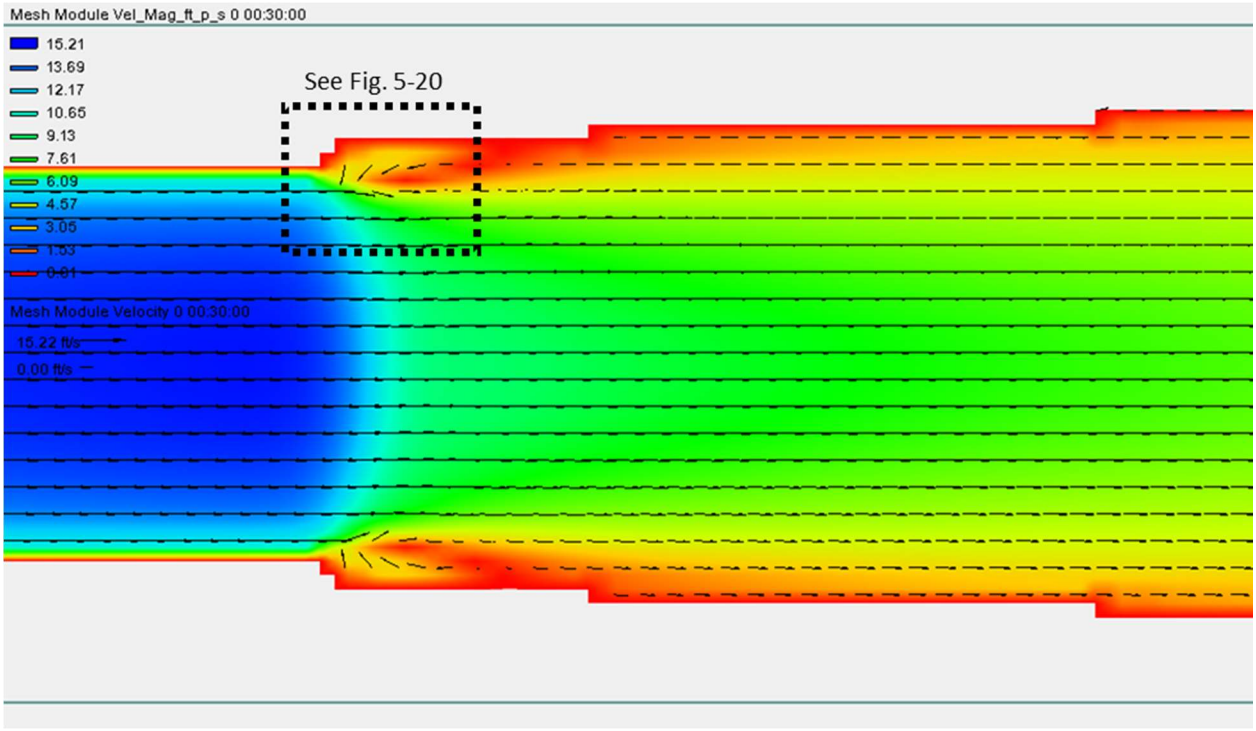

Figure 5-19. Velocity Details near Hydraulic Jump from SRH-2D Viewed in SMS

Furthermore, discrepancies arise from the fact that a hydraulic jump in a trapezoidal channel is simply not a one-dimensional problem. As can be seen from Figure 5-19, the velocity is far from uniform for any given cross section perpendicular to the channel centerline. This, and the fact that the depth varies across the cross section, means that the Froude number varies laterally. So, a single cross section may be at once super- and subcritical simultaneously (Figure 5-21). Also, there is some recirculating flow on this trapezoidal channel's side slopes that is actually travelling upstream. Clearly, a hydraulic jump in a trapezoidal channel is at least a two-dimensional problem. Even more accurately though, it is a three-dimensional problem – this is due to the recirculating

flow that exists on the surface of a hydraulic jump known as “rollers”. While these rollers cannot be directly modeled by SRH-2D, it is unknown if the program makes an attempt to account for them. Despite all of this, as can be seen in 5-22, the water surface profiles from the direct step method spreadsheet and that from the channel centerline for the SRH-2D simulation closely resemble one another.

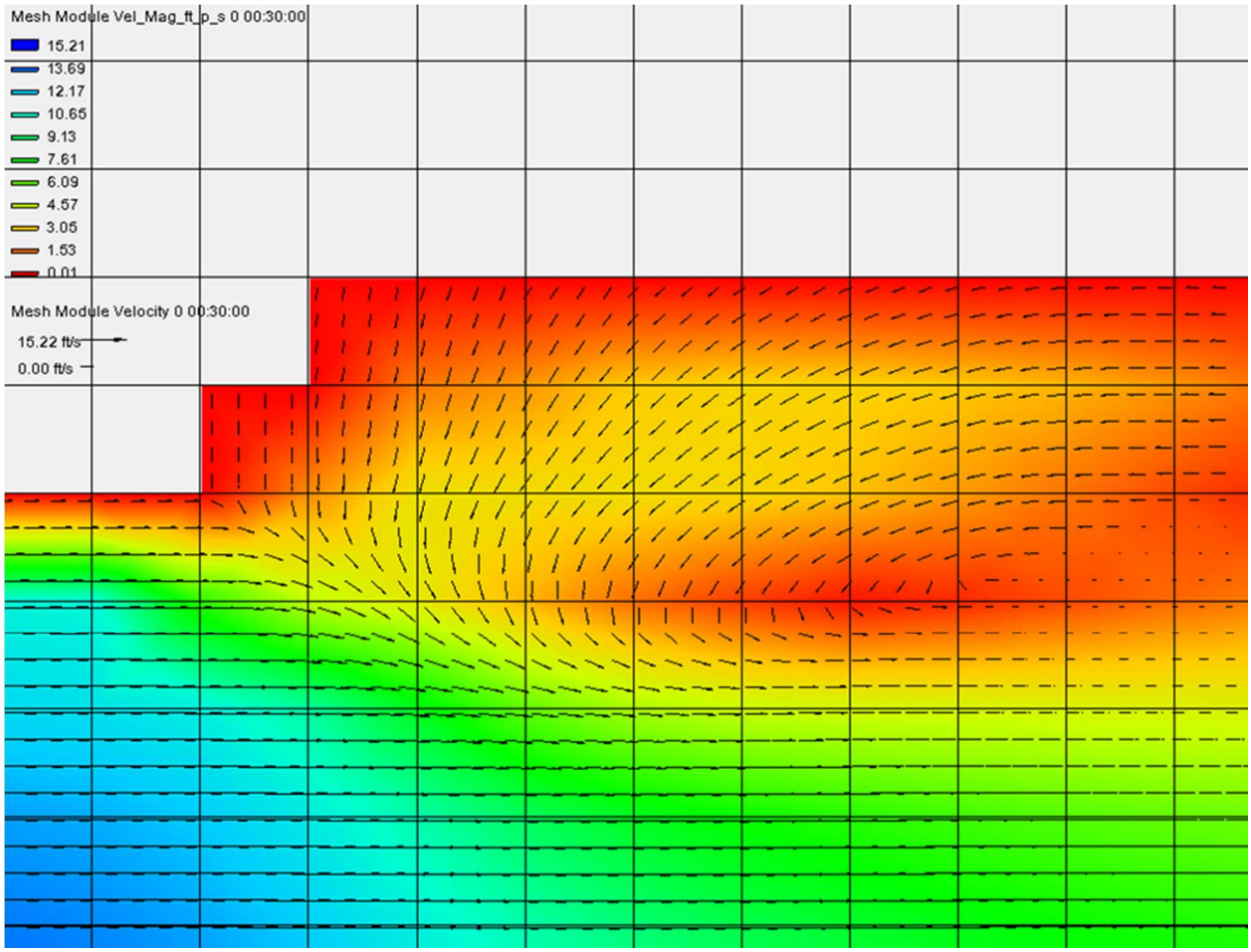

Figure 5-20. Close-up of Recirculating Flow where Extents are defined in Figure. 5-19

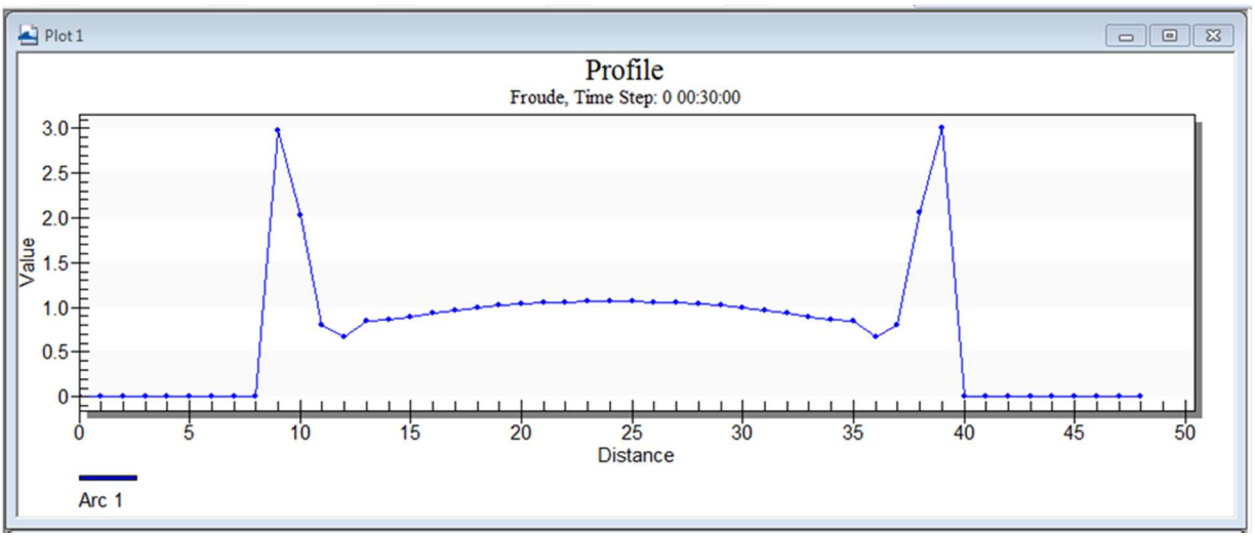

Figure 5-21. Froude Number Data across Cross Section at Station 408.50

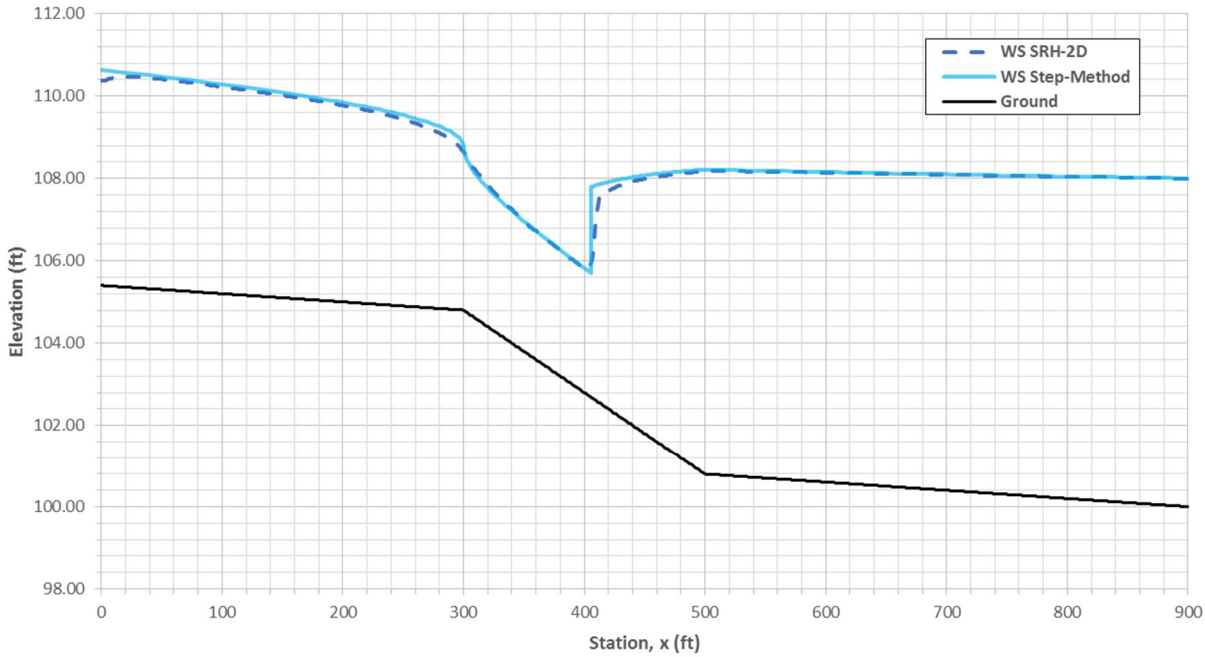

Figure 5-22. Gradually Varied Flow Profiles for Hydraulic Jump Test Reach from Step Method and SRH-2D

One interesting detail noticeable in the figure above is that the depth of flow at the transition from mild to steep, located at station 300', predicted by SRH-2D is below that calculated within the spreadsheet following standard hydraulic engineering assumptions. It is ordinary practice to assume critical depth exists right at the station where such a slope transition occurs, in reality this

is generally not true, but this consideration is usually neglected. From "Open Channel Flow," Henderson – 1966, Chapter 6, "Channel Controls", there is a discussion on the free overfall in the text. At this location, it states, for subcritical flow travelling off the brink, the critical section will upstream from the drop-off point by a distance equal to about 3 to 4 times the critical depth, and downstream of that point the pressure within the flow is not hydrostatic. It goes on, further in the chapter, saying that if a mild slope transitions into a very steep slope "the flow would have some of the character of flow over an overfall – in which […] the critical section retreats upstream to some ill-defined location […]." In order to determine whether this were indeed the case, the following figure was created using the output of the simulation.

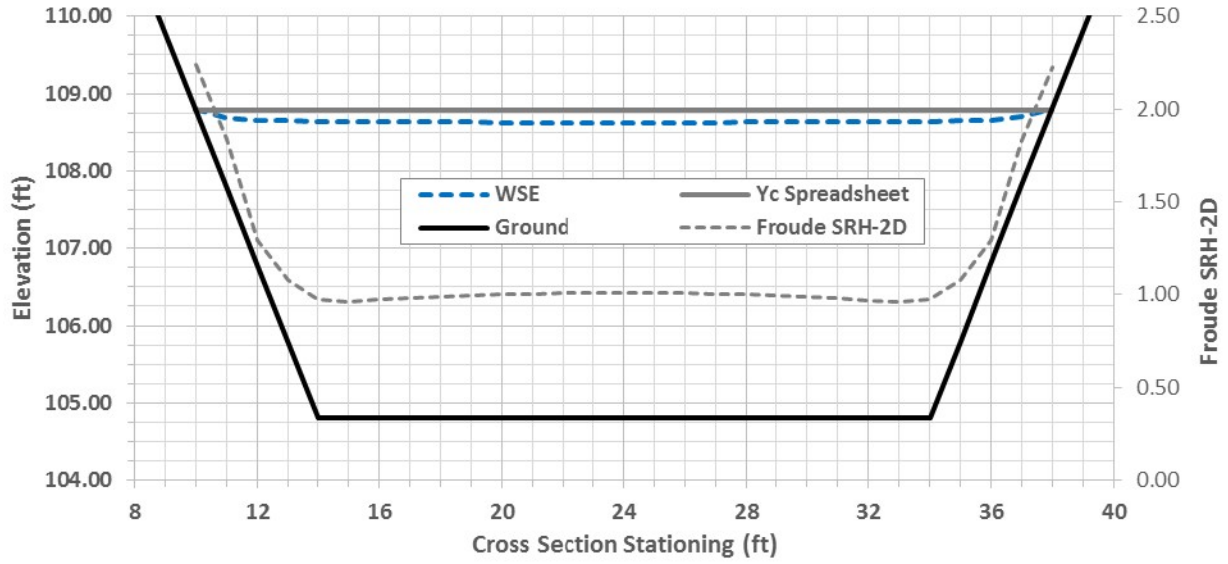

Figure 5-23. Detailed Summary of Cross Section at Station 300

At this cross section all types of flow exist – subcritical, critical, and supercritical. On both side slopes all flow is supercritical, but within the central part of the channel things are more complex. The flow near the center of the channel is very slightly supercritical, while within several feet on each side of the supercritical flow is critical flow. Between the side slopes and this critical

flow, very slightly subcritical conditions exist. The following table concisely contains this same information.

Table 5-6. SRH-2D Froude Numbers across Cross Section at Station 300 for Hydraulic Jump Test

XS Station	10	11	12	13	14	15	16	17	18	19	20	21	22	23	24
Froude #	2.236	1.836	1.295	1.078	0.977	0.960	0.972	0.982	0.990	0.997	1.002	1.006	1.008	1.010	1.011
XS Station	25	26	27	28	29	30	31	32	33	34	35	36	37	38	
Froude #	1.010	1.008	1.006	1.002	0.997	0.990	0.982	0.972	0.959	0.976	1.077	1.293	1.831	2.228	

In light of Table 5-6, it is possible to say that something resembling the conditions which exist at a free overfall are present in the SRH-2D results. However, it is not known the extent to which SRH-2D could model this phenomenon. If the channel were to transition from mild to a very extreme steep slope, the drawdown that occurs upstream of the break-in-grade would involve a non-negligible vertical velocity component, thus turning the problem into a three-dimensional one.

5.7. One-Dimensional HEC-RAS Hydraulic Jump Test

In order to determine depths at various cross sections HEC-RAS employs a form of the step method that differs from the above in that, rather than specifying the change in depth and directly calculating a station, the station is known and the change in depth must be determined. Since head losses due to friction depend on several factors, chiefly among them being depth, and in order to apply the step method the friction slope must be averaged between cross sections, the solution to this form of the step-method requires an implicit solution whereas the form of the step-method used above can be solved explicitly (see Henderson, 5.4, “Step Method – Depth Calculated from Distance” for an in-depth discussion).

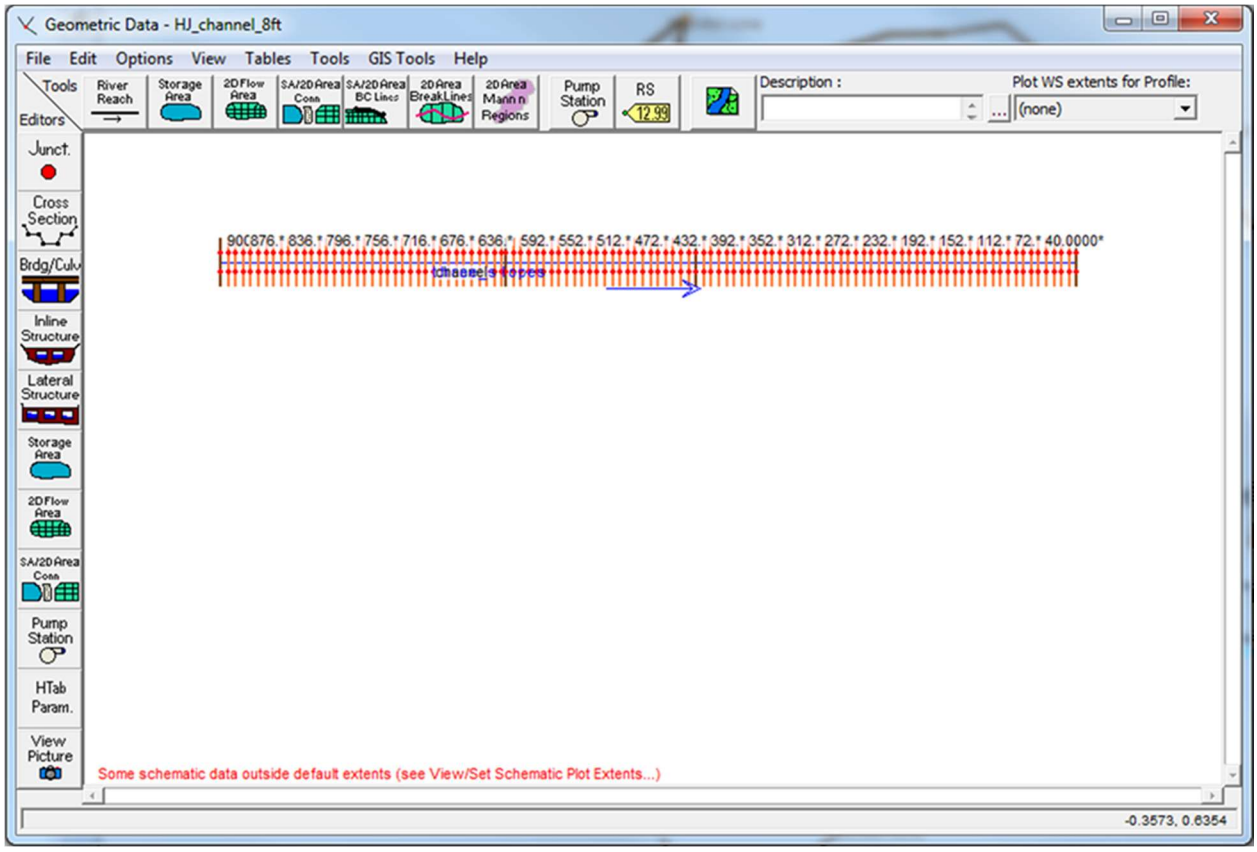

Figure 5-24. Graphical Representation of HEC-RAS 5.0 Cross Sections for Hydraulic Jump Test at 8 foot Spacing.

For the one-dimensional HEC-RAS model shown in Figure 5-24, the primary cross sections were created at four stations: the upstream lake, the downstream lake, and at each break-in-grade. All other cross-sections were generated using the Cross Section Interpolation tool shown in the figure below. These interpolated cross sections are those in Figure 5-24 labeled with an asterisk. This brought the total number of cross sections to 114 as opposed to the 203 locations used for the depth-step method above.

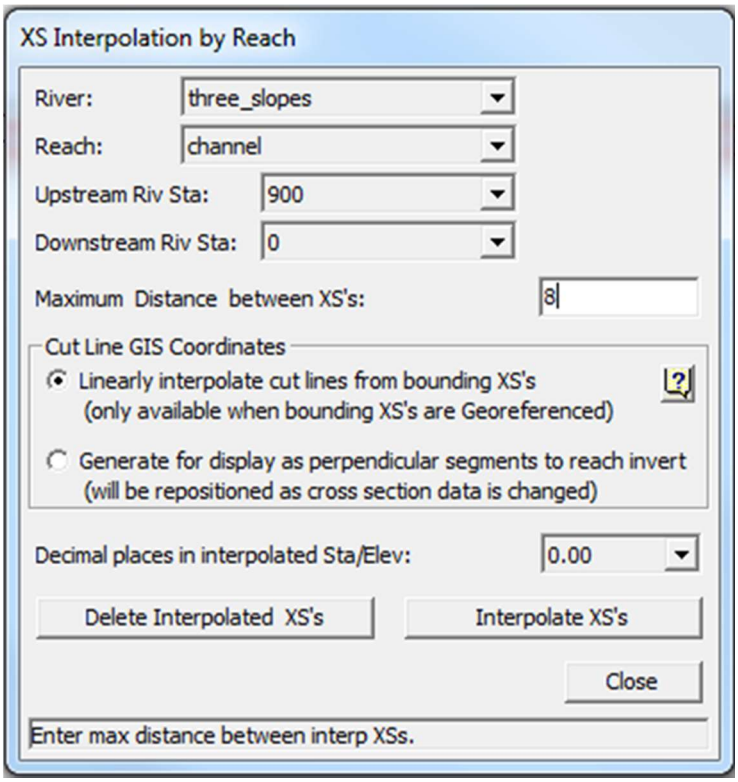

Figure 5-25. HEC-RAS Cross-Section Interpolation Tool Located within the Geometric Data Editor

The upstream and downstream boundary conditions for this model were both set to "known water surface elevations" – 108.00' for the lower lake, and 110.64' for the upper lake. The value for the top lake was obtained from the GVF profile in the depth-step method spreadsheet. The flow for the profile was set to 1000 cfs at station 900'. In order for HEC-RAS to calculate a hydraulic jump, the option for a "Mixed" Flow Regime must be selected before running the steady simulation. Typically, for floodplain mapping the flow regime is left as "Subcritical" to force the results to have the greatest depths, and thus for the floodplain to be as large as possible. This is considered to be conservative. Also, realistically, in most natural channels subcritical flow is by far the most common. Figures 5-26 through 5-28 show the results of a subcritical run, the menu containing the option for changing the flow regime, and the results of a mixed run.

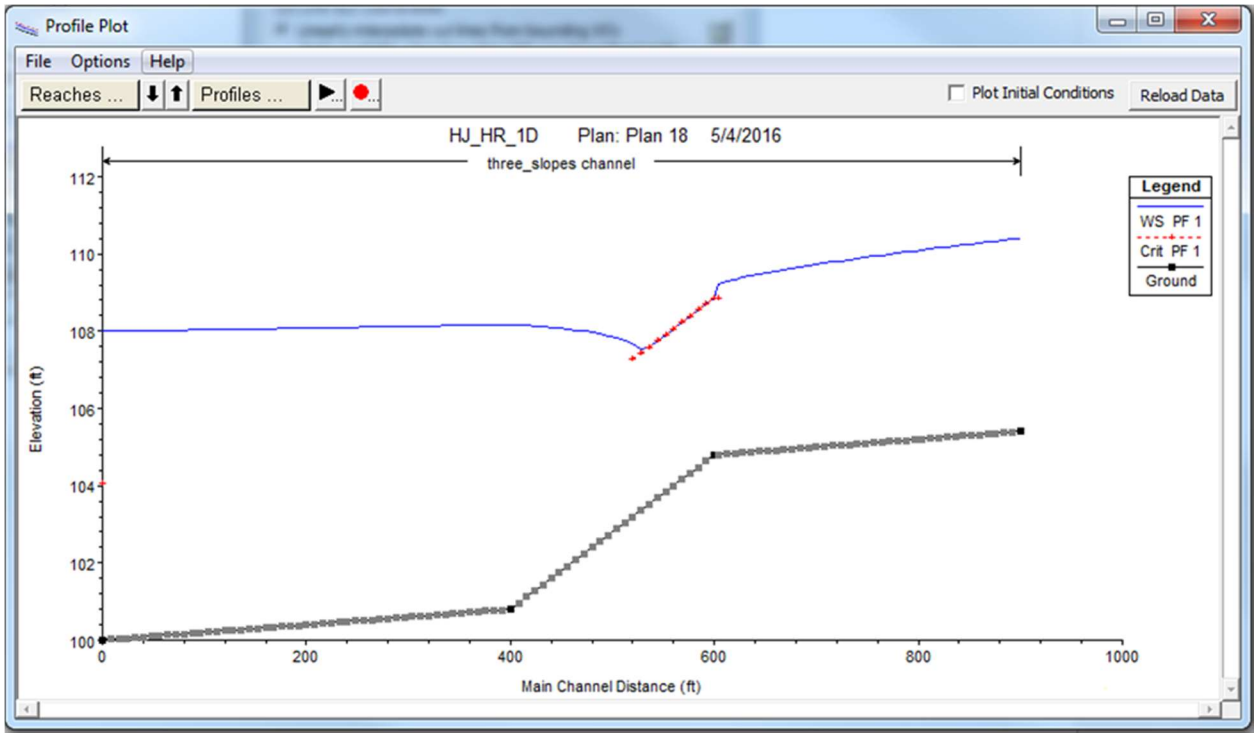

Figure 5-26. Poor Results of Hydraulic Jump Test for One-Dimensional HEC-RAS Simulation using Subcritical Flow Regime Option

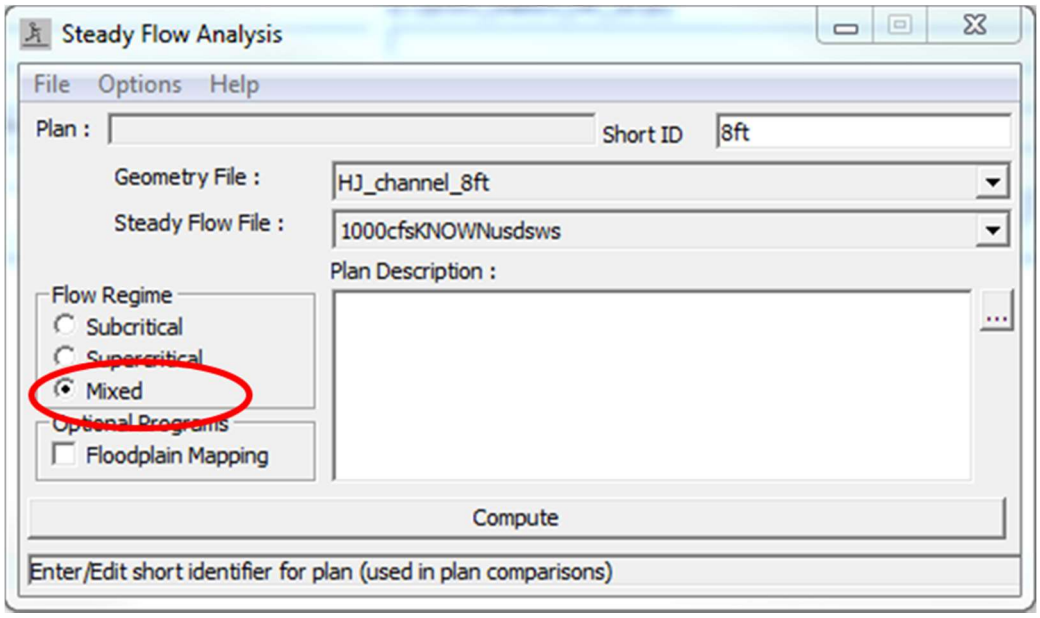

Figure 5-27. Option to Allow HEC-RAS to Compute Hydraulic Jumps

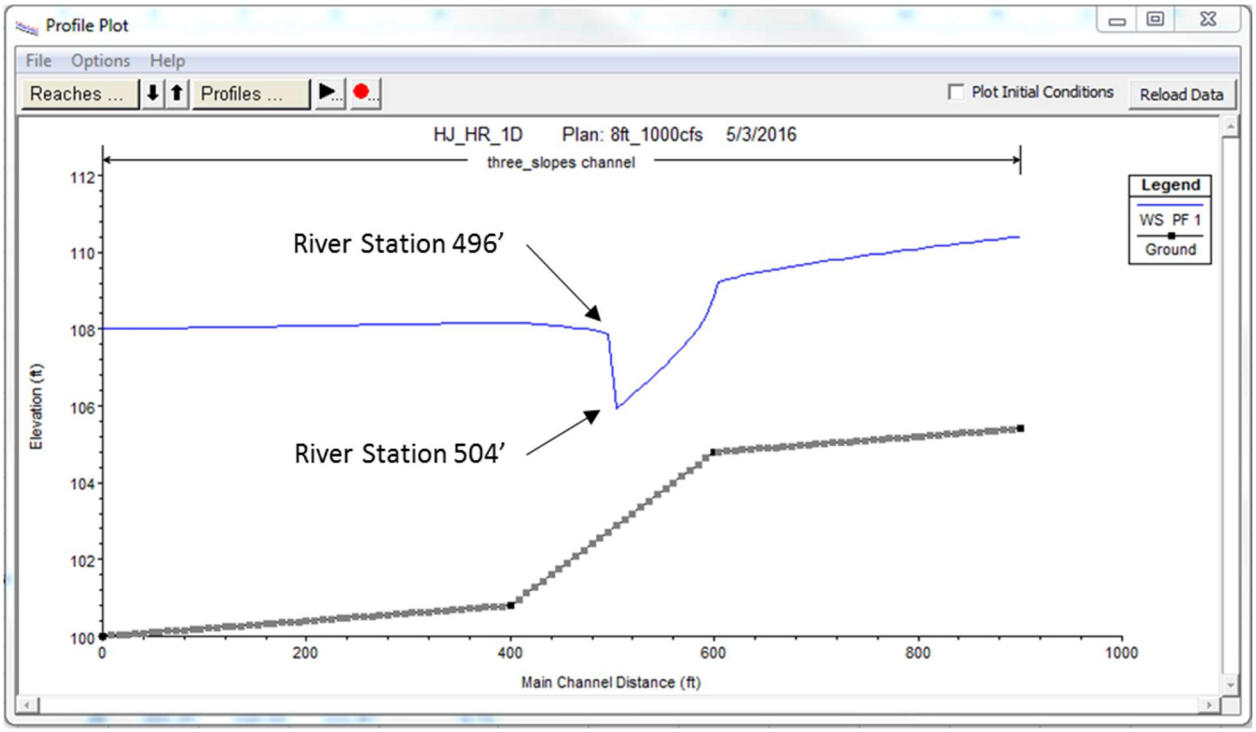

Figure 5-28. Initial HEC-RAS 1D Simulation to Locate Hydraulic Jump Using 8 foot Spacing for Cross Sections

The results of this first test appeared quite good. The stationing is reversed from the spreadsheet and the SRH-2D simulation as HEC-RAS numbers cross sections increasing from downstream to upstream and thus this profile plot is backwards from the cross section display from Figure 5-24, but River Stations 496' and 504' correspond with spreadsheet and SRH-2D stations 404' and 396', respectively (subsequent profile plots were adjusted in Excel to resemble other plots). Thus, HEC-RAS 1D determined that a hydraulic jump should occur between those two stations. This estimate was close to the value of 405.77' obtained from the spreadsheet, and partially falls within the range of 399.00' to 417.00' for the hydraulic jump obtained from SRH-2D. The HEC-RAS estimate is upstream of the value from the spreadsheet though. Originally, it was expected that the hydraulic jump would occur between stations 404' and 412', properly bracketing the solution obtained from the spreadsheet. It was assumed that by reducing the spacing of the cross sections within the HEC-RAS model, the similarity to the value obtained from the

spreadsheet would increase – however, this was not the case. Figure 5-29 shows the results of the subsequent test.

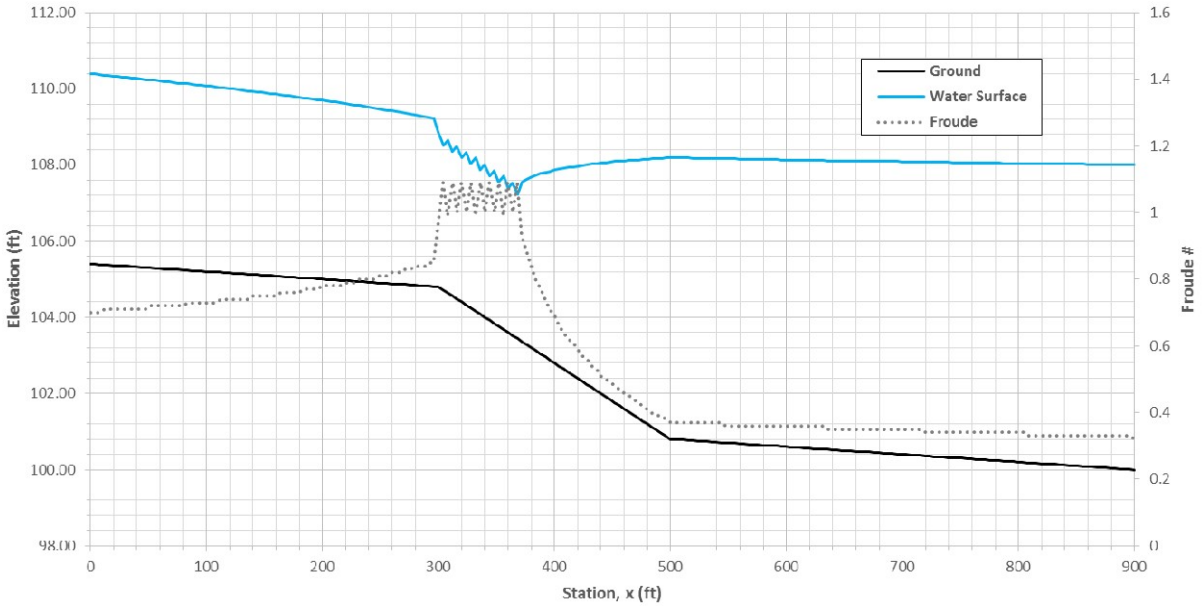

Figure 5-29. HEC-RAS 1D Simulation to Locate Hydraulic Jump Using 4 foot Spacing for Cross Sections

Clearly, merely doubling the number of cross sections did not increase the accuracy of the results. In fact, they are quite dubious. From the first break-in-grade at station 300', until about a third of the way down the steep section at station 368', the depth oscillates weirdly around critical depth. From station 372' until the end of the channel the depth remains subcritical. The reason why these HEC-RAS simulations are behaving thusly is two-fold – first, the bank points are in the wrong places, and the second reason has to do with expansion and contraction losses included in the Energy Equation used by HEC-RAS. The bank points were dealt with first, and an explanation of this problem is what follows.

From Chapter 2, Theory, it was explained that HEC-RAS uses Manning's equation to compute a depth from discharge which satisfies the energy equation. However, each cross section is subdivided into smaller parts and the conveyance is calculated separately for each section. In

this case, the conveyance sections for this channel include each side slope and the central part of the channel. The following example seeks to illustrate the impact of this approach by analyzing this channel using the HEC-RAS conveyance equations, and the normal depth calculated in the depth-step spreadsheet for the mild sections of this channel using the given discharge of 1000 cfs.

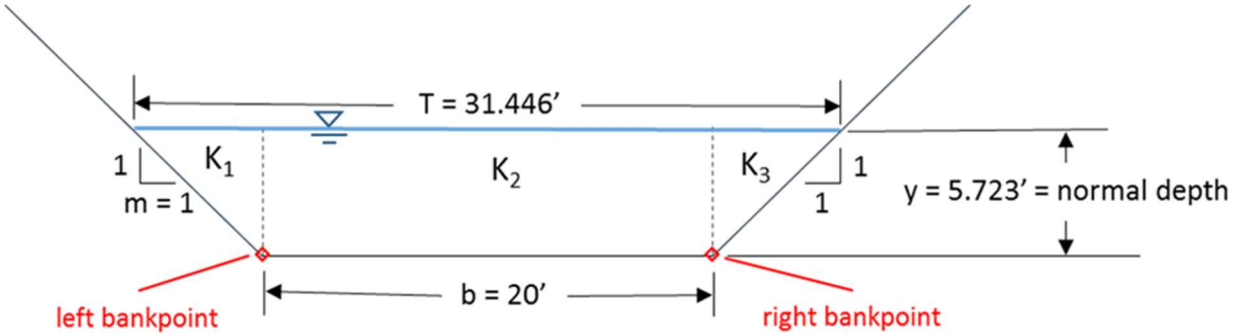

Figure 5-30. Conveyance Sections for Normal Depth on the Hydraulically Mild Portion of the Hydraulic Jump Test Reach with Incorrect Placement of Bank points

$$Q = (K_1 + K_2 + K_3)S_f^{1/2}$$

$$= \left(\frac{1.486}{n_1}\cdot\frac{A_1^{5/3}}{P_{w1}^{2/3}} + \frac{1.486}{n_2}\cdot\frac{A_2^{5/3}}{P_{w2}^{2/3}} + \frac{1.486}{n_3}\cdot\frac{A_3^{5/3}}{P_{w3}^{2/3}}\right)S_o^{1/2}$$

where $n_1 = n_2 = n_3 = n$ and 1.486 (= 1.49 to match spreadsheet's value for English units).

$$= \frac{1.49}{n}\left(\frac{A_1^{5/3}}{P_{w1}^{2/3}} + \frac{A_2^{5/3}}{P_{w2}^{2/3}} + \frac{A_3^{5/3}}{P_{w3}^{2/3}}\right)S_o^{1/2}$$

$$= \frac{1.49}{n}\left(\frac{\left(\frac{1}{2}\cdot y_n^2 m\right)^{5/3}}{\left(y_n\sqrt{1+m^2}\right)^{2/3}} + \frac{(by_n)^{5/3}}{(b)^{2/3}} + \frac{\left(\frac{1}{2}\cdot y_n^2 m\right)^{5/3}}{\left(y_n\sqrt{1+m^2}\right)^{2/3}}\right)$$

$$= \frac{1.49}{0.025}\left(\frac{\left(\frac{1}{2}\cdot(5.72ft)^2\right)^{5/3}}{\left(5.72ft\sqrt{1+1^2}\right)^{2/3}} + \frac{(20ft\cdot 5.72ft)^{5/3}}{(20ft)^{2/3}} + \frac{\left(\frac{1}{2}\cdot(5.72ft)^2\right)^{5/3}}{\left(5.72ft\sqrt{1+1^2}\right)^{2/3}}\right)$$

$$= Q_1 + Q_2 + Q_3 = 69.8cfs + 976cfs + 69.8cfs = 1116cfs = Q.$$

What the above shows is that it would take a discharge 11.6% higher than used for these tests to have the same normal depth as calculated in the spreadsheet using Manning's equation where the entire cross section was used as a single conveyance section. Figure 5-31 shows the cross section editor within HEC-RAS with adjusted bank points. This was applied to every cross section by deleting the interpolated cross sections, manually fixing the bank points for the four primary cross sections, and then re-interpolating the cross sections.

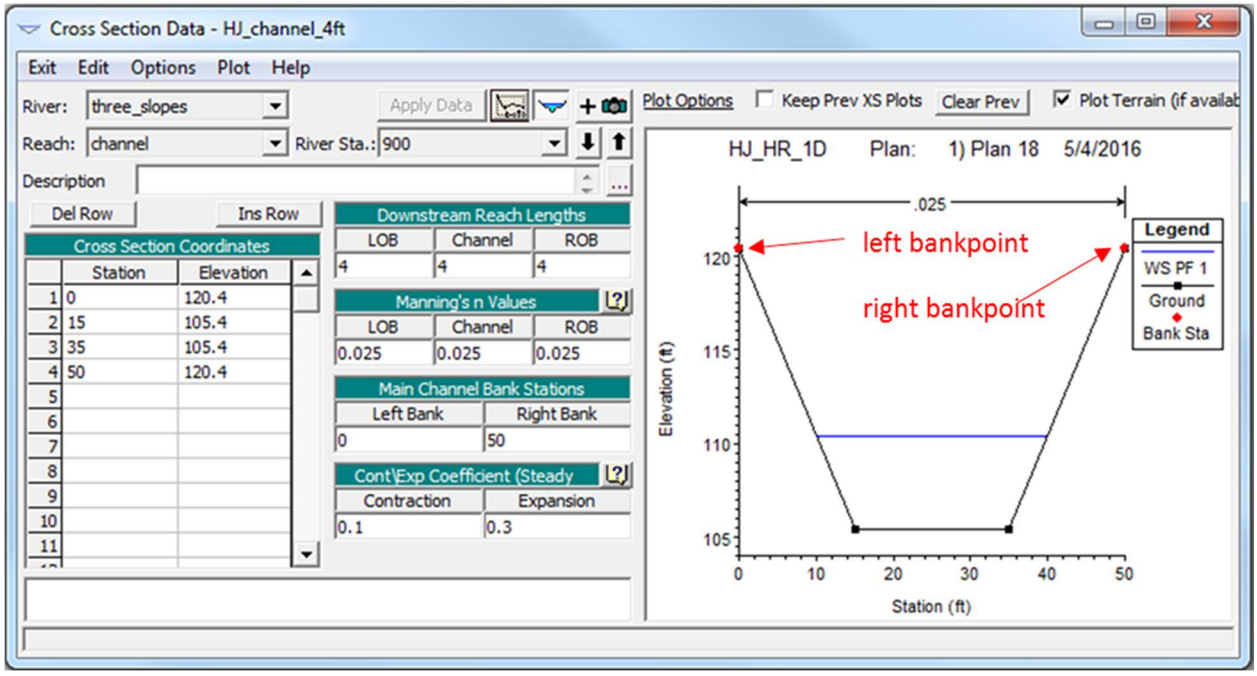

Figure 5-31. Proper Placement of HEC-RAS Bank points on the Trapezoidal Channel

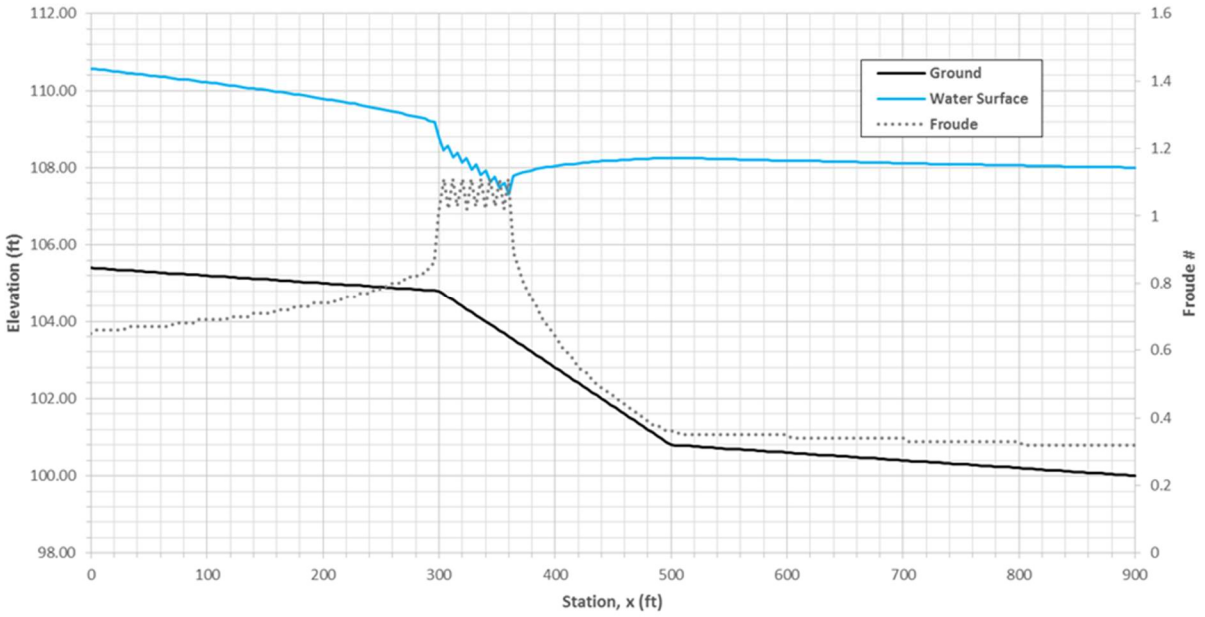

Figure 5-32. HEC-RAS 1D Simulation to Locate Hydraulic Jump Using 4 foot Spacing for Cross Sections and Proper Placement of Bank points

Obviously, the results shown in Figure 5-32 are not correct. The strange oscillation around critical depth was still occurring. Also, fixing the bank points for the HEC-RAS model that used 8 foot spacing for the cross sections still failed to properly bracket the solution – the upstream and downstream stations of the hydraulic jump actually moved further upstream, to stations 388' and 396', when the jump was already located upstream of where it was predicted using the depth-step method. Although, for that model the flow managed to properly achieve supercritical depths leading up to the hydraulic jump. Something else was going here – which leads to the next point, the expansion and contraction losses. The only type of losses accounted for when applying the depth-step method within the spreadsheet were those due to friction. In order to get a direct comparison between methods, those needed to be removed from the HEC-RAS simulation. Figure 5-33 through 5-36 describe this process.

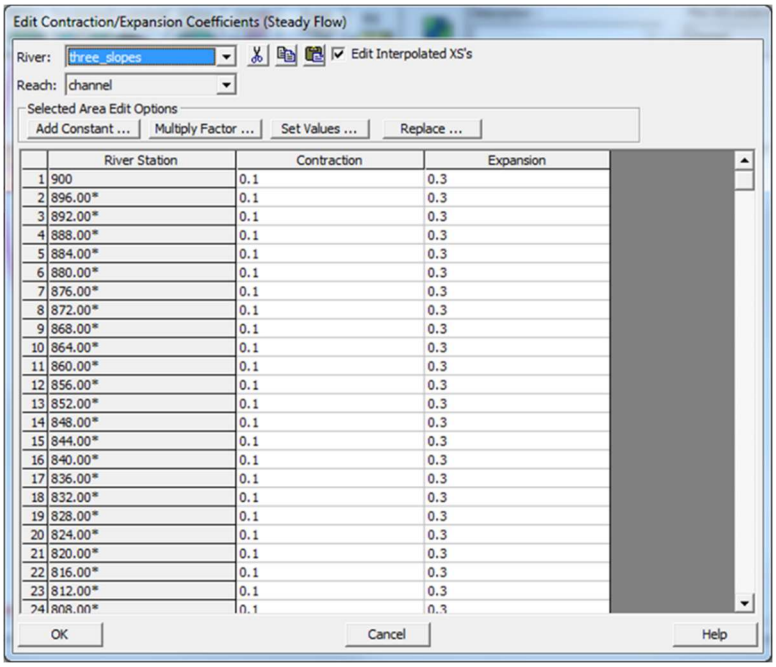

Figure 5-33. Default Values for HEC-RAS Expansion and Contraction Loss Coefficient Table for all Cross Sections in the Model with 4 foot spacing

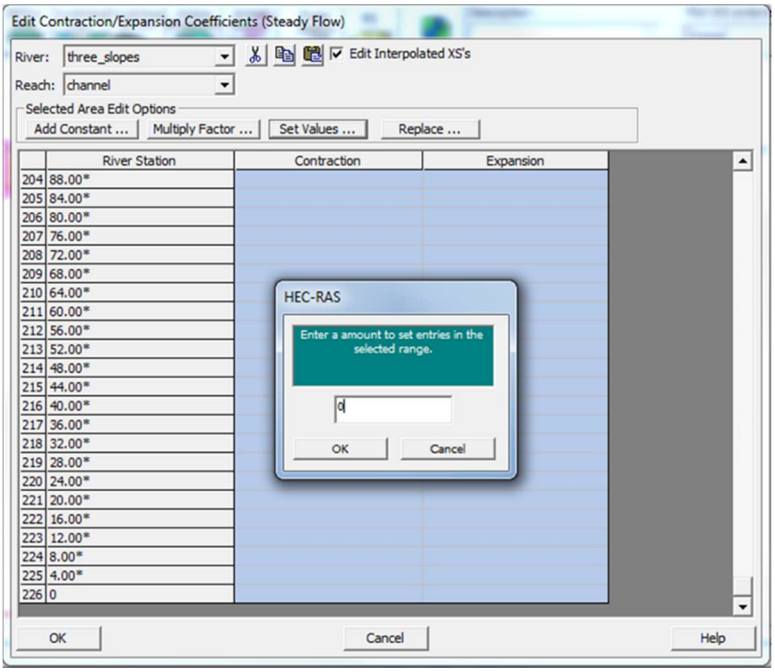

Figure 5-34. Selecting and Setting Expansion and Contraction Coefficients Loss Coefficients to Zero Simultaneously

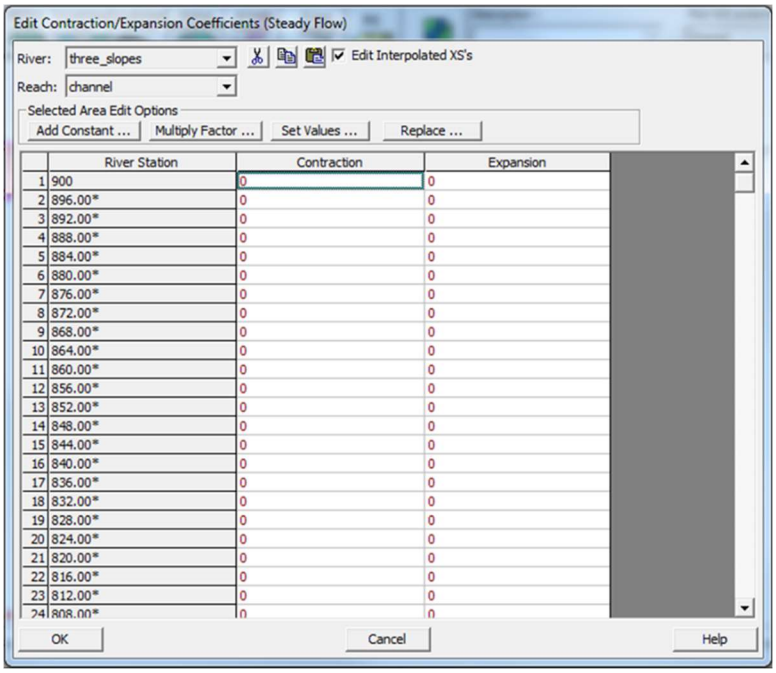

Figure 5-35. All Expansion and Contraction Coefficients Set to Zero

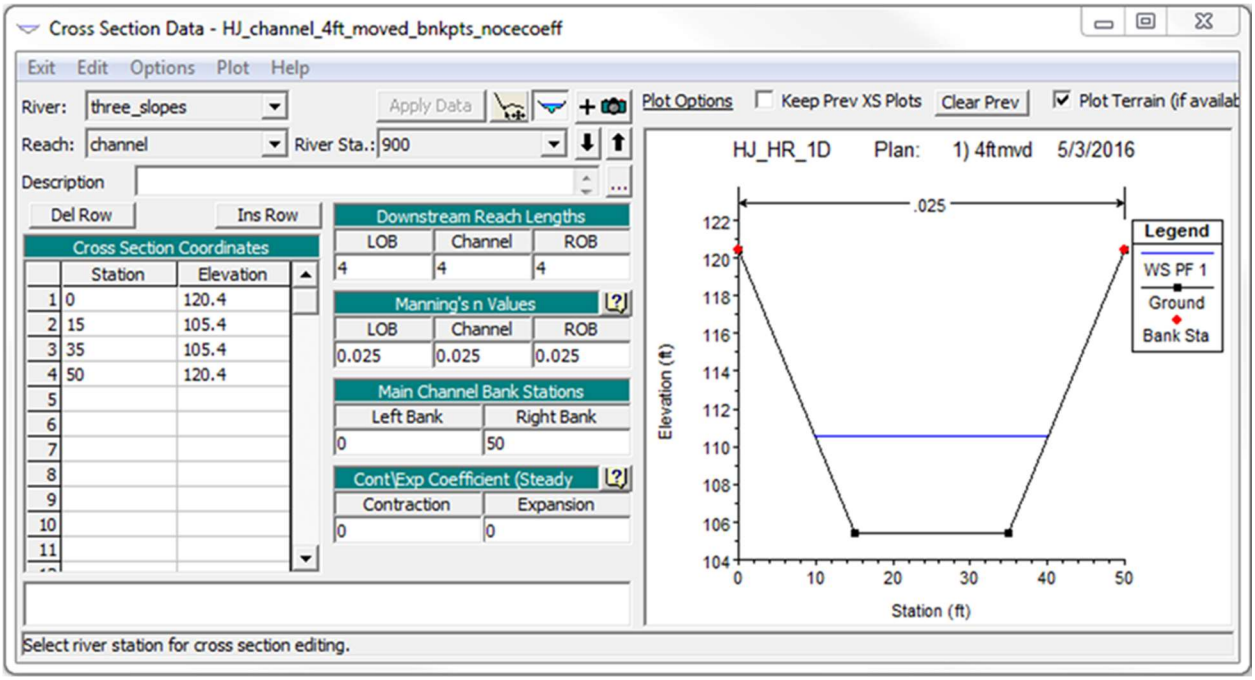

Figure 5-36. Cross Section Data Showing Adjusted Bank points and No Contraction or Expansion Loss Coefficients

One last simulation was performed using the one-dimensional HEC-RAS model for this hydraulic jump test. It finally provided results in close agreement with both the depth-step method and with SRH-2D. The location of the hydraulic jump was properly bracketed by stations 404’ and

408’. The model contained a total of 226 cross sections. It is expected that by further increasing the number of cross sections, at the very least in the sections where depth changes rapidly such as near the hydraulic jump itself, the solution would converge on the same location as determined within the depth-step method spreadsheet.

It is possible that HEC-RAS 1D could provide better results than were achievable within the spreadsheet since HEC-RAS accounts for expansion and contraction losses of the flow, but clearly some problems arise with these when a large number of cross sections are include in the model. The oscillation around critical depth is simply not physically realistic. While that result is certainly not desirable perhaps some manual fine-tuning of these coefficients may produce superior results. This situation was not investigated in this report.

5.8. Two-Dimensional HEC-RAS Hydraulic Jump Test

Lastly, this hydraulic jump test was performed using the two-dimensional capabilities of HEC-RAS 5.0, using both sets of equations offered within the application – the diffusion wave equation and the full momentum equation. The set up was identical for each model, although before each simulation was run the desired equation had to be selected. The upstream boundary condition was a ramped up hydrograph that used an energy grade line of 0.00274 to distribute flow at the inlet. The downstream boundary condition was normal depth with an energy grade line of 0.00062. Both energy grade lines for the boundary conditions were approximated using the nearest average friction slope obtained from the depth-step method spreadsheet (although these could have also been obtained, probably more precisely, from the first and last cross sections from the 1D model). The flow area was composed of 2’ x 2’ square elements. The computational time step used was 0.2 seconds. The model ran for a simulated time of 1 hour. It is possible to allow the model to warm up before the simulation begins, but this step was skipped, and the model was allowed to

start with all cells dry and to just use the boundary conditions to begin the analysis. It was thought necessary to check the option for mixed flow regime profiles, although this may only be required for one-dimensional sections that are connected to a two-dimensional model. The results of each test were saved as maps in the form of rasters within HEC-RAS. These rasters were then opened in ArcMap, and the 3D analyst tool, the interpolate line, was used to extract the water surface elevation data from the channel centerline. Figures 5-37 through 5-49 describe the details above and the subsequent results of the simulations.

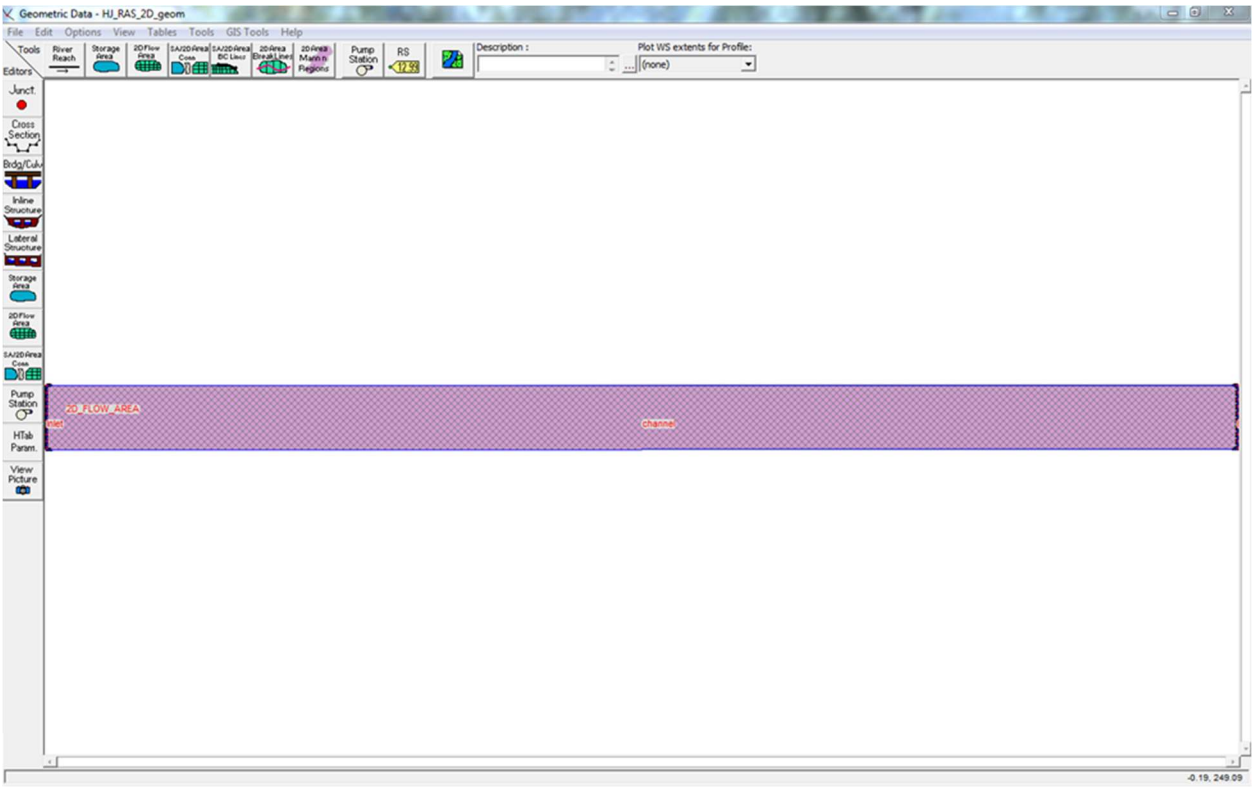

Figure 5-37. 2D Flow Area for HEC-RAS Hydraulic Jump Test Model

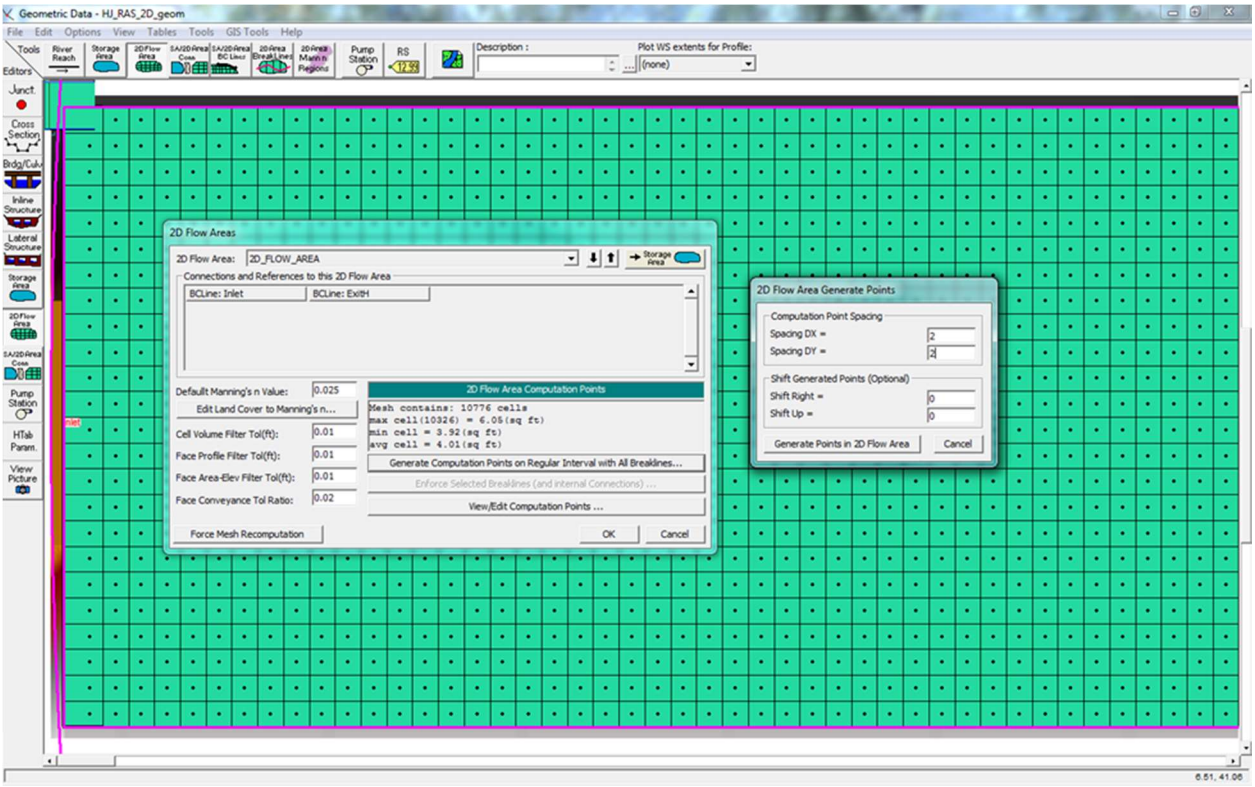

Figure 5-38. Default Manning's Roughness Coefficient and Grid Spacing for the 2D Flow Area

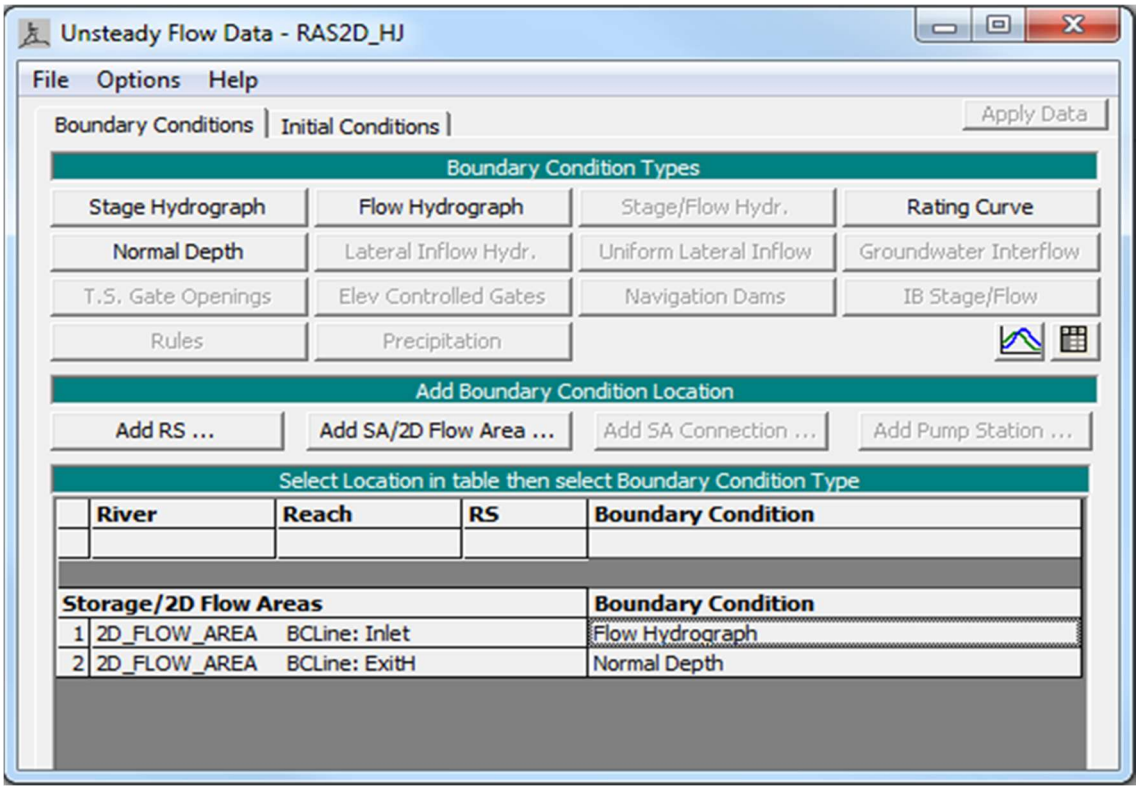

Figure 5-39. Boundary Conditions for the HEC-RAS 2D Hydraulic Jump Test

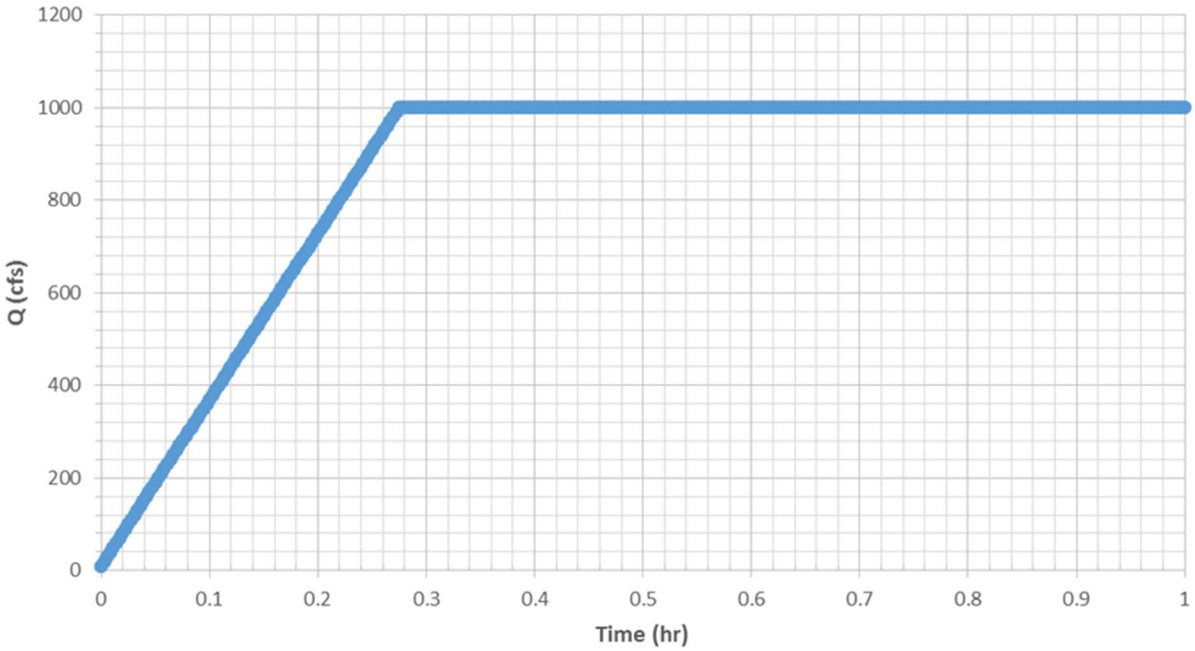

Figure 5-40. Hydrograph Used for the HEC-RAS 2D Hydraulic Jump Test

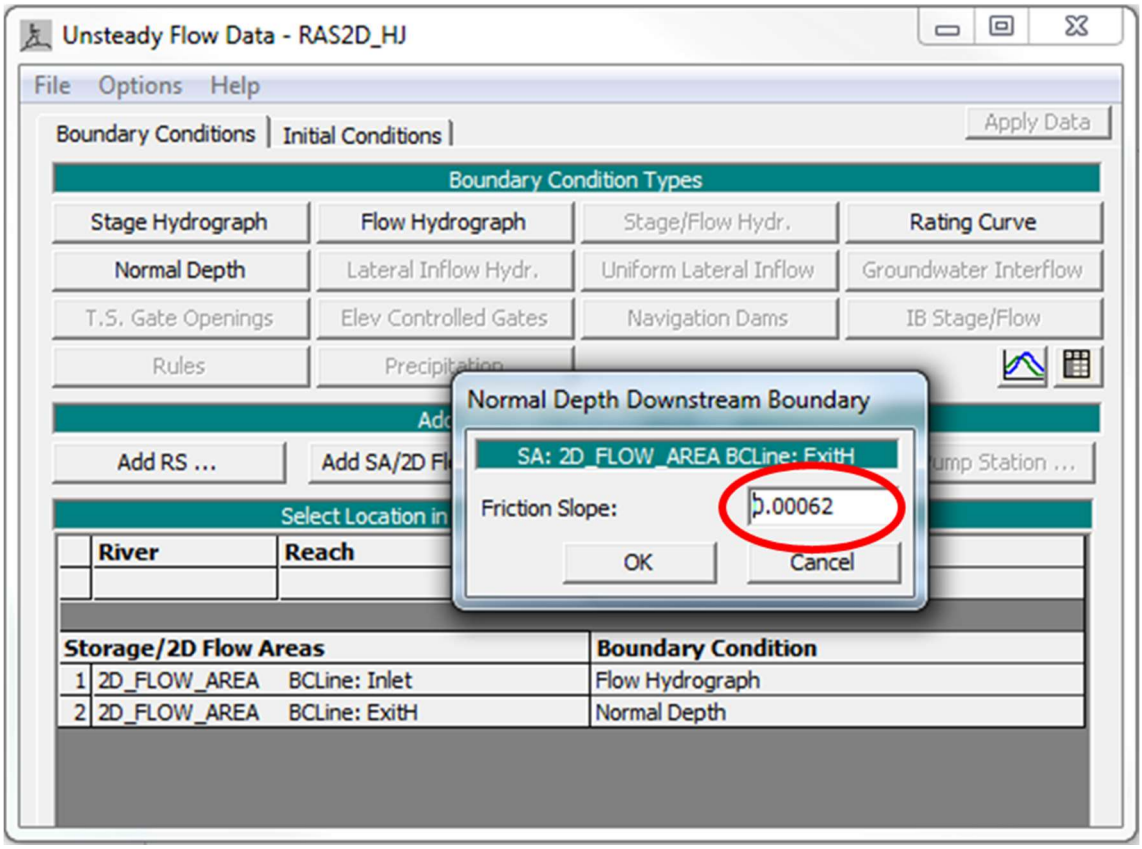

Figure 5-41. Energy Grade Line Slope for Station 900' Used to Distribute Flow at the Exit

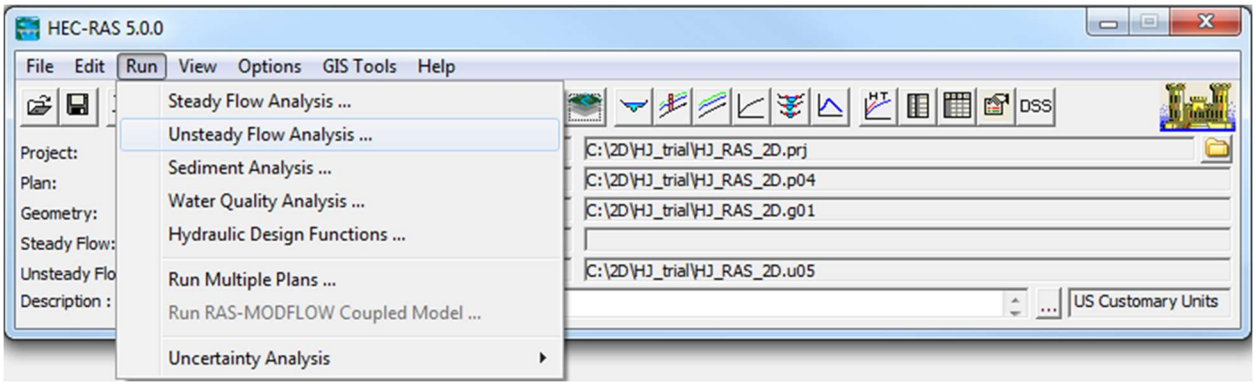

Figure 5-42. Access to Unsteady Flow Analysis Menu from HEC-RAS 5.0 Main Project Window

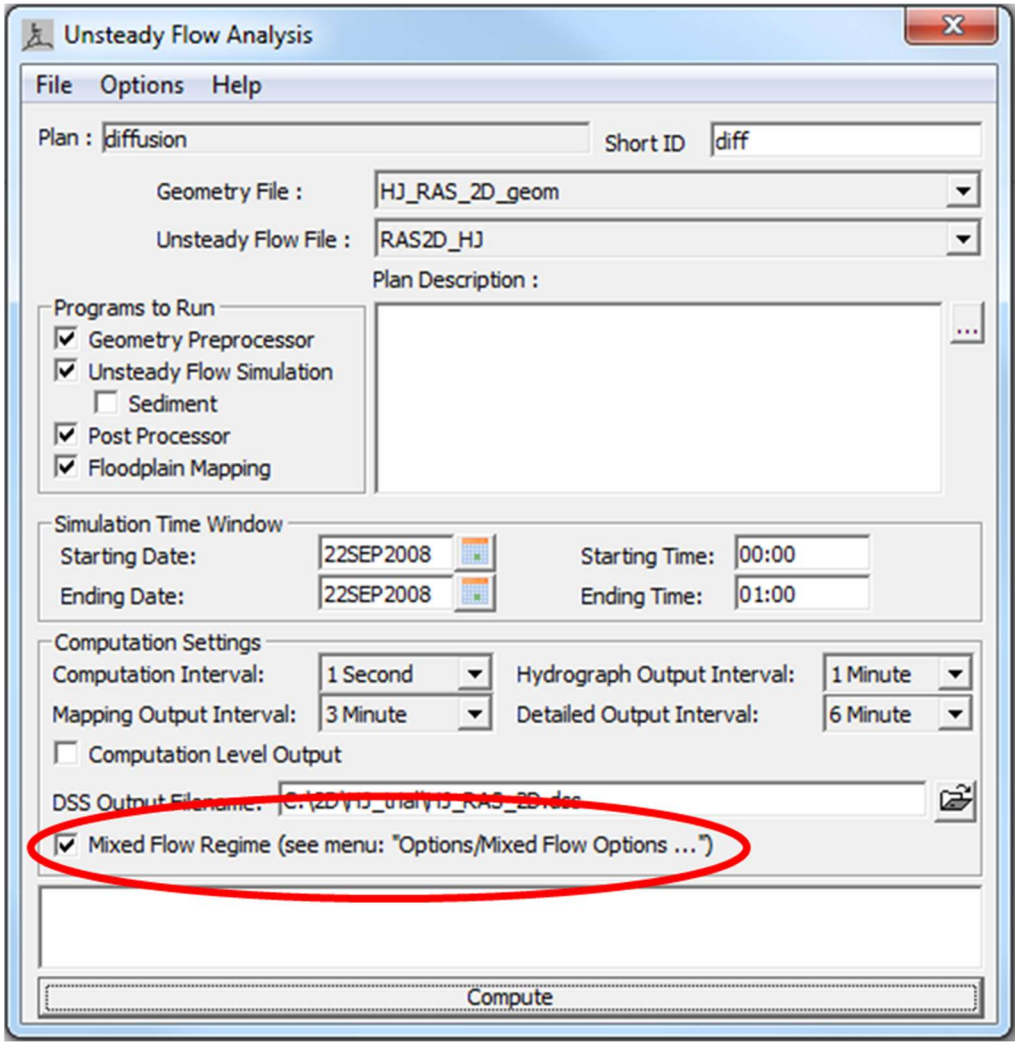

Figure 5-43. Option for Sub- and Supercritical Flow in the Unsteady Flow Analysis Menu

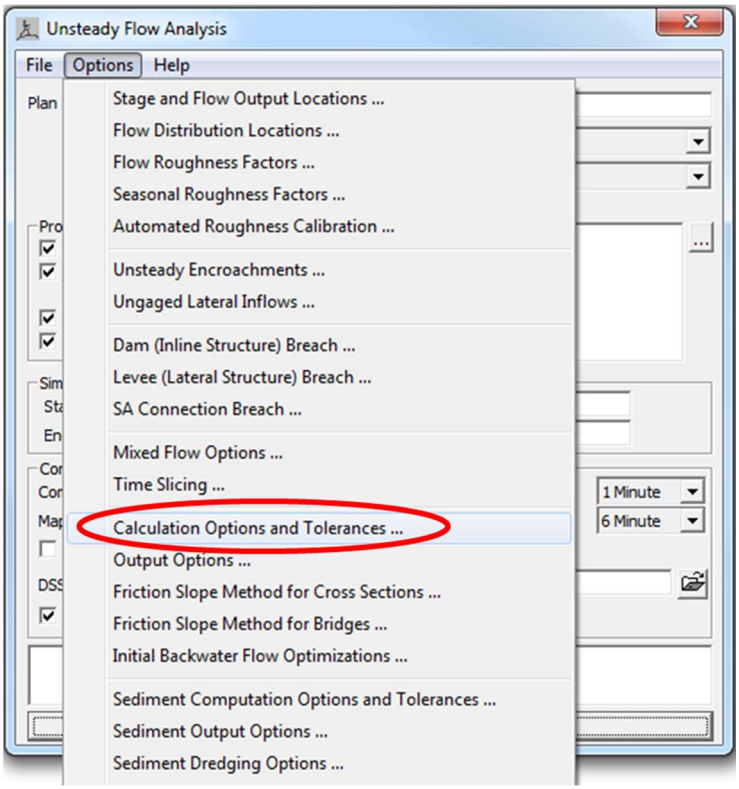

Figure 5-44. Options leading to the Governing Equations Used for Two-Dimensional Simulation

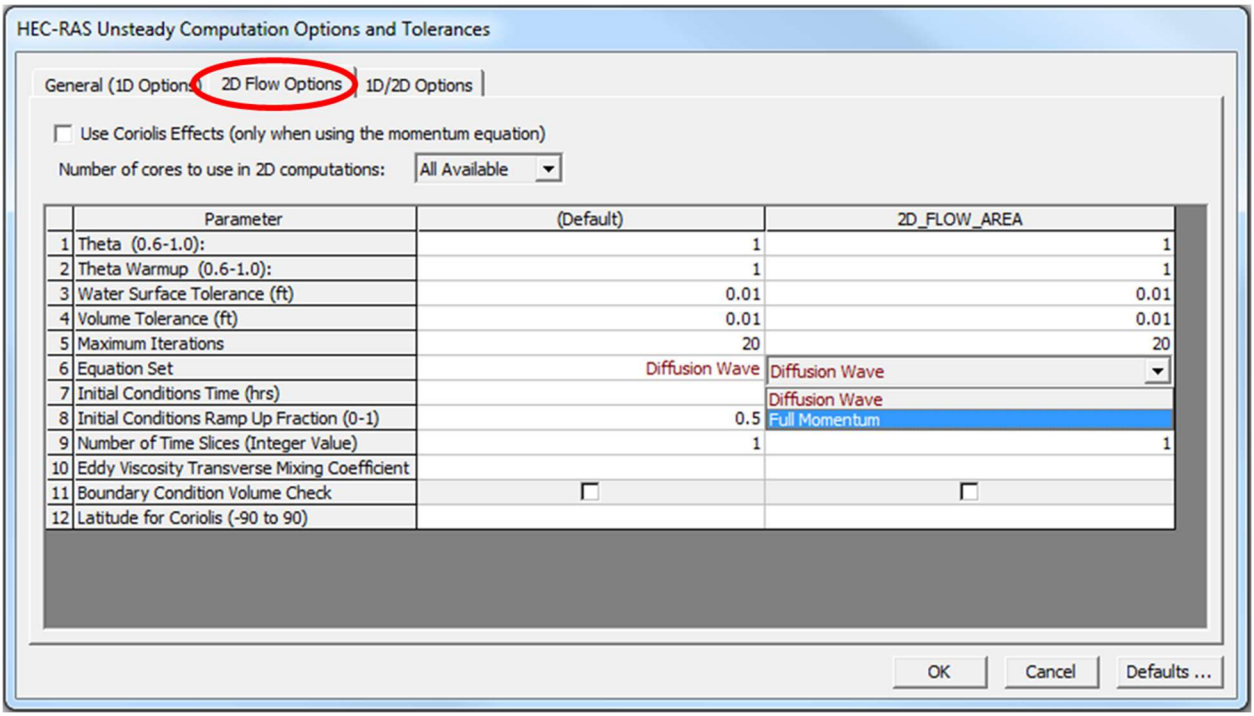

Figure 5-45. Tab Including Options for Selecting Equations of Fluid Motion

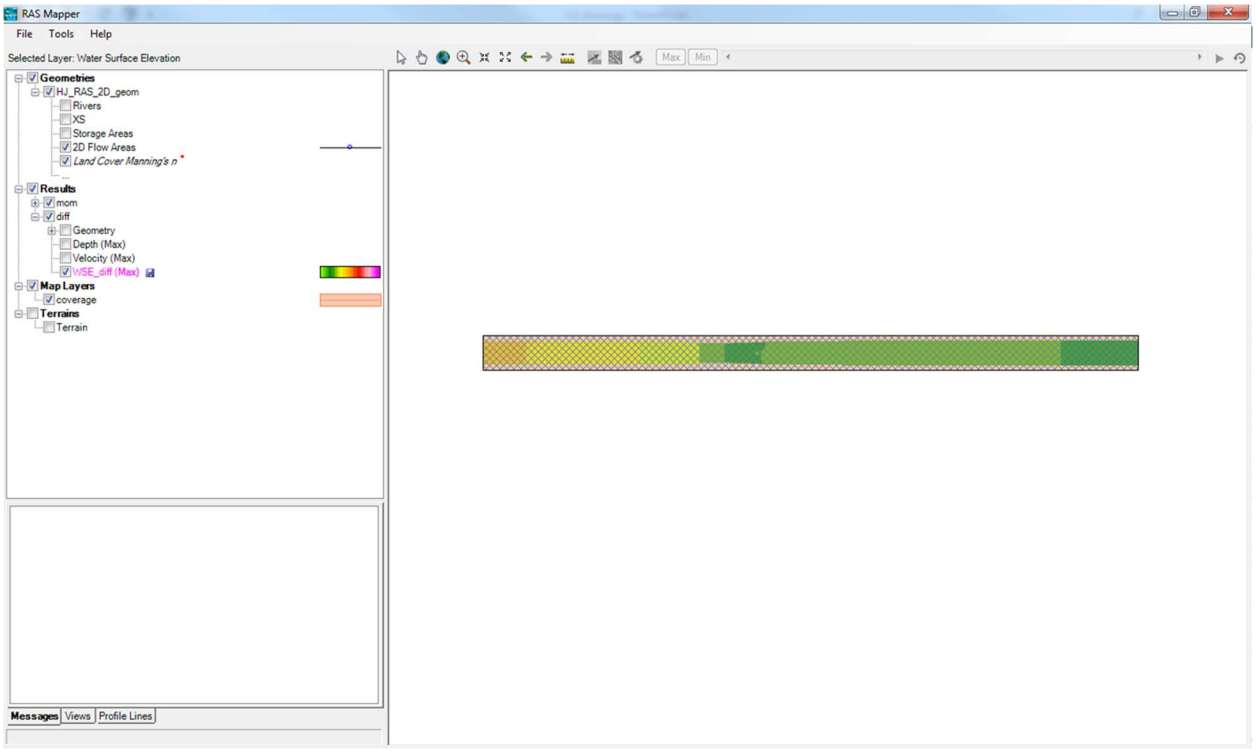

Figure 5-46. RAS Mapper Window Showing Results of the Simulation Using the Diffusion Wave Equation

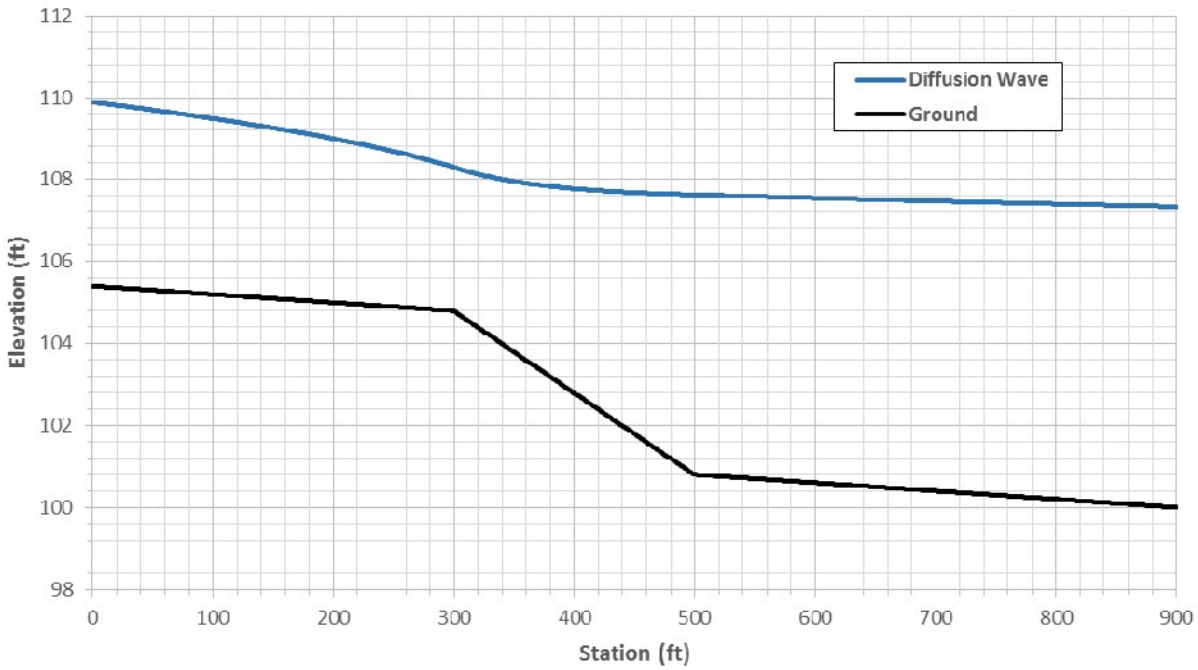

Figure 5-47. Water Surface Profile for HEC-RAS 2D Hydraulic Jump Test Using Simplified Equation of Fluid Motion

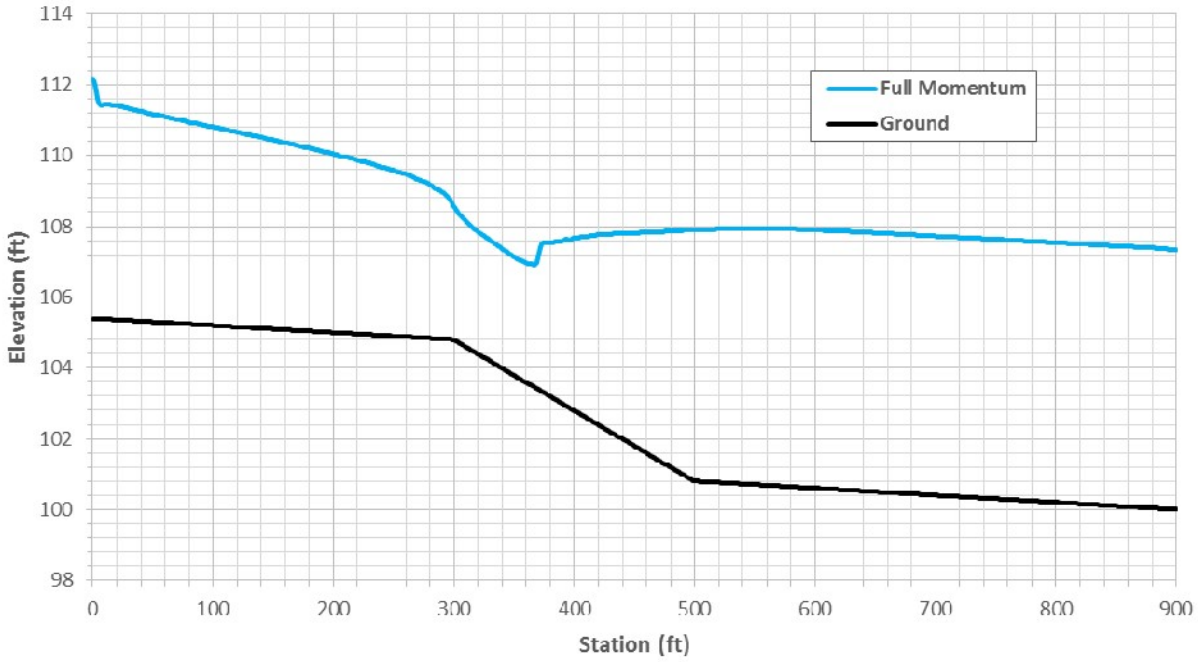

Figure 5-48. Water Surface Profile for HEC-RAS 2D Hydraulic Jump Test Using Saint Venant Equation

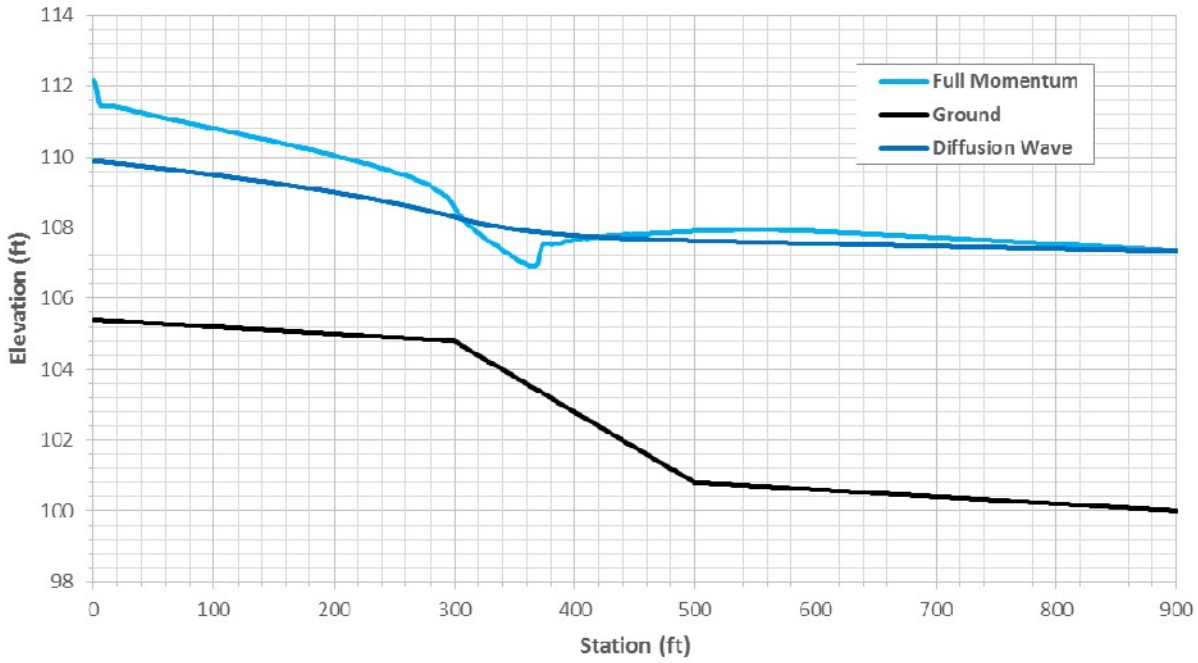

Figure 5-49. Both Water Surface Profiles from HEC-RAS 2D Simulations for Hydraulic Jump Test

From Figure 5-47 it is apparent that the Diffusion Wave equation completely missed the hydraulic jump and thus shows subcritical flow throughout the entire reach. From Figure 5-48 there is some strange behavior at the upstream-most section, where the water starts out very deep, drops rapidly, and then progresses in a more coherent manner. However, the Full Momentum simulation does show a hydraulic jump in the steep section of the channel, and realistically it shows it occurring over some difficult-to-determine distance. The depth increases rapidly from stations 366' to 372', progresses with very marked waves from 372' to about 410', and then continues with smaller waves the whole rest of the length of the steep reach. The hydraulic jump occurs well before the predictions from the depth-step method spreadsheet, SRH-2D, and HEC-RAS 1D. The figure below shows all final profiles determined.

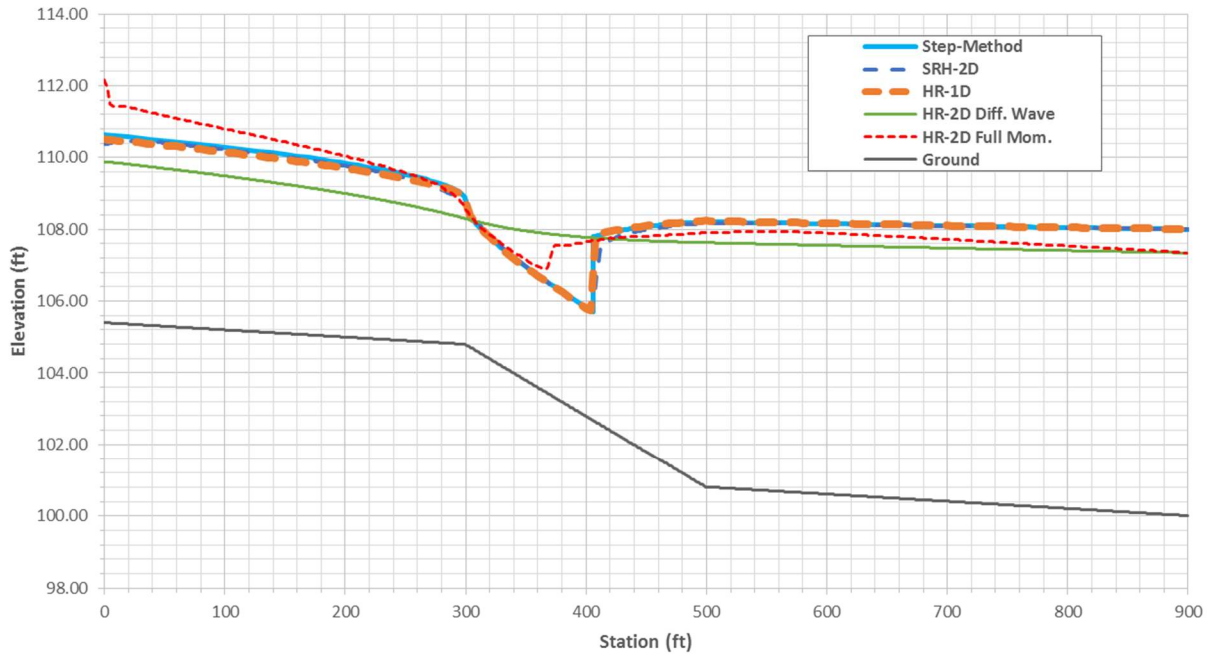

Figure 5-50. Summary of Profiles from Hydraulic Jump Tests

Chapter 6

Bridge Flume Modeling Study

6.1. Background for the Bridge Flume Modeling Study

This chapter seeks to address some concerns raised in the report, "A Model Study of Bridge Hydraulics, Edition 2" (Parr, Milburn, Malone, and Bender, 2010). The original study, performed at the University of Kansas in cooperation with the Kansas Department of Transportation, "[…] was intended to add some insight into the effect of bridge hydraulic features such as ineffective flow regions, weir overflow and flow through skewed bridges". To achieve this goal, a laboratory flume was constructed to do specifically this. Three types of configurations were examined using the flume: the first type was a regular bridge with abutments, bridge piers, and a roadway, the second a simple bridge opening with weir flow in one overbank, and the third a simple skewed bridge. All configurations were tested using a range of flow and tailwater conditions. The laboratory results were then compared to one-dimensional HEC-RAS models. Version 2 of the report contained improvements to the HEC-RAS models based on input provided by Gary W. Brunner, Senior Technical Hydraulic Engineer at the Hydrologic Engineering Center (developers of the HEC-RAS software). His recommendations improved agreement between the HEC-RAS models and the laboratory results. However, the improved models did not overturn a result presented in the initial report – and that is for cases where the Froude number at the downstream bridge face cross section exceeded a Froude number of about 0.7 the water surface profiles upstream of the bridge were largely unaffected by the tailwater conditions (and particularly for the middle-range discharge). For these conditions, the HEC-RAS models assumed inlet control at the bridge section, and the subcritical flow upstream could not sense what was happening downstream

of this critical section. Despite the fact that the laboratory models showed a very definite change in the headwater depth corresponding to a change in the tailwater depth for all cases.

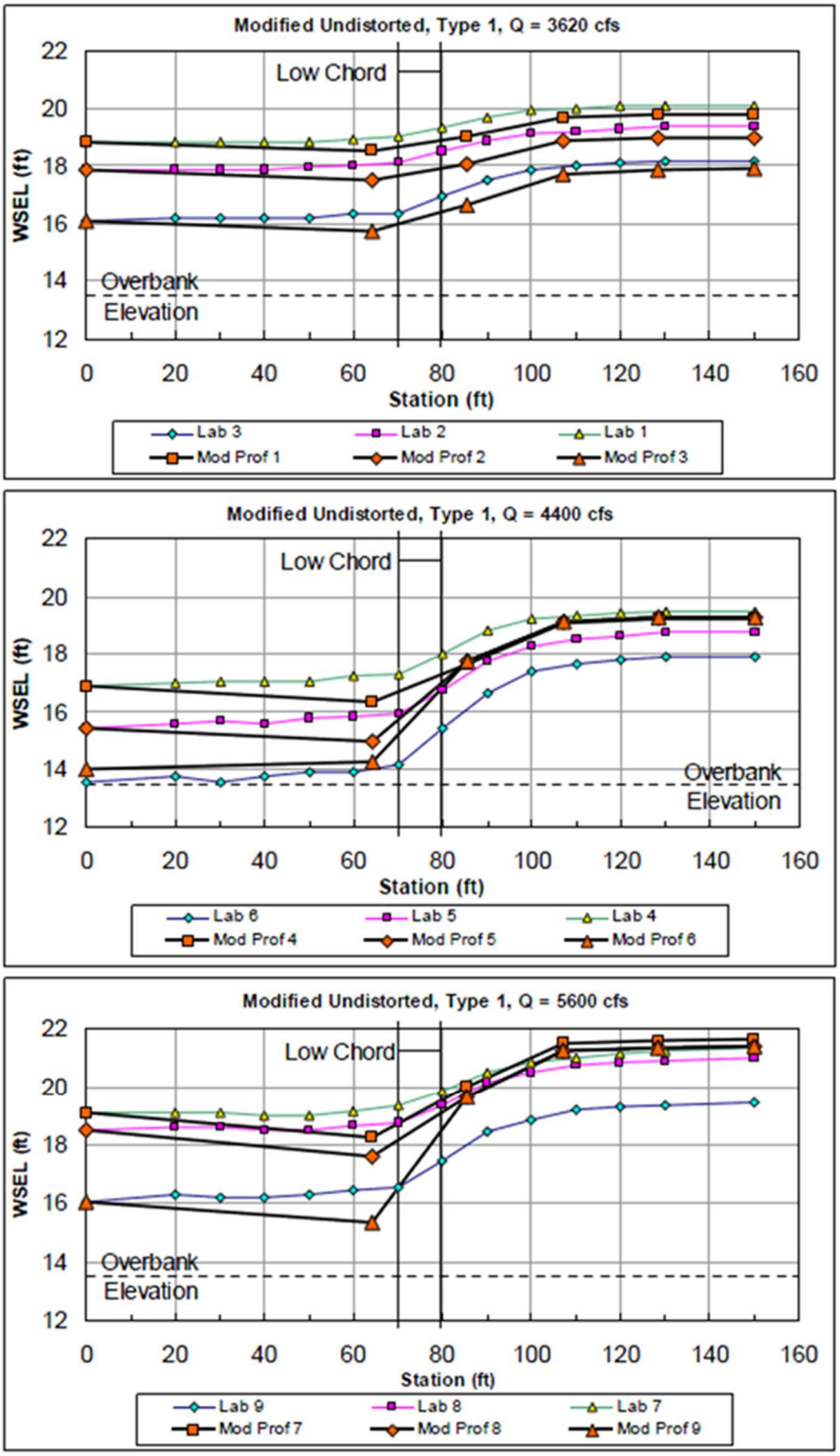

Figure 6-1. Results from Previous Study for the Type 1 Bridge Configuration

It should be noted that, unless stated otherwise, all water surface profiles shown in this chapter are representative of the channel centerline. Now, as can be seen from the plots in the figure above, the results from the type 1 experiments showed that for the middle and high discharges, the undistorted HEC-RAS models (the analyses in the previous report used distorted x and y scales in some places) were only slightly responsive to the tailwater depth. These simulations were run using the previous version of the HEC-RAS software, and they have since been rerun using HEC-RAS 5.0.1 – Figures 6-2 through 6-4 show the subsequent results. They show a slight sensitivity to the tailwater depth, but not one nearly as distinct as was exhibited by the flume model.

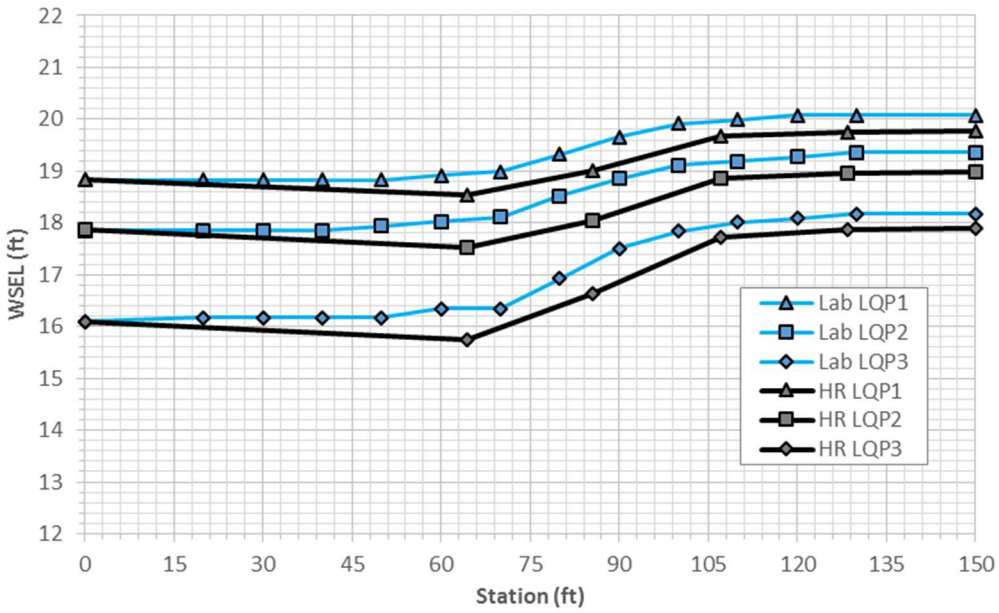

Figure 6-2. Comparison of Lab and Modified, Undistorted 1D HEC-RAS Models from Previous Study for 3620 cfs

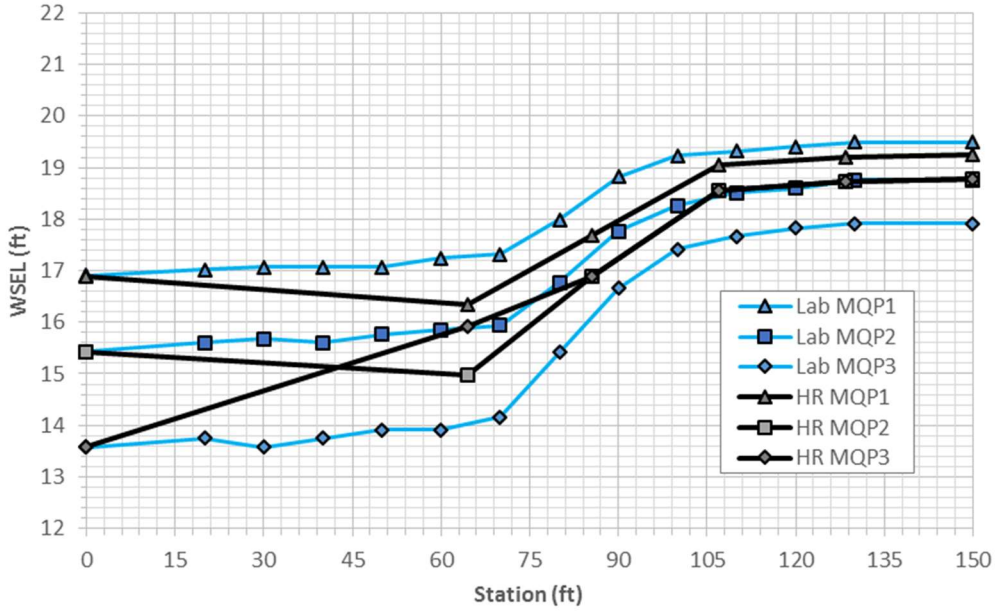

Figure 6-3. Comparison of Lab and Modified, Undistorted 1D HEC-RAS Models from Previous Study for 4400 cfs

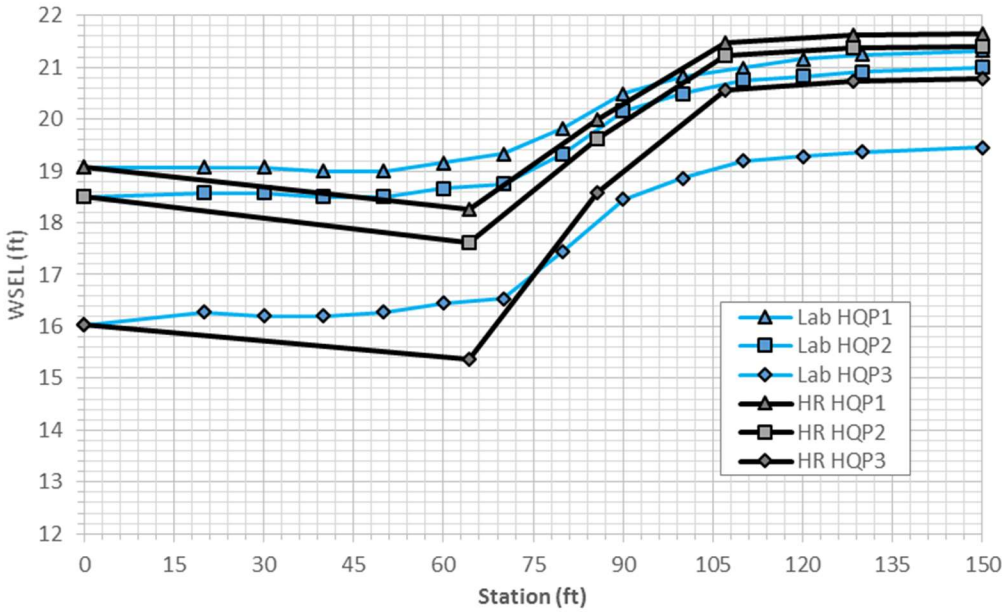

Figure 6-4. Comparison of Lab and Modified, Undistorted 1D HEC-RAS Models from Previous Study for 5600 cfs

The type one bridge experiments for the undistorted case were rerun using HEC-RAS 2D with the full momentum equations and SRH-2D in order to see if these models, which preserve more of the physics of the flow, would exhibit behavior more similar to that seen in the flume.

Since such a great deal of the losses that occurred through this section were due to the rapid contraction and subsequent expansion of the flow, the diffusion equation was not considered for these tests as a preliminary run using that equation set in HEC-RAS showed a total lack of ineffective flow upstream and downstream of the bridge – a result which is far from realistic.

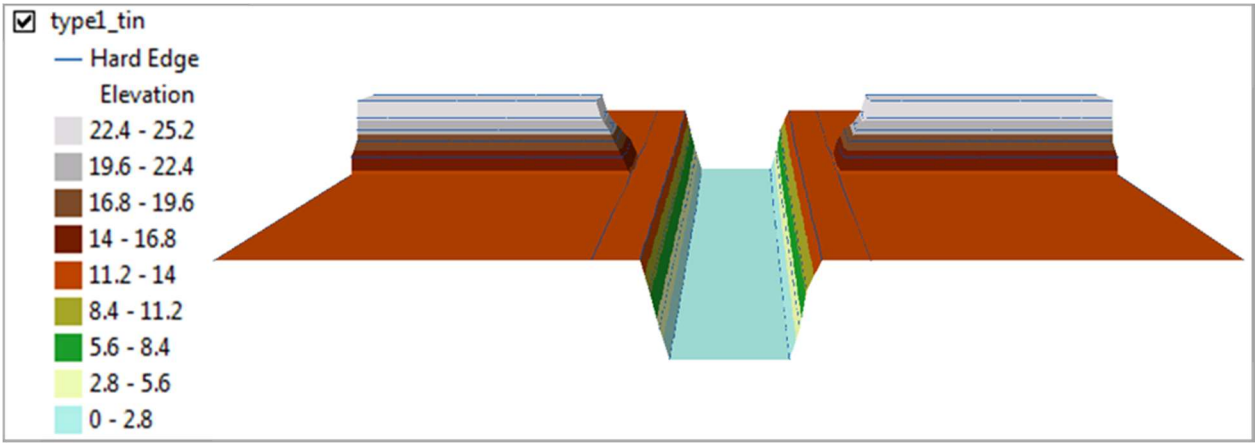

Figure 6-5. View from ArcScene of TIN for Type One Bridge Experiments with Elevations Given in feet

The terrain for use in both the HEC-RAS and SRH-2D models was prepared in ArcMap using the details given in the previous report. This was easily accomplished for the horizontal channel by drawing lines along key features – such as the upper limits of the main channel, toes of the embankments, etc. – and assigning the proper elevations to each line, then using the Feature to 3D by Attribute tool to produce a shapefile capable of being used to generate a TIN. The results of this process can be seen in the figure above. The four circular piers (not shown in the figure above) were also defined in ArcMap. Both models used the same Manning's n value of 0.0233 as in the previous study everywhere except at the locations of the piers in the HEC-RAS model where a Manning's n of 1,000,000 was used to simulate their effect. The SRH-2D model did not need to use this extraordinarily high roughness coefficient as the model is capable of simply generating a "wall" boundary condition line around each pier that does not allow water to cross it. The

hydrographs used for each test were the same for both models and are shown in Table 6-1 and Figure 6-6. Details specific to each model were discussed in their respective sections.

Table 6-1. Ordinates of Hydrographs Used for Type One Bridge Study 2D Simulations

Time (min.)	Discharge (cfs)		
	Low	Mid.	High
0	360	400	500
15	3620	4400	5600
30	3620	4400	5600

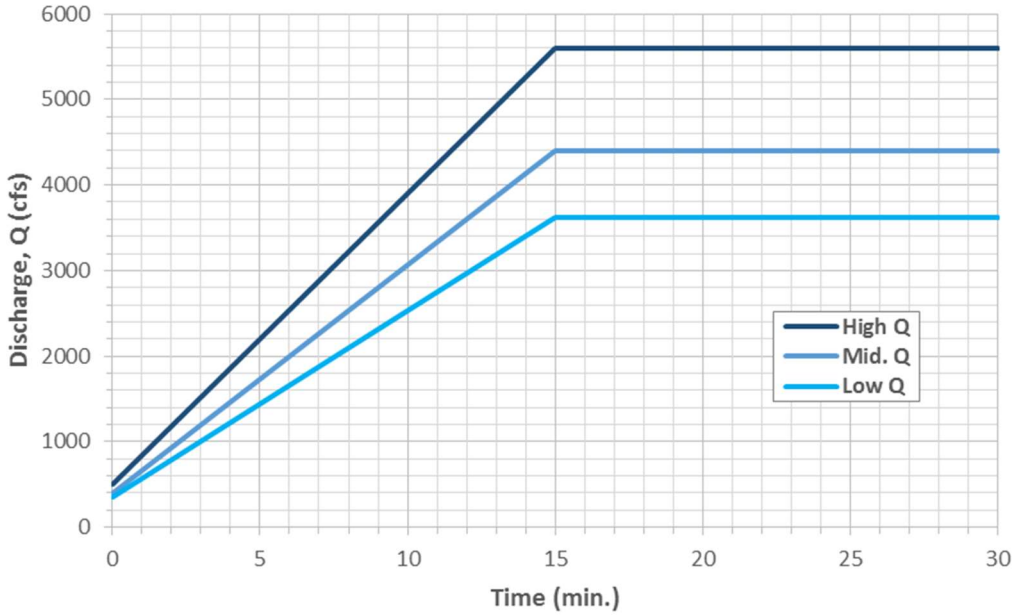

Figure 6-6. Hydrographs Used for Type One Bridge Study 2D Simulations

6.2. HEC-RAS 2D Modeling of Type One Bridge Experiments from Flume Study

The 2D flow area used for the HEC-RAS full momentum model contained elements generated as 2 foot squares, and then the piers were defined by breaklines with 1 foot spacing for cell centers around them which is currently the closest they are allowed to be in HEC-RAS. Some manual editing of cell centers was necessary in order to actually satisfy the 1 foot spacing criteria, but also to ensure that the cell faces near the piers correctly gained the exceptionally high Manning's roughness coefficient of 1,000,000 corresponding to the piers (see figure below).

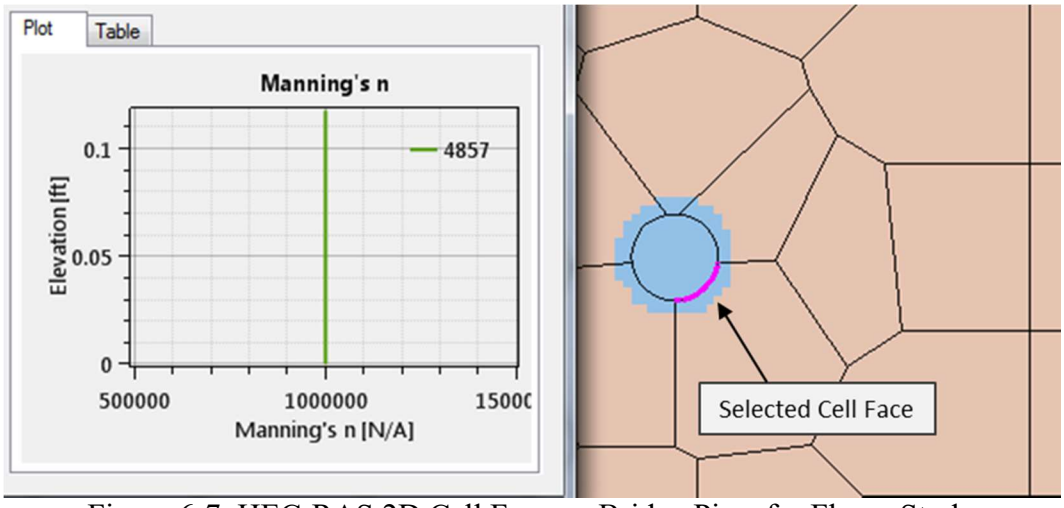

Figure 6-7. HEC-RAS 2D Cell Face on Bridge Piers for Flume Study

In order for the 2D elements of HEC-RAS to capture the Manning's n for the 1.04 foot diameter piers the shapefiles that represented them in the landuse coverage within ArcMap were buffered by 0.2 feet, and when the coverage was brought into HEC-RAS via the RAS Mapper, the coverage polygons were specified to have a grid spacing of 0.1 feet so that the pier polygons would be approximately circular. All of this needed to be done because through practice it's been found that in order for a cell face to have a given roughness coefficient, at least 50% of its length needs to coincide with the coverage type that has that coefficient. Also for this reason, care needed to be exercised to not buffer the pier polygons too much.

The energy grade line for determining the conveyance at the upstream boundary was estimated by comparing the depths recorded in the lab for the two most upstream cross sections. Where the difference in depths between the two sections was equal to zero, the EGL was estimated as 0.0001 – a value considered sufficiently small so as not to have a significant impact on the results. The following table contains the values used for all HEC-RAS 2D simulations.

Table 6-2. Determination of Upstream EGL from Flume Data for HEC-RAS 2D Simulations

Q	Profile	$y_{@x=150}$	$y_{@x=130}$	|del.y/L|	U/S EGL
(cfs)	-	(ft)	(ft)	(ft/ft)	(ft/ft)
3620	1	20.08	20.08	0.00000	0.00010
3620	2	19.36	19.36	0.00000	0.00010
3620	3	18.18	18.18	0.00000	0.00010
4400	1	19.49	19.49	0.00000	0.00010
4400	2	18.77	18.77	0.00000	0.00010
4400	3	17.91	17.91	0.00000	0.00010
5600	1	21.33	21.24	0.00417	0.00417
5600	2	21.00	20.91	0.00417	0.00417
5600	3	19.45	19.37	0.00417	0.00417

The 2D flow area used contained 5163 cells with a maximum size of 6.00 square feet, an average of 4.02 square feet, and a minimum of 0.78 square feet. All RAS-2D simulations were executed with a computational timestep of 0.1 seconds and with a warmup period of 1 hour where the model was allowed to run with the minimum discharge for a given hydrograph and the results at the end of this period would become the initial condition of the simulation proper. While this warmup feature can be very useful for large and complicated sites it was likely unnecessary here, and almost certainly not needed to last for an entire hour. Despite this fact, the HEC-RAS models each took about 20 minutes to run, where the warmup period made up about 7 minutes of that, and this was much faster than accomplished by the SRH-2D simulations (see following section). The results of these simulations using the output from the final timestep at 30 minutes are displayed alongside the flume data in the figures below.

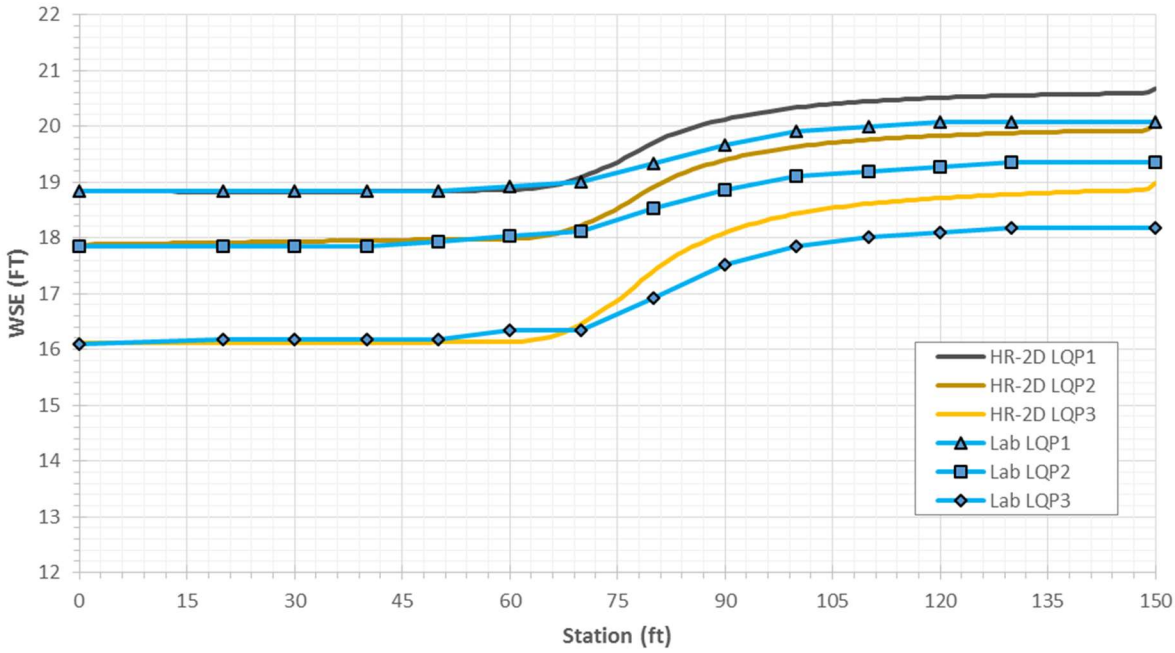

Figure 6-8. Lab and HEC-RAS 2D Full Momentum Equation Model Results for Type One Bridge Configuration and 3620 cfs

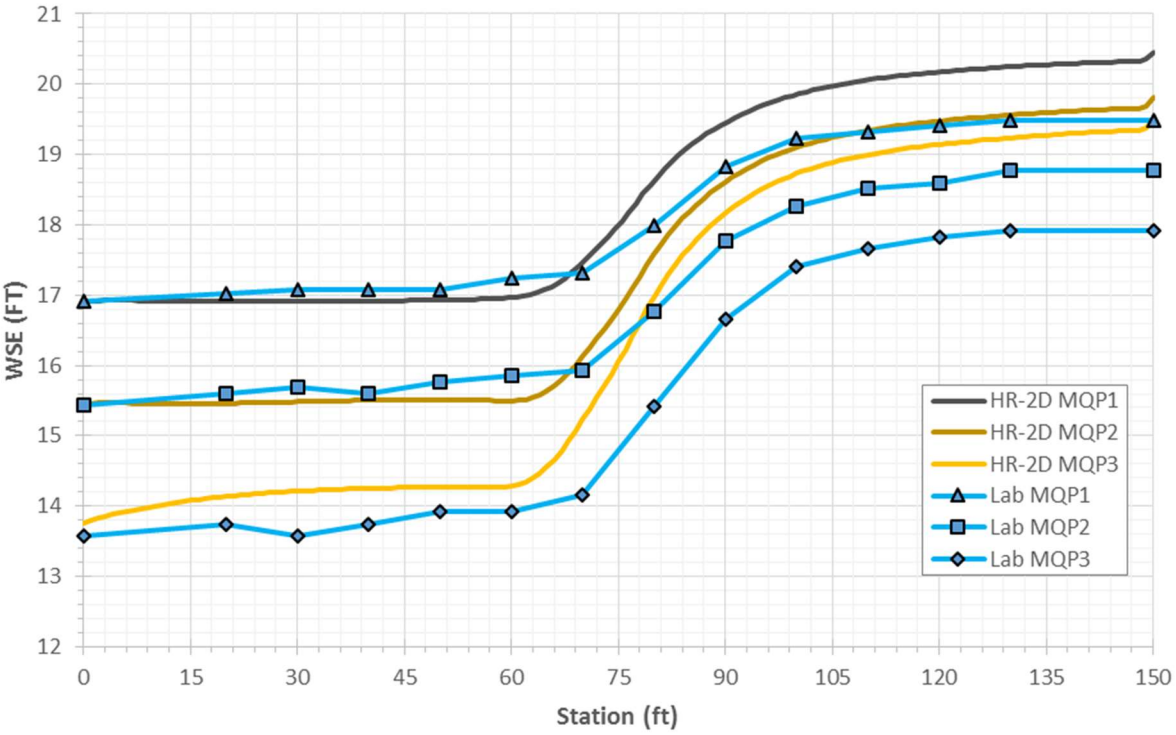

Figure 6-9. Lab and HEC-RAS 2D Full Momentum Equation Model Results for Type One Bridge Configuration and 4400 cfs.

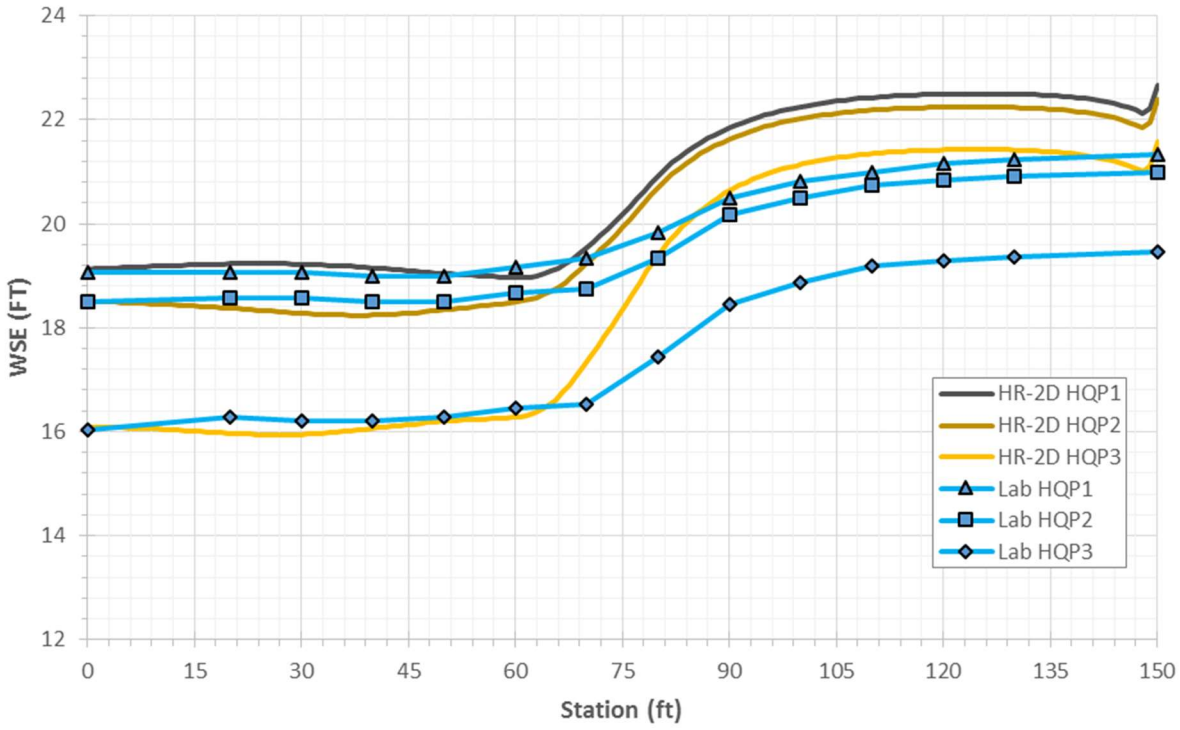

Figure 6-10. Lab and HEC-RAS 2D Full Momentum Equation Model Results for Type One Bridge Configuration and 5600 cfs

The profiles in Figure 6-8 through 6-10 show that HEC-RAS 2D solving the full momentum equations show the relationship observed in the lab – that, for a given discharge, an increase in the tailwater should result in a higher depth upstream of the bridge. However, while this trend exists in the HEC-RAS 2D models, the actual values do not agree well with those observed in the flume. In fact, HEC-RAS 2D overestimates the headwater in every single case. For the lowest discharge (Figure 6-8), the simulated profiles show almost the same sensitivity to tailwater depth as the physical flume model, yet the actual values for the headwater depths are much higher than seen in the flume with the middle RAS-2D profile having approximately the same headwater depth as the highest seen in the lab. For the middle discharge (Figure 6-9), the steps upwards in headwater depth from the HEC-RAS 2D simulations are somewhat similar to those from the lab, but the lowest headwater from the simulations is almost the same as the highest

from the lab. For the highest discharge (Figure 6-10), the pattern between profiles, that the headwater depths between the profiles corresponding the to the highest and the middle tailwater depths are much more similar than those between profiles for the middle and lowest tailwater depths exists, but again, the lowest headwater depth seen in the HEC-RAS 2D results is nearly the same as the highest value from the flume (only slightly lower).

As an explanation for the above it was considered that by increasing the EGL at the inlet the flow would enter the model at a lower depth and a higher velocity. This was not expected to solve the problem as it would likely only introduce new problems and an initial test revealed this was indeed true. Figure 6-11 shows the results for the final timestep of one such test case.

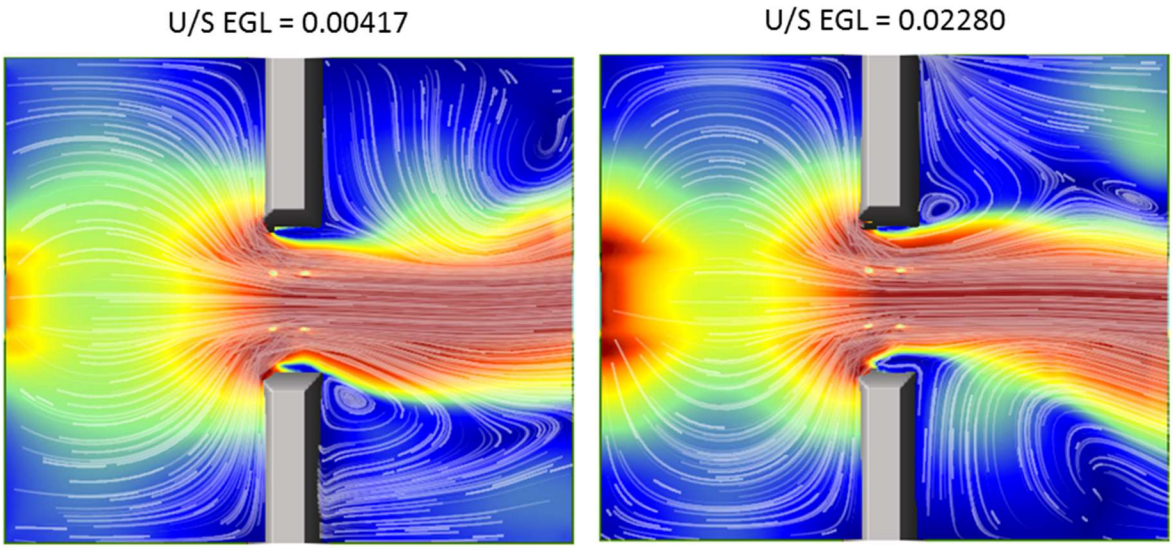

Figure 6-11. Velocity Contour Maps Ranging for 0 to 15 fps with Tracers for the Third High Discharge Profile Using Two Different Upstream EGLs

The image on the left shows the results from the simulation included as the "HR-2D HQP3 series in Figure 6-10, while the one on the right shows a test case using a much higher upstream EGL obtained by dividing the change in depth across the entire reach by the length of the reach. The lowest velocities are represented by dark blue while the highest by dark red. The tracers for the simulation shown in the image at the right show a very unusual and unrealistic flow pattern

that spreads rapidly out from the main channel near the inlet, and then converges again to pass through the bridge opening. This flow pattern resulted in a lower depth at the inlet, but only in the main channel, in the corners of the model at the inlet the depths were actually higher for the case with the EGL equal to 0.02280.

The HEC-RAS 2D full momentum simulations represented in Figures 6-8 through 6-10 all gave very realistic flow patterns downstream of the bridge, where once steady state conditions had been reached at the maximum discharge for a given profile, the flow instability known as vortex shedding began to occur. This was evidenced by the oscillation of the downstream flow from side to side. The higher the discharge the more pronounced the oscillation of this downstream flow, and then even more so for the same discharge when the tailwater was lower.

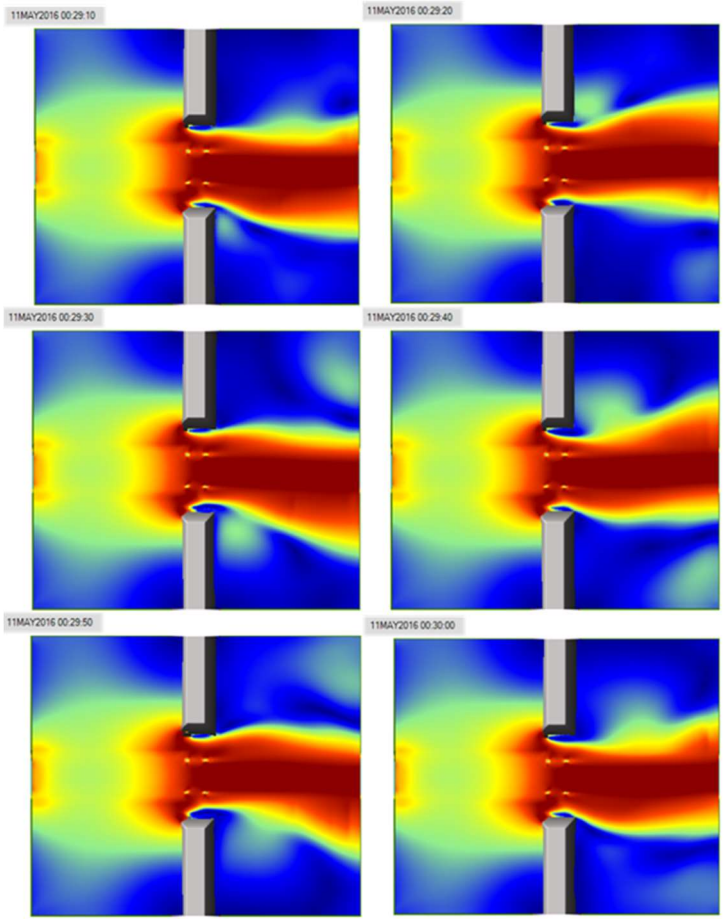

Figure 6-12. Time Series of Velocity Contour Maps Ranging from 0 to 15 fps for the Second Middle Discharge Profile

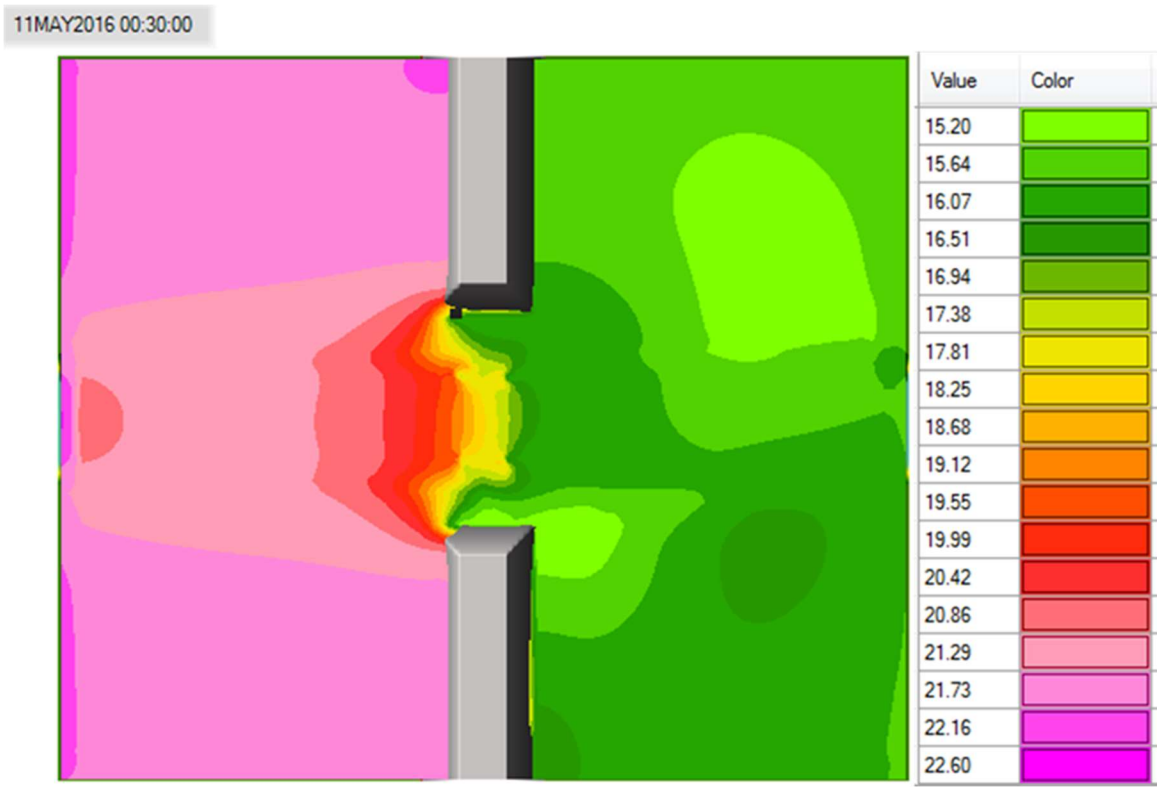

Figure 6-13. Water Surface Elevation Contour Map for the Final Timestep of the Second Middle Discharge Profile

One of the most challenging parts of using one-dimensional HEC-RAS to model bridge openings is the placement of ineffective flow areas. The HEC-RAS Hydraulic Reference manual contains some guidance on establishing where these should be placed, and their locations depend on the expansion and contraction ratios assumed for the incoming and outgoing flow at the bridge. In the manual, the criteria for selecting an acceptable range where the actual ratios might fall suggests that these values are a function of the ratio of the Manning's roughness coefficient of the overbank to that of the main channel, the ratio of the bridge opening width to the total floodplain width, and the longitudinal slope of the channel. Some difficulty arises in that the total width of the floodplain can depend on the contraction and expansion ratios used in the model. Due to this difficulty, the values for the contraction and expansion ratios are often approximated as 1 and 2,

respectively. Figure 6-14 shows the results of one simulation for these bridge tests which more or less showed these values. This profile was the only one with these typical values though.

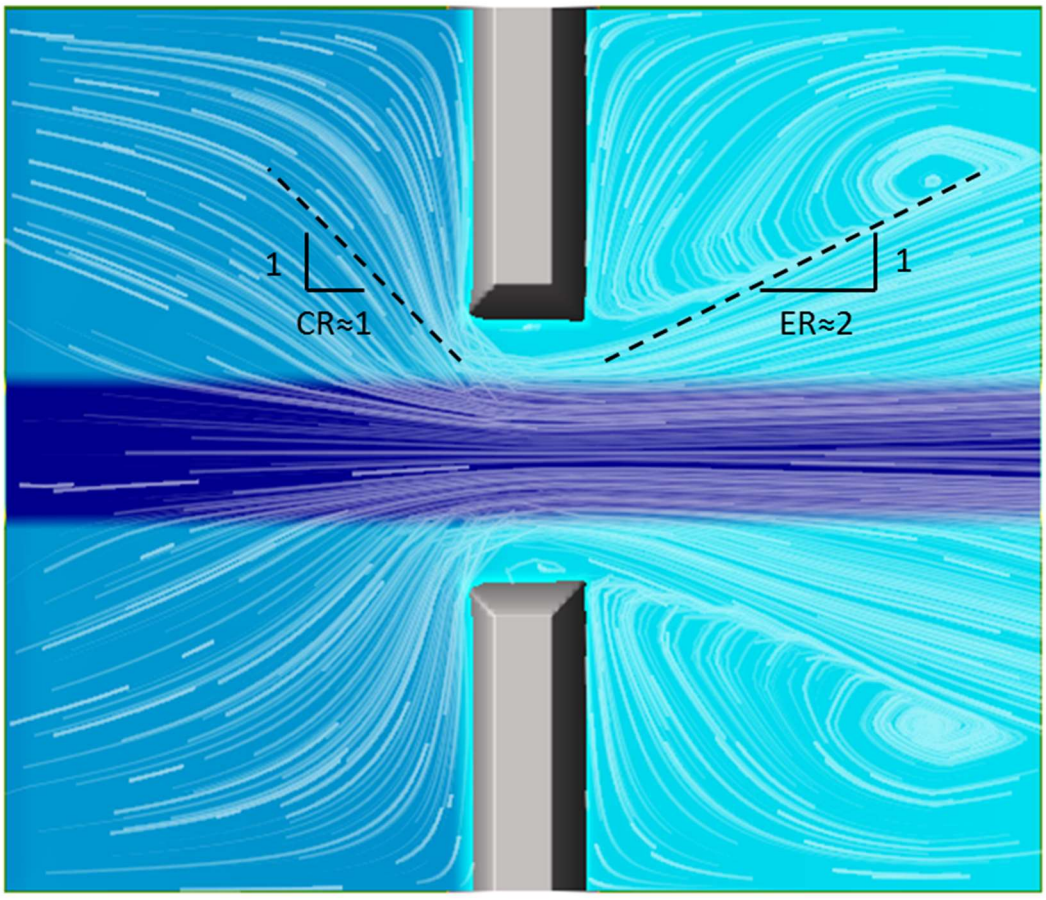

Figure 6-14. Depth Map with Tracers for the Second Middle Discharge Profile Showing Typical Expansion and Contraction Ratios

While the behavior upstream of the bridge was very similar for all profiles, the flow expansion witnessed for the lower discharge profiles was much less pronounced (with almost no expansion occurring) than that seen above. Yet for the highest discharge profiles the expansion was quite drastic. Thus, this shows a case where a simple two-dimensional model may be used to inform a one-dimensional one, if such a thing were judged to be desirable.

6.3. SRH-2D Modeling of Type One Bridge Experiments from Flume Study

The SRH-2D mesh generated in SMS (visible in the figure below) contained elements of various size and shape. The number of elements was densest in the vicinity of the piers and wherever else flow velocities were expected to be highest. There was a combination of both triangles and quadrilaterals. The total quantity of elements was 16,183 with an average cell size of 1.13 square feet, a maximum of 8.84 square feet (found in one of the corners of the model space), and a minimum of 0.02 square feet (found adjacent to one of the piers). It was necessary to draw and enforce breaklines with the correct elevations after mesh generation to properly define the high and low points of the sidewalls of the main channel and to force mesh elements to have the proper elevations near the piers.

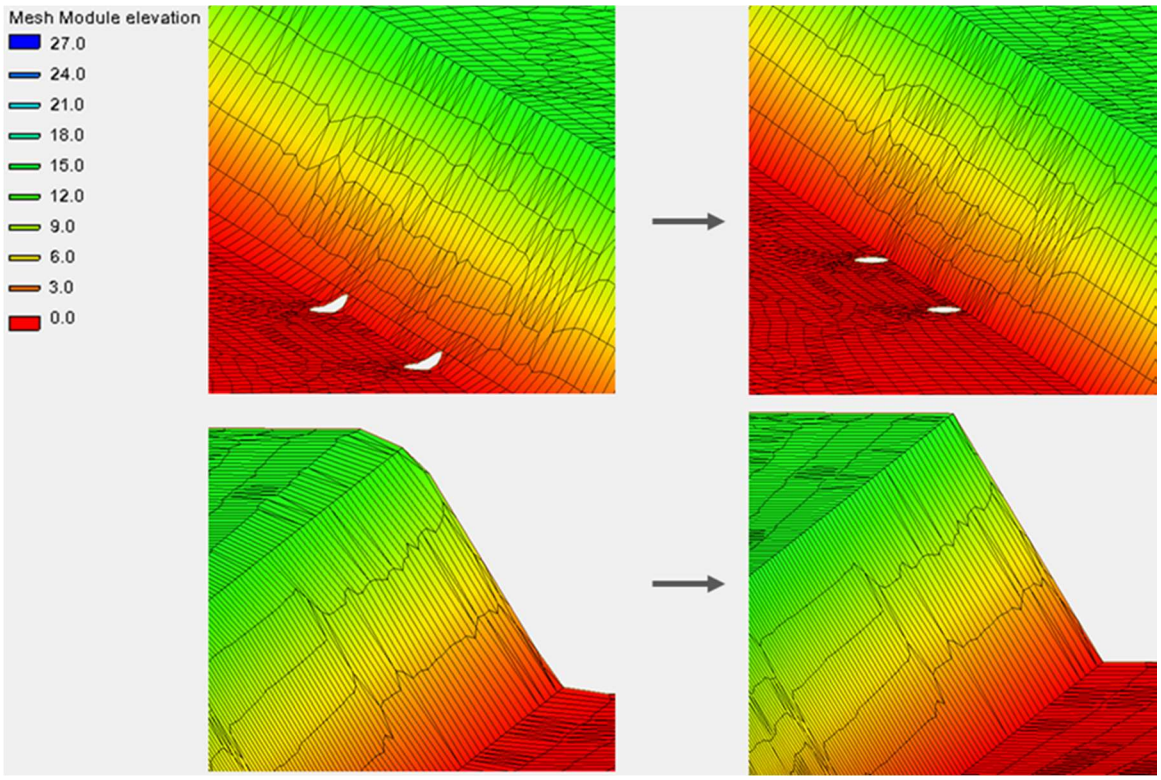

Figure 6-15. Before and After Manual Mesh Adjustment for SRH-2D Bridge Flume Model

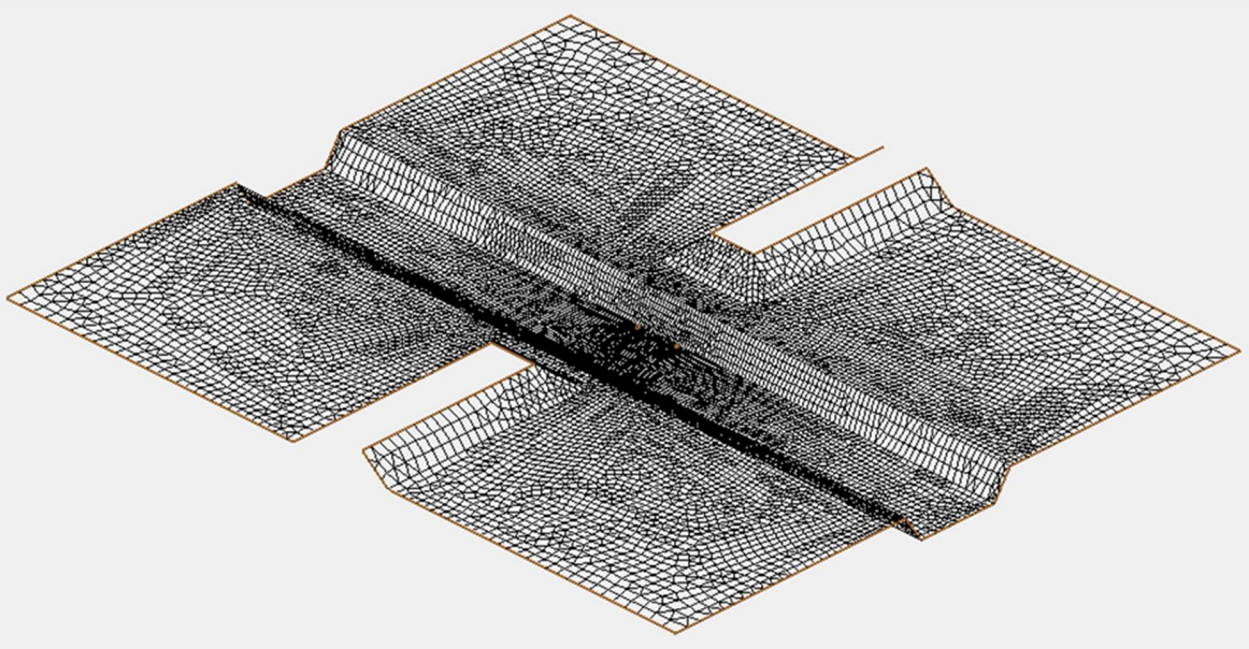

Figure 6-16. Oblique View from SMS 12.1 of the SRH-2D Computational Mesh Used for Type One Bridge Flume Simulations

Once the mesh was suitably defined it was a simple matter setting up the boundary conditions and simulation parameters for each discharge (distributed at the inlet using the conveyance method) and their respective tailwater depths. Every simulation used a timestep of 0.05 seconds and required approximately two hours to run to completion. The results of these tests using the output from the final timestep at 30 minutes of simulation time are displayed alongside the flume data in Figures 6-17 through 6-19.

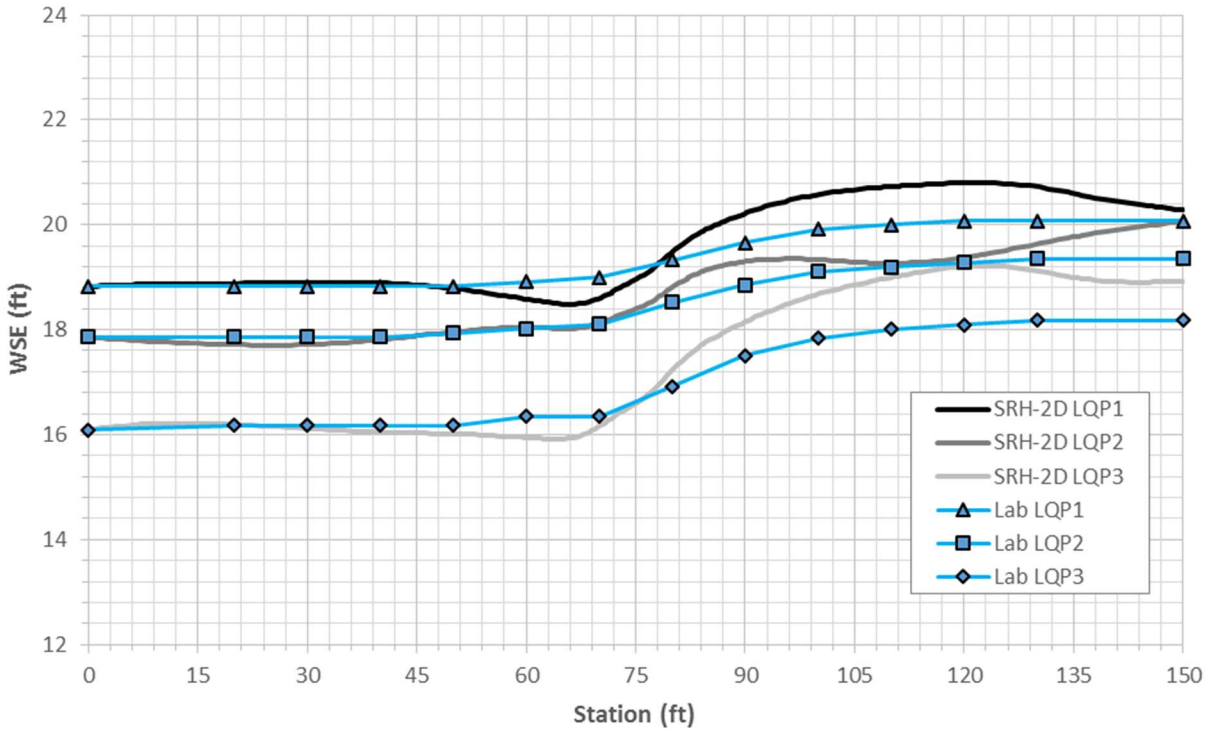

Figure 6-17. Lab and SRH-2D Model Results for Type One Bridge Configuration and 3620 cfs

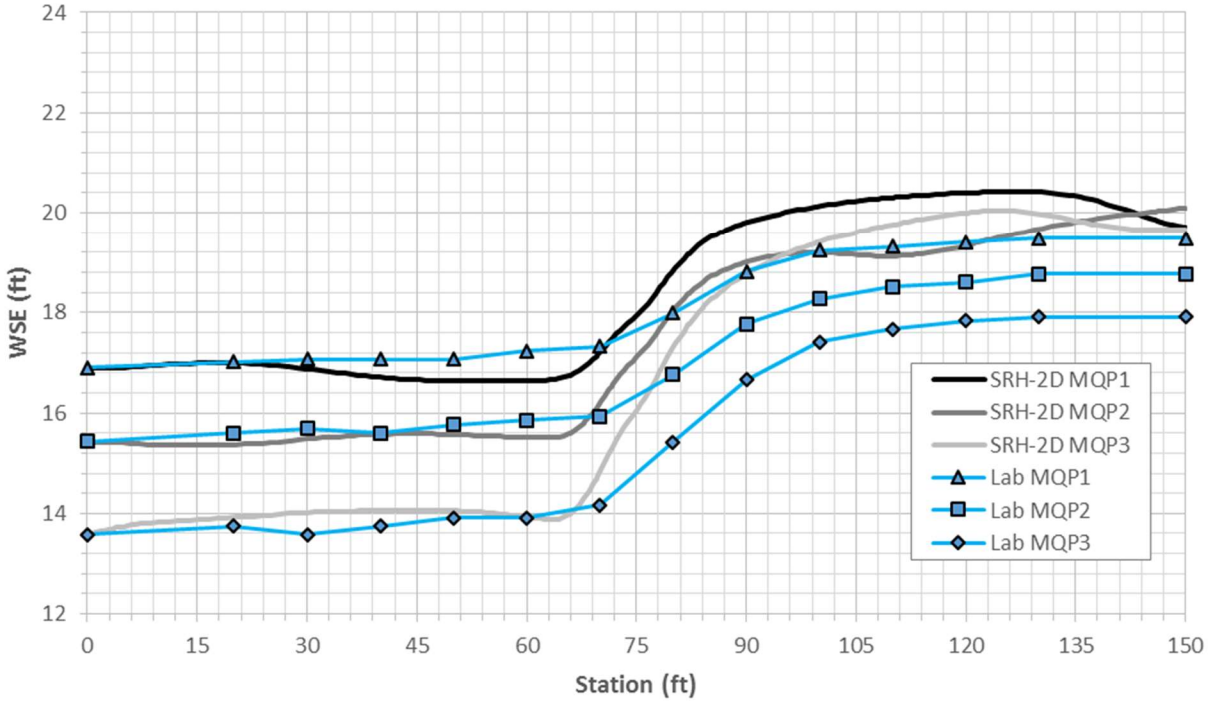

Figure 6-18. Lab and SRH-2D Model Results for Type One Bridge Configuration and 4400 cfs

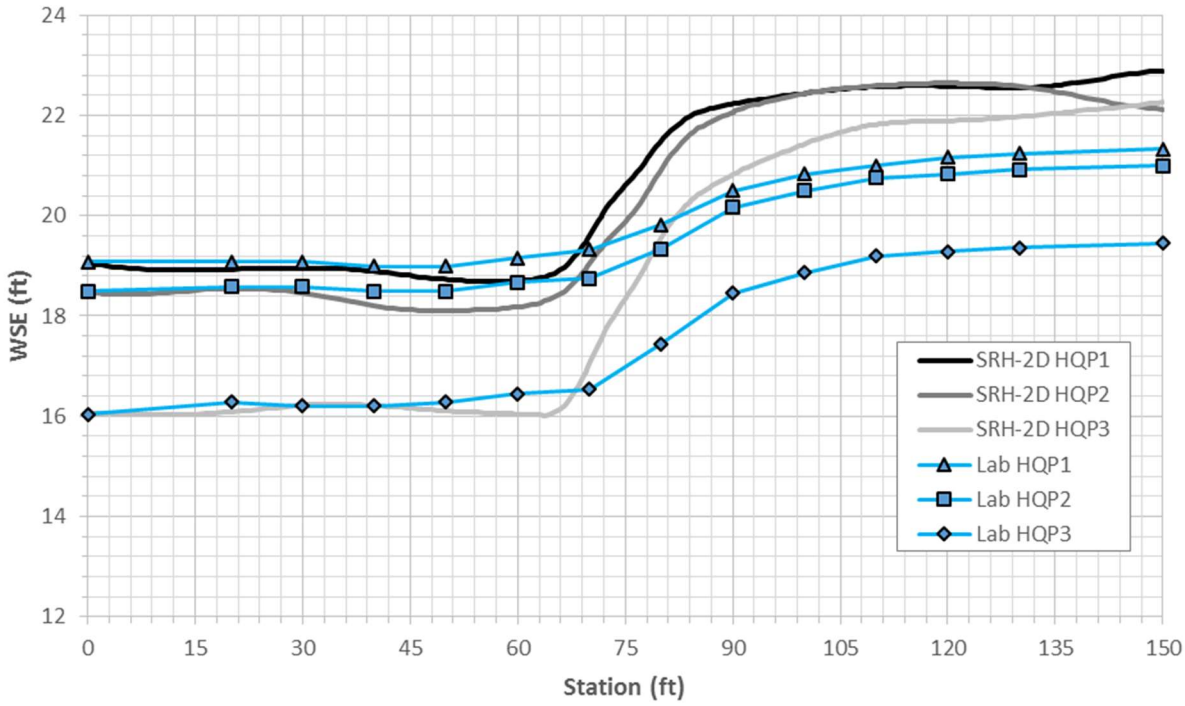

Figure 6-19. Lab and SRH-2D Model Results for Type One Bridge Configuration and 5600 cfs

From these figures it is difficult to determine whether the SRH-2D results show any clear relationship between headwater and tailwater depth for a given discharge. The results from the lowest discharge trials (Figure 6-17) are the only to apparently adhere to the pattern that a higher tailwater depth for the same discharge should result in a greater headwater depth. For the results from the middle and highest discharge trials (Figures 6-18 and 6-19) it would appear that the opposite result as well as the expected result might both be possible – thus really suggesting no pattern at all.

The reason for this is a peculiar flow pattern witnessed for every trial with SRH-2D. Whereas one would expect the flow upstream of the bridge to be relatively stable over time and to see the downstream flow oscillating due to vortex shedding (a result seen in the HEC-RAS 2D simulations), strangely, for the SRH-2D simulations the upstream flow was oscillating back and forth.

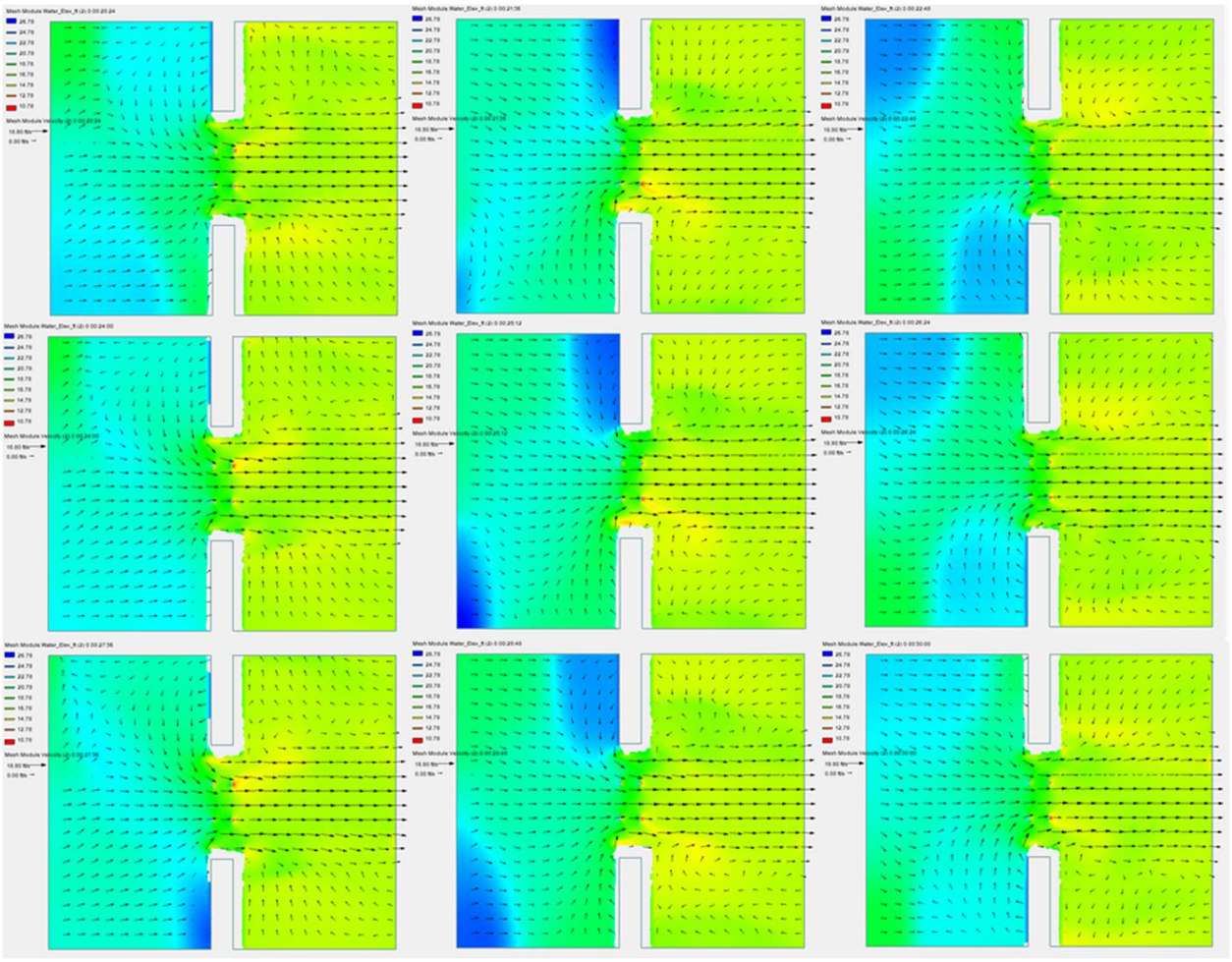

Figure 6-20. Time Series Showing Water Surface Elevation for the Third High Discharge Profile SRH-2D Simulation

The oscillating flow shown in Figure 6-20 had a period approximately equal to the output mapping interval of 0.02 hours (1 minute 12 seconds) or possibly some smaller multiple of this time. For this reason, the depth was averaged for the duration ranging from 15 minutes and 36 seconds to the end of the simulation at 30 minutes. The flows were considered to have reached steady state after reaching their peak discharges at 15 minutes – this was accomplished by visual inspection of the model results, and by considering that in the 36 seconds that elapsed between when the discharges peaked and the timestep when the data for this averaging process began, the

flow in the main channel would need to be travelling at about 4.17 fps to traverse the entire 150 foot length from inlet to exit, and this criteria was easily satisfied by the model results.

Table 6-3. Results for Averaging Process at the Most Upstream Point for SRH-2D Bridge Flume Simulations

Time	Depth (ft)								
(min:sec)	LQP1	LQP2	LQP3	MQP1	MQP2	MQP3	HQP1	HQP2	HQP3
15:36	20.27	19.39	18.61	20.56	19.75	19.73	23.14	22.23	21.12
16:48	20.69	19.99	18.91	20.58	19.98	19.63	23.03	22.53	22.42
18:00	20.25	19.82	18.71	20.60	20.02	19.32	22.91	22.68	22.05
19:12	20.70	19.84	18.87	20.60	19.16	18.91	22.42	22.75	21.92
20:24	20.55	20.00	18.98	20.58	20.09	19.26	22.24	22.81	22.26
21:36	20.23	19.43	18.44	20.54	19.95	19.57	22.99	22.87	21.50
22:48	20.70	19.95	18.91	20.47	19.68	19.77	23.33	22.94	22.41
24:00	20.27	19.99	18.86	20.38	20.02	19.83	23.22	23.03	22.17
25:12	20.69	19.64	18.76	20.28	19.63	19.81	23.07	23.09	21.32
26:24	20.56	19.97	18.97	20.16	20.03	19.76	22.96	23.04	22.41
27:36	20.20	19.68	18.31	20.02	19.99	19.77	22.60	22.85	22.01
28:48	20.70	19.89	18.92	19.85	19.27	19.76	22.17	22.53	22.11
30:00	20.29	20.06	18.93	19.71	20.09	19.65	22.88	22.12	22.26
AVG (ft):	20.47	19.82	18.78	20.33	19.82	19.60	22.84	22.73	22.00
TW (ft)	18.83	17.86	16.09	16.90	15.43	13.58	19.08	18.50	16.03

After accounting for the oscillating depth at the upstream point it becomes clear that the relationship between the headwater and tailwater depths holds true for the SRH-2D simulations as well. Although, like with HEC-RAS 2D, SRH-2D overestimates the depths of flow at the upstream cross section. Besides that, the steps between profiles follow trends similar to those seen in the lab data, where with the low and medium discharges, those steps are fairly uniform, and then for the highest discharge, the difference between the highest and middle headwater depths are much more similar than the middle and the lowest values.

One detail of interest in the hydraulics of channel constrictions is the assumption of inlet control at the entrance of bridges and culverts made in many one-dimensional analyses, and which was likely the culprit for the dubious results given by the previous version HEC-RAS and discussed in the previous report but which does not appear to be so poor in the latest one-

dimensional bridge routines employed by HEC-RAS. This assumption of inlet control depends on the existence of critical depth at the upstream bridge cross section, and while for simple geometries this is a perfectly valid assumption, for complex geometries it will likely not completely apply. Currently the RAS Mapper portion of the HEC-RAS software is not capable of mapping the spatial variation of the Froude number for a given simulation – SMS 12.1, however, is capable of mapping these results of an SRH-2D simulation. The following figure shows the Froude number in the vicinity of the bridge opening for one profile.

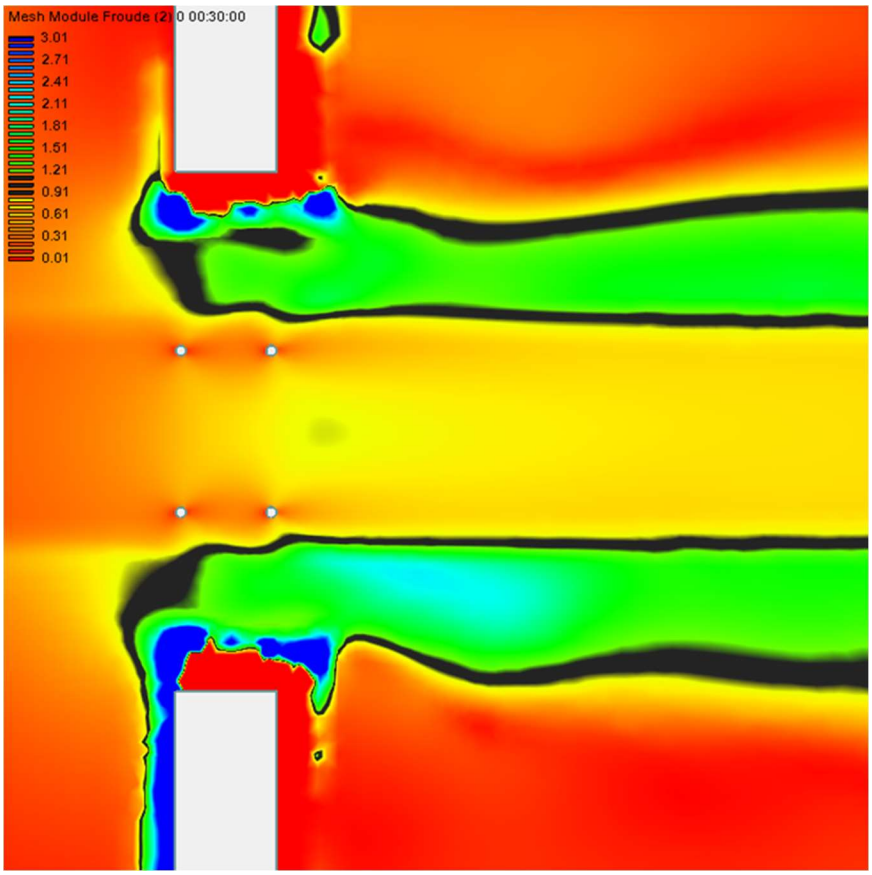

Figure 6-21. Froude Number Contour Map from SMS 12.1 for the Third High Discharge Profile SRH-2D Simulation

In Figure 6-21, Froude numbers greater than or equal to 0.91 yet less than or equal to 1.11 are represented by black and thus are either critical or near critical depth, red to yellow hues represent subcritical flow, and green to blue represent supercritical flow. So, knowing that

subcritical flow is controlled from downstream, and supercritical from upstream, it seems reasonable that for this section which experiences both flow regimes it should be at least partially controlled from downstream.

6.4. Summary of Water Surface Profiles for the Type One Bridge Experiments

Table 6-4. Summary of Water Surface Profiles for the Type One Bridge Experiments

Flow	Profile	Tailwater	Headwater (ft)				HW-TW (ft)				(HW-TW)/L -			
(cfs)	-	(ft)	Lab	HR 5.0 - 1D (GWB)	HR-2D	SRH-2D*	Lab	HR 5.0 - 1D (GWB)	HR-2D	SRH-2D	Lab	HR 5.0 - 1D (GWB)	HR-2D	SRH-2D
3620	1	18.83	20.08	19.78	20.68	20.47	1.25	0.95	1.85	1.64	0.008	0.006	0.012	0.011
3620	2	17.86	19.36	18.99	20.03	19.82	1.50	1.13	2.17	1.96	0.010	0.008	0.014	0.013
3620	3	16.09	18.18	17.89	18.98	18.78	2.09	1.80	2.89	2.69	0.014	0.012	0.019	0.018
4400	1	16.90	19.49	19.24	20.46	20.33	2.59	2.34	3.56	3.43	0.017	0.016	0.024	0.023
4400	2	15.43	18.77	18.77	19.81	19.82	3.34	3.34	4.38	4.39	0.022	0.022	0.029	0.029
4400	3	13.58	17.91	18.77	19.50	19.60	4.33	5.19	5.92	6.02	0.029	0.035	0.039	0.040
5600	1	19.08	21.33	21.65	22.65	22.84	2.25	2.57	3.57	3.76	0.015	0.017	0.024	0.025
5600	2	18.50	21.00	21.41	22.39	22.73	2.50	2.91	3.89	4.23	0.017	0.019	0.026	0.028
5600	3	16.03	19.45	20.78	21.59	22.00	3.42	4.75	5.56	5.97	0.023	0.032	0.037	0.040

*Average over time at steady state conditions

Flow	Profile	Tailwater	(HW - Lab HW)/Lab HW * 100% (ft)			ΔHW (ft)				ΔHW/ΔTW (ft)			
(cfs)	-	(ft)	HR 5.0 - 1D (GWB)	HR-2D	SRH-2D	Lab	HR 5.0 - 1D (GWB)	HR-2D	SRH-2D	Lab	HR 5.0 - 1D (GWB)	HR-2D	SRH-2D
3620	1	18.83	-1.5%	3.0%	1.9%	-	-	-	-	-	-	-	-
3620	2	17.86	-1.9%	3.5%	2.4%	0.25	0.18	0.31	0.32	-0.26	-0.19	-0.32	-0.33
3620	3	16.09	-1.6%	4.4%	3.3%	0.59	0.67	0.72	0.73	-0.33	-0.38	-0.41	-0.41
4400	1	16.90	-1.3%	5.0%	4.3%	-	-	-	-	-	-	-	-
4400	2	15.43	0.0%	5.5%	5.6%	0.75	1.00	0.82	0.96	-0.51	-0.68	-0.56	-0.65
4400	3	13.58	4.8%	8.9%	9.4%	1.00	1.85	1.54	1.63	-0.54	-1.00	-0.83	-0.88
5600	1	19.08	1.5%	6.2%	7.1%	-	-	-	-	-	-	-	-
5600	2	18.50	2.0%	6.6%	8.3%	0.25	0.34	0.32	0.47	-0.43	-0.59	-0.55	-0.81
5600	3	16.03	6.8%	11.0%	13.1%	0.92	1.84	1.67	1.74	-0.37	-0.74	-0.68	-0.70

From Table 6-4 it can be seen that the HEC-RAS 2D full momentum and the SRH-2D results differ only slightly from each other, but both models overestimated the headwater depth in every case. Remarkably, the HEC-RAS 1D model (which took the greatest level of expertise to develop) gave answers most similar to that found in the lab, although for the middle discharge, the one-dimensional model still shows a slight insensitivity to the tailwater depth as suggested by the total lack of change for the headwater depths between profiles 2 and 3.While the HEC-RAS 1D results occasionally underestimate and other times overestimate, but are always rather close to the observed headwater depths, the 2D models both always overestimate the values. The magnitude of this overestimation increases as discharge does, and for a given discharge increases as tailwater

decreases, and it always comparable between HEC-RAS 2D and SRH-2D. Thus, the best agreement occurs at the lowest discharge for the highest tailwater depth, with a 3.0% and a 1.9% overestimation for the RAS-2D and SRH-2D models, respectively, and the greatest deviation from the lab data occurs at the highest discharge with the lowest tailwater depths, with an 11.0% and a 13.1% overestimate from each model. All models seem to agree fairly well at the low discharges, but their accuracy at reproducing the lab results diminishes as discharge increases. This pattern is not as distinct for the one-dimensional model, but for both two-dimensional ones is completely supported by the results – with SRH-2D performing slightly better than RAS-2D at the lowest discharge and the opposite occurring at the highest discharge.

Based upon a measured Manning's roughness coefficient of 0.0141 from the flume tests, Froude number similarity was used to determine the prototype coefficient of 0.0233 that was used in all HEC-RAS 1D models in the previous study, and subsequently, in all two-dimensional models discussed in this report. The dimensional scaling based on the Froude number similarity depends on the depth and velocity of the flow, and thus the Manning's roughness coefficient should vary with the discharge as well as from one profile to the next. The following section considers varying the roughness coefficient for the two-dimensional models using the same discharge and profile as corresponds to the one-dimensional results that already agree with the laboratory value for the headwater depth in order to match the two-dimensional results to that headwater depth observed in the lab.

6.5. Calibration of the Two-Dimensional Models to the Laboratory Results.

The trial selected for calibration purposes was the second profile of the middle discharge, so with a discharge of 4400 cfs and a tailwater depth of 15.43 feet. This was done because the one-dimensional results showed the same headwater depth as the laboratory model. Due to this and the

fact that it used the middle tailwater depth with middle discharge, it was considered fairly representative of all trials. The point selected for comparison was one along the channel centerline 90 feet upstream from the downstream boundary, and thus 4.4 feet upstream from the toe of the upstream embankment. The laboratory value for depth at this point was 17.77 feet.

The Manning's roughness coefficient was the main parameter adjusted throughout these calibration trials, but one trial using SRH-2D also reduced the Parabolic Turbulence constant, K, from the default value of 0.7 to 0.1. The eddy viscosity was not adjusted for the HEC-RAS 2D full momentum model because, as stated in the Chapter 3, this feature currently does not work correctly in HEC-RAS (simulations will fail to run and return an error message if this variable is adjusted). Four roughness coefficients were examined in addition to the one used in the profile simulations, and so the five roughness coefficients used were 0.0233, 0.0141 (that measured from the flume before dimensional scaling), 0.0050, 0.0010, and 0.0001.

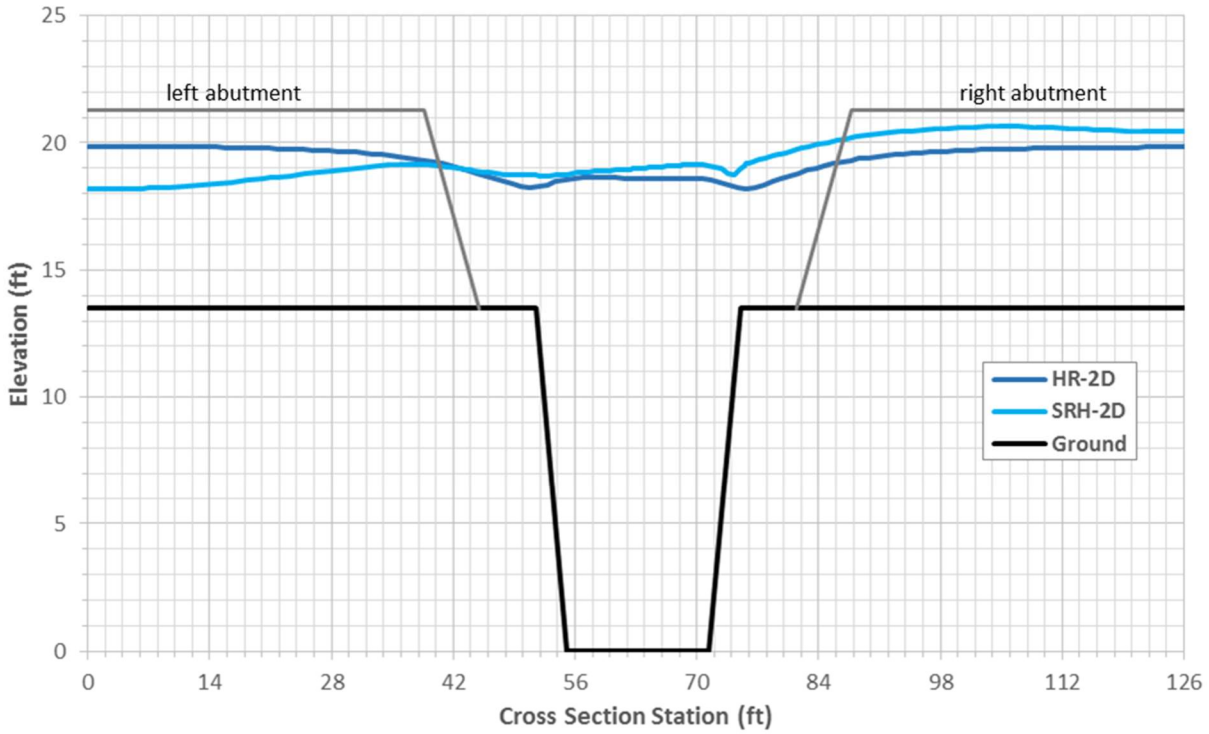

Figure 6-22. Water Surface Profiles at the Cross Section 90 feet upstream for the Final Timestep of the Profile with a Discharge of 4400 cfs and a Tailwater Depth of 15.43 feet

The SRH-2D profile shown in the figure above demonstrates the oscillatory flow described for this model in section 6.3. These results were taken from the final timestep of each simulation, but at the previous timestep (28 minutes and 48 seconds) the SRH-2D results showed that the deeper flow was on the left side of the cross section rather than the right. The HEC-RAS 2D profile is mostly symmetrical around the longitudinal axis along the stream centerline, but the water surface was noticed to undulate up and down with respect to time – perhaps due to disturbances propagating upstream related to the vortex shedding downstream of the bridge. The conditions upstream of the bridge from the HEC-RAS 2D simulations were, however, much more stable than those determined from SRH-2D.

To account for the transient nature of the flow at steady state conditions, the water surfaces at the selected point were averaged over time using data points collected at discrete times in a manner similar to what was done for the upstream point in SRH-2D (section 6.3). From the SRH-2D models data existed every 1 minute and 12 seconds, and so every point available from 15 minutes and 36 seconds to 30 minutes was used. The HEC-RAS models had data available every 10 seconds, but values were only taken every 1 minute starting at 16 minutes and continuing until 30 minutes. This was regarded as appropriate because the depth of flow only varied slightly with time, and because of the rather manual process for retrieving the water depth at the desired point from RAS Mapper the extra effort required to use all available data would not have been worth it. A point was created at the desired location upstream of the bridge in ArcMap, and this shapefile was imported into both SMS and RAS Mapper. In SMS an entire time series for the observation point could be easily extracted and then copied and pasted into Excel, while the data from HEC-RAS had to be mapped to the point separately for every timestep and all trials and then that value had to be manually entered into Excel. Figure 6-23 shows an example of the depth written to this

point in RAS Mapper for one trial. Tables 6-5 through 6-7 show the data collected, the average depth for each trial, and more.

Figure 6-23. Example of Depth at a Discrete Time Mapped to an Observation Point in the RAS Mapper

Table 6-5. HEC-RAS 2D Results for Time-Averaged Depth at a Point Upstream of the Bridge

	n				
	0.0233	0.0141	0.0050	0.0010	0.0001
Time	**y**				
(min:sec)	(ft)				
16:00	18.60	18.61	18.58	18.56	18.60
17:00	18.60	18.60	18.56	18.56	18.55
18:00	18.60	18.59	18.58	18.68	18.54
19:00	18.60	18.63	18.78	18.70	18.69
20:00	18.61	18.67	18.57	18.57	18.64
21:00	18.61	18.68	18.56	18.55	18.58
22:00	18.61	18.68	18.75	18.80	18.60
23:00	18.61	18.68	18.66	18.58	18.63
24:00	18.62	18.68	18.57	18.57	18.63
25:00	18.63	18.67	18.56	18.73	18.63
26:00	18.64	18.66	18.78	18.67	18.62
27:00	18.63	18.65	18.57	18.57	18.61
28:00	18.62	18.63	18.56	18.57	18.61
29:00	18.61	18.62	18.75	18.78	18.61
30:00	18.61	18.62	18.66	18.57	18.61
AVG. (ft):	18.61	18.65	18.63	18.63	18.61
Std. Dev. (ft):	0.01	0.03	0.09	0.09	0.04

Table 6-6. SRH-2D Results for Time-Averaged Depth at a Point Upstream of the Bridge

	n					
	0.0233	0.0141	0.0050	0.0010	0.0001	0.0001
	K					
	0.7	0.7	0.7	0.7	0.7	0.1
Time	y					
(min:sec)	(ft)					
15:36	18.74	18.06	17.89	18.10	18.10	17.89
16:48	18.71	18.27	17.91	18.01	18.01	18.07
18:00	18.66	18.39	18.02	17.64	17.64	18.10
19:12	18.69	18.27	18.06	18.24	18.24	18.18
20:24	18.49	18.34	17.67	17.93	17.93	17.98
21:36	18.42	18.27	18.22	17.68	17.68	17.85
22:48	18.50	18.10	18.03	18.11	18.11	17.76
24:00	18.67	18.03	17.82	17.84	17.84	17.82
25:12	18.79	18.23	17.99	17.87	17.87	17.91
26:24	18.74	18.41	17.99	17.92	17.92	18.00
27:36	18.68	18.25	18.11	17.94	17.94	18.02
28:48	18.64	18.35	17.75	17.95	17.95	18.00
30:00	18.69	18.29	18.27	17.82	17.82	17.90
AVG. (ft):	18.65	18.25	17.98	17.93	17.93	17.96
Std. Dev. (ft):	0.11	0.12	0.17	0.17	0.17	0.12

Table 6-7. Comparison of the Calibration Test Results from Both Two-Dimensional Models to the Laboratory Depth of 17.77 feet

Model	n	K	y	Simul. y - Lab y
	-	-	(ft)	(ft)
HEC-RAS 2D Full Momentum	0.0233	-	18.61	0.85
	0.0141	-	18.65	0.88
	0.0050	-	18.63	0.87
	0.0010	-	18.63	0.86
	0.0001	-	18.61	0.84
SRH-2D	0.0233	0.7	18.65	0.88
	0.0141	0.7	18.25	0.48
	0.0050	0.7	17.98	0.21
	0.0010	0.7	17.93	0.16
	0.0001	0.7	17.93	0.16
	0.0001	0.1	17.96	0.19

The HEC-RAS 2D model showed virtually no sensitivity to the Manning's roughness coefficient used. This is a surprising outcome in light of the results discussed in Chapter 3 of this report, where the geometry for the test reach in that section involved a series of channel

constrictions not totally unlike what was being modeled here, and where the model showed a strong sensitivity to the roughness coefficient. The SRH-2D models showed some sensitivity to the roughness coefficient, but even when the coefficient used was as low as 0.0010, the calculated depth still exceeded the laboratory value by 0.16 feet. Further reduction of the roughness coefficient to 0.0001 (10^-4) netted no corresponding decrease in the depth – suggesting a bottom limit for the decrease in depth achievable by reducing the Manning's n. An attempt was made to run an SRH-2D simulation using a roughness coefficient equal to 0.00001 (10^-5) but the code could not converge on a solution no matter how small the timestep. Since the bulk of the head losses through this reach were local effects associated with the bridge, reducing the parabolic turbulence constant, and thus reducing energy dissipation in the eddies, would lead to a corresponding decrease in the depth. However, this was not the case – in fact, the depth increased slightly when a lower value for K was used – seemingly contradicting the results presented in Chapter 3. It is unknown if these results were particular to the discharge and the tailwater depth used or if similar results would be found by doing this same analysis for one of the other eight flow profiles discussed in this chapter. It is possible that if the eddy viscosity term could be adjusted in HEC-RAS when performing a 2D analysis with the full momentum equations, then that type of analysis could be an excellent match with the laboratory data. Further investigation may be warranted.

Chapter 7

Neodesha Floodplain Study

7.1. Background for the Neodesha Floodplain Study

The complexity of the Neodesha site is of particular interest to hydraulic modelers of river systems. HEC-RAS 1D, HEC-RAS 2D run with the full momentum equations, and SRH-2D were all used to model a section of the Fall River upstream of where it joins the Verdigris River. The city of Neodesha, KS (Wilson County) exists at the confluence of these two rivers. The following image in Figure 7-1 delineates the boundary of the model space.

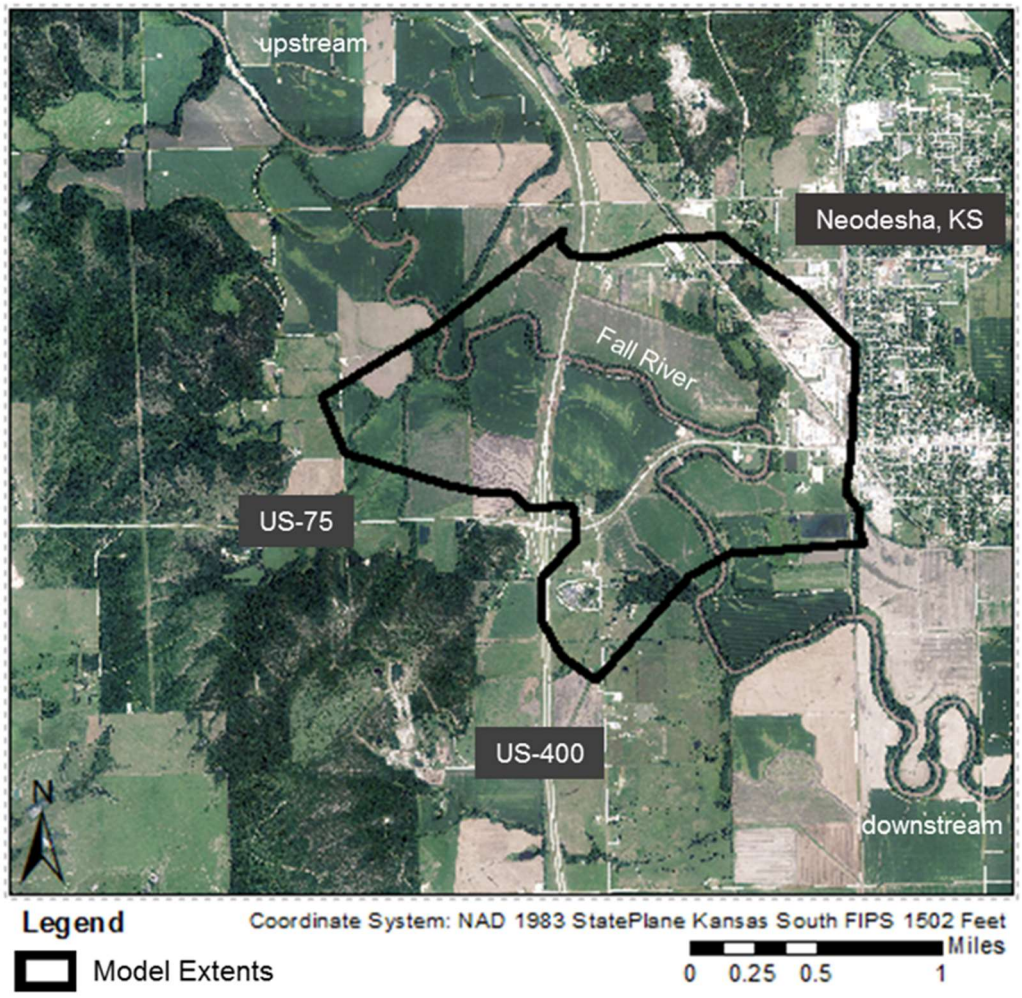

Figure 7-1. Neodesha Floodplain Study Site and Surrounding Area

The aerial photographs composing the image were obtained from the USGS online National Map Viewer. The total model area was 2.15 square miles and the reach length 15,907 feet. The major bases for comparison between models were the floodplain extents, the area inundated, the water surface profile along the main channel's centerline, and flow divisions through the bridge openings.

The section of interest of this reach possesses many features that make a standard one-dimensional analysis difficult. On the upstream end the channel changes direction frequently, widely meandering as it progresses across the relatively flat floodplain. The flow then encounters Highway 400 where there exist four hydraulic structures: a bridge over the main channel, a relief bridge and a relief culvert south of the main bridge, and a small culvert north of the main channel. The river then proceeds eastward to run nearly parallel to Highway 75 before it turns abruptly to pass through the main bridge under the road. In addition to the main bridge on Highway 75, there are two relief structures to the southwest. Once the flow has bypassed the main bridge under Highway 75 it curves back to the west, the opposite direction it was heading before, once again running parallel to the highway. The flow from the two relief bridges then recombines with the main channel flow as it heads by a water treatment plant whose ponds on the eastern side of the downstream extent of the model space are protected from flooding by levees. These details frustrate the task of defining cross sections that do not overlap and that suitably approximate the complicated flow patterns.

The space chosen was intended to include the notable features of the site, those that make it difficult to model, but was also reduced in size for the sake of computational efficiency for the two-dimensional models. Great care was exercised in the placement of the upstream and downstream boundaries. At the upstream end, the boundary needed to be placed far enough away

from the bridge to ensure realistic flow patterns for the incoming water, but also in a location where the flow is approximately one-dimensional (at least for a reasonably high flow and thus one that is outside of the channel). At the downstream end the boundary needed to be far enough away such that the separate flows issuing from the three bridges located along Highway 75 have sufficiently recombined, and the flow is approximately one-dimensional.

Currently, neither two-dimensional model can accommodate pressure flow directly but must rely on supplemental routines – in the case of HEC-RAS, it must use the standard 1D culvert and bridge routines, and for SRH-2D, it must use the Federal Highway Administration's culvert analysis software, HY-8. Thus, the discharge selected was one intended to be high enough for the flow to include the overbanks but not so high as to cause overtopping of the roadways or pressure flow through the bridges. To this end, 40,000 cfs was used as the target discharge. This value was near the "Full Valley Discharge" of 39,800 cfs listed in the KDOT as-built plans for HW 400 (96-103 K-3295-01). After first using the flow for the one-dimensional HEC-RAS model and finding it satisfactorily met the criteria listed above, it was deemed appropriate for use in the two-dimensional models. As was often the case for analyses included in this report, the inflow hydrographs used for the 2D models were simply ones that ramped up to the maximum discharge and maintained this constant discharge for a duration sufficient for steady state conditions to be reached. This was done primarily for numerical stability, as rapid changes in the hydrodynamics of a model may result in unrealistic flow behavior like extreme changes in depths and velocities (especially near obstructions such as piers), but also because the intermediate details are also of interest. The total hydrograph durations vary for each two-dimensional model and will be discussed further in their respective sections. The HEC-RAS 1D model did not require an inflow hydrograph as it was run as a steady state simulation. All models used a water surface elevation of

795 feet as the downstream boundary condition. This value was obtained from the HEC-RAS 1D model using a normal depth downstream boundary condition.

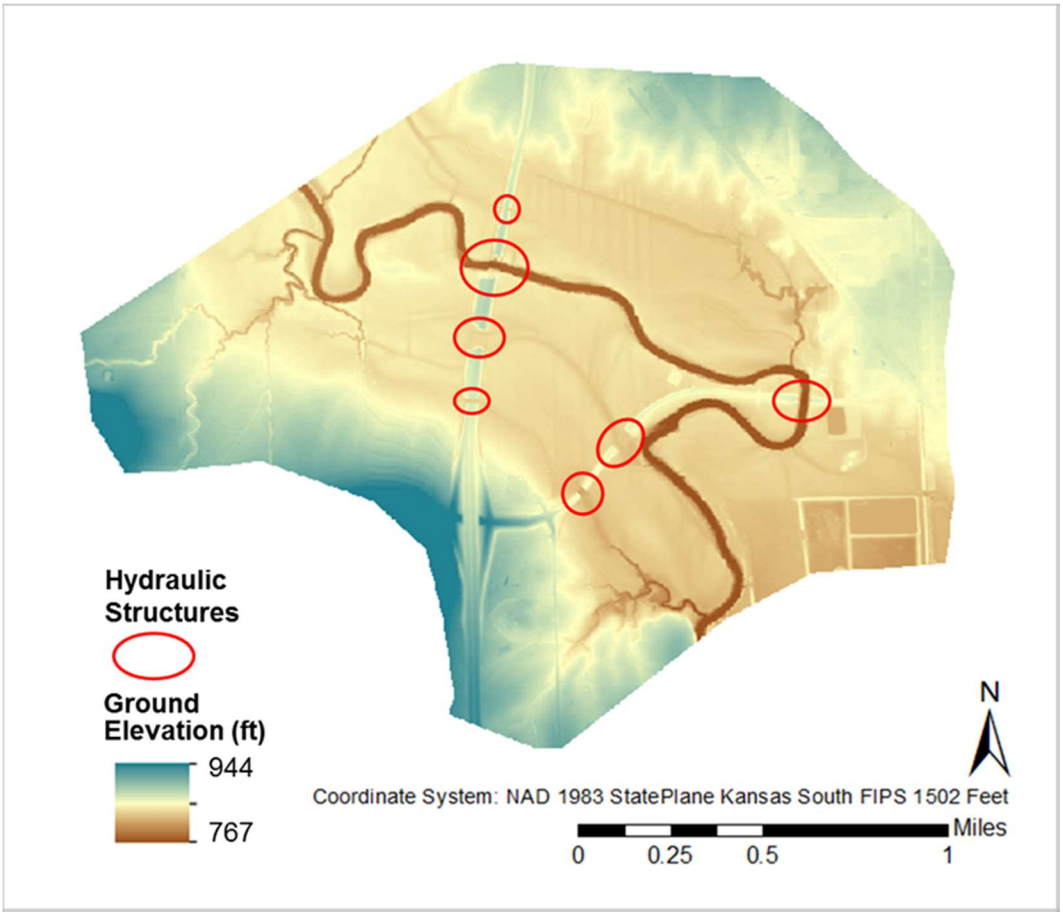

Figure 7-2. Digital Elevation Model for the Neodesha Floodplain Study

The above map shows the raster defining the terrain for the study site. Unlike the aerial imagery, this data was obtained from the Kansas Applied Remote Sensing (KARS) online resource rather than from the National Map Viewer. The elevation grid downloaded had a resolution of 1 meter square, which was the highest resolution available. A raster must have a uniform grid spacing throughout its domain for the 2D models. Consequently, the 1-m raster was converted to a TIN and then resampled to a tighter grid spacing of 1 foot square. This was done to ensure that changes made to the terrain were adequately represented within each model and to facilitate acceptable modeling of the geometry of the structures. The effects of several changes can be clearly

seen in Figure 7-2. Along Highway 400 they included the southernmost relief culvert, which based on the KDOT bridge plans was approximated with a 64 foot wide opening on a plane 127 feet long and given a constant elevation of 795.20 feet. The raw elevation data (LIDAR) included only information for the road in this location, and so this section needed to be dropped to create a channel for the flow to travel through. Also along Highway 400, a small culvert was similarly added to the terrain to the southernmost relief bridge, but since no plans were available for this structure, it was approximated using aerial imagery as being 12 feet wide, and, based on the surrounding contours, given a change in elevation from 795.87 feet to 794.92 feet from upstream to downstream over a horizontal distance of 80 feet, thus long enough to span the width of the road and its embankments. The first relief bridge south of the main channel on Highway 400 was left as it was in the raw LIDAR data. The relief bridge nearest to the main channel along Highway 75 was also left untouched. The southwestern-most relief bridge (culvert) along Highway 75 was, based upon KDOT plans, approximated with a 100 foot wide opening on a plane 60.5 feet long and given a constant elevation of 789.10 feet. Where the main channel crosses both Highways 400 and 75, pseudo "survey data" was created from the bridge plans. The elevations of points along the upstream face of each bridge and along the abutments were used to assign elevation values to 3D lines drawn parallel to the channel centerline. These lines were used to generate TINs with dimensions corresponding to the extents of these 3D lines. The TINs were then used to generate rasters that had a resolution of 1 foot by 1 foot. Here, as well as for the portions of the terrain edited mentioned above, the ArcMap Mosaic tool was used to merge the separate rasters, with the higher priority given to the newly created rasters. The results of this process for the two main bridges on this section of the Fall River are included in the figures 7-3 and 7-4.

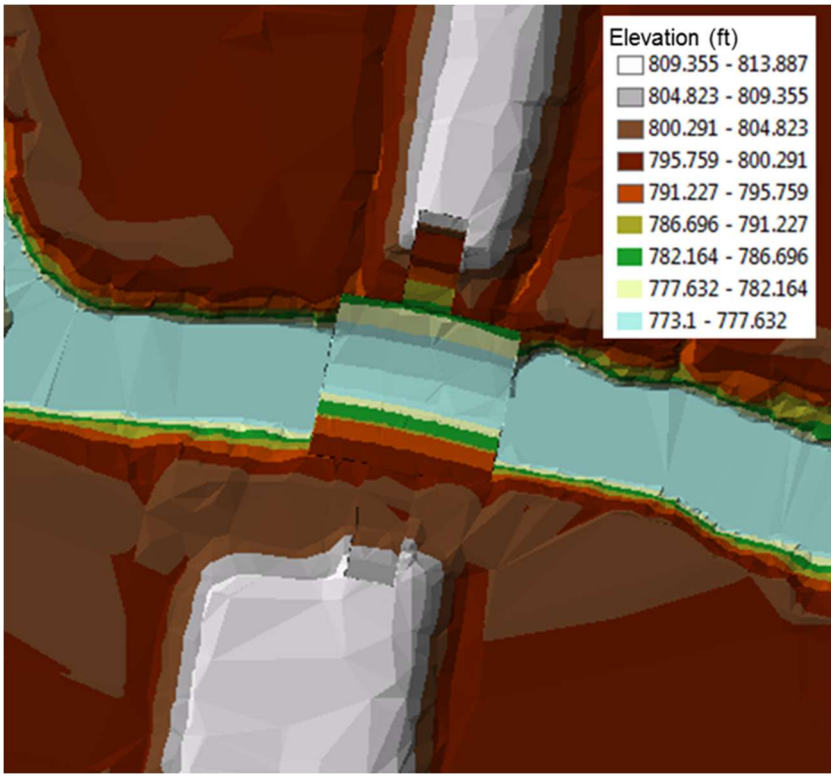

Figure 7-3. Composite TIN of Raw Data and As-Built Plan Bridge Data for Main Bridge on Highway 400

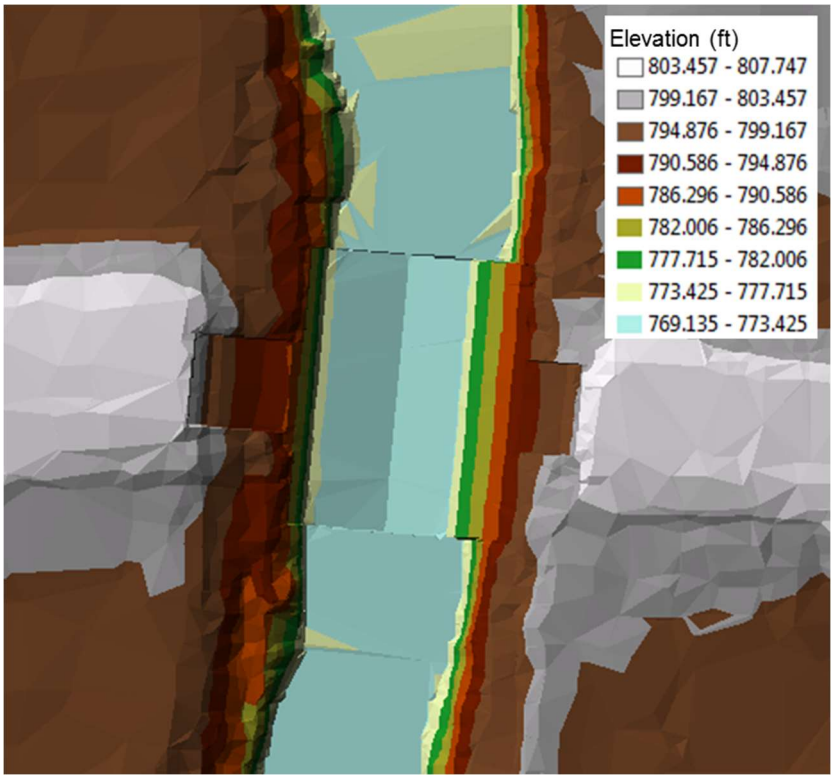

Figure 7-4. Composite TIN of Raw Data and As-Built Plan Bridge Data for Main Bridge on Highway 75

It is readily apparent that some disagreement exists between the as-built plan data and the LIDAR, and two likely reasons exist for this. The first is that the two sources of data correspond with different dates. Several years may have elapsed between the collection of the LIDAR that was processed into the raster downloaded and the time when the field data for the bridge plans was gathered, and the channel bed is not likely to have exactly the same geometry each time data is collected due to bank erosion or soil accumulation. The second reason is that the flow through the river was probably different on each occasion. This is important because the LIDAR beams do not penetrate the water surface, and so the river bathymetry is not reflected in the dataset. The effect of this can be seen in Figures 7-3 and 7-4 in the channels away from the bridges where the channel appears unusually flat. Also, the survey included in the bridge plans actually measured the ground elevation, and so the low point of that survey data through each bridge is below that of the LIDAR – by about 4 feet and about 2 ½ feet through the main bridges under Highways 400 and 75, respectively. The channel away from the bridges as represented by the LIDAR data was left intact because, while doing so artificially reduces the conveyance of the main channel, the reduction relative to the large discharge modeled was deemed sufficiently insignificant. Also, for the sake of making comparisons amongst the various models, what is important is that every model share the same bias if one exists. If this reach were being modeled for design purposes (or some other critical task), then it would be advisable to carve out the channel through some sort of manipulation of the DEM. This could be accomplished fairly easily within ArcMap using 3D elevation lines in a manner similar to that described in Chapter 3 (Computation Test). These 3D elevation lines would be related to the survey data for each bridge but would also take into consideration the slope of the channel. The elevation lines could be used to generate TINs, and those could be used to generate rasters. This would be done for multiple segments of the channel. Next, it would require a series

of mosaic operations using the blend option for these multiple sections to smoothly merge the channel rasters. Then, the mosaic tool would be used again to join the merged channel rasters to that based on the LIDAR, but with the value priority set to minimum. Following this procedure would guarantee a greater conveyance through the main channel, but surely other methods exist to accomplish this goal.

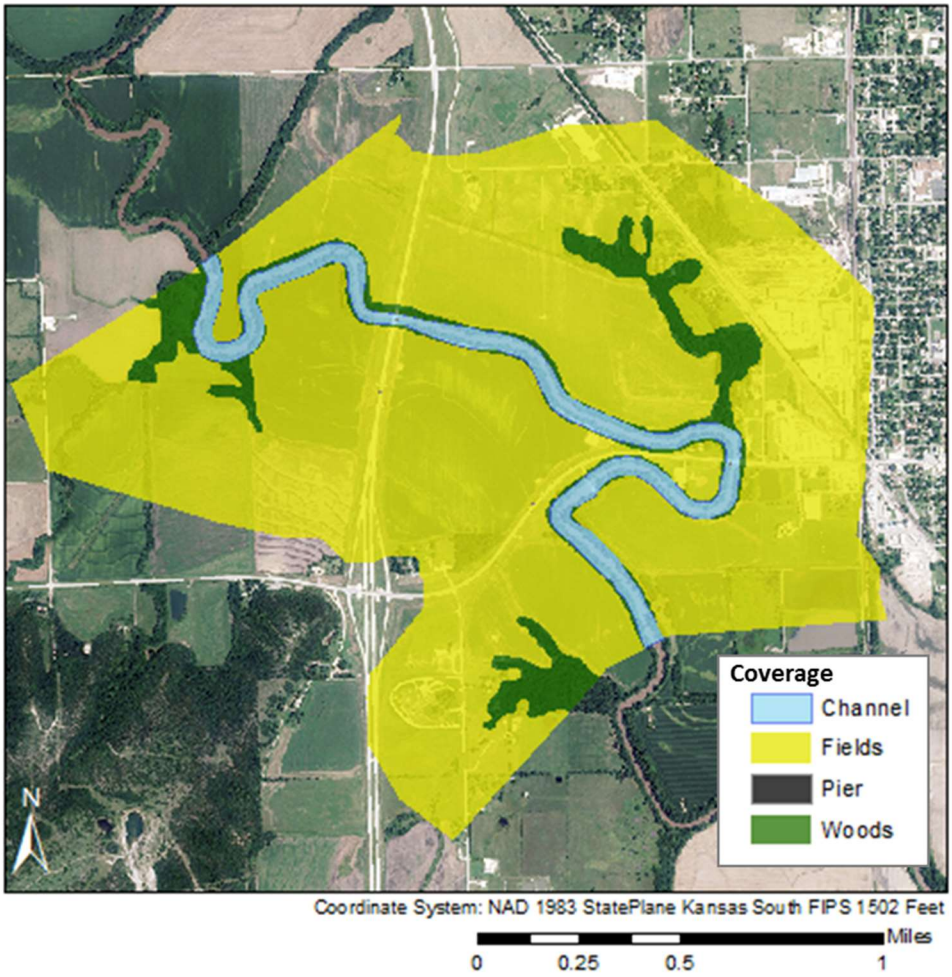

Figure 7-5. Manning's Roughness Coverage Polygons for the Neodesha Floodplain Study Site

The regions delineated in the figure above correspond to Manning's roughness coefficients of 0.035 for the channel, 0.1 for the woods, 0.055 for the fields, and, for use in the HEC-RAS 2D simulation, the piers were assigned an n-value of 1,000,000 (10^6) to minimize conveyance through the piers. These polygons were drawn in ArcMap and there were assigned their respective

values. Since no overtopping of the roadways was anticipated, separate roughness coefficients were not assigned to the roadways and thus are included in the "fields" category (although it should make no difference which type they belong to). The number of land use types defined were kept to a minimum in order to preserve computational efficiency and the site was mostly fields. This coarse description of land use for the site was expected to be wholly capable of simulating the primary flow features without overly complicating the issue of building the model. Sections 7.2 7.3, and 7.4 describe the details and results of each model individually.

7.2. One-Dimensional HEC-RAS Model for Neodesha

7.2.1. One-Dimensional HEC-RAS Neodesha Model Setup

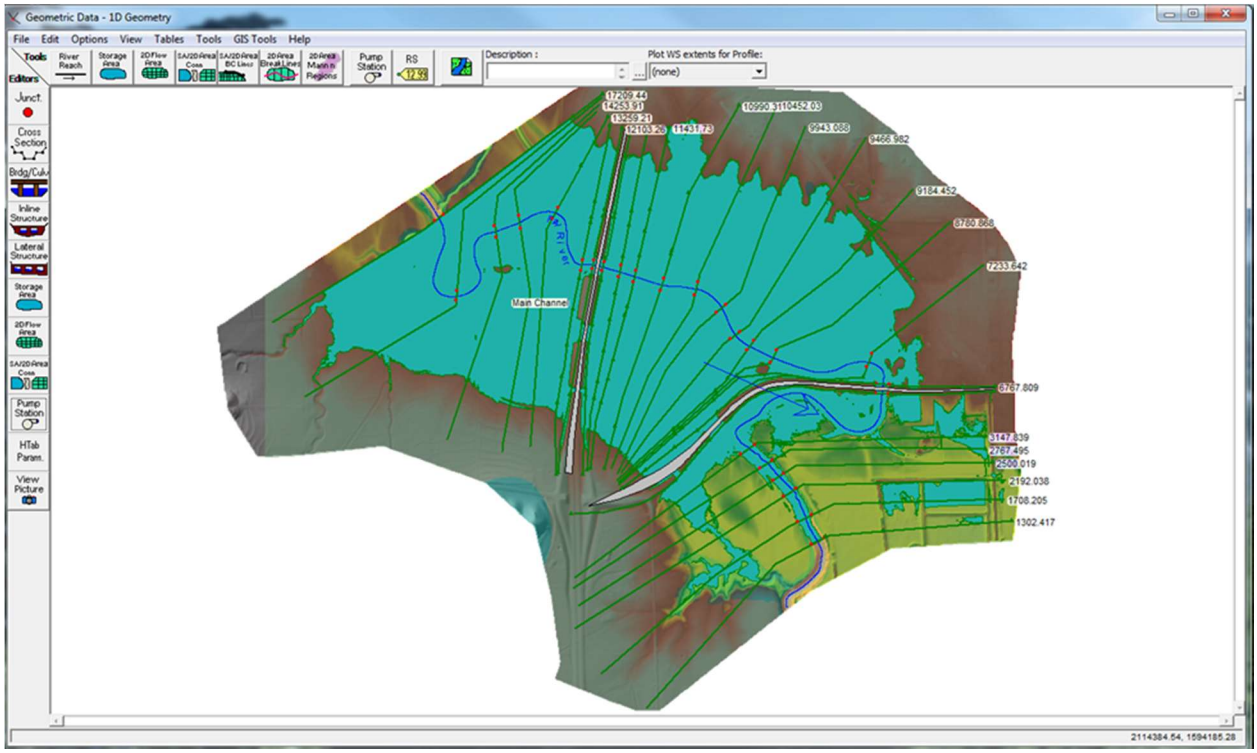

Figure 7-6. One-Dimensional HEC-RAS Geometry and Flood Map for the Neodesha Floodplain Study

The model depicted in Figure 7-6 was composed of twenty-five cross sections and two bridge sections. It included ineffective flow areas upstream and downstream of each hydraulic

structure to account for the reduced conveyance through nearby cross sections related to the contraction and subsequent expansion of flow as it passes through these constrictions. The boundaries of each ineffective flow areas were drawn at 1:1 and 2:1 ratio (longitudinal to lateral with respect to the flow direction) for the contraction and expansion sections, respectively. Blocked ineffective flow areas were used on the east sides of the three most downstream cross sections to bar the low elevation areas bounded by the levees near the water treatment plant from being used for conveyance. Details for the bridges, such as pier sizes and distributions, opening width, roadways, and guard rails were determined from the KDOT plans. The upstream and downstream bounding bridge cross sections had their stationing and channel elevation data manually adjusted in Excel so that they lined up with each bridge opening and so that their channel elevations matched that of the field "survey data". Figures 7-7 through 7-9 show the blocked ineffective flow areas near most downstream cross section and the bridge cross sections from HEC-RAS.

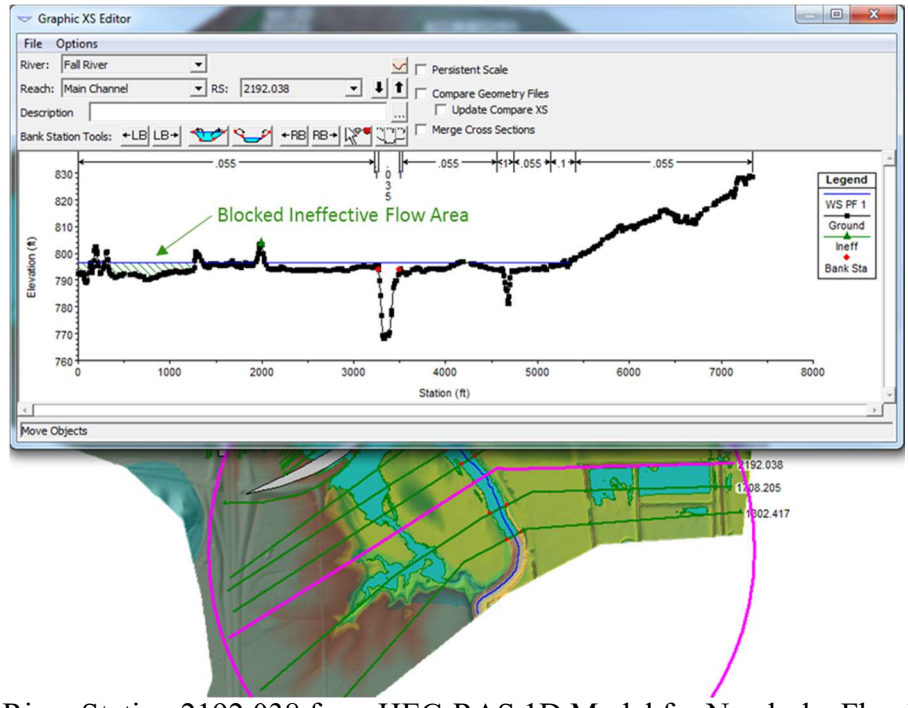

Figure 7-7. River Station 2192.038 from HEC-RAS 1D Model for Neodesha Floodplain Study Showing Blocked Ineffective Flow Areas Typical of the Three Most Downstream Cross Sections

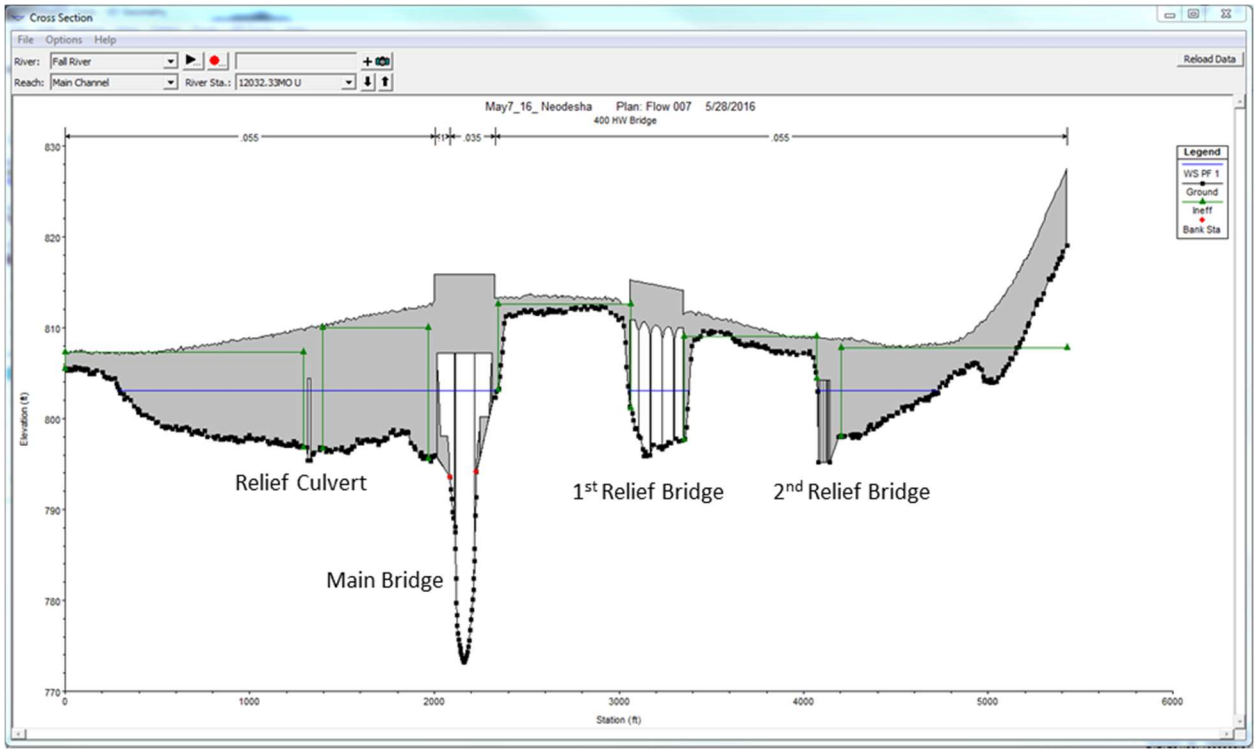

Figure 7-8. Upstream Bounding Bridge Cross Section for Highway 400

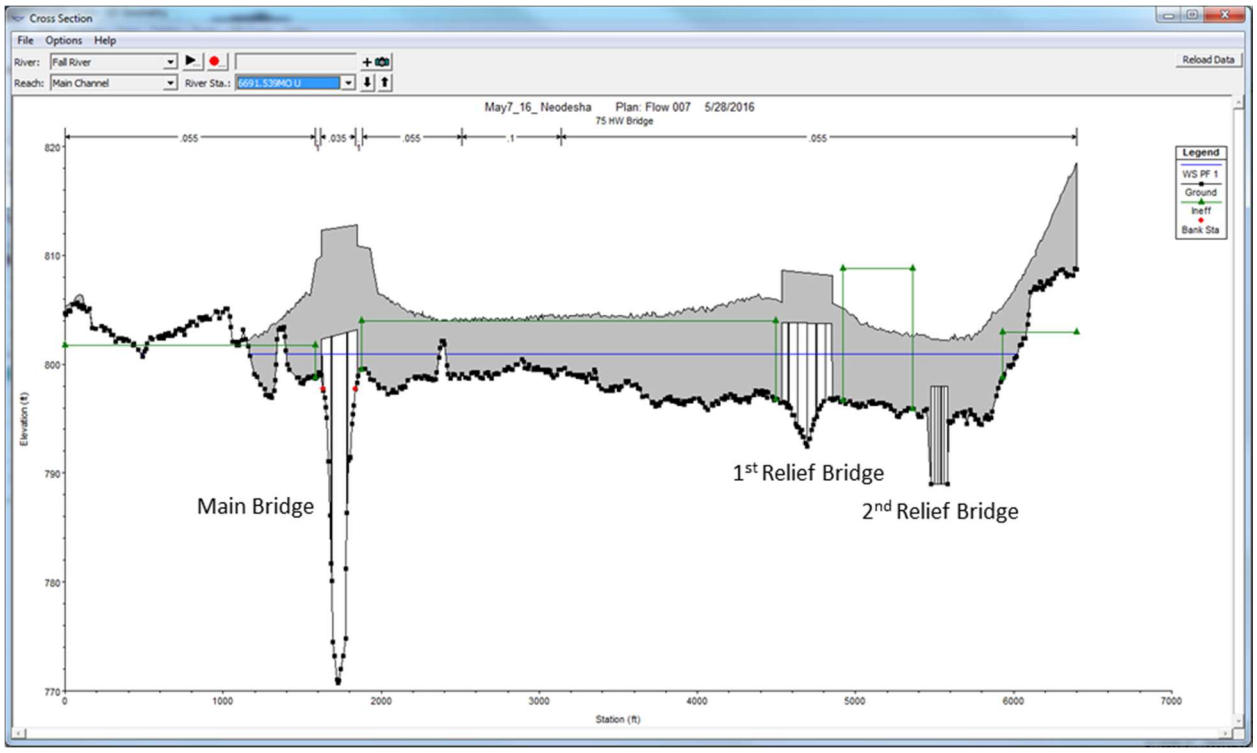

Figure 7-9. Upstream Bounding Bridge Cross Section for Highway 75

Thirty-nine piers were included for the 2D models. HEC-RAS 1D only models the upstream pier for multiple column pier groups. At the main bridge on Highway 400 there were 6 piers each with a diameter of 3.5 feet. At the first relief bridge on that Highway there were 12 piers each with a diameter of 2.5 feet. At the time the simulations were run there were no plans available for the main bridge on Highway 75, and so the piers were estimated as 6 piers each with a diameter of 4.5 feet – although, bridge plans have since become available showing that the correct details were 4 piers each with a diameter of 3 feet. Since the two-dimensional simulations require such a long time to run, the results which were determined using the estimated pier diameters at the main bridge on Highway 75, are presented in this report. Finally, the remaining 15 piers were located at the first relief bridge on Highway 75 and each one had a diameter of 2.5 feet. The multiple barrels of the second relief bridges for both Highways 400 and 75 were approximated in the two-dimensional models by using single barrels and reducing the total opening widths by amounts equal to the sum of the thicknesses of the walls separating each barrel. Taking this approach would underestimate the amount of losses experienced through both of these relief bridges, but considering that the discharge passing through each structure is rather small relative to the total discharge, this is an acceptable approximation.

7.2.2. One-Dimensional HEC-RAS Neodesha Model Results

The figures that follow summarize the results of the one-dimensional HEC-RAS model. The runtime for this model was 9 seconds. For the floodplain map in Figure 7-10, the disconnected flow areas produced during the “cut and fill” operation of HEC-GeoRAS were deleted in ArcMap and then the area of the single remaining polygon was determined to be 1.35 square miles, or 63.1% of the total study area. It is vital to note that the flow did not overtop either roadway, nor

did the water surface elevation exceed the height of the levee near the downstream cross sections. Also, that the flooded extents were adequately bounded by the model domain.

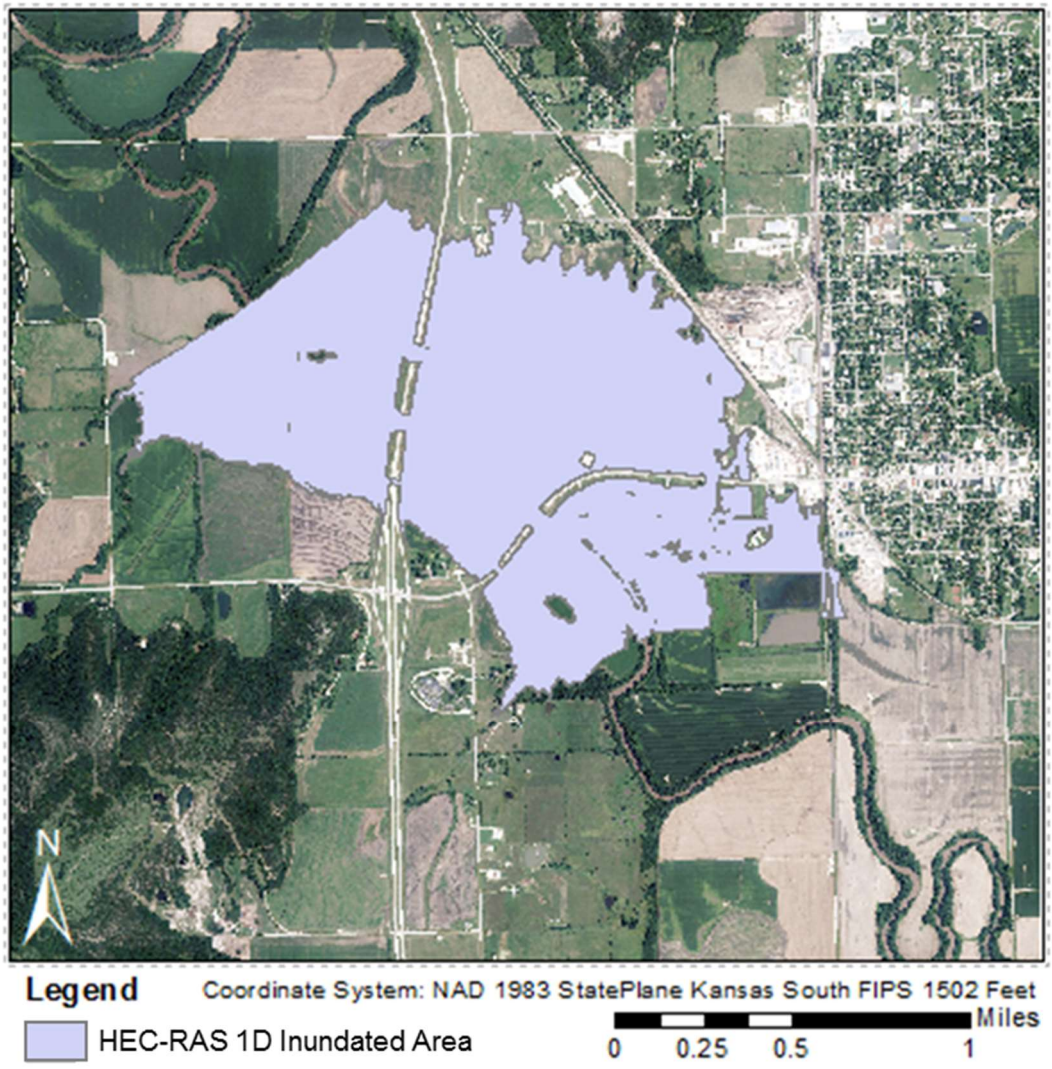

Figure 7-10. Map Showing Inundated Area from HEC-RAS 1D Neodesha Floodplain Model

From the water surface profile in Figure 7-11 it can be seen that the bed drop and subsequent rise through each bridge opening does not appear to produce suspicious results. The change in water surface elevation from two cross sections upstream of the main bridge on Highway 400 at River Station 12,276.80 feet (station 10,974 feet on the plot) to two cross section downstream of the bridge at River Station 11676.45 feet (station 10374.03 feet on the plot), a

distance of 160.05 feet, is 1.44 feet. This drop is reasonable given the maximum depths at each respective cross section are 27.65 and 26.48 feet. The decrease in water surface elevation is even less distinct at the downstream bridge through Highway 75.

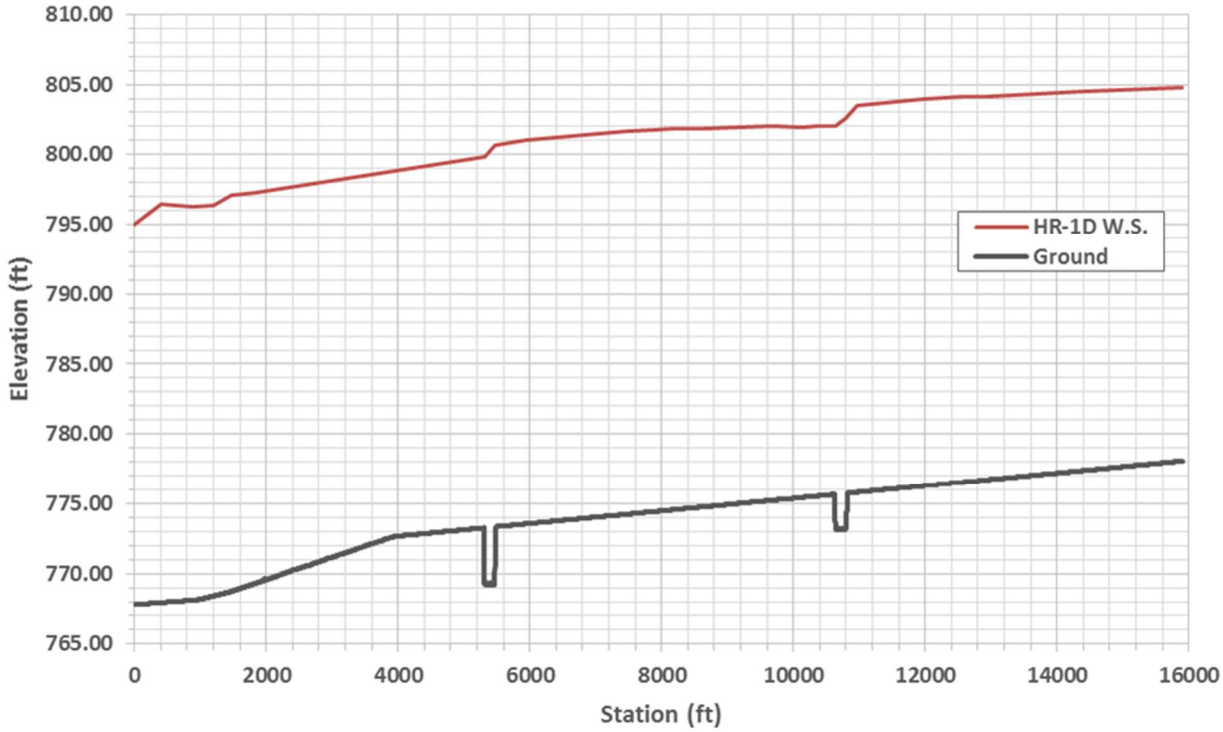

Figure 7-11. Channel Centerline Water Surface Profile from HEC-RAS 1D Neodesha Floodplain Model

Table 7-1. Flow Divisions for the Hydraulic Structures of the HEC-RAS 1D Neodesha Floodplain Model

	Structure Designation	Q (cfs)	Percent of Q_{MAX}*
Highway 400	Main Bridge	29952	74.9%
	First Relief Bridge	7267	18.2%
	Second Relief Bridge	2363	5.9%
	Relief Culvert	419	1.0%
Total Q:		40000	100.0%
Highway 75	Main Bridge	29554	73.9%
	First Relief Bridge	6565	16.4%
	Second Relief Bridge	3881	9.7%
Total Q:		40000	100.0%

Q_{MAX} = 40,000 cfs

The flow splits shown in Table 7-1 were determined by entering the Geometric Editor window and left-clicking the desired bridge section to select it, choosing “Tabular Output”, and then selecting “Profile Table”. The opening of interest for the cross section must be selected from the drop down menu circled in the figure below. Each Multiple Opening Output Table contains a variety of information about the particular opening including results pertaining to the internal bridge cross sections. For example, in this table it could be determined what amount of the total discharge passed over the road as weir flow, but in this case all discharge in the vicinity of this opening passed through the bridge opening.

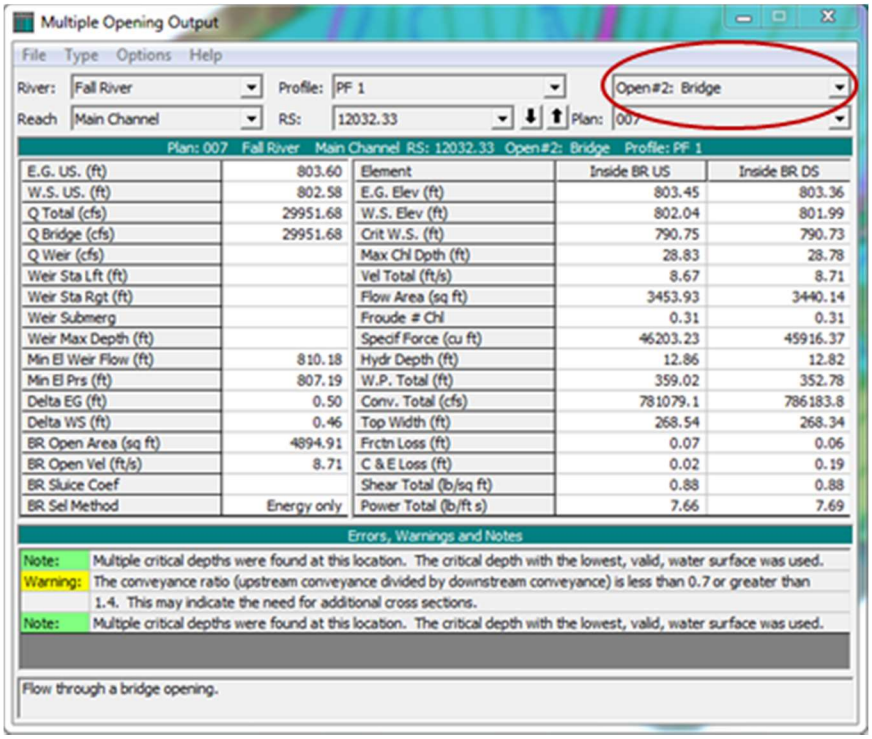

Figure 7-12. Flow Results for the Main Bridge Opening on Highway 400 for the HEC-RAS 1D Neodesha Floodplain Model

7.3. Two-Dimensional HEC-RAS Full Momentum Model for Neodesha

7.3.1. Two-Dimensional HEC-RAS Full Momentum Neodesha Model Setup

In order to more accurately account for losses through the bridge openings and the more dynamic effects of converging and diverging flow, only the full momentum equation set was considered for this fully two-dimensional analysis. For a combined 1D/2D HEC-RAS model, using the one-dimensional bridge routines to account for those losses and the two-dimensional diffusion equation set everywhere else may be adequate, but such a case was not considered for this study. This model contained 158,484 elements, with a minimum cell size of 1.07 square feet, a maximum cell size of 738.30 square feet, and an average cell size of 393.09 square feet. These cell attributes actually result in an area for the model equal to 2.23 square miles, which is slightly larger than the intended study area of 2.15 square miles. The reason for this is because of a small area included near the downstream boundary on the east side. In this region, some rather unusual ponding occurred that was visible at the beginning of the simulation. The initial conditions of the simulation were the result of a 2 hour warmup period that used a constant discharge of 1000 cfs with the same downstream boundary as the simulation proper of a constant water surface elevation equal to 795 feet. The results from the early timesteps of the simulation show water in places where it could not have flowed into, and in this area that was not intended to be part of the model domain. The velocities in this region were virtually zero, and thus the area was removed from the floodplain map that is described further within this section. The energy grade line used to establish the flow distribution at the inlet was 0.0003. The computational timestep for the model was 1 second, and the total simulated time spanned 66 hours and 30 minutes, and thus the inflow hydrograph was defined as shown in Figure 7-13.

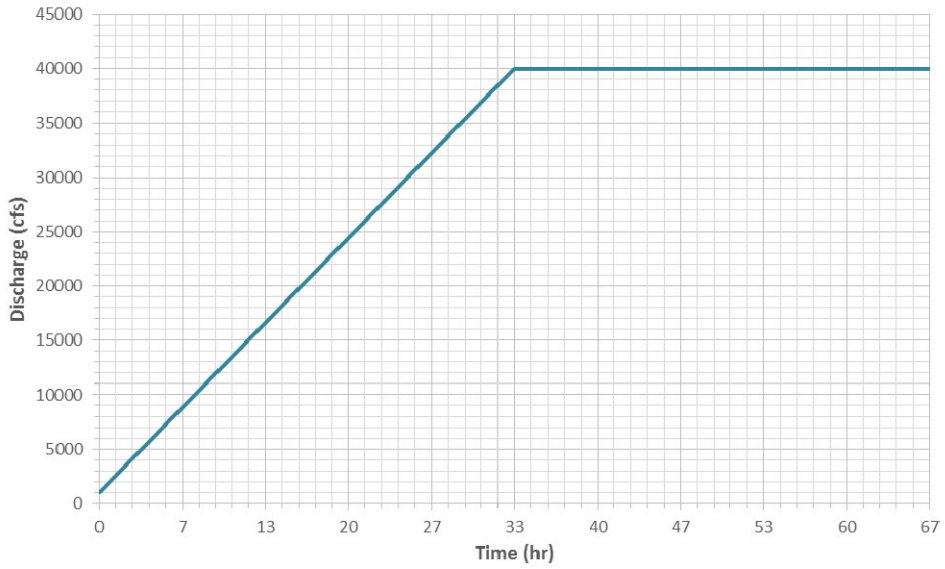

Figure 7-13. Inflow Hydrograph for HEC-RAS 2D Neodesha Floodplain Model

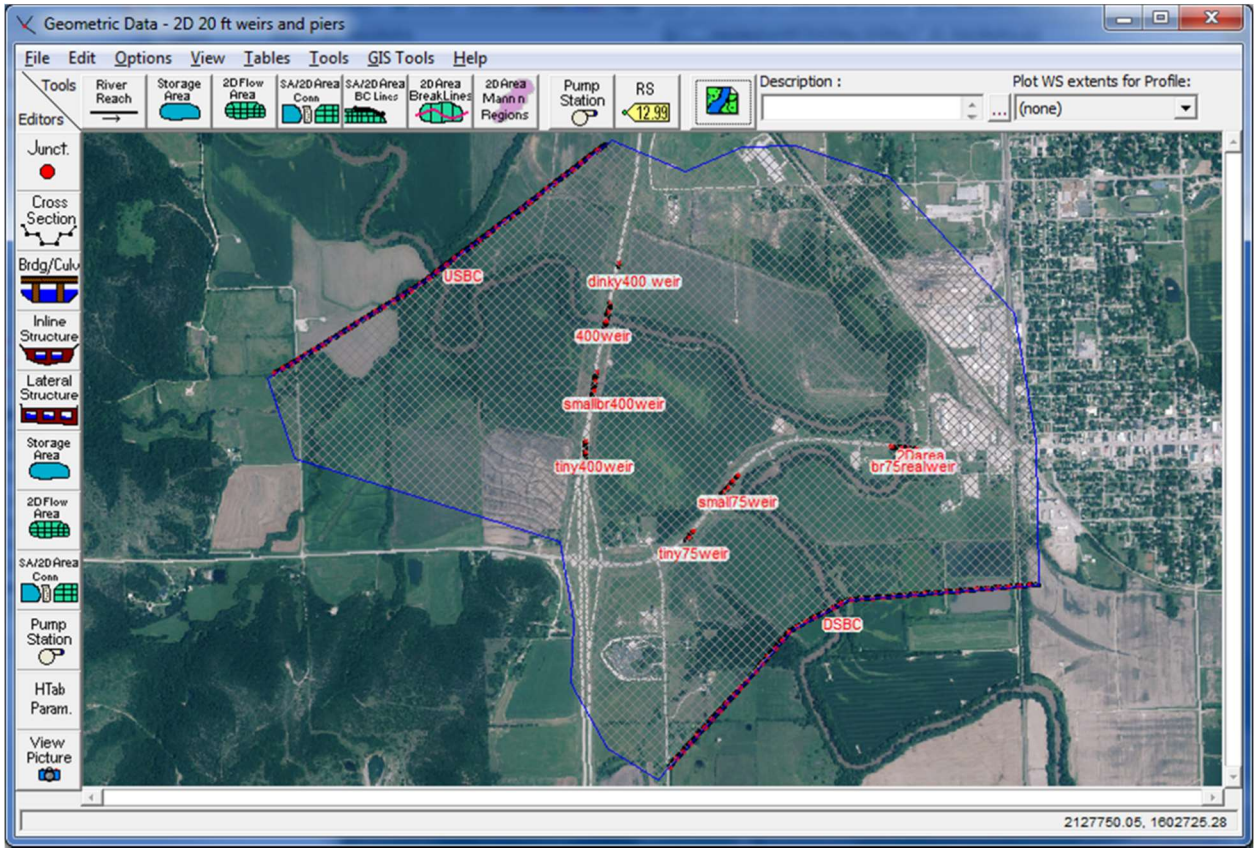

Figure 7-14. Transparent 2D Flow Area and Aerial Imagery for the HEC-RAS 2D Neodesha Floodplain Model

The geometry shown in Figure 7-14 was generated by enforcing a general spacing for the model area of 20 feet by 20 feet. Individual breaklines were used to define the spacing of elements around each pier and to ensure cell faces coincided with the Manning's roughness coefficient associated with the piers (see Chapter 6). This meant that the points defining the outside boundary of each pier needed to be determined separately, which was accomplished using ArcMap. The spacing of cells around the piers was designated such that there would be 6 elements surrounding each pier, thus the spacing enforced around each pier was one-sixth of its circumference. Additional breaklines were added that spanned the width of each hydraulic structure through the roadways. This was a necessary step involved in a work-around procedure for determining the flow through each opening. In HEC-RAS 2D there is no direct way of just measuring the flux across a line, however, the model does record a hydrograph for the flow that passes over a weir, and a weir can be included in the 2D solution space of HEC-RAS. A weir must be drawn such that it follows the cell boundaries, and so, weirs were defined that were of the same dimensions and in the same locations as these breaklines. It would not be desirable for these weirs to have an effect on the flow characteristics though, so they were made to be of approximately the same height as the ground. They could not be of exactly the same height as the ground, because to do so almost invariably causes the simulation to fail in execution. For this reason, the elevation data along the breaklines was copied from HEC-RAS into an Excel spreadsheet, a value of 0.1 feet was added to every data point, and this new elevation series was pasted into the appropriate weir table. After all breaklines were enforced, a great deal of manual editing in the form of adding and moving points needed to be done to in order to avoid poor transitions in cell sizes, to reduce as much as reasonable the number of sides of each cell, to avoid thin elements, to make sure piers were properly included, and also points were removed that were too close together and violated the 1 foot spacing limit.

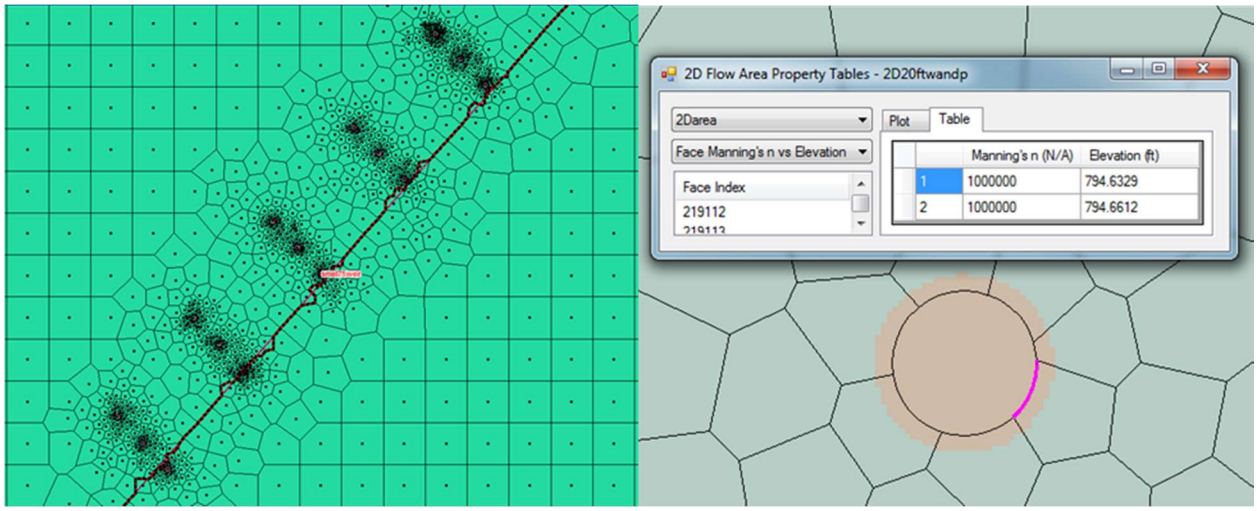

Figure 7-15. Results of Mesh Editing and Breaklines at the First Relief Bridge for the HEC-RAS 2D Neodesha Model

Figure 7-15 shows the results of manual editing and the inclusion of breaklines. From this it is apparent that after editing the near-ground level weir was no longer exactly on top of the breakline. This is because the weir is automatically readjusted to follow cell faces that lead from its starting point to its end. This will not affect the flux calculations over the weir, and since the weir was raised 0.1 feet over its initial position, this should avoid any errors that may arise from its movement.

7.3.2. Two-Dimensional HEC-RAS Full Momentum Neodesha Model Results

Once all model parameters were defined and the mesh prepared the simulation was run. The code took 24 hours, 16 minutes, and 3 seconds to completely execute. The following figures describe the results.

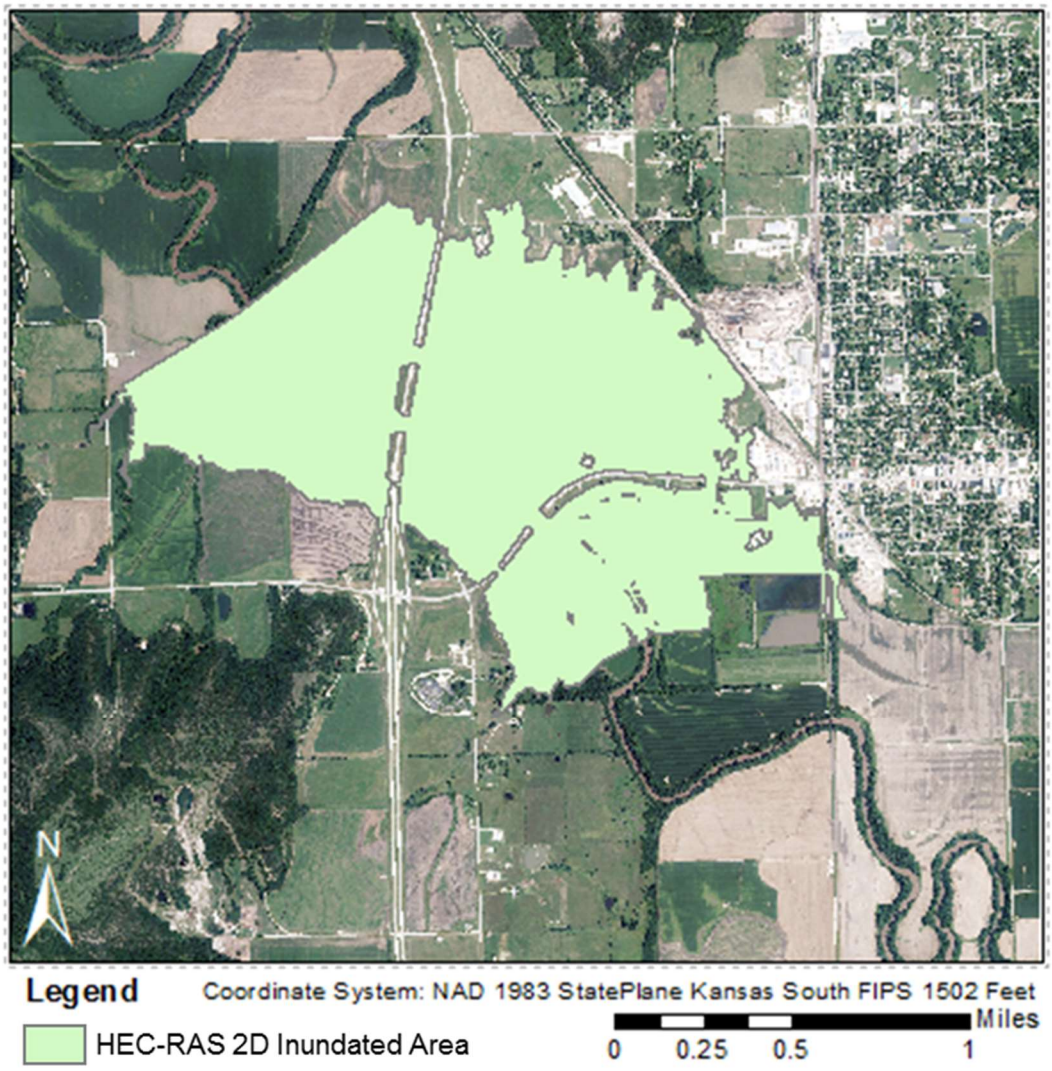

Figure 7-16. Map Showing Inundated Area from HEC-RAS 2D Full Momentum Neodesha Floodplain Model

The floodplain depicted in Figure 7-16 was determined by saving the water surface elevation raster from RAS Mapper for the final timestep of the model as a stored map. This raster was then loaded in ArcMap and the 3D Analyst tool called "Raster Domain" was used to determine its extents. A few small disconnected flow areas that were located near the small road and train tracks in the northeastern part of the 2D flow area that nearly form a triangle with Highways 400 and 75 were removed. These disconnected areas can be seen in the following figure. They occurred due to the fact that the 20 foot square elements in that region of the model were large enough to

span the roadway from one corner to the diagonal corner across the element. Since flow is allowed to enter one mesh face of an element and then exit out of another, numerically the highpoint of the road centerline manifested itself merely in the stage versus storage relationship for the cell, and this interior feature of the cell was bypassed entirely by the flow. Velocities were essentially zero in this region, and by viewing the results the extents of the ponding due to this apparently disconnected flow area were stable, and so they were deemed appropriate for removal from the final floodplain map. This problem could be easily avoid by adding a breakline along the road centerline. However, due to time constraints, this breakline was not added to the geometry and the simulation was not rerun. The total area of this cleaned up polygon was 1.40 square miles, or 65.0% of the total study area.

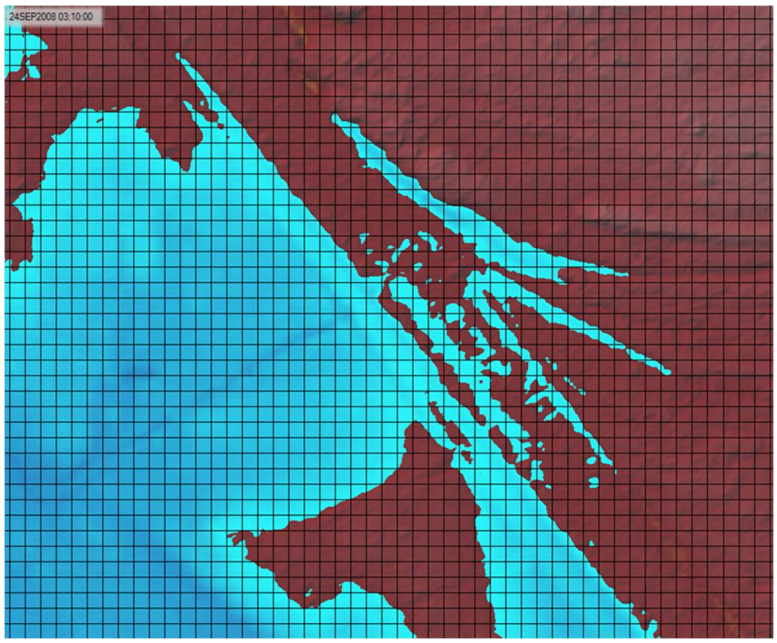

Figure 7-17. Disconnected Flow Areas from the HEC-RAS 2D Model for Neodesha Floodplain Model

Table 7-2. Flow Divisions at the Final Timestep for the Hydraulic Structures of the HEC-RAS 2D Neodesha Floodplain Model

	Structure Designation	Stage HW Elev. (ft)	Stage TW Elev. (ft)	Q (cfs)	Percent of Q_{MAX}*
Highway 400	Main Bridge	803.60	803.56	25090	62.7%
	First Relief Bridge	803.95	803.88	10583	26.5%
	Second Relief Bridge	803.76	803.65	3686	9.2%
	Relief Culvert	803.74	803.67	639	1.6%
Total Q:				39998	100.0%
Highway 75	Main Bridge	799.97	799.95	20924	52.3%
	First Relief Bridge	800.20	800.18	10573	26.4%
	Second Relief Bridge	799.79	799.69	8504	21.3%
Total Q:				40000	100.0%

Q_{MAX} = 40,000 cfs

The flow splits shown in Table 7-2 were obtained from the HEC-RAS Stage and Flow Hydrograph tables related to plots like that shown in the following figure and which were compiled in Figure 7-18. The data show that steady state conditions had been reached by the model. As these results were taken from the final timestep of the model, it's extremely likely that the inability of the flow through Highway 400 to sum to the total discharge of 40,000 cfs was due to periodic oscillations in the flow through the openings. Hydrograph details were only available at 10 minute intervals thus making it difficult to capture exactly 40,000 cfs, but at the timestep corresponding to 65 hours and 30 minutes the total flux through the Highway 400 openings was indeed equal to the total inflow rate of 40,000 cfs. This demonstrates that the volume conservation of the HEC-RAS 2D model was quite good for this simulation.

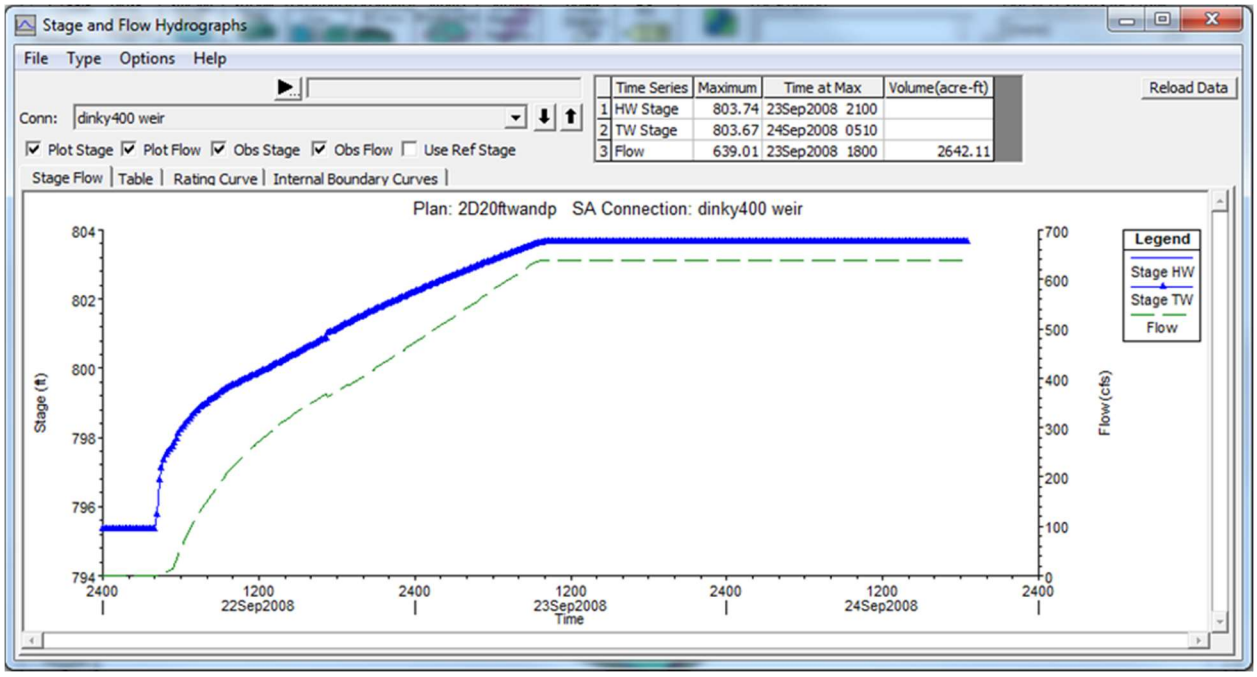

Figure 7-18. Weir Flow Hydrograph from HEC-RAS 2D for the Relief Culvert on Highway 400

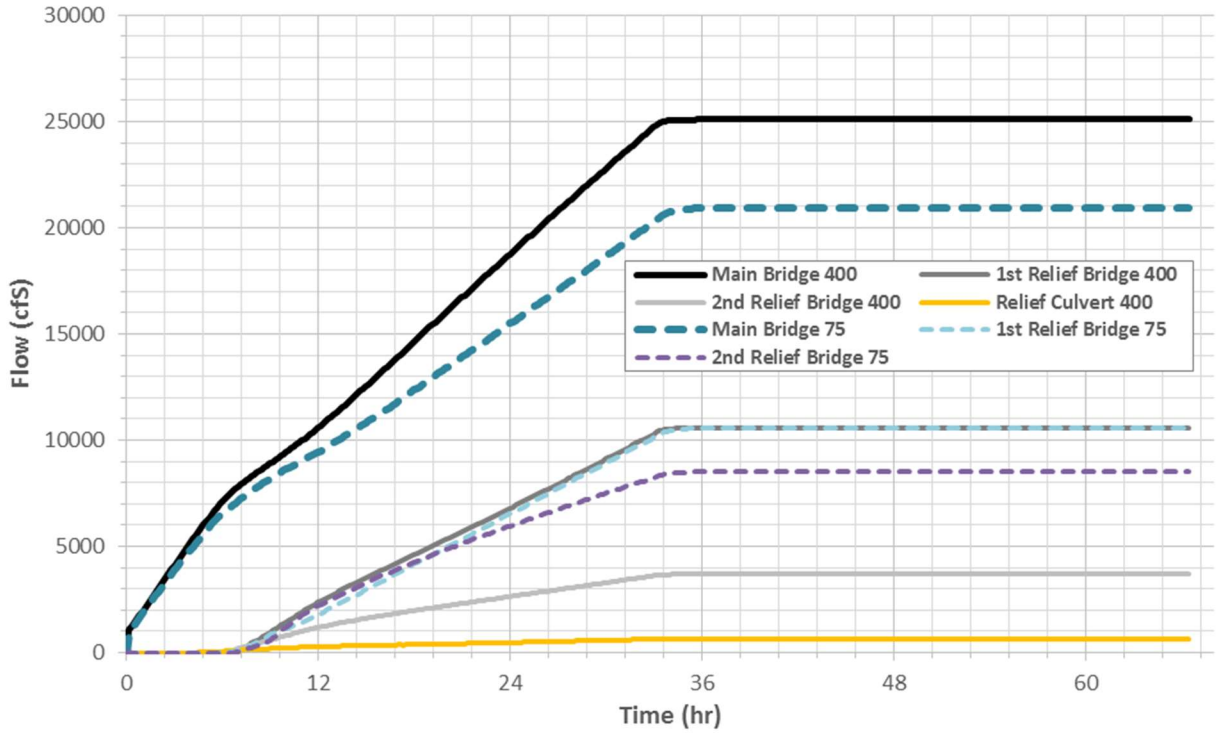

Figure 7-19. Hydrographs of the HEC-RAS 2D Hydraulic Structures for the Neodesha Floodplain Study

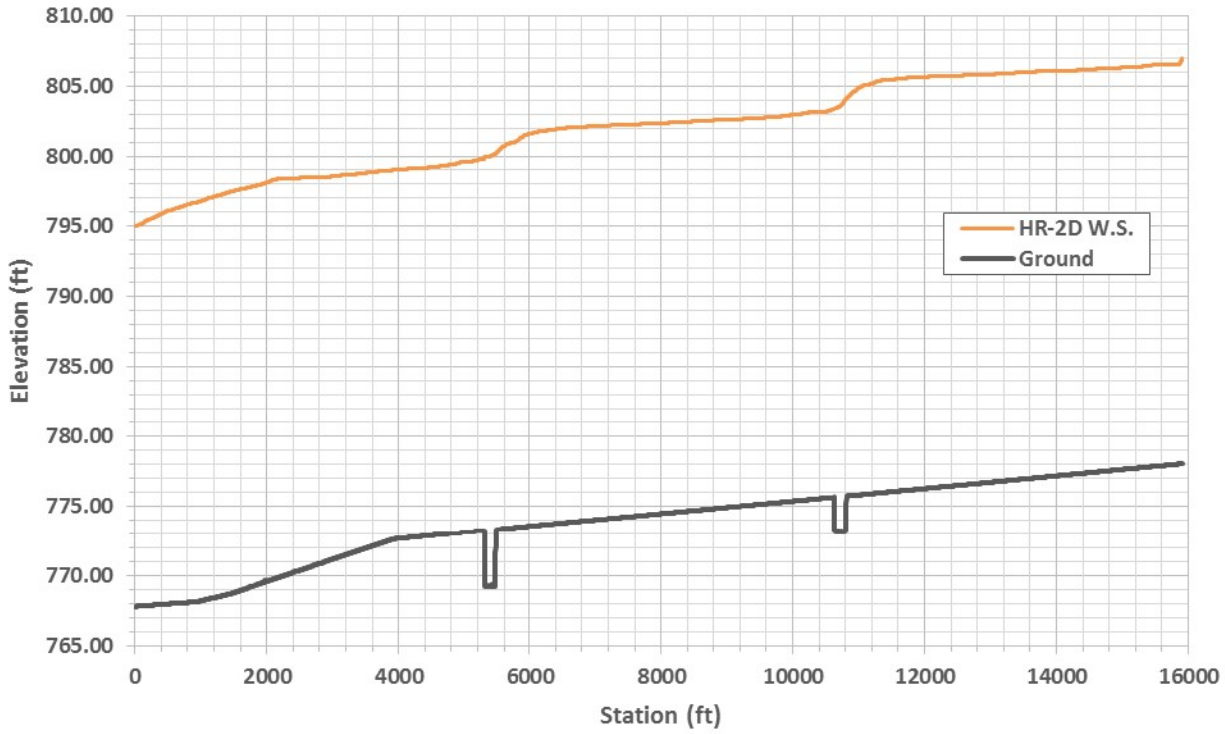

Figure 7-20. Channel Centerline Water Surface Profile from HEC-RAS 2D Neodesha Floodplain Model

The above water surface profile was determined by tracing the channel centerline in ArcMap with an interpolate line accessed via the 3D Analyst toolbar. The surface this line related to was the water surface elevation raster saved in RAS Mapper that corresponded with the data from the final timestep. It can be seen that the downstream boundary condition was satisfied, and that at the upstream end, the curious behavior observed in various places elsewhere in the analyses discussed in this report was also present. The flow at the inlet entered the model space at a depth higher than seems reasonable and thus highlights the importance of placing boundary conditions far enough away from the area that is desired to be studied in detail so that the boundaries do not adversely affect the results.

Figures 7-21 and 7-22 demonstrate the overall flow patterns for this model of the Neodesha Floodplain. The series of images are taken from the vicinity of each hydraulic structure. These

images could be used to either verify or dispute the ineffective flow markers for a one-dimensional model; however, this was not done here.

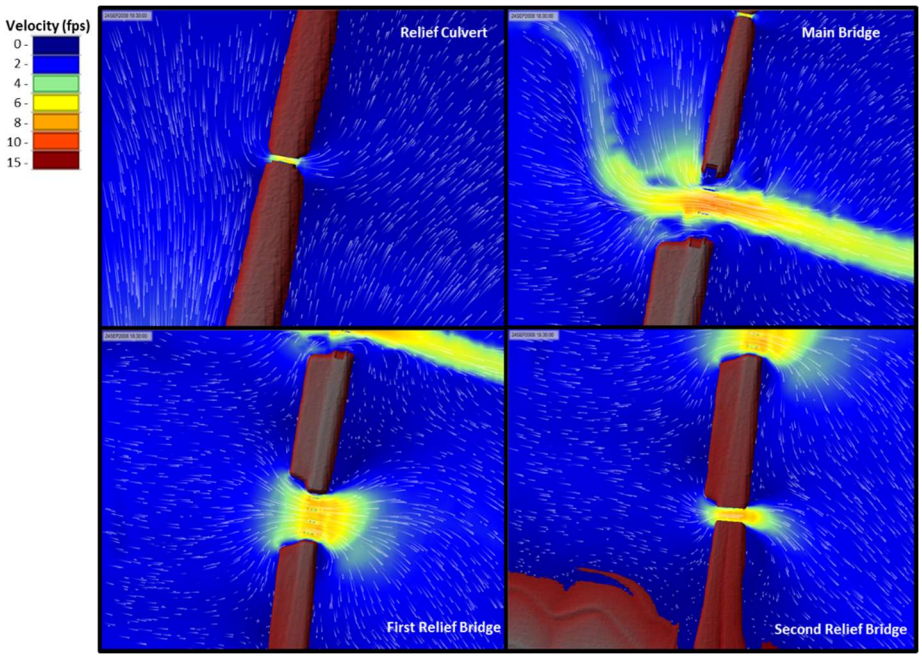

Figure 7-21. Velocity Contours with Tracers for the HEC-RAS 2D Highway 400 Openings

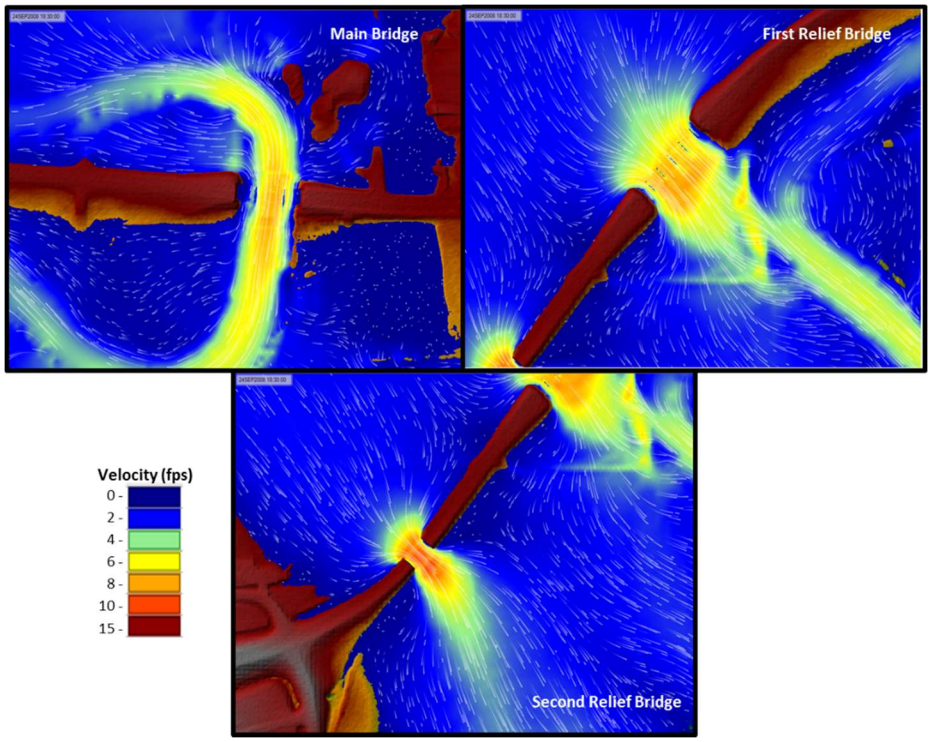

Figure 7-22. Velocity Contours with Tracers for the HEC-RAS 2D Highway 75 Openings

7.4. SRH-2D Model for Neodesha

7.4.1. SRH-2D Neodesha Model Setup

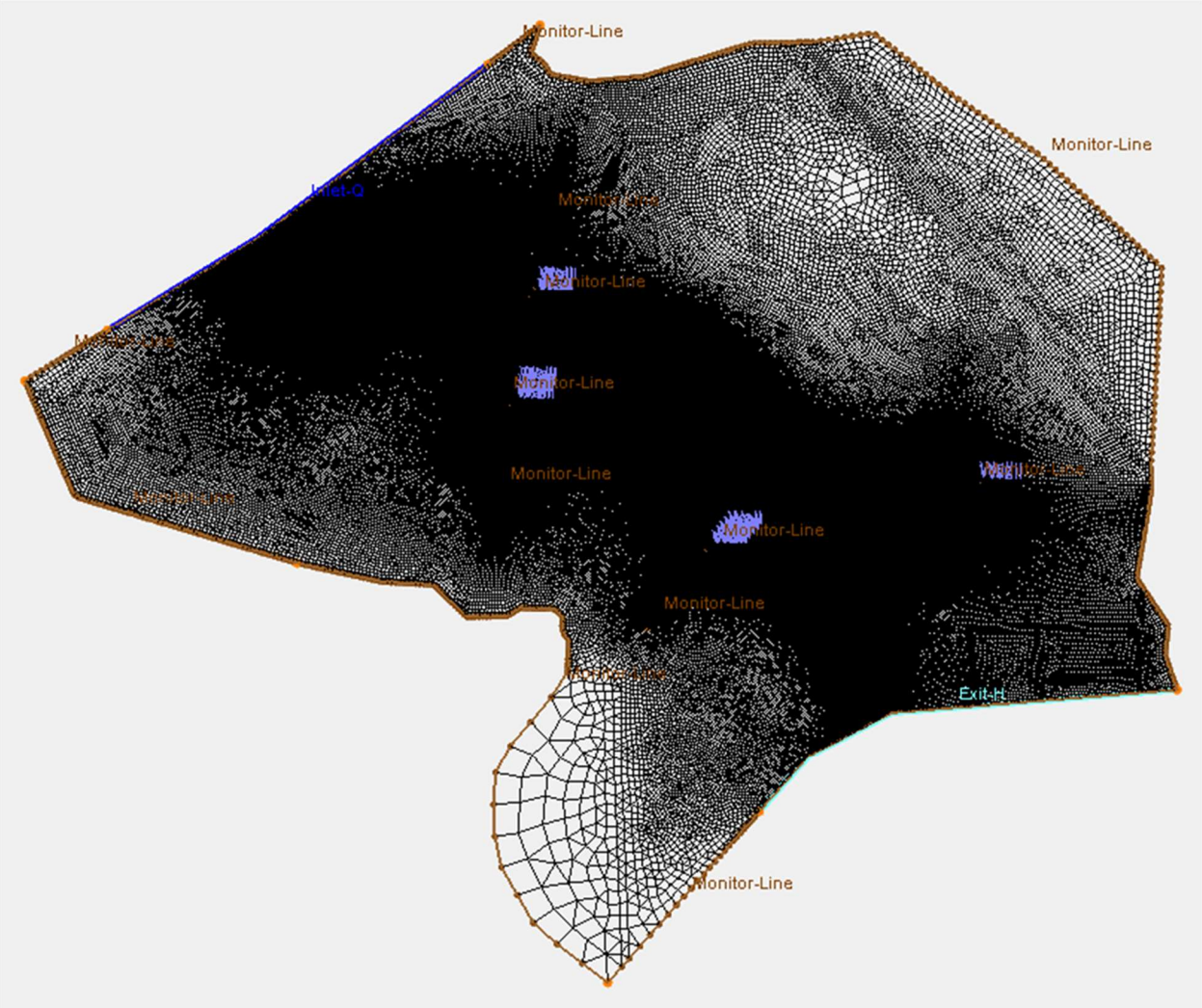

Figure 7-23. Finite-Element Mesh for SRH-2D Neodesha Floodplain Model Viewed in SMS

The mesh generated in SMS for the SRH-2D model and shown above was composed of 420,269 elements with a minimum element size of 0.34 square feet, a maximum element size of 81,956.42 square feet, and an average element size of 142 square feet. The total area for the model was 2.15 square miles and so matched that of the intended study area. The mesh contained a mixture of triangular and quadrilateral elements. The size and distribution of elements depended

on the quantity of nodes along arcs defining the boundaries of the land coverage polygons shown in Figure 7-5. The spacing of these nodes along arcs was determined manually for each arc individually with the intent of achieving an appropriate balance between computational efficiency, model stability, and precision of results. The node spacings on the arcs defining the pier boundaries were specified as 1 foot to satisfy the criteria above. Additional arcs were manually drawn, using the raster as a guide, to define key features such as the roadway embankments and the levees at the downstream boundary. A close-up view of the results of mesh generation can be seen in the figure below. Also in the figure, two lines can be seen, each called "Monitor Line". Seven of these were added to the SRH-2D boundary condition layer – one for each hydraulic structure represented within the model. When the SRH-2D code was executed, the instantaneous flux across each of these lines is written to separate text files stored in the same folder as the rest of the output from the simulation. These files can then be easily retrieved and brought into an Excel spreadsheet.

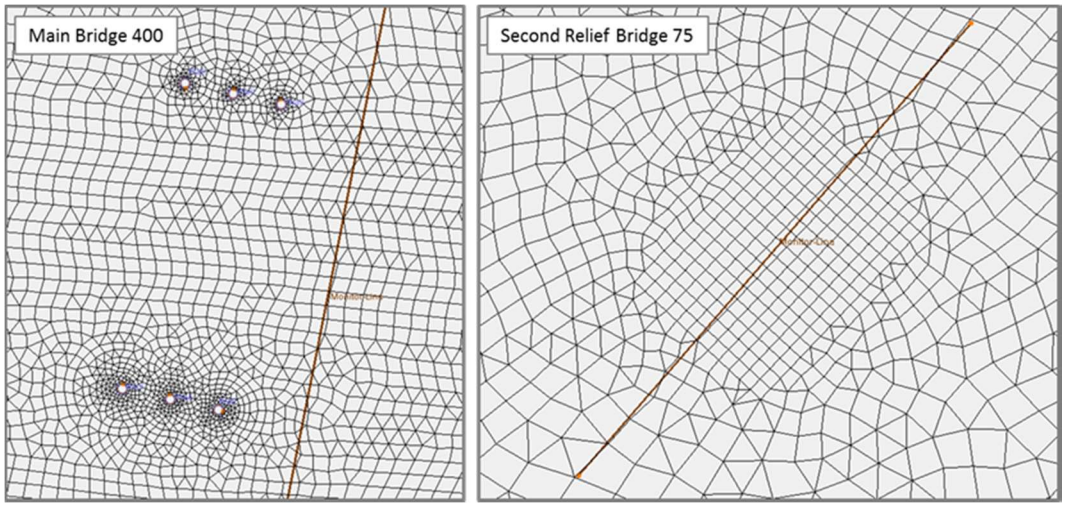

Figure 7-24. Two Plan Views Typical of the SRH-2D Mesh Construction near the Hydraulic Structures for the Neodesha Floodplain Model

For the SRH-2D simulation the initial condition was set to "Dry". "Conveyance" was selected as the method for distributing flow at the inlet. The computational timestep for the simulation was 0.2 seconds. The total simulated time was specified as 8 hours and so, following a

similar pattern as specified elsewhere in this report, the inflow hydrograph for the model was developed as follows.

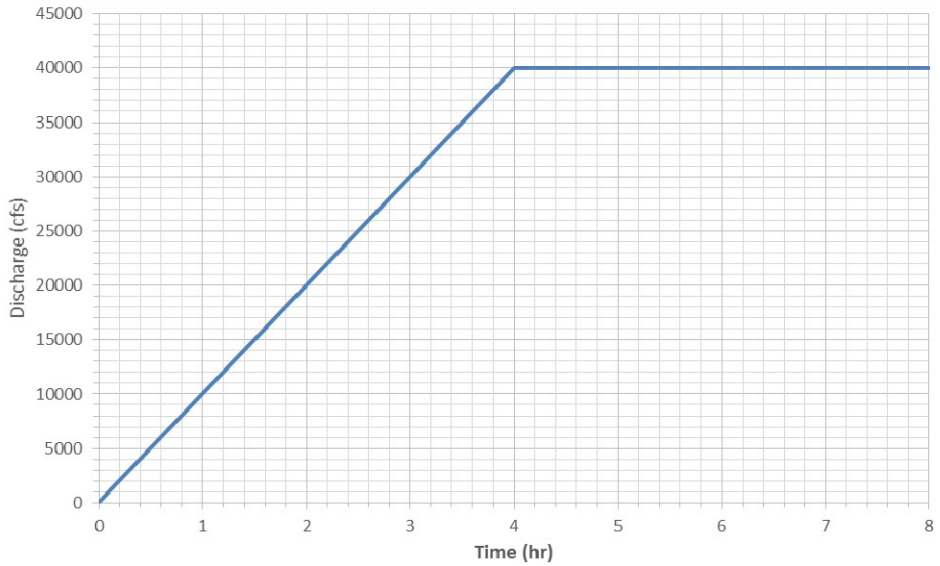

Figure 7-25. Inflow Hydrograph for SRH-2D Neodesha Floodplain Model

The total CPU time required for the model to run to completion was 166 hours and 59 minutes. A restart of the model was required after about 106 hours due to an unforeseen computer shut down. Fortunately, by default SRH-2D generates an extensive amount of restart files that can be used to resume a model. This adds up to 6.96 days just to run the model, and including the time that elapsed between the interruption of the simulation's execution and when it was able to be restarted almost 9 days had passed (the shutdown occurred late at night over a weekend). This reveals one problem of using a model that involves such long computation times. Possibly the model could have used a slightly larger timestep than 0.2 seconds, but definitely not more than 1 second. Experience suggests that for numerical stability SRH-2D requires smaller computational timesteps than the HEC-RAS 2D full momentum model.

7.4.2. SRH-2D Neodesha Model Results

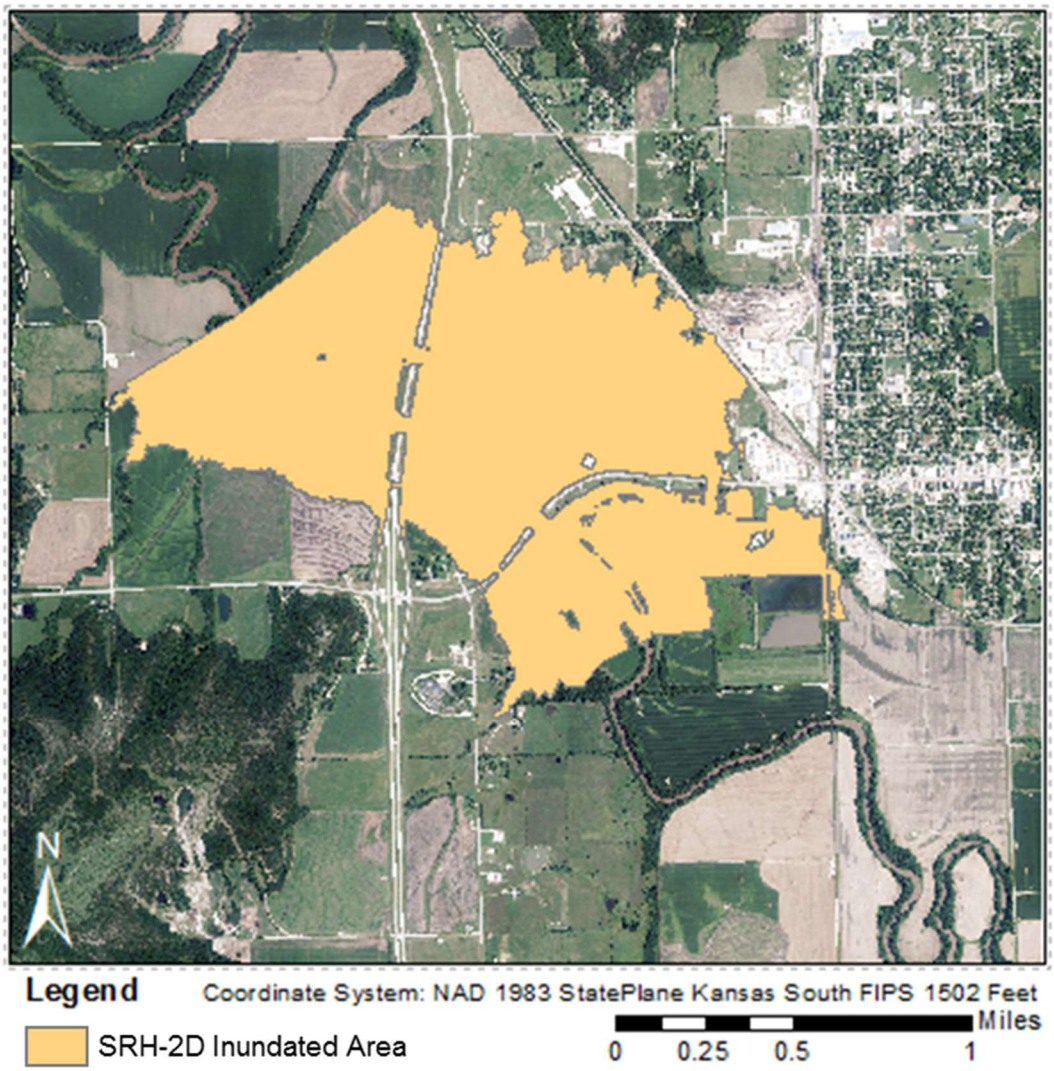

Figure 7-26. Map Showing Inundated Area from SRH-2D Neodesha Floodplain Model

In order to generate the above inundation map in ArcMap quite a large number of steps needed to be performed. Summarizing, the depth contour map needed its display options set to ”Linear” rather than “Color Fill”, where the number of contour intervals was set to one, and the single contour displayed corresponded to a depth of 0.01 feet. This contour map then had to be exported from SMS as an AutoCAD shapefile. This linear AutoCAD shapefile was brought into ArcMap containing a great number of layers and line types. The single layer that corresponded to

the desired boundary was exported from its parent set so that it would be alone and in the ArcMap shapefile format. This linear shapefile was then manipulated in a variety of ways until it was finally of the form shown in Figure 7-26. The area inundated by the final timestep equaled 1.37 square miles, thus accounting for 64.0% of the total study area.

Table 7-3. Flow Divisions at the Final Timestep for the Hydraulic Structures of the SRH-2D Neodesha Floodplain Model

	Structure Designation	Avg. WSE (ft)	Q (cfs)	Percent of Q_{MAX}*
Highway 400	Main Bridge	801.81	27711	69.3%
	First Relief Bridge	803.71	8246	20.6%
	Second Relief Bridge	802.38	3417	8.5%
	Relief Culvert	801.56	591	1.5%
Total Q (cfs):			39965	99.9%
Highway 75	Main Bridge	798.94	25511	63.8%
	First Relief Bridge	799.28	7535	18.8%
	Second Relief Bridge	798.29	6818	17.0%
Total Q (cfs):			39864	99.7%

While Table 7-3 may suggest that there are somewhat significant volume conservation issues with the SRH-2D model, the more likely situation is that the model had not yet reached fully steady state conditions. By looking at the following figure this seems even more likely. The series called “Exit” contains the data for the downstream boundary condition for the simulation and can be seen to be asymptotically approaching the maximum discharge of 40,000 cfs but to have not quite reached this. It is plausible that another hour of simulation time would be sufficient to reach fully steady-state conditions, but as that would have taken approximately another 24 hours to execute, was not done. However, a visual inspection of the model results over the final half hour suggested that the floodplain extents were very nearly constant, and since the sum of the discharges through the openings were within 0.1 – 0.3% of the maximum inflow, these results were deemed acceptable for comparison purposes. The additional volume that would have been stored in the

model at truly steady state conditions is unlikely to have made any significant impact on the observed depths or floodplain extents, but this situation highlights one of the challenges involved in mathematically complex and thus time-consuming hydraulic models.

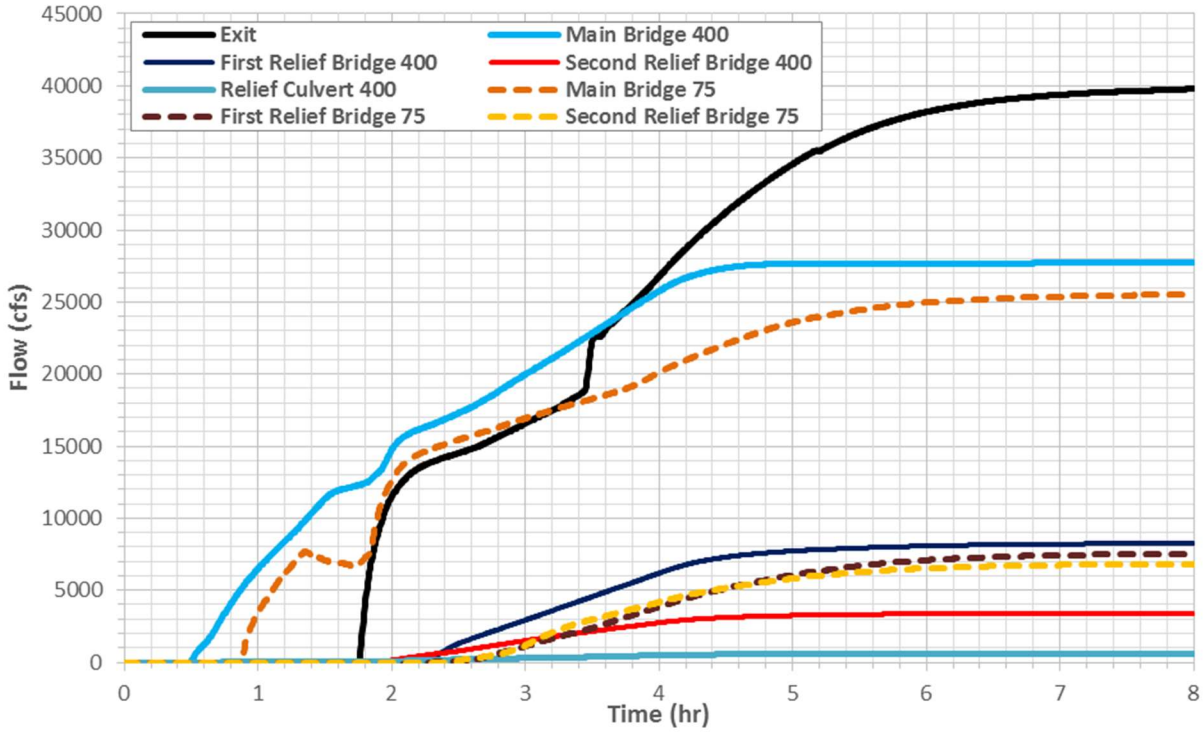

Figure 7-27. Hydrographs of the SRH-2D Hydraulic Structures for the Neodesha Floodplain Study

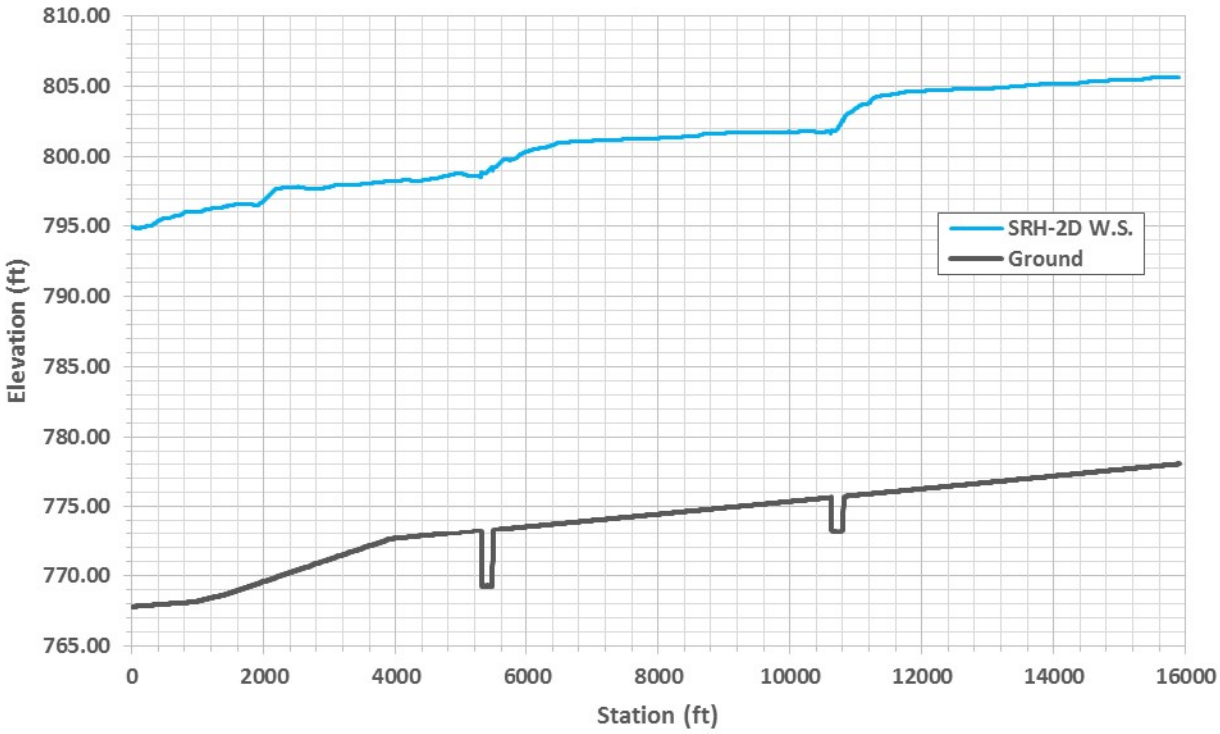

Figure 7-28. Channel Centerline Water Surface Profile from SRH-2D Neodesha Floodplain Model

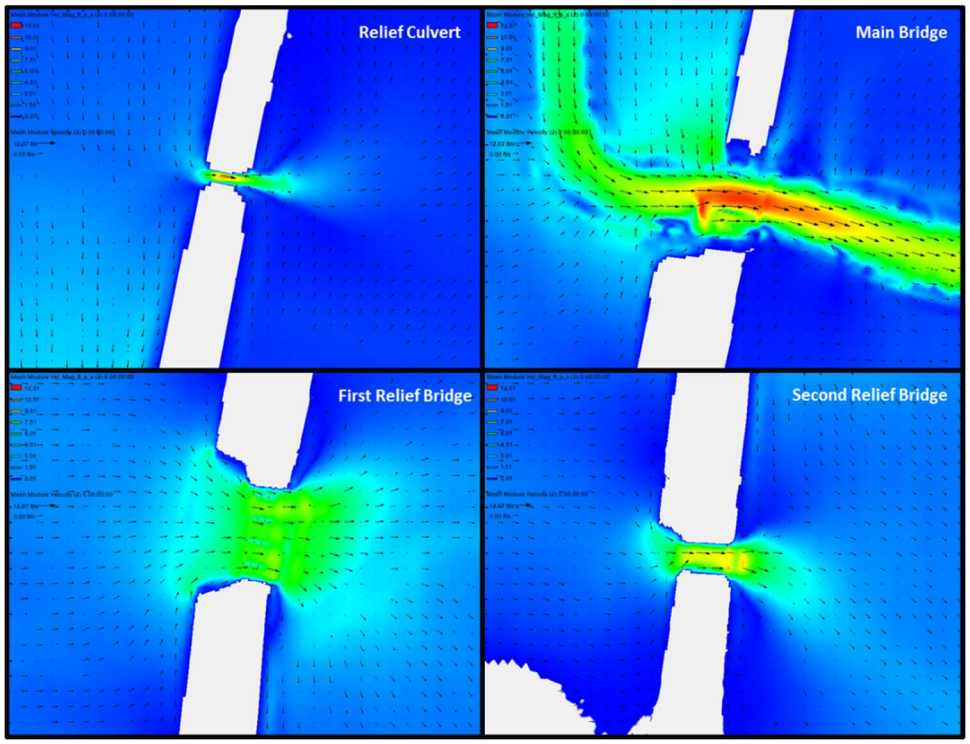

Figure 7-29. Velocity Contours with Vectors for the SRH-2D Highway 400 Openings

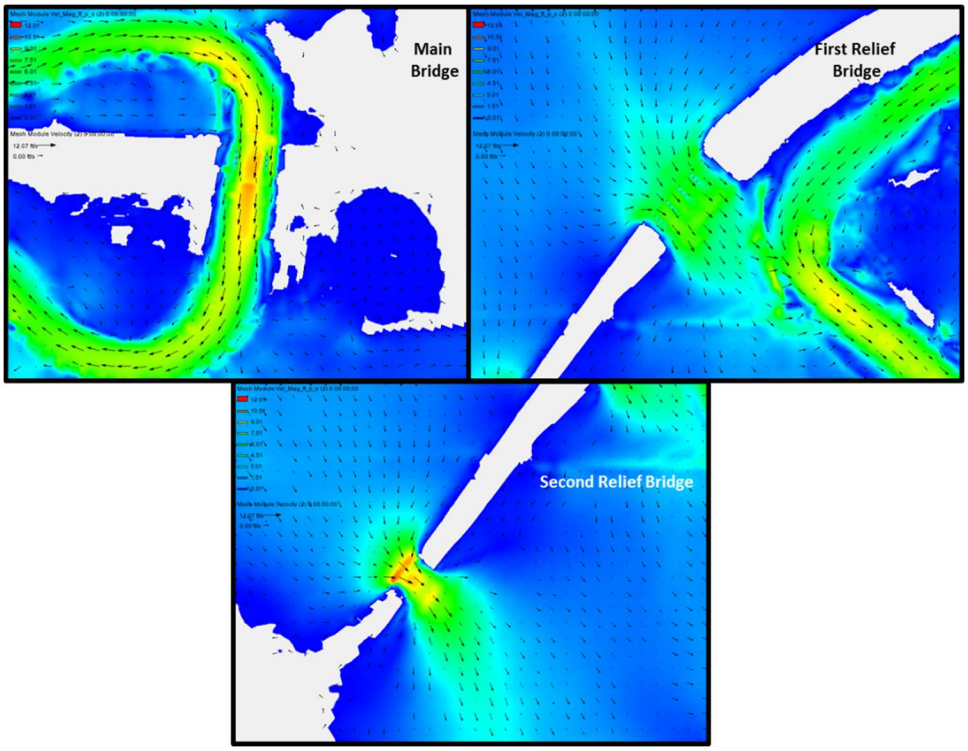

Figure 7-30. Velocity Contours with Vectors for the SRH-2D Highway 75 Openings

7.5. Summary of the Neodesha Floodplain Study Hydraulic Model Results

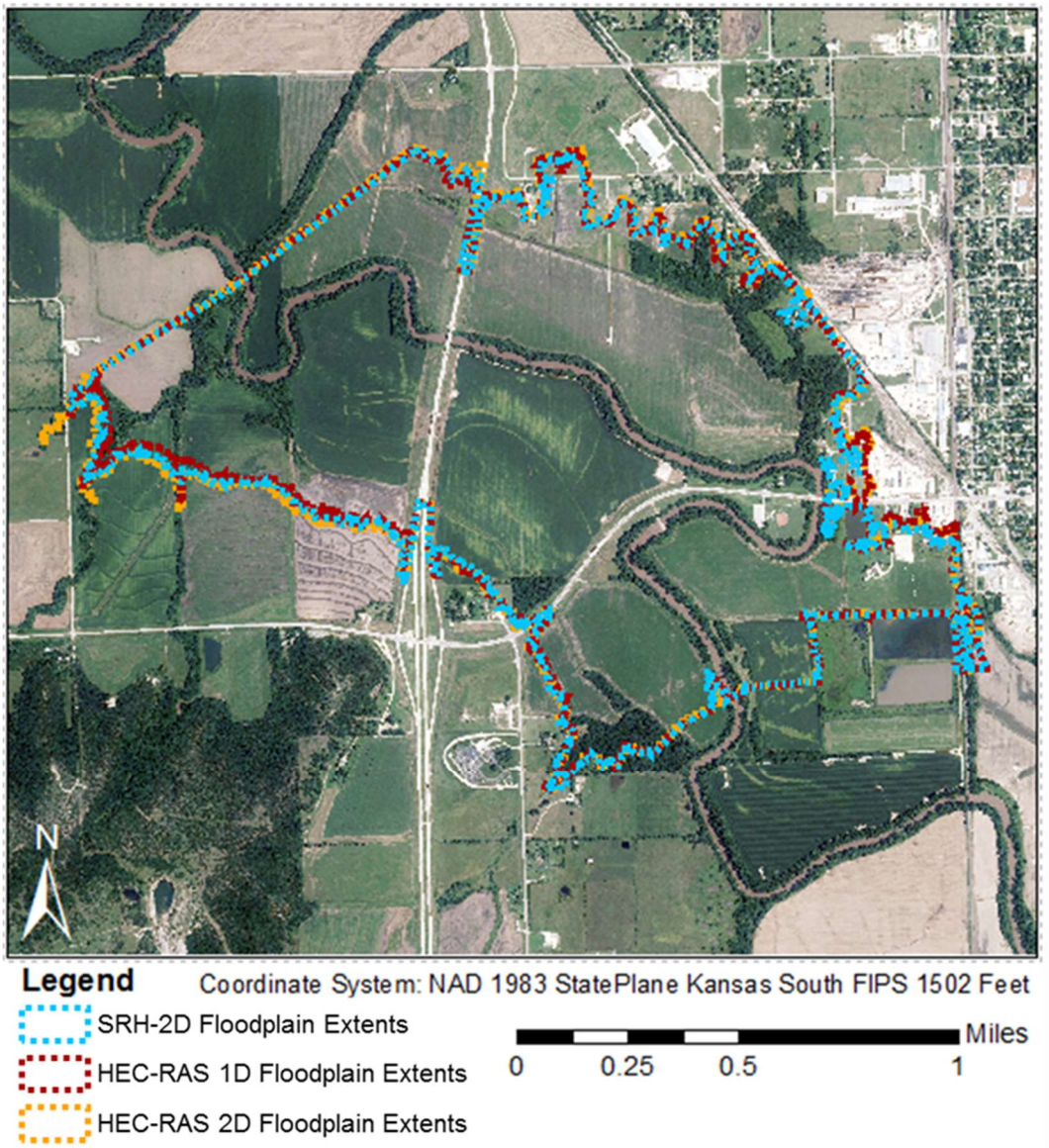

Figure 7-31. Comparison Map Showing the Floodplain Extents from all Three Models for the Neodesha Test Site

From Figure 7-31 it can be seen that the outside bounds of the floodplain are actually very similar for all three models tested – the one-dimensional HEC-RAS model, the two-dimensional HEC-RAS full momentum model, and the SRH-2D model. If comparing either two-dimensional models' extents to those of the one-dimensional model, it is difficult to assess which predicts a wider floodplain because sometimes the two-dimensional floodplain extents are inside and

sometimes outside, but if the comparison is limited to the two-dimensional models, it appears that the SRH-2D derived floodplain has extents either at approximately the same limits as the HEC-RAS 2D full momentum model or just inside of it. However, they are all more or less equal. This becomes even more apparent if one considers the actual portions of the model that were determined to be underwater at steady state conditions for the site. The following table contains the inundation data presented in previous sections. All models predict roughly the same amount of flooded land.

Table 7-4. Summary of Flooded Area for all Three Models for the Neodesha Test Site

Model	Wet Area	Percent Inundation
-	(sq.mi.)	
HR-1D	1.35	63.1%
HR-2D	1.40	65.0%
SRH-2D	1.37	64.0%

By considering the steady state flow from the one-dimensional model and the final timesteps of the two-dimensional models as shown in Table 7-5, one sees that the one-dimensional model predicted the highest flows through both of the main bridges. Both two-dimensional models distributed the flow more widely across the floodplain, resulting in more flow going through the relief structures present on both highways. Strikingly, the flow divisions through the openings determined by SRH-2D are more often than not closer to the conveyances determined by the HEC-RAS 1D model than by the HEC-RAS 2D model. The four cases out of seven where the SRH-2D values are more similar to the one-dimensional model include, on both Highways 400 and 75, the main bridges and the first relief bridges. It is not known which division of flow is the most accurate, further testing, including either laboratory or field data to calibrate the models to would be required to make such a claim, but in the event that the two-dimensional models are more accurate, these could be used to guide one-dimensional scour analyses which may be over predicting the amount

of scour expected to occur through the main channel structures. One thing to keep in mind is that the HEC-RAS 2D model could be set up very quickly if only the raw LIDAR data were used and details such as piers were not considered. The terrain should, however, be adjusted to include any culverts. Fairly large grid size could be used to allow one to produce a reasonable flow distribution.

Table 7-5. Summary of Flow Divisions for all Three Models through the Hydraulic Structures within the Neodesha Test Site

		Model								
		HEC-RAS 1D		HEC-RAS 2D Mom.			SRH-2D			
	Structure Designation	Q (cfs)	Percent of Q_{MAX}*	Q (cfs)	Percent of Q_{MAX}*	$Q_{1D} - Q_{2D}$ (cfs)	Q (cfs)	Percent of Q_{MAX}*	$Q_{1D} - Q_{2D}$ (cfs)	$Q_{HR-2D}-Q_{SRH-2D}$ (cfs)
Highway 400	Main Bridge	29952	74.9%	25090	62.7%	4862	27711	69.3%	2240	-2622
	First Relief Bridge	7267	18.2%	10583	26.5%	-3317	8246	20.6%	-979	2337
	Second Relief Bridge	2363	5.9%	3686	9.2%	-1323	3417	8.5%	-1054	269
	Relief Culvert	419	1.0%	639	1.6%	-220	591	1.5%	-172	48
	Total Q:	40000	100.0%	39998	100.0%	2	39965	99.9%	35	33
Highway 75	Main Bridge	29554	73.9%	20924	52.3%	8631	25511	63.8%	4043	-4587
	First Relief Bridge	6565	16.4%	10573	26.4%	-4008	7535	18.8%	-970	3038
	Second Relief Bridge	3881	9.7%	8504	21.3%	-4623	6818	17.0%	-2937	1686
	Total Q:	40000	100.0%	40000	100.0%	0	39864	99.7%	136	136

Q_{MAX} = 40,000 cfs

By comparing the flow patterns at the location of the first relief bridge on Highway 400, as shown in the following figure, it suggests that the two-dimensional models both predict similar rates of contraction and expansion through constrictions when the model extents exist relatively far away from the site of the constriction (see Chapter 6). While the rate of contraction appears close to a 1 to 1 ratio, which was assumed for the one-dimensional model, the flow is seen to expand much more rapidly to the south on the downstream side than was accounted for in that model.

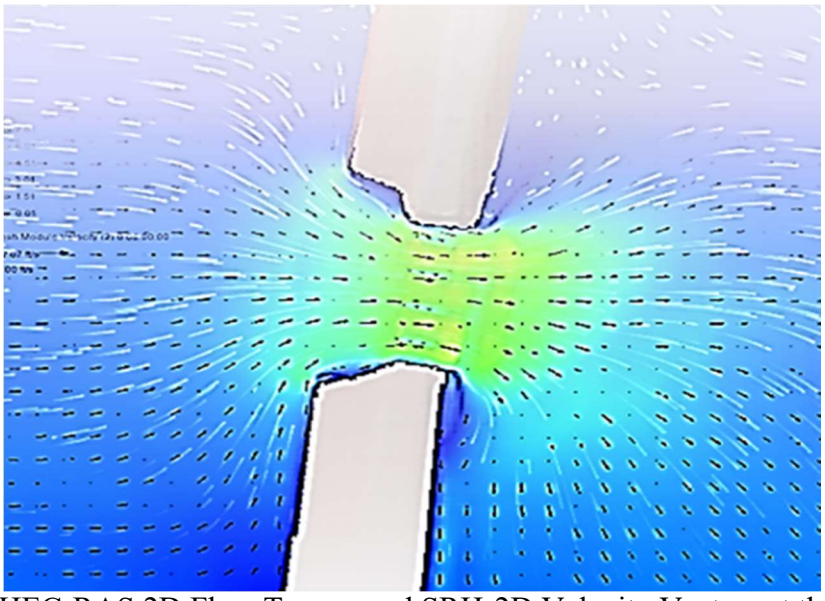

Figure 7-32. HEC-RAS 2D Flow Tracers and SRH-2D Velocity Vectors at the First Relief Bridge on Highway 400

These two-dimensional models were used to examine the unrealistic, but essential, assumption inherent in the one-dimensional HEC-RAS models that the water surface is constant across the entire length of any given cross section. Two cross sections were considered, the bounding upstream cross sections of the HEC-RAS one-dimensional model for Highways 400 and 75. The results of the models at these locations are contained in Figures 7-33 and 7-34. By looking at the water surface profiles in these figures the inaccuracy of the constant water surface elevation assumption quickly becomes apparent. For all three models, the surface width of the flow at these cross sections exceeds 4000 feet. The one-dimensional model is simply averaging properties across too great a distance. Another readily apparent detail, is that the HEC-RAS 2D model predicts the highest depths across the cross sections almost without exception. These profiles exceed those of SRH-2D by a foot or more in most locations – interestingly though, their overall shapes are very similar to each other.

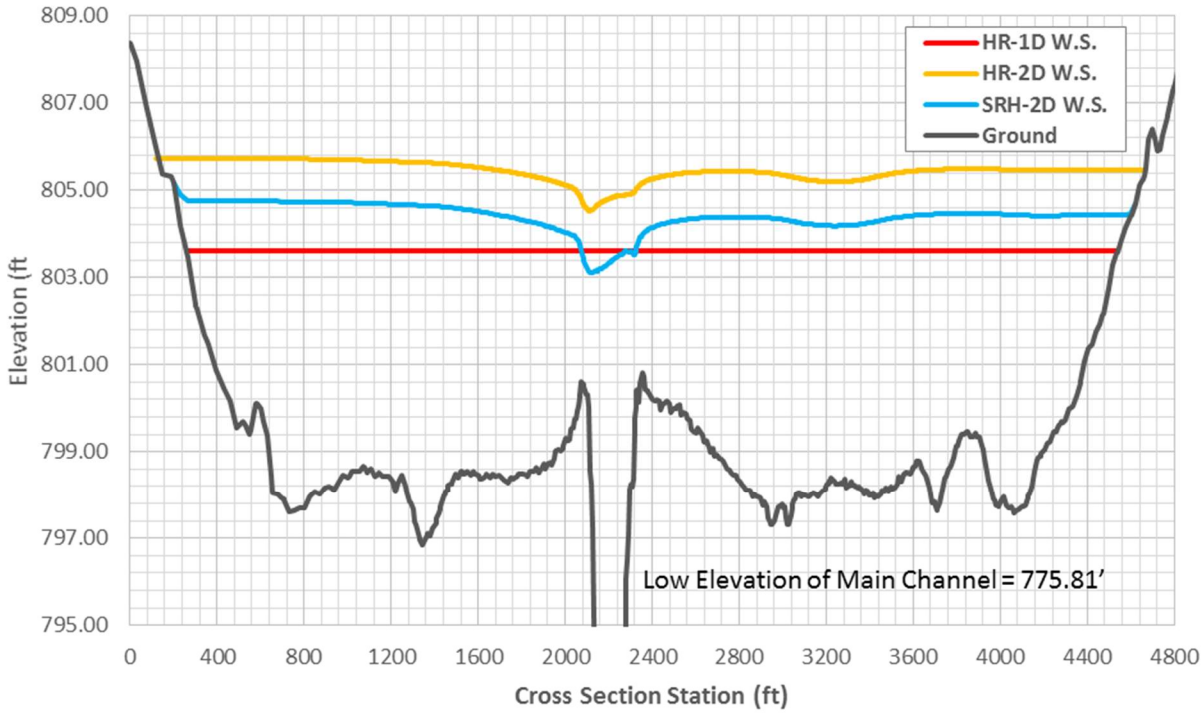

Figure 7-33. Water Surface Profiles for the Three Models at the Upstream Bounding Cross Section of Highway 400

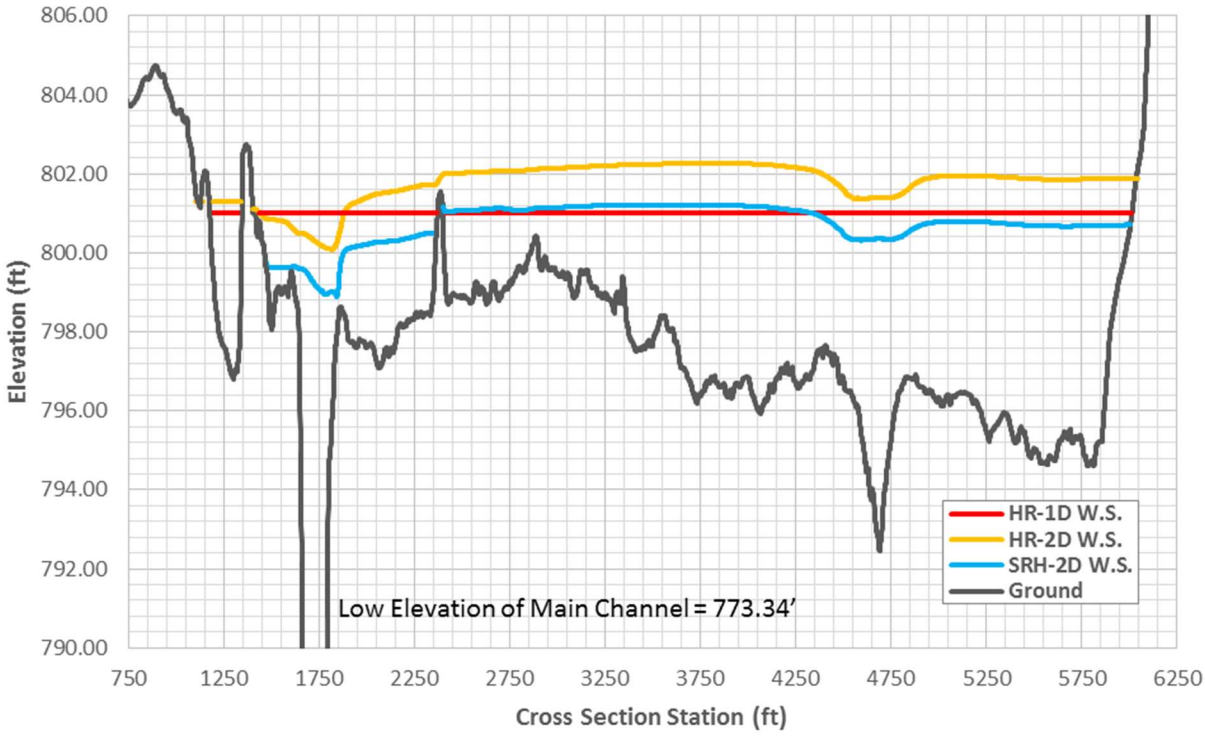

Figure 7-34. Water Surface Profiles for the Three Models at the Upstream Bounding Cross Section of Highway 75

The assumption that the energy is equal across the cross section is a much more realistic one, as, for truly steady state conditions, the flow will seek to balance energy losses that occur along comparable paths. So, if the cross sections are properly located, the problem becomes analogous to the well-documented situation of flow through parallel pipes between two reservoirs. This assumption would be a fascinating subject to study in greater detail, but was not addressed in regards to this site. One option that exists but was not used for the 1D HEC-RAS model was to split the flow upstream from HW 400, having it come back with the main channel flow just downstream from the larger relief structure for HW 75. This would require introducing two junctions and a *supplementary* stream that would pass through both of the relief bridges. This approach would also need to employ a ground level lateral weir between the two flow fields to avoid discontinuities at the adjoining edges of the cross sections.

Lastly, the water surface profiles along the stream centerline were considered for these three models, and are included in the following figure. All three profiles follow mostly the same pattern, yet those from the HEC-RAS 2D simulation exhibit a strong tendency towards higher depths than the other two models tested. The SRH-2D and HEC-RAS 1D profiles are sometimes below and other times above each other, and, to a much lesser extent, the same thing holds true for the HEC-RAS 2D and 1D profiles, but the HEC-RAS 2D profile is always above that from SRH-2D. This suggests, that for floodplain studies, HEC-RAS 2D may be the more conservative of the two-dimensional models since it predicts so much higher depths than SRH-2D does which translates to larger floodplains mapped. This has been a typical result for all tests conducted for this report. Also, the curious tendency of the HEC-RAS 2D models to let flow into the model space at unusually high depths has been a recurring issue.

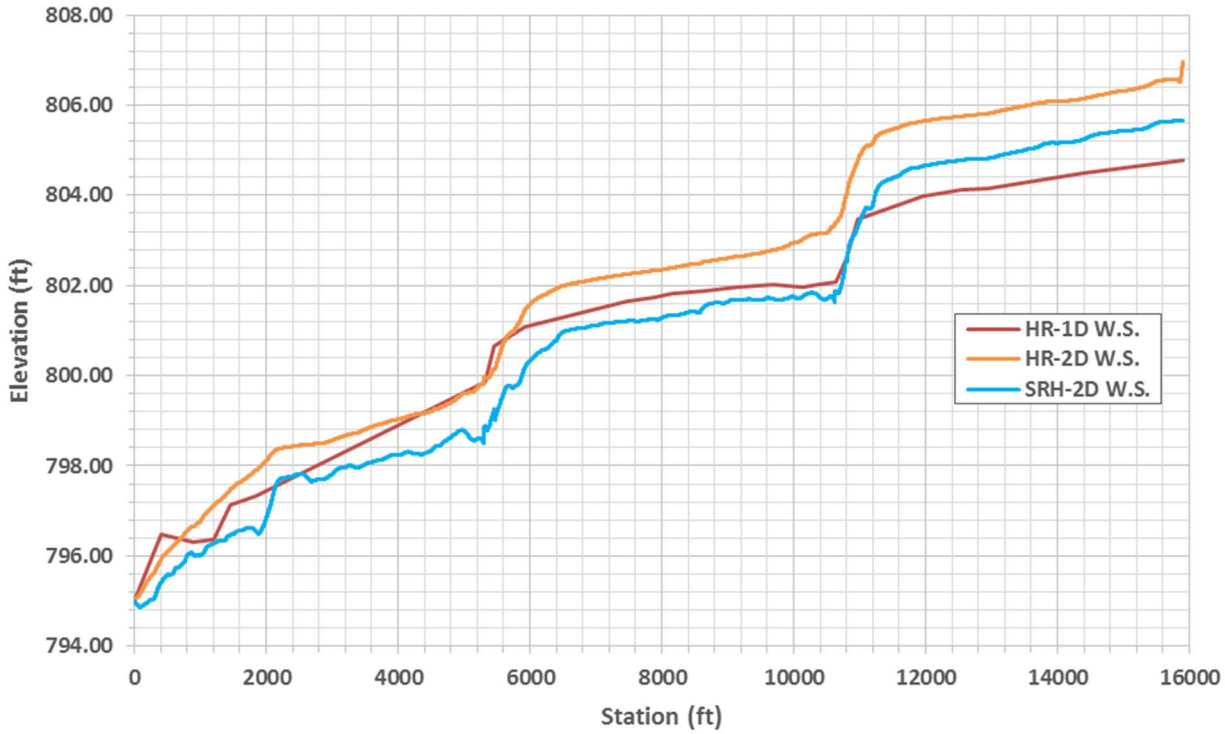

Figure 7-35. Water Surface Profiles from the Stream Centerline of the Three Models Tested for the Neodesha Floodplain Study

Chapter 8

Conclusion

The work presented in this report has led to the following conclusions:

1. There is still a place for one-dimensional hydraulic models in the repertoire of the hydraulic engineer. This is in large part due to the much longer computation times required for the 2D models over 1D models. For the Neodesha test reach (Chapter 7), the HEC-RAS 1D model took 9 seconds to complete, the HEC-RAS 2D full momentum model took 24 hours, 16 minutes, and 3 seconds, and the SRH-2D model took by far the longest at 166 hours and 59 minutes. This consideration may make the two-dimensional models prohibitively time-consuming for many engineering firms for iterative bridge design projects.
2. The two-dimensional models require a great deal of judgement and editing in order to build a sophisticated representation of a site. However, even more judgement is often required for 1D HEC-RAS modeling at complex sites. In regard to the 2D models, subjectivity remains in the selection of the computational timestep as well as the mesh element locations, sizes, and distributions in order to achieve a balance between physically realistic results and computational efficiency. However, a simplified HEC-RAS 2D model could be set up very quickly using only the raw LIDAR data if details such as piers were not included.
3. The use of relatively coarse representations of a site for a simplified two-dimensional model, using either HEC-RAS 2D or SRH-2D, could greatly aid in directing the construction of 1D models by helping the engineer visualize general flow patterns for the site, flow distribution for multiple openings, and placement of cross sections and ineffective flow areas. In this manner the 2D models could help reduce the subjectivity

inherent in building a proper HEC-RAS 1D model. Also, if hydraulic engineers begin to adopt this practice of using a 2D model to aid construction of a 1D model, then the field may begin to shift towards a heavier reliance on the more mathematically advanced 2D models.

4. There are some serious concerns raised by the unresponsiveness of the 2D models to the Manning's roughness coefficient observed for the bridge model that was discussed in Section 6.5. The water depth upstream of the bridge cross section for the HEC-RAS 2D full momentum model showed no obvious connection to the value used for the channel roughness, while the SRH-2D model did – although even when the roughness coefficient for this model was reduced to all the way to 0.0001 from 0.0233, the reduction in depth was not enough to cause the 2D model to match the laboratory data. This and the fact that both two-dimensional models responded so differently to the change in the roughness coefficient when both were using the full Saint Venant equations is troubling and warrants further investigation.
5. The divisions of flow through multiple opening bridges obtained from the 2D models are significantly different than those from the 1D HEC-RAS model. Thus the 2D models may be useful in guiding more accurate analyses of scour through bridges as well as sizing relief structures.
6. Virtually every analysis in this report shows that HEC-RAS 2D using the full momentum equations predicts the highest overall depths for any given site. This suggests that any analysis performed using exclusively that model to obtain results where high water levels are the critical variable would be the most conservative option. SRH-2D tends to return

higher depths than HEC-RAS 1D as well, but not to such a degree as the HEC-RAS 2D full momentum model.

7. HEC-RAS 2D with the diffusion equation will underestimate losses over a reach, but for situations where local losses are relatively small this solution bears more resemblance to those from SRH-2D than from HEC-RAS 2D with the full momentum equation. This suggests a strong possibility that a combined one- and two-dimensional HEC-RAS model using 1D routines through bridges and the diffusion equation set for the 2D flow areas would provide solutions that are a good balance between manual model set up, computational efficiency, and physically meaningful depictions of the flow behavior. Such an approach is particularly appealing for sites with highly sinuous streams that require accurate floodplain delineation.

References

Brunner, G.W. (2016) *HEC-RAS River Analysis System User's Manual.* Report No. CPD-68, Version 5.0. U.S. Army Corps of Engineers, Hydrologic Engineering Center, Davis, CA.

Brunner, G.W. (2016) *HEC-RAS River Analysis System Hydraulic Reference Manual*. Report No. CPD-69, Version 5.0. U.S. Army Corps of Engineers, Hydrologic Engineering Center, Davis, CA.

CEIWR-HEC (1991) *HEC-2 Water Surface Profiles User's Manual*. Report No. CPD-2A. U.S. Army Corps of Engineers, Hydrologic Engineering Center, Davis, CA.

Chow, V.T. (1959) *Open-Channel Hydraulics*. New York, NY: McGraw-Hill, Inc.

Henderson, F.M. (1966) *Open Channel Flow.* New York, NY: Macmillan Publishing Co., Inc.

Kundu, P. K., Cohen, I. M. (2008) *Fluid Mechanics, Fourth Edition*. Burlington, MA: Academic Press.

Lai, Y. G. (2008) *SRH-2D version 2: Theory and User's Manual: Sedimentation and River Hydraulics – Two-Dimensional River Flow Modeling*. U.S. Department of the Interior, Bureau of Reclamation, Technical Service Center, Denver, CO.

McEnroe, B.M., Young, C. B., Shelley, J. E. (2009) "Guidelines for Stream Realignment Design" *Kansas DOT Rep. No. K-TRAN: KU-08-2. Kansas Department of Transportation, Topeka, KS.*

Parr, A.D., Milburn, S., Malone, T., Bender, T. (2010) "A Model Study of Bridge Hydraulics, Edition 2" *Kansas DOT Rep. No. K-TRAN: KU-03-4R*. Kansas Department of Transportation, Topeka, KS.